External Noise in Stochastic Population Dynamics: The Case of Binary Environmental Switching

Robert E. L. West

Department of Mathematics

University of Leeds

A thesis submitted for the degree of

Doctor of Philosophy

October 5, 2020

Acknowledgements

I would firstly like to thank my supervisors, Mauro Mobilia and Alastair Rucklidge for their invaluable advice, guidance and support during my time at Leeds. Secondly, Sandro Azaele, Mike Evans and Michael Assaf for timely advice at crucial points in my studies. Finally I would like to thank all my friends and family who have put up with my mathematical ramblings over the last four years, particularly Josh and Harriet for their hospitality and company during the writing of this thesis.

Abstract

Understanding the factors that affect species survival and coexistence is a problem of significant importance. Species survival and reproduction can be affected by intrinsic (*i.e.* the composition of the population) and environmental factors (*e.g.* light, moisture, heat), and analysing their combined effect is a difficult task. This thesis will investigate the combined effect of internal (demographic) noise, caused by random birth-death events in a finite population, and external (environmental) noise on two models of microbial competition. These models are inspired by the well known Prisoner's Dilemma and Rock-Paper-Scissors games of Evolutionary Game Theory, and their dynamics in a static environment is well known. In well mixed (*i.e.* non-spatial), finite populations without mutation between species, internal noise ultimately leads to the death of all but one species. The strength of these demographic fluctuations is dependent on the population size, hence the probability that a certain species takes over (fixates) the population depends on the structure of the game and the size of the population. The majority of this thesis will focus on the case where external noise is modelled as a randomly switching carrying capacity, following a dichotomous Markov process to mimic periods of abundant and scarce resources. This results in a fluctuating population size, coupling the demographic noise to the environmental noise, leading to interesting, complex effects on the population dynamics. The effects of this coupling within these models is analysed using numerical and analytical techniques, and in general it is found that external noise promotes the fixation of the species that is the least likely to fixate in a static environment, but does not prolong species coexistence.

Abbreviations

IN	Internal (demographic) Noise
EN	External (environmental) Noise
DMN	Dichotomous Markov noise
PN	Periodic Noise (rectangular wave)
OU	Ornstein-Uhlenbeck
cCLV	chemical cyclic Lotka-Volterra model
MLM	May-Leonard model of cyclic competition
BDCLV	Birth-Death cyclic Lotka-Volterra model
LNA	Linear noise approximation
IDH	Intermediate Disturbance Hypothesis

Contents

Chapter 1

Introduction

Understanding the factors that affect the extinction and survival of species in ecological communities is one of the most important questions in modern science (Pennisi (2005)). Initially, biological processes were modelled as continuous processes with ordinary differential equations describing the population densities. However this necessarily ignores the random nature of biological processes: the number of individuals of a species does not change continuously, but is rather the result of births and deaths within the population. Hence this continuous description does not describe the dynamics exactly. In situations without mutation, demographic fluctuations (internal noise - IN) caused by birth-death events can ultimately lead to fixation - where one species takes over the whole community (Crow & Kimura (2009); Ewens (2004); Gardiner (1985); Van Kampen (1992)). The strength of these fluctuations is inversely proportional to the square root of size of the population, and hence decreases with the size of the community, and their nature depends on the internal community structure and composition. Furthermore, external factors like temperature, humidity, light *etc.* also have an influence on the community, leading to periods that are more or less favourable to growth and/or survival. Detailed knowledge about exogenous factors is generally unknown, so they are often modelled as external noise (EN) by assuming that the birth and/or death rates of one or all species varies in time (Acar *et al.* (2008); Ashcroft *et al.* (2014); Assaf *et al.* (2013a,b); Balaban *et al.* (2004); Chesson & Warner (1981); Danino & Shnerb (2018); Dobramysl & Täuber (2013); He *et al.* (2010); Hidalgo *et al.* (2017); Hufton *et al.* (2016, 2018); Kussell & Leibler

(2005); Kussell *et al.* (2005); May (1974); Melbinger & Vergassola (2015); Thattai & Van Oudenaarden (2001); Visco *et al.* (2010); West *et al.* (2018); Xue & Leibler (2017)). In this thesis I will present the effects of dichotomous Markov noise (DMN) (see Bena (2006) for a review of this process) on two paradigmatic models of species competition.

DMN, also known as the telegraph process, is a two-state Markov process that switches randomly between two values. The amount of time it spends at either value is drawn from an exponential distribution, with rate parameters that are constant, but not necessarily the same for each state. When applied to the death rates of a system, it is used to mimic the effects of a fluctuating level of resources available. This is particularly relevant for bacterial communities, in which relatively small changes in environmental factors can lead to population bottlenecks: a large fraction of the population die, and the community is repopulated by a small number of survivors. When the population size is small, demographic fluctuations are more important, leading to scenarios different from the case of a constant environment (West & Mobilia (2020); West *et al.* (2018); Wienand *et al.* (2015, 2017, 2018)). Dichotomous noise also has the advantage of being straightforward to simulate, and sufficiently simple that analytical results are possible for some systems, whilst also being a form of *coloured* noise (Bena (2006)). This means that it is correlated in time, which makes it more relevant for biological modelling of external fluctuations than white noise. White noise, which is uncorrelated in time, is relevant when the environmental fluctuations occur on a much shorter timescale than the biological processes in the system. In this case the rapid environmental fluctuations are in effect not felt by the system, and it feels the average effect of the noise. By contrast, when the environmental fluctuations and internal biological processes occur on similar timescales, or the timescale of the biological process is much shorter than the environmental noise, the external noise becomes a driving process within the main system, and its correlations must be taken into account (Ridolfi *et al.* (2011)). Furthermore, white noise and white shot noise can be recovered by taking appropriate limits in dichotomous noise (Bena (2006)). Another noise process relevant in biological settings is the Ornstein-Uhlenbeck process, a coloured Gaussian process. This cannot be recovered by taking a limit in DMN, but is not the focus of this thesis

as it has a couple of limitations (however, see Appendix A.2). Firstly, it is an unbounded process. Hence if it is used to drive the population size via the carrying capacity, it can go negative leading to unphysical results. This can be avoided by imposing a reflecting boundary at zero, and by using a small variance so that the probability of going negative is small. The first of these changes the distribution leading to inaccurate analytical results, and the second places a large restriction on the parameters of the process. Secondly, since it is a continuous process, it is more difficult to simulate systems where this drives the rates of another process. The quickest method is to approximate the OU process as a birth-death process with suitable rates so that the Fokker-Planck equation is the same (Roberts *et al.* (2015)), but this still leads to slow simulations since these rates are much larger than those for the rest of the system. Furthermore, analytical results even in one-species systems are only recoverable in the limits of fast and slow correlation times (Assaf *et al.* (2013a,b); Bena (2006)).

The bacterial models I will investigate are inspired by two classical examples from game theory, the *Prisoner's Dilemma* and *Rock-Paper-Scissors Game*. Originally developed in the 1940s and 1950s by John von Neumann, Oskar Morgenstern and John Nash, Game Theory attempts to address situations where a player may choose from certain strategies, bearing in mind the decisions of their competitors. In the 1970s, John Maynard Smith and George Price developed *Evolutionary* Game Theory by applying these ideas to the natural world, making predictions about how the composition of biological communities change over time (Smith (1982)). Since then advances in computing power have enabled the study of demographic fluctuations, as well the effects of spatial and network structure.

In the Prisoner's Dilemma, a two-person symmetric game, individuals may choose from two pure strategies: co-operation (C), where an individual chooses to share resources with its opponent, or defection (D) where they choose to take all the resources for themselves (Smith (1982)). Co-operation comes at an individual cost, but often with a global benefit (i.e. shared with all individuals). In evolutionary game theory, these are interpreted as 'population games', with the strategies (C) and (D) becoming species and their frequencies as the fractions of the population that are type C- or D- players/species respectively. This is

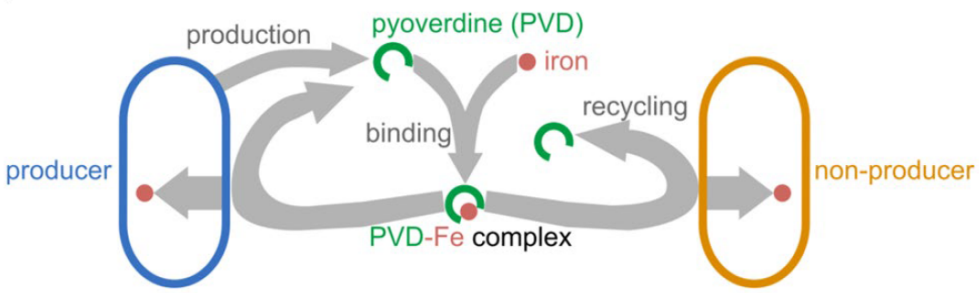

Figure 1.1: Cooperation and defection in *Pseudomonas aeruginosa*. Cooperators (blue) produce the siderophore pyoverdine (green) that binds to the iron (red) in the environment. The resulting complex is taken into the periplasm (membrane between the cytoplasm and outer membrane) of both cooperators and defectors (non-producers, orange), where the iron is reduced and incorporated into cells, while the pyoverdine is recycled back into the environment. Reproduced from Becker *et al.* (2018).

particularly relevant in biofilm formation, where some cells sacrifice their own metabolic rate and/or motility, in favour of developing features like thicker cell walls, antimicrobial factors and/or inhibitors, molecules that release nutrients from the environment and extracellular structures that benefit the whole community (Caro-Astorga *et al.* (2020)). For example, in *Pseudomonas aeruginosa* colonies, co-operative strains produce iron-scavenging molecules (siderophores) when iron is lacking in the environment (Becker *et al.* (2018); Buckling *et al.* (2007); Diggle *et al.* (2007); Griffin *et al.* (2004) - see Figure 1.1). The 'defectors' in this setting are the strains that do not produce siderphores, but still feel the benefit of their production due to increased increased iron uptake. Previous work has found that in finite, well mixed populations defectors fixate (i.e. the whole population is defectors) with a much larger probability than co-operators (Ewens (2004); Gardiner (1985); Hofbauer & Sigmund (2003); Hofbauer *et al.* (1998); Nowak & Sigmund (2004); Smith (1982)), due to their fitness advantage (because of a selective bias towards the defection strategy - in the deterministic counterpart, defection is an evolutionary stable strategy i.e. a stable fixed point), that manifests itself as a faster growth rate than the co-operators.

Why then is co-operative behaviour so prevalent in nature? Answering this

question is one of the central questions in modern evolutionary biology (Frank (1998); Hamilton (1995); Smith & Szathmary (1997)) and several possible mechanisms have been suggested. Spatial structure in terms of a lattice or more general networks, where individuals interact with their nearest neighbours has been shown to result in both cooperators and defectors coexisting for a time that scales roughly exponentially with the system size (Doebeli & Knowlton (1998); Durrett & Levin (1994); Hassell *et al.* (1994); Killingback *et al.* (1999); Lieberman *et al.* (2005); May (2006); Nowak & May (1992)). Here co-operators can form groups within the network mostly only helping each other, meaning that the benefit they produce is shared with other co-operators[1]. This is known as 'Network Reciprocity' and is one of the factors that can lead to selection of co-operative behaviour (Nowak (2006b)). Another consideration is the life-cycle of microbial colonies. In Cremer *et al.* (2012) and Melbinger *et al.* (2015) the authors describe the evolution of microbial colonies in three stages: a large group splits randomly into smaller groups, these then evolve independently, and then recombine after a certain time. In this case, when the average size of the smaller groups is small enough, the fact that groups with more cooperators will reach bigger sizes before the recombination favours co-operative traits. Here the selection occurs on two scales, first defectors out-compete co-operators within groups, but groups with more cooperators outcompete those with less. This 'Group Selection' counteracts the effect of individual level selection to favour co-operation.

There is also evidence that aforementioned population bottlenecks (where a large proportion of the community dies out, and is repopulated from the small amount of remaining survivors) can promote cooperation in bacterial biofilms (Brockhurst (2007); Brockhurst *et al.* (2007)). These experiments have found that cooperative strains of the bacteria are promoted when the disturbances that

[1]It should be noted that this is due to the underlying microscopic structure of the Prisoner's Dilemma, where cooperators survive by forming large compact clusters that reduce potential for exploitation by defectors. By contrast, in the snowdrift game, an alternative model of cooperation/defection that allows for stable coexistence of both strategies in the well mixed case, spatial structure reduces the frequency of cooperation. This is because the best reply to any strategy is the opposite one. Hence, cooperators act as a base for expanding finger-like structures, but cannot form clusters that protect against exploitation (Hauert & Doebeli (2004))

cause the bottlenecks occur at an intermediate rate. Too slow and selective advantage of non-cooperation leads to the defectors being promoted, while if the disturbances occur at a fast rate, the population never reaches a large enough size for co-operation to be beneficial (Brockhurst *et al.* (2007)). Furthermore, it has also been found that in this intermediate disturbance regime, larger disturbances (i.e. where a larger proportion of the population die out) are more likely to favour cooperators (Brockhurst (2007)).

After this brief overview, I will now more directly focus on the lines of research pursued in this thesis. These build on two recent works Wienand *et al.* (2017, 2018) where the authors show that symmetric dichotomous noise (i.e. the noise process spends on averate the same time in each state) applied to the death rate in the form of a randomly switching carrying capacity can also promote co-operation in a well mixed setting, as co-operators in some cases can have a higher fixation probability than without external noise. In Chapter 3, I will analyse the effect of asymmetric dichotomous noise on a version of the Prisoner's Dilemma. These results are more general, since they account for environmental noise that spends more time in either state and are also compared with a periodically switching environment.

The other model that I will consider is the Rock-Paper-Scissors game. This is the archetypal model of cyclic competition: rock blunts scissors, scissors cut paper, and paper wraps rock. Similar interactions have been observed in toxin producing-susceptible-resistant strains of *Escherichia coli* and the mating strategies of male *Uta stansburiana* lizards (Hibbing *et al.* (2010); Kerr *et al.* (2002); Kirkup & Riley (2004); Nahum *et al.* (2011); Sinervo & Lively (1996); Smith (1996); Zamudio & Sinervo (2000)). The *E. coli* community is comprised of three different strains; one that produces a toxin that kills the sensitive strain, and a resistant strain that does not produce the toxin. The sensitive strain grows faster than the resistant strain (since it is not subject to the cost of resistance), which in turn grows faster than the producing (since it does not incur the cost of producing the toxin). The cycle is closed by producing strain killing the sensitive strain (see Figure 1.2). In the case *U. stansburiana* lizards, males have three phenotypes characterised by different sizes and colours: large orange, medium blue and small yellow; while females are all small and yellow. Large orange males command a

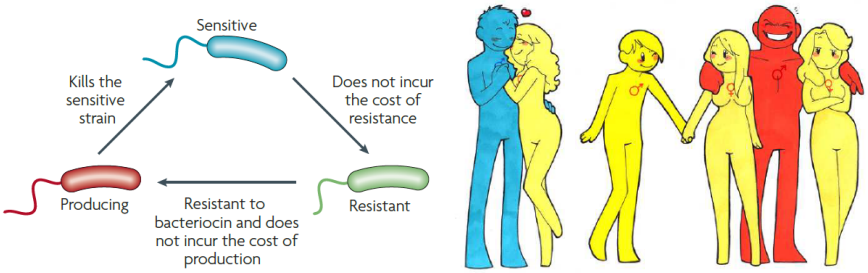

Figure 1.2: Examples of Rock-Paper-Scissors games in nature: (Left): toxin mediated cyclic dominance between sensitive, resistant and producing strains of *E. coli*. Reproduced from Hibbing *et al.* (2010). (Right): Mating strategy cyclic dominance in *U. stansburiana* lizards. Reproduced from HumonComics (2012).

large territory due to their size, meaning that they have many partners with whom they form weak bonds; medium blue males have smaller territories, within which they form strong bonds with fewer females. Hence the orange lizards dominate the blue ones. The small yellow males are indistinguishable from the females and do not have their own territories. Instead they sneak into those of others and try to mate with the females there. In orange territories they are successful because the host males have weak bonds with the females; while in blue territories they are not, due to the strong bonds between the host males and the females (see figure Fig. 1.2). Hence, orange dominates blue, blue dominates yellow and yellow dominates orange.

Mathematically, this is described by the cyclic Lotka-Volterra model (zero-sum case) and May-Leonard model (non-zero-sum case) (see Chapter 2 for more on zero- and non-zero-sum games). Ignoring all forms of noise, species densities oscillate around a coexistence fixed point, which is stable, neutrally stable or unstable. Together with the fact that the states corresponding to fixation of each species are saddle points, this can result in spirals towards the interior fixed point, limit cycles, neutral orbits or heteroclinic cycles depending on the parameters, this will be discussed in more detail in Chapter 4. Similarly to two species models, the inclusion of demographic fluctuations means that fixation is certain in the well mixed case, resulting various fixation and survival scenarios in populations of different size, with two simple laws for fixation in large and small

populations. (Berr *et al.* (2009); Frean & Abraham (2001); Frey (2010); Ifti & Bergersen (2003); Szolnoki *et al.* (2014)). Again, spatial and network structure have been shown to have a profound effect on the dynamics, in particular the interaction of the former coupled with mobility can promote or jeopardise species coexistence (Mobilia *et al.* (2016); Reichenbach *et al.* (2007a,b, 2008); Szczesny *et al.* (2013, 2014); Szolnoki *et al.* (2014)), while the latter results in limit cycles and noisy oscillations of species densities (Sato *et al.* (1997); Szabó *et al.* (2004); Szolnoki & Szabó (2004); Tainaka (1994)). Environmental noise in form of white noise on the reaction rates has been shown to have a minimal effect on the system dynamics (He *et al.* (2010)), but our understanding of the effects of coloured external noise is still poor. In Chapter 5 I will present the effects of a fluctuating population size (i.e. subject to both internal and external noise) on the fixation properties of the non-spatial rock-paper-scissors game, and in Chapter 6 I will present the results of a fluctuating reaction rate on a similar, but simpler model of cyclic competition. In both cases, the results are compared against the previously established laws for fixation in small and large population sizes (described in Chapter 4). Chapter 6 is a departure from the rest of the thesis, where instead of a fluctuating population size, we suppose that the fluctuating environment result in more/less favourable conditions for one of the species.

Having read this thesis, it is my goal that the reader should understand the effects of: Firstly, fluctuating population size driven by a dichotomous Markov noise on the two models introduced above. In the case of the Prisoner's dilemma I show that the fixation probability of the co-operators depends non-trivially on the asymmetry of the underlying external noise and the rate at which the switching takes place. Furthermore I will compare these results with periodic switching, where it will be shown that the transition between fast and slow switching occurs much earlier (i.e. for smaller switching rates) in the periodic case. In the case of Rock-Paper-Scissors games, due to the complicated dependence of the fixation probability of each species on the system size, letting this vary in time produces intricate, novel fixation scenarios that would not be possible with constant population size. External noise makes the competition more egalitarian, but does not prolong coexistence. Finally, I will present the results of a variable reaction rate on the zero-sum Rock-Paper-Scissors game. Again, external noise

produces new fixation scenarios, but does not prolong species coexistence. I hope that understanding the effect of simple, but coloured noise sources on these relatively simple models of species competition will become a small piece in the large, incomplete jigsaw of our understanding of the world around us (which we are trying to complete without the lid). First, in the next Chapter I will introduce the mathematical techniques I will use in the remainder of the Thesis.

Chapter 2

Mathematical Methods and Preliminary Results

This Chapter will introduce the mathematical techniques and results that will be used in the subsequent chapters. First I will review two methods for stochastic modelling of biotic populations: the Moran process where the total population size is fixed, and the birth-death process where the total population size fluctuates in time, and show how the first can be used to approximate the second. Then I will introduce dichotomous Markov noise and present its effect on the population size distribution of the logistic growth model, as these results will be central to the analysis in later chapters.

2.1 Mathematical Modelling of Biotic Populations

Mathematical modelling of biotic systems is by no means a new discipline. The famous Fibonacci sequence $1, 1, 2, 3, 5, 8, ...$, introduced in 1202 in his book *Liber Abaci* by Fibonacci[1] can crudely describe the population growth of mating pairs: Suppose that we start with one mating pair, that each mating pair takes one timestep to reach maturity, once they have they give birth to another mating

[1]This was its first appearance in Western Mathematics, however it was known to Indian Mathematicians in as early as 200 BC.

pair in each timestep, and that there are no deaths. The number of mating pairs after the first time step is $n_1 = 1$. In the next timestep they reach sexual maturity, $n_2 = 1$, then in the following they give birth to another mating pair, $n_3 = 2$. For a general time k, the number of mating pairs n_k will be the number at the last timestep n_{k-1}, plus the number of sexually mature pairs that will give birth to another i.e. the number of pairs two timesteps ago, n_{k-2}. After many timesteps, the number of pairs is roughly $\left(\frac{1+\sqrt{5}}{2}\right)^k$: the growth is exponential.

The first model for human population growth was proposed by Malthus in his seminal work *An Essay on the Principle of Population* in 1789, where he observed that the global population was growing exponentially. Due to a linearly increasing food supply, a point would be reached where this is no longer sustainable, subjecting much of the population to famine, poverty and ultimately death. This idea of population growth being limited by a resource was formalised by Verhulst in a series of papers between 1838 and 1847: in small population sizes growth is still exponential but reduces as the number of individuals increases and approaches the maximum supportable size, known as the carrying capacity. This maximum supportable population size can be thought of as relating to the amount of resources available to individuals in the system. If N is a variable representing the total population size, b is the per-capita growth rate at small population sizes and K is carrying capacity then we write this with the well-known formula

$$\frac{dN}{dt} = bN\left(1 - \frac{N}{K}\right). \tag{2.1}$$

A similar, historically important model for two species systems was introduced in 1926, simultaneously but independently by Vito Volterra and Alfred James Lotka, who were trying to model predator-prey and chemical oscillations respectively. Taking Volterra's ecological context, the growth of the prey is exponential in small population sizes but is limited by the presence of predators, who die without prey to feed on:

$$\begin{aligned} \frac{dN_1}{dt} &= N_1\left(b - \alpha N_2\right) \\ \frac{dN_2}{dt} &= N_2\left(\beta N_1 - d\right), \end{aligned} \tag{2.2}$$

where b is the per-capita birth rate of prey in the absence of predators, d is the death rate of predators in the absence of prey, and α, β are parameters that are related the rate of predation, efficiency of biomass conversion and carrying capacity. This model admits periodic solutions around the non-trivial steady state $(d/\beta, b/\alpha)$, and has been derived in several disciplines: not only ecology (Lotka (1926); Volterra (1926a,b)) and chemistry (Semenov *et al.* (1935)), but others such as economics (Galbraith (2008)) and epidemics (Kermack & McKendrick (1927, 1932, 1933)). It should be noted that this model is fundamentally flawed: the periodic orbits are neutrally stable, set by the initial conditions and are therefore not robust - different initial conditions lead to different orbits. This can be seen by noting that the quantity $C = b \ln N_2(t) - \alpha N_2(t) - \beta N_1(t) + d \ln N_1(t)$ is conserved. The orbits will therefore be those along which this is constant. In later chapters we will also see that a form of cyclic competition, the cyclic Lotka-Volterra model also has orbits defined by a conserved quantity. These are both examples of *zero-sum* games, which always exhibit a conserved quantity (see below).

As humanity's understanding of the world around us has improved we started asking larger scale scientific questions. A natural extension of the Lotka-Volterra predator-prey model above is to ask, if we knew the relative strengths of interactions between all species in a community, could we model a system of M different species in the same way? In this case we write:

$$\frac{dN_i}{dt} = r_i N_i \left(1 - \frac{1}{K_i} \sum_{i=1}^{M} \alpha_{ij} N_j\right), \tag{2.3}$$

where r_i are the species growth rates, K_i is the carrying capacity of species i (the maximum number of species i individuals that can be supported) and the signs of α_{ij} and α_{ji} tell us about the type of relationship between species i and j: if they are both zero then the species do not directly affect one another, if they are both positive then they are in direct competition, negatively affecting one another. If one is positive and the other negative then there is a predator-prey relationship, while the rarer case of the both being negative indicates to a mutualistic relationship where both species promote the other. Due to the large number of parameters and variables, this system has rich, varied possible behaviour. These

include, but are not limited to: extinction of all but one species, limit cycles, strange attractors and chaos. In practice it is difficult to accurately quantify the intra- and interspecific interaction strengths (α_{ii} and α_{ij} respectively), so in practice these are drawn from a normal distribution with mean 0 and variance σ^2 with probability c (called 'connectance') and are zero otherwise. Similar assumptions are made for the growth rates r_i and carrying capacities K_i. Models of this type were first studied by R. M. May, who found that stability decreases with the number of species M, the connectance c and the variance of the interaction strength σ^2 (May (1971, 1972, 1974)). This result seems to be at odds with the wide variety of diverse co-habiting species observed in nature, and has inspired a large body of work to try and address this (see, for example Allesina & Tang (2012); Biroli *et al.* (2018); Bunin (2017); Donohue *et al.* (2013); Galla (2018); Ives & Carpenter (2007); Loreau & De Mazancourt (2013); McCann (2000)). Interestingly it has been found that spatial structure in terms of a meta-population model with dispersal between patches can promote stability (Gravel *et al.* (2016)), while saturating non-linear feedback between species can lead to either a unique stable fixed point, multiple fixed points or non-convergent dynamics (chaotic or periodic orbits) (Sidhom & Galla (2020)).

An important limitation of these models is that they assume that the populations change continuously in time. We know that this is not the case: populations fluctuate due to birth and death events, and these happen with a certain rate. A further complication is that these rates are in general not constant: they may depend explicitly on time, some external variables like temperature or sunlight and on the composition of the system.

Concurrently to our understanding of ecology, Game theory was formalised by Von Neumann and Morgenstern in 1944, with further seminal contributions by John Nash in the 1950s, in order to explain human economic behaviour (Morgenstern & Von Neumann (1944); Nash (1951, 1953, 1950); Nash *et al.* (1950)). It is concerned with situations where interacting individuals ('players') make decisions, depending on the available options ('strategies') and the choices of those they are interacting with. Their decisions come with an associated payoff against other strategies, and players act in a rational, self-interested manner in order to maximise their individual payoff. Thus everything that a player uses to make

their decision is summarised in a payoff table, which shows the resulting payoff of playing each strategy against another. Furthermore, we must suppose that every player knows everything about the structure of the game, in particular knows all the possible strategies and is able to play all of them. This thesis will focus on pairwise contests between identical players, so-called *symmetric two-player* games, with M strategies. In this case the payoff matrix for each player is the same, defined by an $M \times M$ matrix. For example the following matrix defines a symmetric two-player game where two individuals playing strategy S_1 both receive the payoff a against each other, two S_2 individuals both receive d, while when S_1 receives b against S_2 and S_2 receives c against S_1:

$$\mathcal{P} = \begin{array}{c|cc} \text{Strategy} & S_1 & S_2 \\ \hline S_1 & a & b \\ S_2 & c & d \end{array}$$

The goal is to find a strategy $\vec{x}$ (here meaning a vector where the entry in the i-th column gives the probability of playing the pure strategy S_i, the entries must be non-negative and sum to 1) such that if almost all individuals adopt it, a player playing a different one cannot invade the population. This is called a *strict Nash equilibrium (sNE)*, defined as a strategy that is the unique best reply itself, i.e. satisfies $\vec{x} \cdot \mathcal{P}\vec{x} > \vec{y} \cdot \mathcal{P}\vec{x}\ \forall \vec{y} \neq \vec{x}$ ($\vec{y} \cdot \mathcal{P}\vec{x}$ is the payoff of strategy $\vec{y}$ against strategy $\vec{x}$). The simplest case is when this is always playing S_1 or S_2 (i.e. $\vec{x} = [1, 0]^T$ or $[0, 1]^T$) ('pure strategies'), however if $a < c$ and $d < b$ the sNE is a *mixed* strategy, playing S_1 with probability $p = \frac{b-d}{b+c-a-d}$ and S_2 with probability $1 - p$ (Smith (1982)).

These ideas were applied to the behaviour of animals by John Maynard Smith and George Price in 1973 (Smith & Price (1973)) and then further formalised in Smith (1982). There are a few differences between classical game theory and this new *evolutionary* game theory (EGT). First, the strategy sets are no longer strategies that individuals choose, but are now inherited genotypic variants. Hence, pure strategies become species. Secondly, strict Nash equilibriums now, with a slight relaxation of the conditions become *evolutionary stable strategies* (the inequality above for a strict Nash equilibrium must hold, or if there is instead an equality then the condition $\vec{x} \cdot \mathcal{P}\vec{x} > \vec{y} \cdot \mathcal{P}\vec{y}\ \forall \vec{y} \neq \vec{x}$ must also be satisfied). Finally, mixed strategies $\vec{x} = \sum_{i=1}^{M} x_i \vec{e}_i$ now correspond to a population with

a fraction x_i individuals of species i. These populations then evolve according to repeated random parings of individuals, with outcomes defined in the payoff matrix. These models are called 'population games' and EGT aims to describe the dynamics of these populations. The dynamics of the population densities x_i follows $dx_i/dt = x_i\left[(\mathcal{P}\vec{x})_i - \vec{x}\cdot\mathcal{P}\vec{x}\right]$, which is the celebrated replicator equation (see, for example Schuster & Sigmund (1983)) The first term is the expected payoff of and individual of species i, while the second is the average payoff of the population. From this, the steady states and their stability can be found using traditional methods (linear stability analysis, bifurcation theory).

In a stochastic setting, births and deaths occur with a randomly, each with a certain rate. In this context, the expected payoff to a species i individual, given by $(\mathcal{P}\vec{x})_i$, (where $\vec{x} = [N_1/N, N_2/N]^T$, $N_i, i = 1, 2$ refers to the number of individuals playing strategy i and $N = N_1 + N_2$ is the total population size) is interpreted as its fitness, and is proportional to the per-capita birth rate. We also suppose that deaths are due to competition for resources, manifested by a per-capita death rate N/K, where K is the carrying capacity - the maximum supportable population size. I will refer to processes where births and deaths happen separately, leading to fluctuating total population size around the carrying capacity K, as a 'Birth-Death Process', however it is sometimes more convenient mathematically to assume that a birth and death occur simultaneously, keeping the population size fixed (at K) and reducing the number of variables by 1. This is known as the 'Moran Process' and will also be used extensively in this thesis.

In Sections Sec. 2.1.1 and Sec. 2.1.2 I will describe the Moran process and the Birth-Process in static environments. These are two classical formulations of bacterial competition with slightly different properties (Benaim *et al.* (2004); Doebeli *et al.* (2017); Ewens (2004); Fudenberg *et al.* (2004); Hofbauer *et al.* (1998); Kimura (1957); Méndez *et al.* (2015); Moran *et al.* (1962); Nee *et al.* (1994); Nowak (2006a); Nowak *et al.* (2004)). The second is used in Chapters 3 and 5 when considering fluctuating population size, and the first is used in Chapter 6 where the population size is fixed. However I will also show that the considering the Moran process approximation of Birth-Death processes in useful in Chapters 3 and 5. Section 2.2 introduces external noise, its importance in biological modelling and the form that I will use - dichotomous Markov noise

(Section 2.2.1). To prepare the reader for analysis of its effects on two and three species models, I will show its effects on the one species logistic growth model.

2.1.1 The Moran Process

We first consider the case where the total population size of the system is fixed, known as the Moran Process. This describes competition between individuals of different species where at each time-step firstly an individual is chosen for reproduction, creating an exact copy of itself. Simultaneously, another is chosen to die so that the total population size (here denoted by K) remains fixed. The exact reaction network and rates at which these reactions occur is related to the population composition and the parameters of your system, and to illustrate the methods used I first consider populations of two competing species. In this case there are two possible reactions:

$$\begin{aligned} [N_1, N_2] &\xrightarrow{W_{21}} [N_1 + 1, N_2 - 1] \quad \text{and,} \\ [N_1, N_2] &\xrightarrow{W_{12}} [N_1 - 1, N_2 + 1] \end{aligned} \tag{2.4}$$

where the transition rates W_{12} and W_{21} are general functions of the population densities $\vec{x} = [N_1, N_2]^{\mathrm{T}}/K$ (i.e. $x_1 + x_2 = 1$), of the form $W_{ji} = h_{ji}(\vec{x})x_i x_j K$. This choice of transition rates means that we are considering Markov process with absorbing boundaries, i.e. $\vec{x} = [x_1, x_2]^{\mathrm{T}} = [1, 0]^{\mathrm{T}}$ and $[0, 1]^{\mathrm{T}}$ are absorbing states, and cannot be left once they have been entered. Hence this guarantees that the stochastic dynamics will end up in one of these states. This thesis will be focused on the *fixation probability* of each species, defined (for species i) as the probability that the system reaches the absorbing state in which only species i is present: $\lim_{t\to\infty} P(\vec{x}(t) = \vec{e}_i)$ denoted as ϕ_i ($\vec{e}_i$ is the unit vector in the i direction). Another quantity of interest will be the mean fixation time, defined as the mean time for an absorbing state to be reached, independent of the species that has fixated the population.

The analysis starts with the Master equation, written as:

$$\frac{d}{dt}P(\vec{N}, t) = \left[\left(\mathbb{E}^-_{N_1}\mathbb{E}^+_{N_2} - 1\right) W_{21} + \left(\mathbb{E}^+_{N_1}\mathbb{E}^-_{N_2} - 1\right) W_{12}\right] P(\vec{N}, t), \tag{2.5}$$

where $\mathbb{E}^{\pm}_{N_i}$ are shift operators such that $\mathbb{E}^{\pm}_{N_i} h(\vec{N}) = h(\vec{N} \pm \vec{e}_i)$ and $P(\vec{N}, t) = 0$ whenever any $N_i < 0$. From this a recursive formula for the fixation probability of species 1 can be obtained from a first-step analysis of the underlying Markov process. In this case one can define the recursive formula for $\phi(m)$, the probability that a population of focal species (w.l.o.g. species 1) of size m will fixate the population:

$$\phi(m) = \frac{W_{21}(m)}{W_{21}(m) + W_{12}(m)}\phi(m+1) + \frac{W_{12}(m)}{W_{21}(m) + W_{12}(m)}\phi(m-1), \tag{2.6}$$

the first term accounts for a species of type 1 replacing one of type 2, and the second accounts for the opposite. This has boundary conditions $\phi(0) = 0$ and $\phi(K) = 1$. Following Ewens (2004) we define $\chi_m = \phi(m) - \phi(m-1)$, to find that $\frac{\chi_{m+1}}{\chi_m} = \frac{W_{12}(m)}{W_{21}(m)}$, from which it is simple to show that:

$$\chi_m = \chi_1 \prod_{i=1}^{m} \frac{W_{12}(i)}{W_{21}(i)} \quad \text{and} \quad \phi(m) = \chi_1 \sum_{q=1}^{m} \left(\prod_{i=1}^{q} \frac{W_{12}(i)}{W_{21}(i)} \right). \tag{2.7}$$

When the ratio in the product is constant ($= \alpha$) the expression above reduces to a geometric series. Using this and the boundary condition for $m = K$ we find that:

$$\phi(m) = \frac{\alpha^m - 1}{\alpha^K - 1}. \tag{2.8}$$

A similar first-step analysis can be used to find the unconditional mean fixation time. In this case the recursive formula for $T(m)$, the mean fixation time for a system starting with m individuals of species 1 is (Antal & Scheuring (2006); Assaf & Mobilia (2010); Gardiner (1985)):

$$W_{21}(m)\left[T(m+1) - T(m)\right] + W_{12}(m)\left[T(m-1) - T(m)\right] = -1, \tag{2.9}$$

With boundary conditions $T(0) = T(K) = 0$. The solution to this problem, given by

$$T(m) = -T(1) \sum_{k=m}^{N-1} \prod_{j=1}^{k} \frac{W_{12}(j)}{W_{21}(j)} + \sum_{k=m}^{N-1} \sum_{l=1}^{k} \frac{1}{W_{21}(l)} \prod_{j=l+1}^{k} \frac{W_{12}(j)}{W_{21}(j)}, \tag{2.10}$$

$$\text{where} \quad T(1) = \phi(1) \sum_{k=1}^{N-1} \sum_{l=1}^{k} \frac{1}{W_{21}(l)} \prod_{j=l+1}^{k} \frac{W_{12}(j)}{W_{21}(j)}, \tag{2.11}$$

is in general too complicated and unwieldy to be useful, however approximations may be made in the limit of large population sizes, for example see Antal & Scheuring (2006).

These results are for two species systems with a fixed population size. However I will also consider populations of three competing species. In this case, while it is possible to use the first-step analysis to write down expressions similar to (2.6) and (2.9), the equations are not easily solvable, so expressions similar to (2.8) and (2.10) for the fixation probability and mean fixation time are not readily available. However, from the Master equation, it is possible to derive the mean field equations, as I will now show. The mean field equations are a deterministic theory describing how the averages $\langle x_i \rangle = \langle N_i \rangle / K = \frac{1}{K} \sum_{\vec{N}} N_i P(\vec{N}, t)$ vary in time. Due to the correlations between the x_i's, this results in an infinite hierarchy of equations. Progress is made by treating the x_i's as independent variables (ignoring the correlations). We write:

$$\begin{aligned}
\frac{\partial}{\partial t}\langle x_i \rangle &= \sum_{\vec{N}} \frac{N_i}{K} \frac{\partial}{\partial t} P(N,t) = \sum_{\vec{N}} \frac{N_i}{K} \sum_{i=1}^{3} \sum_{\substack{j=1 \\ j \neq i}}^{3} \left(\mathbb{E}^{-}_{N_i} \mathbb{E}^{+}_{N_j} - 1 \right) W_{ji}(\vec{N}) P(\vec{N}, t) \\
&= \sum_{\vec{N}} \frac{N_i}{K} \sum_{i=1}^{3} \sum_{\substack{j=1 \\ j \neq i}}^{3} \left[W_{ji}(\vec{N} - \vec{e}_i + \vec{e}_j) P(\vec{N} - \vec{e}_i + \vec{e}_j, t) - W_{ji}(\vec{N}) P(\vec{N}, t) \right] \\
&= \sum_{\vec{N}} \left(\frac{N_i + 1}{K} - \frac{N_i}{K} \right) \sum_{\substack{j=1 \\ j \neq i}}^{3} W_{ji}(N) P(N,t) \\
&+ \sum_{\vec{N}} \left(\frac{N_i - 1}{K} - \frac{N_i}{K} \right) \sum_{\substack{j=1 \\ j \neq i}}^{3} W_{ij}(N) P(N,t) \\
&= \sum_{\substack{j=1 \\ j \neq i}}^{3} \left\langle \frac{W_{ji} - W_{ij}}{K} \right\rangle = \sum_{\substack{j=1 \\ j \neq i}}^{3} \left\langle x_i x_j \left[h_{ji}(\vec{x}) - h_{ij}(\vec{x}) \right] \right\rangle \\
&\approx \sum_{\substack{j=1 \\ j \neq i}}^{3} \langle x_i \rangle \langle x_j \rangle \left[\langle h_{ji}(\vec{x}) \rangle - \langle h_{ij}(\vec{x}) \rangle \right], \qquad (2.12)
\end{aligned}$$

where the last line is a result of factorising $\langle x_i x_j g(\vec{x}) \rangle = \langle x_i \rangle \langle x_j \rangle \langle g(\vec{x}) \rangle$ for general $g(\vec{x})$. This comes from the fundamental assumption of the mean field approxi-

mation: that the effect of all the other individuals in the system on any given individual can be approximated by a single averaged effect. Then, due to the central limit theorem, the ratio of the size of demographic fluctuations to the mean is of order $N^{-1/2}$. One may then write:

$$x_i \approx \langle x_i \rangle + \frac{1}{\sqrt{N}} d_i, \tag{2.13}$$

where $d_i \sim \mathcal{O}(1)$. When substituted into the penultimate line of (2.12) this gives:

$$\sum_{\substack{j=1 \\ j\neq i}}^{3} \left\langle x_i x_j \left[h_{ji}(\vec{x}) - h_{ij}(\vec{x}) \right] \right\rangle \approx \sum_{\substack{j=1 \\ j\neq i}}^{3} \langle x_i \rangle \langle x_j \rangle \left[\langle h_{ji}(\vec{x}) \rangle - \langle h_{ij}(\vec{x}) \rangle \right] + \mathcal{O}\left(\frac{1}{\sqrt{N}} \right), \tag{2.14}$$

yielding the final line of (2.12) in the deterministic limit when $N \to \infty$ and demographic fluctuations are ignored.

This is a crude and uncontrolled approximation, and as a result the mean field equations (which are deterministic) omit a lot of information about the system. They describe the dynamics of the average values reasonably well for large population sizes, and can tell us the location of the fixed points of the system. However, in the full stochastic system these will only remain fixed points if they absorbing (i.e. there is no pathway by which to escape once entered). If there is more than one of these such fixed points (as in the models considered in later chapters) these equations tell us nothing about the probability of each one being hit.

At this point, it is convenient to write the probability distribution in terms of the population densities, $\vec{x}$, where the shift operators are now defined as $\mathbb{E}_i^{\pm} g(\vec{x}) = g(\vec{x} \pm e_i/K)$ (with a slight abuse of notation $g(x_i) \equiv g(x_i K) = g(N_i)$) for a general function g. Then one can perform a size expansion of (2.5) in $1/K$ (known as van Kampen's system size expansion), keeping the terms of $\mathbb{E}_i^{\pm}$ up to order $\frac{1}{K^2}$

so that $\mathbb{E}_i^{\pm} = 1 \pm \frac{1}{K}\frac{\partial}{\partial x_i} + \frac{1}{2K^2}\frac{\partial^2}{\partial x_i^2} + \mathcal{O}\left(\frac{1}{K^3}\right)$, and to first order in $\frac{1}{K}$ we have:

$$\begin{aligned}
\frac{\partial}{\partial t}P(\vec{x},t) &= \left[\left(\mathbb{E}_1^-\mathbb{E}_2^+ - 1\right)W_{21} + \left(\mathbb{E}_1^+\mathbb{E}_2^- - 1\right)W_{12}\right]P(\vec{x},t) \\
&= -\left[\left(\frac{\partial}{\partial x_1} - \frac{\partial}{\partial x_2}\right)h_{21}(\vec{x})x_1x_2 + \left(\frac{\partial}{\partial x_2} - \frac{\partial}{\partial x_1}\right)h_{12}(\vec{x})x_2x_1\right]P(\vec{x},t) \\
&+ \frac{1}{2K}\left[\left(\frac{\partial}{\partial x_1} - \frac{\partial}{\partial x_2}\right)^2 h_{21}(\vec{x})x_1x_2 + \right. \\
&\left.\left(\frac{\partial}{\partial x_2} - \frac{\partial}{\partial x_1}\right)^2 h_{12}(\vec{x})x_2x_1\right]P(\vec{x},t) + \mathcal{O}\left(\frac{1}{K^2}\right), \qquad (2.15)
\end{aligned}$$

With absorbing boundaries at $\vec{x} = \vec{e}_i$, $i = 1, 2$, i.e. $P(\vec{e}_1, t) = P(\vec{e}_2, t) = 0$. Since I am considering two species, and the total population size is fixed, this equation is simplified by writing $x_1 = x$ and $x_2 = 1 - x$. From (2.15) the Fokker-Planck equation can be written:

$$\frac{\partial P(x,t)}{dt} = -\frac{\partial}{\partial x}A(x)P(x,t) + \frac{1}{2}\frac{\partial^2}{\partial x^2}B(x)P(x,t) \qquad (2.16)$$

Where $A(x) = x(1-x)\left[h_{21}(x) - h_{12}(x)\right]$ and $B(x) = x(1-x)\left[h_{21}(x) + h_{12}(x)\right]/K$.

From this one can use the results of Gardiner (1985) to find closed equations and solutions for the fixation probability of the either species and the mean time to fixation. The fixation probability of the focal species, $\phi(x)$ is the solution of the equation:

$$\begin{aligned}
&A(x)\frac{d}{dx}\phi(x) + \frac{1}{2}B(x)\frac{d^2}{dx^2}\phi(x) = 0, \\
&\text{with boundary conditions: } \begin{cases}\phi(0) = 0 & \text{and} \\ \phi(1) = 1\end{cases} \qquad (2.17)
\end{aligned}$$

which is shown to be

$$\phi(x) = \frac{\int_0^x \Psi(y)dy}{\int_0^1 \Psi(y)dy}, \quad \text{where} \quad \Psi(x) = \exp\left[2\int_0^x \frac{A(x')}{B(x')}dx'\right]. \qquad (2.18)$$

The unconditional mean fixation time $T(x)$ is the solution to the equation

$$\begin{aligned}
&A(x)\frac{d}{dt}T(x) + \frac{1}{2}B(x)\frac{d^2}{dx^2}T(x) = -1, \\
&\text{with boundary condition: } \quad T(0) = T(1) = 0. \qquad (2.19)
\end{aligned}$$

There is a closed solution to this equation however when both the boundaries are absorbing the given expression is singular. In practice this equation is solved numerically.

2.1.2 The Birth-Death Process

The above formulation is applicable to systems with fixed population size, however I will chiefly be interested in modelling competition in populations with variable population size as a birth-death process, in which births and death events that increase/decrease the total population size by 1 individual occur separately, with different rates. As before, N_i is the number of species i and the events and probabilities are defined as follows:

$$N_i \xrightarrow{T_i^+} N_i + 1 \quad \text{and} \quad N_i \xrightarrow{T_i^-} N_i - 1, \quad \text{with} \quad i \in \{1, ..., M\}$$
$$\text{where} \quad T_i^+ = g(\vec{N}) f_i(\vec{N}) N_i / \bar{f}, \quad T_i^- = d(\vec{N}) \omega_i(\vec{N}) N_i / \bar{\omega}, \tag{2.20}$$
$$\bar{f} = \sum_{i=1}^{M} N_i f_i \quad \text{and} \quad \bar{\omega} = \sum_{i=1}^{M} N_i \omega_i, \tag{2.21}$$

where, in this thesis $M \in \{2, 3\}$. This is the most general setting, where the biological factors determining the birth and death rates are written as the product of global and relative terms: $g(\vec{N})$ and $d(\vec{N})$ are referred to as the global birth fitness and global weakness respectively and are species-independent acting similarly on all strains, whereas $f_i(\vec{N})$ and $\omega_i(\vec{N})$ are species-dependent relative birth fitness and relative weakness respectively (Cremer *et al.* (2011); Melbinger *et al.* (2010)). Hence, g and f_i affect the species birth rates, while d and ω_i affect their survival or viability. Various evolutionary scenarios have been investigated within this framework (Cremer *et al.* (2011, 2012); Melbinger *et al.* (2010, 2015); West & Mobilia (2020); Wienand *et al.* (2017, 2018)).

In this thesis the relative birth fitness ('fitness'), f_i, will depend on the population composition via the payoff matrix (which will be defined in the relevant subsequent Chapters) but not the environment, while the global fitness will generally be assumed to be constant (*i.e.* $g(\vec{N}) = 1$) apart from in Section 3.4 where we model a public good game by supposing that it depends linearly on the density of one of the species. Additionally, I will assume that all strains have equal survival

chances and are subject to logistic growth, hence $\omega_i = 1\ \forall i$ and $d(\vec{N}) = N/K$, where K is the carrying capacity of the system and $N = \sum_{i=1}^{M} N_i$ is the total population size. In Chapters 3 and 5 we will assume that K varies in time so the population size will fluctuate not only due to the natural demographic noise in the birth-death formulation, but also due to the carrying capacity changing in time. For now, we assume it is constant.

In general, even when there are only two species, it is not possible to find expressions like (2.18) and (2.19) for the fixation probability and mean fixation time. This is because the Master equation is multivariate, and approximation methods (van Kampen's system size expansion also known as the diffusion approximation) lead to equations that are themselves multidimensional and difficult or impossible to solve. However it is possible to find mean field equations for the total population size and population densities which we will use later on. The Master equation for N can be written as:

$$\frac{\partial}{\partial t}P(\vec{N},t) = \sum_{i=1}^{M}\left[\left(\mathbb{E}_{N_i}^{-}-1\right)T_i^{+} + \left(\mathbb{E}_{N_i}^{+}-1\right)T_i^{-}\right]P(\vec{N},t), \tag{2.22}$$

from which a similar calculation to (2.12) gives the mean field equation for N:

$$\frac{\partial}{\partial t}\langle N\rangle = \sum_{i=1}^{M}\left[\langle T_i^{+}\rangle - \langle T_i^{-}\rangle\right] \approx \langle N\rangle\left(\langle \overline{h}(\vec{N})\rangle - \frac{\langle N\rangle}{K}\right), \tag{2.23}$$

where $\langle \overline{h}(\vec{N})\rangle = \sum_{i=1}^{M}\langle h_i(\vec{N})\rangle\langle N_i\rangle/\langle N\rangle$ and $h_i(\vec{N}) = g(\vec{N})f_i(\vec{N})/\bar{f}$. To derive the mean field equations for the population densities x_i we first write the master equation for $\vec{N}$:

$$\frac{\partial}{\partial t}P(\vec{N},t) = \sum_{i=1}^{M}(\mathbb{E}_{N_i}^{-}-1)\left[T_i^{+}P(\vec{N},t)\right] + \sum_{i=1}^{M}(\mathbb{E}_{N_i}^{+}-1)\left[T_i^{-}P(\vec{N},t)\right]. \tag{2.24}$$

Now we find the differential equation for $\langle x_i\rangle = \sum_{\vec{N}}(N_i/N)P(\vec{N},t)$, paying at-

tention to the fact that now both N_i and N vary in time:

$$\begin{aligned}
\frac{\partial}{\partial t}\langle x_i\rangle &= \sum_{\vec{N}} \frac{N_i}{K}\frac{\partial}{\partial t}P(N,t) \\
&= \sum_{\vec{N}} \frac{N_i}{N}\Big\{T_i^+(\vec{N}-\vec{e}_i)P(\vec{N}-\vec{e}_i,t) + T_i^-(\vec{N}+\vec{e}_i)P(\vec{N}+\vec{e}_i,t) \\
&- \left(T_i^+(\vec{N}) + T_i^-(\vec{N})\right)P(\vec{N},t)\Big\} \\
&+ \sum_{j\in\{1,\ldots,M\}\neq i,\vec{N}} \frac{N_i}{N}\Big\{T_j^+(\vec{N}-\vec{e}_j)P(\vec{N}-\vec{e}_j,t) + T_j^-(\vec{N}+\vec{e}_j)P(\vec{N}+\vec{e}_j,t)\Big\} \\
&- \sum_{j\in\{1,\ldots,M\}\neq i,\vec{N}} \frac{N_i}{N}\left(T_j^+(\vec{N}) + T_j^-(\vec{N})\right)P(\vec{N},t) \\
&= \sum_{\vec{N}} \Big\{\frac{N_i+1}{N+1}T_i^+(\vec{N})P(\vec{N},t) + \frac{N_i-1}{N-1}T_i^-(\vec{N})P(\vec{N},t) \\
&- \frac{N_i}{N}\left(T_i^+(\vec{N}) + T_i^-(\vec{N})\right)P(\vec{N},t)\Big\} \\
&+ \sum_{j\in\{1,\ldots,M\}\neq i,\vec{N}} \Big\{\frac{N_i}{N+1}T_j^+(\vec{N})P(\vec{N},t) + \frac{N_i}{N-1}T_j^-(\vec{N})P(\vec{N},t) \\
&- \frac{N_i}{N}\left(T_j^+(\vec{N}) + T_j^-(\vec{N})\right)P(\vec{N},t)\Big\}. \qquad (2.25)
\end{aligned}$$

Rearranging the right hand side we have:

$$\begin{aligned}
\frac{\partial}{\partial t}\langle x_i\rangle &= \left\langle \left(\frac{N_i+1}{N+1} - \frac{N_i}{N}\right)T_i^+(\vec{N})\right\rangle + \left\langle \left(\frac{N_i-1}{N-1} - \frac{N_i}{N}\right)T_i^-(\vec{N})\right\rangle \\
&+ \sum_{j\in\{1,\ldots,M\}\neq i,\vec{N}} \left\{\left\langle \left(\frac{N_i}{N+1} - \frac{N_i}{N}\right)T_j^+(\vec{N})\right\rangle + \left\langle \left(\frac{N_i}{N-1} - \frac{N_i}{N}\right)T_j^-(\vec{N})\right\rangle\right\} \\
&= \left\langle \frac{T_i^+(\vec{N}) - T_i^-(\vec{N})}{N}\left(1 + \mathcal{O}\left(\frac{1}{N}\right)\right)\right\rangle \\
&- \left\langle \frac{x_i}{N}\left(1 + \mathcal{O}\left(\frac{1}{N}\right)\right)\sum_{j=1}^{M}\left(T_j^+(\vec{N}) - T_j^-(\vec{N})\right)\right\rangle \\
&\approx \frac{\langle T_i^+(\vec{N})\rangle - \langle T_i^-(\vec{N})\rangle}{\langle N\rangle} - \frac{\langle x_i\rangle}{\langle N\rangle}\frac{\partial\langle N\rangle}{\partial t}, \qquad (2.26)
\end{aligned}$$

where we make the same assumptions as for (2.12) for the factorisation in the last line, and that N is large enough for the $\mathcal{O}\left(\frac{1}{N}\right)$ terms to be ignored. This

equation is similar to (2.12), where the second additional term on the right hand side accounts for the fact that the total population size also varies in time.

When we are investigating the effect of a variable carrying capacity in Chapters 3 and 5 we will principally be interested in the effect of external noise on the fixation probability for each species. Even in the case without external noise, it is not possible to find formula for $\phi(x)$ and $T(x)$ directly. However, progress can be made by approximating the birth-death process defined above as a Moran process (with fixed $N = K$), with transition rates $W_{ji} = T_i^+ T_j^- / K$. We are then in a position to use the results of Section 2.1.1 to find $\phi(x)$ and $T(x)$ for $N = K$. The fixation probability and mean fixation time under the influence of external noise are then found by weighting this over the relevant probability distribution for N. We will now discuss the effect of dichotomous Markov noise on the probability distribution for N in the logistic birth death equation. This form of external noise will be the focus of this thesis, but it should be noted that other forms of noise are relevant. In Chapter 3 we will compare the results with periodic noise, for which the effect on the probability distribution for N can be found in Section 3.3.2. I also have some preliminary work on Ornstein-Uhlenbeck noise, details of which can be found in Appendix A.2.

2.2 Dichotomous Noise and the Logistic Birth-Death Process

In this section I will present the results of a randomly switching carrying capacity on logistic growth. This will underpin much the later work, in which the total population size follows this process. We will start with a logistic birth death process, defined by (2.20) with number of species $M = 1$, $f, g, \omega = 1$ and $d = N/K$ (where the subscript 1 has been dropped because we have only one species). In the case without external noise, i.e. $K(t) = K$, this gives the following Master equation for N:

$$\frac{dP_K(N)}{dt} = (N-1)P_K(N-1) + \frac{(N+1)^2}{K} P_K(N+1) - \left(N + \frac{N^2}{K}\right) P_K(N), \quad (2.27)$$

from which it is possible to find a recursion relation equation for the stationary probability distribution of N, $P_K(N)$, by setting (2.27) equal to zero and imposing a reflecting boundary at $N = 1$. This assumes that the probability flux to the extinction state is negligibly small, justified by the fact that it takes a time of order e^K to reach this (Assaf & Meerson (2010); Assaf *et al.* (2008); Doering *et al.* (2005); Méndez *et al.* (2015)). In the stochastic setting, $N = 0$ (extinction) is the only absorbing state, but since the expected time to reach it is much larger than the timescale of fixation (i.e. all but one species dying out), we can ignore this. The normalised solution is:

$$P_K(N) \approx \frac{K^{N+1}e^{-K}}{(N+1)!} \tag{2.28}$$

which we see from inset of Fig. 2.1 agrees very well with simulation results.

Considering the mean field equation, and writing $\langle h(N)\rangle \to h(N)$ (for general h) we have:

$$\frac{dN}{dt} = N\left(1 - \frac{N}{K}\right). \tag{2.29}$$

Hence in the deterministic setting, (2.29) predicts that the N will initially grow/decline exponentially if $N(0) < K$ (resp. $N(0) > K$), reaching the stationary state $N = K$ in time $t \sim \mathcal{O}(1)$. However, given that the process is stochastic, in reality after the 'exponential phase' of growth/decline, $N(t)$ will not be constant but fluctuate around K with fluctuations scaling with $\sqrt{K}$. In this case, the probability distribution of N relaxes to (2.28) on a timescale $\mathcal{O}(1)$(see Fig. 2.1).

A natural way that fluctuating environmental conditions (*e.g.* moisture, sunlight, temperature, pH/nutrient/toxin level *etc*) might affect a population is by changing the maximum supportable population size, here modelled by the carrying capacity K. Thus we let the carrying capacity vary in time, focusing on the case where it switches randomly between two values. As K changes, the intensity of the fluctuations changes, coupling the external (environmental) variability (noise) with the demographic (internal) fluctuations (noise). As we will see in later chapters, this has a significant effect on the outcome of two and three species competition models, for now we will concentrate on single species models, and investigate the effects on the probability distribution of N.

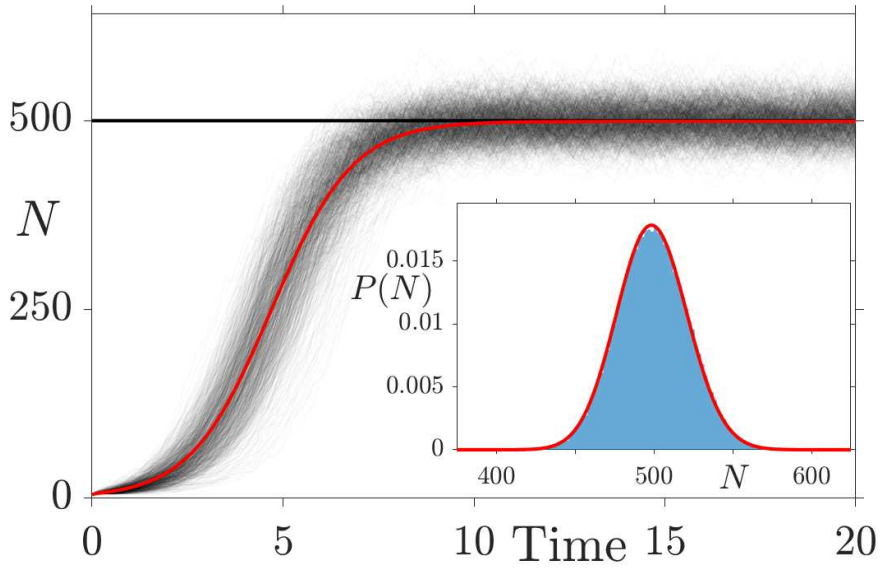

Figure 2.1: Logistic growth in a fixed environment with $K = 500$. Grey lines are 10^3 individual realisations of the stochastic process, the red line is the average of these. We see that $N \to K$ in a time $t = \mathcal{O}(1)$. Inset: Histogram of the numerical distribution from 10^5 realisations, red line is the prediction from (2.28) which we see agrees with simulations almost perfectly.

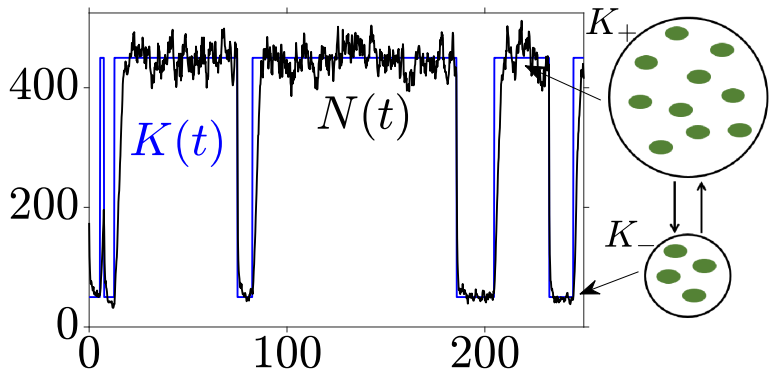

Figure 2.2: Asymmetric dichotomous noise switching between $K = K_+$ and $K = K_-$, spending on average $\nu_\pm^{-1}$ in either state (blue), along with a typical realisation of N (black) vs time. Parameters: $(K_0, \nu, \gamma, \delta) = (250, 0.03, 0.8, 0.6)$. After a switch the total population size is of order $K_\pm$ in a time of order 1, fluctuating around the carrying capacity until another switch occurs. Strength of relative fluctuations is greater for smaller population sizes.

2.2.1 Dichotomous Markov Noise

The primary form of external noise this thesis will consider is dichotomous Markov noise (DMN). This form of noise received a lot of attention in the 1980s, and since then its effects on single variable deterministic and stochastic systems have been thoroughly studied (see, for example Balakrishnan (1993, 2003); Balakrishnan & Van den Broeck (2001); Balakrishnan *et al.* (2001); Bena (2006); Bena *et al.* (2002, 2003); Bressloff (2017); Bressloff & Lawley (2017); Doering & Horsthemke (1985); Hänggi & Jung (1995); Horsthemke & Lefever (1984); Masoliver *et al.* (1986a,b); Rodriguez & Pesquera (1986); Sancho (1984); Sancho & Miguel (1983); Sancho & San Miguel (1984); Sancho (1985); Schmid *et al.* (1999); Van Den Broeck (1983); Van den Broeck & Hänggi (1984)). In this model the carrying capacity switches between a high (K_+) and low (K_-) value corresponding to abundant or scarce resources respectively. In this way, the external noise mimics population bottlenecks: a large proportion of the community dies due to an environmental disturbance and then is repopulated from the small amount of survivors. Since demographic noise is more important in small population sizes, this can lead to very different behaviour in multispecies systems when compared to the case without external noise. Furthermore, DMN has a finite non-zero correlation time (unlike white noise), is straightforward to implement numerically and is sufficiently simple that it is possible to derive analytical results in some cases (Bena (2006); Ridolfi *et al.* (2011)). An example is shown in Fig. 2.2, where the carrying capacity switches between $K_+ = 450$ and $K_- = 50$, spending more time on average in K_+. We write:

$$K(t) = K_0(1 + \gamma\xi(t)), \quad \text{where} \quad K_0 = \frac{K_+ + K_-}{2} \quad \text{and} \quad \gamma = \frac{K_+ - K_-}{K_+ + K_-} \tag{2.30}$$

and $\xi(t)$ is a random variable taking the values ± 1, defined by the rate equations:

$$\xi = +1 \xrightarrow{\nu_+} \xi = -1 \quad \text{and} \quad \xi = -1 \xrightarrow{\nu_-} \xi = +1. \tag{2.31}$$

Defining the mean of the switching rates $\nu = (\nu_+ + \nu_-)/2$, we write $\nu_\pm = (1 \mp \delta)\nu$ where $\delta = (\nu_- - \nu_+)/(\nu_- + \nu_+)$ is the mean of ξ (see (2.32). This is a form of *coloured* noise, with autocorrelation function $\langle\xi(t)\xi(t')\rangle - \langle\xi(t)\rangle\langle\xi(t')\rangle = (1 - \delta^2)\mathrm{e}^{-2\nu|t-t'|}$ (Bena (2006)) (where $\langle\cdot\rangle$ denotes the ensemble average). From these

it is straight forward to calculate the mean and variance of $K(t)$ as $(1+\delta\gamma)K_0$ and $(\gamma K_0)^2(1-\delta)^2$. In this context, $0 \leq \gamma < 1$ can be thought of as the intensity of the noise: larger values of γ correspond to greater intensity, and $\gamma = 0$ corresponds to the case without external noise with $K(t) = K_0\ \forall t$. The parameter $-1 < \delta < 1$ relates to the asymmetry of the switching rates: when it is zero ξ spends the same amount of average time at $K_\pm$, negative (positive) values mean more time is spent on average at K_- (K_+).

There are two regimes that are particularly relevant: firstly in the slow switching case, $\nu_\pm \ll 1$, we observe that there is a very long time between environmental changes and the population size rapidly approaches $K_\pm$ (depending on ξ), around which it fluctuates for an average time of $\nu_\pm^{-1}$ until the next switch occurs. The population size then approaches the new carrying capacity $K_\mp$ and the process continues indefinitely. In this case we expect (and will show later on) the probability density of N to be peaked around $K_\pm$ (see Fig. 3.4(a)).

However when we consider the fast switching case ($\nu_\pm \gg 1$), the environment switches very rapidly compared to the species reactions. Here the external noise self averages:

$$\langle \xi(t) \rangle = \sum_{\xi'} \xi' P(\xi = \xi') = \frac{\nu_+^{-1} - \nu_-^{-1}}{\nu_+^{-1} + \nu_-^{-1}} = \frac{\nu_- - \nu_+}{\nu_- + \nu_+} = \delta. \tag{2.32}$$

Where $P(\xi = \xi')$ means the probability that ξ takes value ξ'. Here I have omitted the dependence on t because I always consider a stationary process. If the process is non-stationary and starts with $\xi = -1$ with probability p then using Horsthemke & Lefever (1984) we can write $\langle \xi(t) \rangle = \delta + (1 - \delta - 2p)e^{-2\nu t}$. Now, using (2.23), we can write the mean field equation for the average population size $\langle N \rangle$, replacing $\langle \xi \rangle$ with its average δ:

$$\begin{aligned}
\frac{d}{dt}\langle N \rangle &\approx \langle T^+ \rangle - \langle T^- \rangle = \langle N \rangle \left(1 - \left\langle \frac{N}{K_0(1+\gamma\xi(t))} \right\rangle \right) \\
&= \langle N \rangle \left(1 - \left\langle \frac{N(1-\gamma\xi(t))}{K_0(1-\gamma^2)} \right\rangle \right) = \langle N \rangle \left(1 - \frac{\langle N \rangle}{K_0(1-\gamma^2)} \left(1 - \gamma\langle \xi(t) \rangle\right) \right) \\
&\approx \langle N \rangle \left(1 - \frac{\langle N \rangle}{K_0\,(1-\gamma^2)} (1 - \delta\gamma) \right),
\end{aligned} \tag{2.33}$$

where the equality in the second line comes from the fact that $(\xi(t))^2 = 1\ \forall t$. Thus when the environmental switching is very rapid we expect to see a probability

distribution peaked around $\mathcal{K}_\delta = K_0(1-\gamma^2)/(1-\delta\gamma)$. For this result to apply, in addition to ν being very large we also need K_0 to be sufficiently large that demographic fluctuations can be ignored.

The differences between fast and slow regimes illustrate a nice feature of dichotomous external noise: the presence of a phase transition in the probability density of population size (from now on $\rho_{\nu,\delta}(N)$) between bimodal and unimodal, at some intermediate value of ν. In fact it is possible to find a lowest order approximation of $\rho_{\nu,\delta}(N)$, as I will now show, by treating the process as a piecewise-deterministic Markov process, i.e. ignoring all demographic noise and considering only the effect of environmental switching. This is defined by the Master equation (dropping the dependence on t for notational convenience), where N is treated as a continuous deterministic process (note that the Master equation for the full stochastic process will be defined in the relevant sections):

$$\begin{aligned}\frac{dP(N,\xi)}{dt} &= -\frac{d}{dN}\left[N\left(1-\frac{N}{K_0(1+\xi\gamma)}\right)P(N,\xi)\right] \\ &+ \nu\,(1+\xi\delta)\,P(N,-\xi) - \nu\,(1-\xi\delta)\,P(N,\xi),\end{aligned} \tag{2.34}$$

where the first line accounts for the deterministic dynamics, $N \to K_\pm$ depending on the value of ξ, and the second term accounts for the environmental switching. Following the method of Horsthemke & Lefever (1984), we then define the unconditional probability density (i.e. independent of the environmental variable) for the population size $p(N) = P(N,1) + P(N,-1)$, and a complementary function $q(N) = \nu_+ P(N,1) - \nu_- P(N,-1)$, so that we may write the simultaneous equations:

$$\begin{aligned}\frac{dp(N)}{dt} &= -\frac{d}{dN}\left[N\left(1-\frac{N(1-\gamma\delta)}{K_0(1-\gamma^2)}\right)p(N)\right] \\ &- \frac{1}{\nu}\frac{d}{dN}\left[\frac{\gamma N^2}{K_0\,(1-\gamma^2)}q(N)\right], \quad \text{and}\end{aligned} \tag{2.35}$$

$$\begin{aligned}\frac{dq(N)}{dt} &= -\left(\frac{d}{dN}\left[N\left(1-\frac{N(1+\gamma\delta)}{K_0(1-\gamma^2)}\right)\right]+2\nu\right)q(N) \\ &- \left(1-\delta^2\right)\nu\frac{d}{dN}\left[\frac{\gamma N^2}{K_0\,(1-\gamma^2)}p(N)\right].\end{aligned} \tag{2.36}$$

The stationary distributions (p_s and q_s) are then found by setting both of these to 0. The first of these and the fact that - in this deterministic setting - we have

$K_- < N(t) < K_+ \ \forall t$, implies that

$$q_s(N) = -\frac{\nu}{\gamma N}\left(K_0(1-\gamma^2) - N(1-\delta\gamma)\right) p_s(N), \tag{2.37}$$

which can be differentiated and substituted into (2.36) to give the differential equation for $p_s(N)$:

$$\begin{aligned}\frac{dp_s(N)}{dN} &= \Bigg\{ -2\nu \frac{K_0\left[K_0\left(1-\gamma^2\right) - N\left(1-\delta\gamma\right)\right]}{N^2\left[K_0\left(1-\gamma\right) - N\right]\left[K_0\left(1+\gamma\right) - N\right]} \\ &- \frac{d\ln}{dN}\left[\frac{\left(K_0\left(1+\gamma\right) - N\right)\left(K_0(1-\gamma) - N\right)}{\gamma K_0}\right]\Bigg\} p_s(N). \end{aligned} \tag{2.38}$$

This can be integrated to find the unconditional lowest order approximation of the probability density for N, defined within $[K_-, K_+]$ from here on denoted $\rho^{\mathrm{PDMP}}_{\nu,\delta}(N)$:

$$\rho^{\mathrm{PDMP}}_{\nu,\delta}(N) = \frac{\mathcal{Z}_{\nu,\delta}}{N^2}\left[\frac{K_+}{N} - 1\right]^{\nu_+ - 1}\left[1 - \frac{K_-}{N}\right]^{\nu_- - 1}, \tag{2.39}$$

where $\mathcal{Z}_{\nu,\delta}$ is a normalisation constant. This equation predicts peaks in the probability distribution in different places depending on the parameters ν, δ and γ. For a full description see Appendix A.1.1, but if we briefly consider the simpler symmetric case, $\delta = 0$ we see in Fig. 2.3 major differences in the probability distribution of N, $\rho_{\nu,0}(N)$, depending on the switching rate, ν, that are captured well by this approximation $\rho^{\mathrm{PDMP}}_{\nu,0}(N)$: in the slow switching regime $\nu \ll 1$ (2.39) predicts peaks around $K_\pm$ while in the fast switching regime $\nu \gg 1$ it predicts a single peak around $\mathcal{K}_\delta$. Hence this lowest order theory (in K_0^{-1} - equation (2.34) from which (2.39) is derived is a result of expanding the master equation in K_0^{-1} and ignoring terms of order $\mathcal{O}(K_0^{-1})$) captures the position of the peaks of $\rho_{\nu,\delta}(N)$ well, and as we will see is sufficient for most of our needs in Chapters 3 and 5. However, since this approximation necessarily ignores internal fluctuations it fails to capture the width of the peaks and the 'leakage' of probability outside $[K_-, K_+]$. The next order approximation can be found by performing a linear noise approximation (LNA) around the conditional PDMP (i.e. the PDMP given that $\xi = \pm 1$), where one assumes that the fluctuations around the PDMP process for each value of N are Gaussian with mean and variance found to be 0

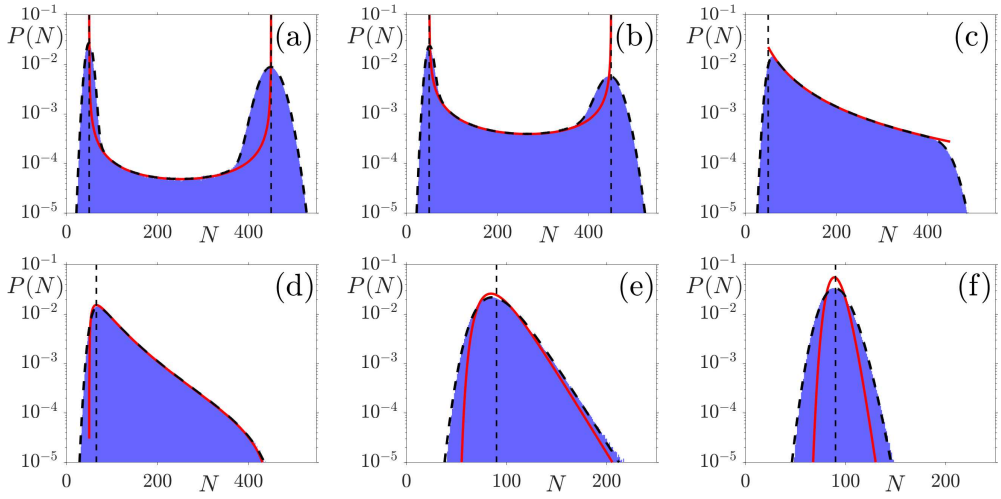

Figure 2.3: N-QSD histogram (blue), $p^{\mathrm{PDMP}}_{\nu,\delta}(N)$ (red) and linear noise approximation (black, dashed) for (a) $\nu = 0.01$, (b) $\nu = 0.1$, (c) $\nu = 1$, (d) $\nu = 2$, (e) $\nu = 10$, (f) $\nu = 50$. Parameters are $(K_+, K_-) = (450, 50)$. Blue shaded areas are histograms from simulations, Solid lines are PDMP predictions from (2.39) and black dashed lines are predictions from LNA (A.5). Vertical lines indicate $N = K_\pm$ in (a,b), $N = N^*$ in (c,d), and $N = \mathcal{K}_\delta$ in (d,e). We see the presence of a noise induced transition in the N-QSD from bimodal to unimodal as from small to large ν, which is well predicted by the PDMP. The LNA captures the width around the peaks for large and small ν, and the leakage of probability outside the support of (2.39) for small ν.

and N respectively, and that the strength of the fluctuations is the same in each environmental state (see A.1.2 for details). This is shown by the black dashed lines in Fig. 2.3, where we see that this is a much better approximation of the full N-QSD, particularly in the very slow and very fast switching regimes.

Chapter 3

Two Species Competition with Variable Carrying Capacity

3.1 Review of Previous work

This Chapter will investigate the coupled effect of internal and external noise on a two-species competition model, where one species has a fitness advantage over the other. First of all I shall review some other relevant work, for context.

One area where the relevance of environmental noise is most obvious is in the evolution of bacterial bet-hedging strategies. This is a survival strategy whereby an organism spreads risks to increase long-term fitness in a fluctuating environment, and other examples are seed banks of annual plants (Cohen (1966)), polyandry in animal mating systems (Yasui (2001)) and foraging behaviour in bumble bees (Burns & Dyer (2008)). It has been observed that, due to stochastic gene expression, bacteria can switch between two phenotypes: one that has a faster growth rate but is highly susceptible to environmental changes, and the other which sacrifices its metabolic growth rate to produce structures that help it survive more stressed environmental conditions (Avery (2006); Casadesús & Low (2006); Dubnau & Losick (2006); Kaern *et al.* (2005); Kaufmann & van Oudenaarden (2007); Kussell & Leibler (2005); Kussell *et al.* (2005); Lachmann & Jablonka (1996); Maheshri & OShea (2007); Paulsson (2004); Samoilov *et al.* (2006); Thattai & Van Oudenaarden (2004); Wolf *et al.* (2005)). Hence there is a trade off between reaching a larger population size in unstressed conditions,

and not dying out when the environment is more adverse (for example due to the presence of an antibiotic). In Hufton *et al.* (2018) they find that for both periodic and random environmental switching, for small and intermediate switching rates there are non-trivial phenotypic-switching rates that maximise the average group growth rate, indicating that heterogeneity (*i.e.* the presence of both phenotypes over time) has a fitness advantage. For fast environmental switching, homogeneity (*i.e.* only one phenotype present) is favoured. Furthermore, they find that the stochastic environment always leads to a higher group growth rate than the equivalent periodic environment. Many other examples have been investigated, both experimentally and theoretically (see, for example Acar *et al.* (2008) and references above). While the details may change, the uniting feature is that the switching rate between phenotypes that confers the greatest benefit, whether through maximising growth rate, protecting best against extinction *etc.* is highly dependent on the rate of environmental switching, rather than intrinsic difference in birth/death rates of the strains in the different conditions, or whether the switching is periodic or random. That being said, populations can generally maintain higher fitnesses in stochastic environments compared to periodic ones (Hufton *et al.* (2018); Thattai & Van Oudenaarden (2004)). This emphasizes the importance of incorporating stochastic and/or periodic environmental variability into models, as it is its presence here that leads to the diversity in phenotypic expression. This is what we observe in the real world, and would not be seen in the these models if the environment was constant.

Another way to model environmental stress is in terms of catastrophes: in Visco *et al.* (2010) the authors analyse the effect of this on a deterministic two species bet-hedging model. Catastrophes occur randomly but dependent on the population composition, reducing the number of faster growing species to a new value with a given probability, leaving the slower growing species unharmed. Here it is again found that bet-hedging is an evolutionary strategy that may be able to mitigate the affect of adverse catastrophes. This is closely related to another mechanism in nature that is thought to promote co-operative behaviour: population bottlenecks. These occur when a large proportion of the population die out, and the small number of remaining survivors then repopulate it (Brockhurst (2007); Brockhurst *et al.* (2007); Wahl *et al.* (2002)). The results of these

models suggest that intermediate disturbance rates promote cooperative species the most, and within this regime cooperation will be further promoted by larger disturbances.

In the context of evolutionary games, much of the previous work has focused on either fluctuating selection between individuals, or on fluctuations that affect the structure of the game. In Ashcroft *et al.* (2014) a model was investigated in which the payoff matrix switches randomly between a coexistence (stable interior fixed point, unstable fixed points on boundaries) and co-ordination (unstable interior fixed point, stable fixed points on boundaries) game, according to a dichotomous Markov process. Here, the fixation probability of a single individual that is selectively disadvantaged in the co-ordination game is increased in the presence of noise with respect to a fixed environment. This increase of the fixation probability of a selectively disadvantaged individual (with respect to a constant environment) was also found in Assaf *et al.* (2013a), where the authors analyse the effect of fluctuating selection as an Ornstein-Uhlenbeck process (see Appendix A.2) on the outcome of the Prisoner's Dilemma. Not only did they find that the fixation probability was increased compared to the static environment, they also find that the functional dependence of the fixation probability on the population size was changed when the variance of the noise was large. In Hidalgo *et al.* (2017) where selection fluctuates but is neutral overall on average, they found that external noise can lead to a marked increase in the time taken for a species to fixate the population, with a super-linear dependence on the population size for fast switching environments. Clearly, environmental noise can have a drastic effect on evolutionary games, affecting not only which species is most likely to fixate the population, but also the time that it takes for this to happen.

The most relevant work for this thesis is that of Wienand *et al.* (2017, 2018), in which they examine the effects of symmetric dichotomous noise on two species of bacteria that compete according to the Prisoner's Dilemma. In contrast to the examples in the last paragraph, the external noise affects the death rates through the carrying capacity, and the total population size fluctuates due this and the internal noise stemming from birth and death processes. They find that in the case of pure resource competition, where the species are identical apart from one having a slower per capita growth rate, survival of the slow growing species is

favoured either by a slow or fast switching environment, according the size of the growth rate difference (selection strength, s), compared to a critical strength s_c. In the public good scenario, the slower growing species sacrifices its own reproductive rate to increase the global growth rate, coupling the evolution of the total population size with the composition. Here the authors use an 'effective theory' to find that although the survival probability of the slower growing species is exponentially reduced, it may still be beneficial to produce the public good due to the large payoff when producers fixate.

This Chapter extends their work in two important ways: Using the same basic model, we consider asymmetric dichotomous external noise. Here the environment spends on average unequal amounts of time in each state. We find that this can produce a non-monotonic dependence on the switching rate, when the noise asymmetry and intensity are large enough. This non-monotonic dependence is also observed for the noise intensity when the DMN process spends more time on average at $\xi = 1$ (*i.e.* $\delta > 0$), but the dependence on δ and s is always monotonically decreasing, as one would expect. Secondly, we compare the effects with asymmetric periodic noise that has the same mean and variance when averaged over the period of variation, and in general find that this produces a sharper transition between switching regimes. In both cases we are able to find a lowest order (in K_0^{-1}) theory that qualitatively describes the dependence of the fixation probability of the slow-growing species on the selection strength, noise intensity and noise asymmetry. In the public good case we are also able to use an 'effective theory' to qualitative describe the effect on the fixation probability of producers, which is shown to have a similar qualitative behaviour as the pure resource competition case.

3.2 The Model

This model of species competition is inspired by the the Prisoner's Dilemma, a prototypical model in Game Theory, defined by the payoff matrix

$$\mathcal{P} = \begin{array}{c|cc} \text{Strategy} & S & F \\ \hline S & 1-s & 0 \\ F & 1 & 0 \end{array}$$

where S and F refer to slow growing 'co-operators' and faster growing 'defectors'. This payoff matrix says that when two S individuals meet, they share the available resources, taking a payoff of $1-s$, where $s \ll 1$. When a defector and co-operator meet the defector steals all the resources for themselves, receiving a payoff of 1, while the co-operator gets nothing. When two defectors meet, they both try to steal the resources for themselves. This is unsuccessful and they both receive nothing. This is the simplest version of a 'social dilemma': The best strategy for any individual is to defect, as this has the higher individual payoff. However the total payoff recieved when both cooperate is $2-2s$, greater than the total payoff when one defects and the other co-operates as long as $s < 1/2$. Thus, the best strategy for the community (everyone co-operating) is not the same as that for individuals.

We suppose that at time t there are $N(t) = N_S(t) + N_F(t)$ individuals, where S and F correspond to slow growing as fast growing strains respectively. These have per-capita fitness $f_S = (1-s)/\bar{f}$ and $f_F = 1/\bar{f}$, where $0 < s \ll 1$, $\bar{f} = (N_F + (1-s)N_S)/N = 1 - sx$ is the average population fitness and $x = N_S/N$. The rescaling of the species fitnesses $f_{S,F}$ by the population average fitness is to ensure that the total population size is independent of the population composition in the pure resource competition case. This average fitness is a function of x, however the location of the fixed points and their stability is unchanged by this (Bladon *et al.* (2010)). Furthermore, we suppose that the slower growing strain provides a public good to the system, increasing the global growth rate by a factor of $g(x) = 1 + bx$. The population size and composition naturally fluctuates due to the birth-death processes:

$$N_i \xrightarrow{T_i^+} N_i + 1, \quad N_i \xrightarrow{T_i^-} N_i - 1, \quad i \in \{S, F\}, \tag{3.1}$$

where $T_i^+ = g(x) f_i N_i$ is the and $T_i^- = N_i N/K(t)$. Thus the species-dependent relative weakness defined in (2.20) is $\omega_i = 1$ for both strains. From the expressions for the birth rates, we see that they differ only in the f_i. This is larger for the F strain, hence why this is called the 'fast' growing species. Environmental noise is modelled by letting the carrying capacity, $K(t)$, vary in time according to an asymmetric dichotomous Markov noise process, defined by (2.30) and (2.31)

(repeated below):

$$K(t) = K_0(1 + \gamma\xi(t)), \quad \text{where} \quad K_0 = \frac{K_+ + K_-}{2} \quad \text{and} \quad \gamma = \frac{K_+ - K_-}{K_+ + K_-}. \tag{3.2}$$

K_0 is the average of the two carrying capacities, γ measures the intensity of the environmental noise and $\xi(t)$ is a random variable taking the values ± 1, defined by the rate equations:

$$\xi = +1 \xrightarrow{\nu_+} \xi = -1 \quad \text{and} \quad \xi = -1 \xrightarrow{\nu_-} \xi = +1. \tag{3.3}$$

The mean of the switching rates is $\nu = (\nu_+ + \nu_-)/2$, and we write $\nu_\pm = (1 \mp \delta)\nu$ where $\delta = (\nu_- - \nu_+)/(\nu_- + \nu_+)$ is the mean of ξ. Hence δ is a measure of the asymmetry of the switching: when $\delta > 0$ the process spends more time on average at K_+, when $\delta < 0$ more time is spent at K_- and when it is zero it spends the same average time in both states. Of course, environmental noise could also affect the birth rates through f_i for example with selection strength changing with the environment according to $s(t) = s_0 + \gamma_s\xi(t)$ where $s_0 \geq 0$ and $\gamma_s > 0$. This would be particularly interesting in the case where $s_0 = 0$ or $\gamma_s > s_0$, since then different strains would be favoured in each environment. This would model the effect of bacteriostatic antimicrobials, which stop cells from reproducing (Marrec & Bitbol (2020)). Another possibility would be to let the species-dependent weakness, ω_i, vary with the environment, which would model the presence bactericidal antimicrobials that induce cell death (Coates *et al.* (2018); Marrec & Bitbol (2020)). These are not studied here, but when combined with and environmentally dependent carrying capacity would be interesting avenues of future research.

Using the results of Section 2.1.2, when all forms of noise are ignored the mean field equations for the average values of N and x can be written as (dropping the $\langle\cdot\rangle$ notation):

$$\frac{d}{dt}N = N\left(g(x) - \frac{N}{K_0}\right) \tag{3.4}$$

$$\frac{d}{dt}x = -g(x)s\frac{x(1-x)}{1-sx}, \tag{3.5}$$

with initial population size N_0 and initial fraction of cooperators x_0. In this deterministic setting N asymptotically approaches K_0, and is of order K_0 in a

time $t \sim \mathcal{O}(1)$, while x decays asymptotically to zero on a timescale $t \sim \mathcal{O}(s^{-1})$. This is not the same when demographic fluctuations are taken into account: The population composition, x, fluctuates in time, and is then fixed once one of the absorbing boundaries $x = 0$ or $x = 1$ is hit. If $x = 1$ then the slow growing species has *fixated* the population, while if $x = 0$ then the fast growing species is the one that has fixated the population. After this, the total population size still fluctuates (due to the birth-death events) around K_0 if the fast growing species fixates (since $g(0) = 0$), while if the slow growing species fixates it fluctuates around $(1+b)K_0$ (since $g(1) = 1+b$). This is in stark contrast to the deterministic mean field equations and is the focus of the chapter: how does the probability that the slow growing species is the one to fixate the population, (*fixation probability*, ϕ) depend on the selection strength s, public good parameter b, noise intensity γ and the noise asymmetry δ? Further, how do these parameters affect the time it takes for fixation to occur?

In order to answer these questions we first need to know what happens in the case without external noise. The master equation for the full process is (2.22):

$$\frac{\partial}{\partial t}P(\vec{N},t) = \sum_{i=1}^{M}\left[\left(\mathbb{E}_{N_i}^{-}-1\right)T_i^{+} + \left(\mathbb{E}_{N_i}^{+}-1\right)T_i^{-}\right]P(\vec{N},t). \tag{3.6}$$

This is a multivariate process, and as discussed in Section 2.1.2 approximation methods lead to multidimensional equations that are not possible to solve in a way that gives meaningful, interpretable results. To get around this, we use the fact that although the total population size fluctuates in time, it is roughly K_0 after the exponential growing phase (i.e. usually after a transient of order $t \sim \mathcal{O}(1)$). We suppose therefore that births and deaths occur simultaneously, keeping the total population size fixed. A further simplification that we must make to validate this assumption is that $b = 0$, since then the mean field equations are decoupled and $N \to K_0$ regardless of the population composition. Thus we approximate the full process as a Moran Process, defined by:

$$\begin{aligned}[N_S, N_F] &\xrightarrow{W_{FS}} [N_S+1, N_F-1] \quad \text{and} \\ [N_S, N_F] &\xrightarrow{W_{SF}} [N_S-1, N_F+1]\,,\end{aligned} \tag{3.7}$$

$$\text{where} \quad W_{FS} = \frac{T_S^+ T_F^-}{K_0} \quad \text{and} \quad W_{SF} = \frac{T_F^+ T_S^-}{K_0}, \tag{3.8}$$

and use the results from Section 2.1.1: The exact formula for the fixation probability of the slow growing species with an initial fraction of x_0 co-operators in a population of size K_0 is given by (2.8), substituting $\alpha = W_{SF}/W_{FS}$:

$$\phi|_{K_0}(x_0) = \frac{(1-s)^{-x_0 K_0} - 1}{(1-s)^{-K_0} - 1}, \tag{3.9}$$

which is an exponentially decreasing function with K_0 (see Figure 3.1). In the realm of the diffusion approximation, valid when $s \ll K_0^{-1/2} \ll 1$, a simpler formula can be derived from the Backward Kolmogarov equation (2.17), given by (2.18) with $A(x) = -sx(1-x)K_0/\bar{f}$ and $B(x) = (2-s)x(1-x)/\bar{f} \approx 2x(1-x)/\bar{f}$ (i.e. keeping the leading order terms in s):

$$\phi|_{K_0}(x_0) = \frac{\exp\left[-K_0 s(1-x_0)\right] - \exp\left[-K_0 s\right]}{1 - \exp\left[-K_0 s\right]}. \tag{3.10}$$

With these baseline results for $b = 0$ without external noise, in the next section I will show how external noise significantly changes these fixation properties. Then in Section 3.4 I will show how *public good games* ($b > 0$) are affected by external noise.

3.3 Pure Resource Competition, $b = 0$

Here I will show that the fixation probability of the slow growing species ϕ is a non-trivial function of the mean switching rate ν and the switching asymmetry δ. This stems from the effect of the external noise on the population size distribution, $\rho_{\nu,\delta}(N)$, which is characterised by three different regimes: slow ($\nu \ll 1$), fast ($\nu \gg 1$) and intermediate ($1/(1+|\delta|) < \nu < 1/(1-|\delta|)$) switching. First, we need to briefly discuss the quasi-stationary probability distribution for N, the N-QSD (so called because the only absorbing state is $N = 0$, but, as discussed in Section 2.2, the time to reach this scales as e^N. Before this the system spends a long time in this quasi-stationary distribution, and is in effect the distribution while the competition between the two species occurs).

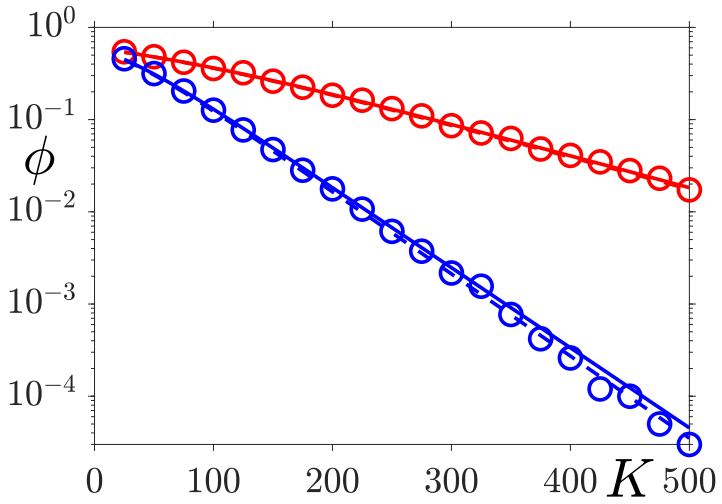

Figure 3.1: Fixation probability, ϕ when K is constant and $x_0 = 0.6$ for $s = 0.02$ (red) and $s = 0.05$ (blue) with logarithmic y-axis. Solid lines are from diffusion approximation (3.10) and dashed lines are from exact solution of the Master equation (3.9). Symbols are results from simulations. In both cases we see that for large K the dependence on K is exponential.

The lowest order approximation $\rho^{\mathrm{PDMP}}_{\nu,\delta}(N)$ can be found using the results of Section 2.2.1 by ignoring internal noise, assuming that the population size is driven only by external noise according to the piecewise-deterministic Markov process (PDMP):

$$\frac{d}{dt}N = N\left(1 - \frac{N}{K_0(1-\gamma^2)}(1-\xi\gamma)\right). \tag{3.11}$$

This is given by equation (2.39) (see Section 2.2.1 for derivation):

$$\rho^{\mathrm{PDMP}}_{\nu,\delta}(N) = \frac{\mathcal{Z}_{\nu,\delta}}{N^2}\left[\frac{K_+}{N} - 1\right]^{\nu_+ - 1}\left[1 - \frac{K_-}{N}\right]^{\nu_- - 1}, \tag{3.12}$$

where $K_\pm = K_0(1 \pm \gamma)$, $\nu_\pm = (1 \mp \delta)\nu$ and $\mathcal{Z}_{\nu,\delta}$ is a normalisation constant. As we see from Figure 3.4 this captures the position of the peaks well, but not the width or skewness (since these are due to the internal noise). Furthermore, $\rho^{\mathrm{PDMP}}_{\nu,\delta}(N)$ has support $[K_-, K_+]$, with $\rho^{\mathrm{PDMP}}_{\nu,\delta}(N) = 0$ for $N \notin [K_-, K_+]$. Internal noise causes a 'leakage' of probability outside $[K_-, K_+]$ which is neglected by the

PDMP approximation. As discussed in Section 2.2.1, performing a linear noise approximation (LNA) around the PDMP gives a much more accurate description of the true N-QSD, but for my purposes (fixation probability and mean fixation time) does not significantly improve the accuracy of the theoretical predictions over the PDMP.

In the slow switching regime we have $\nu_\pm \ll 1$. Here the environmental switching is very slow compared to the birth-death process, spending a long time at $K_\pm$ before switching. Hence, as predicted by (3.12) the distribution of the population size is peaked around $K_\pm$. When $\nu \to 0$ a more accurate formula (that includes internal noise but is simpler than the LNA) can be found by the weighted sum of (2.28) for $K = K_\pm$, where the weights are given by the probability of the environmental noise equal to ± 1, $P(\xi = \pm 1) = (1 \pm \delta)/2$ (see Figure 3.4 (a)):

$$\rho_{\nu\to 0,\delta}(N) = \sum_{\xi=\pm 1} P_{K(\xi)}(N|\xi)P(\xi) \simeq \left(\frac{1+\delta}{2}\right)\frac{K_+^{N+1}\mathrm{e}^{-K_+}}{(N+1)!} + \left(\frac{1-\delta}{2}\right)\frac{K_-^{N+1}\mathrm{e}^{-K_-}}{(N+1)!}. \tag{3.13}$$

In the fast switching regime, $\nu_\pm \gg 1$, the environmental noise self averages $\xi \xrightarrow{\nu\gg 1} \delta$ and the population size fluctuates around $\mathcal{K}_\delta := K_0(1-\gamma^2)/(1-\delta\gamma)$, the weighted harmonic mean of $K_\pm$. Similarly the PDMP approximation predicts a peak at an intermediate value $K_- < N^* < K_+$, given by the smaller solution to the quadratic equation:

$$N^2 - (\nu\,(1-\delta\gamma)+1)\,K_0 N + \left(1-\gamma^2\right)K_0^2\nu = 0, \tag{3.14}$$

found by setting $d\rho_{\nu,\delta}^{\mathrm{PDMP}}(N)/dN = 0$ to find the stationary points. To leading order in $1/\nu$ the solution to this is also $\mathcal{K}_\delta$ (see Figure 3.4 (b)). In this regime, we can use the LNA to discuss the validity of the PDMP formula. When $\nu \to \infty$ (3.12) becomes very sharply peaked around $\mathcal{K}_\delta$, effectively becoming a Dirac-delta function, and the LNA (which takes into account the demographic fluctuations) then predicts that the distribution of N is Gaussian with mean and variance $\mathcal{K}_\delta$ (see Appendix A.1.2). Whilst a saddle point approximation of $\mathrm{var}\left(\rho_{\nu,\delta}^{\mathrm{PDMP}}(N)\right) = \int_{K_-}^{K_+}(N-\langle N\rangle)^2\rho_{\nu,\delta}^{\mathrm{PDMP}}(N)dN$ shows that the variance of the PDMP approximation is $\left(\gamma\mathcal{K}_\delta/(1-\delta\gamma)\right)^2(1-\delta^2)/(2\nu)$ (see B.1.2). Hence we see that the PDMP is valid while $\nu \lesssim K_0$. After this, the variance is driven mainly by the demographic fluctuations, which is not captured by the PDMP.

The intermediate regime is different dependent on the sign of δ. When $\delta < 0$, i.e. the carrying capacity spends more time in the less favourable environment (K_-), $\rho_{\nu,\delta}(N)$ exhibits a peak at $N \approx K_-$, as predicted by the PDMP approximation (3.12) (see Figure 3.4 (d)). When $\delta > 0$ the carrying capacity spends more time at K_+, and $\rho_{\nu,\delta}(N)$ therefore has a peak at $N \approx K_+$. Furthermore for some combinations of (γ, δ, ν) the population size can have an additional peak at N^*, defined as above (see Figure 3.4 (c). More details, including a complete phase diagram are in Appendix A.1.1).

3.3.1 Fixation Probability when $b = 0$

This section will present and explain the effects of random switching on the fixation probability in the pure resource competition scenario. This can by found by using the fact that when $s \ll 1$ the population size distribution reaches its long time quasi-stationary distribution in a time $t \sim \mathcal{O}(1)$, while fixation occurs on a timescale of order $1/s$ (Wienand *et al.* (2017, 2018)). Hence there is timescale separation between the two processes, and ϕ can be approximated by averaging $\phi|_{K_0}(x_0)$ (3.10) over the PDMP approximation of the population size distribution (3.12):

$$\phi^{\mathrm{ADN}}(\nu) \simeq \int_{K_-}^{K_+} \rho^{\mathrm{PDMP}}_{\nu/s,\delta}(N)\phi|_N(x_0)dN, \tag{3.15}$$

where (3.12) uses the rescaling $\nu \to \nu/s$ to reflect the fact that there are $\mathcal{O}(\nu/s)$ switches prior to fixation. This accurately predicts the qualitative behaviour of the fixation probability for all values of ν, δ and γ (see Figure 3.2(a,b)), and again it is useful to consider the three different switching regimes as in the previous section.

In the slow switching regime, $\nu \to 0$, there are no switches before fixation and the population density is peaked at $K_\pm$. Hence one can approximate:

$$\lim_{\nu\to 0} \phi^{\mathrm{ADN}}(\nu) \simeq \phi^{\mathrm{ADN}}(0) = \frac{1}{2}\left[(1-\delta)\,\phi|_{K_-}(x_0) + (1+\delta)\,\phi|_{K_+}(x_0)\right], \tag{3.16}$$

as confirmed in Figure 3.2(a,b).

When $\nu/s \gg 1$ (fast switching), $\rho_{\nu/s,\delta}$ is sharply peaked at $N \simeq K_0(1-\gamma^2)/(1-\delta\gamma) =: \mathcal{K}_\delta$ and to leading order we have:

$$\lim_{\nu\to\infty} \phi^{\mathrm{ADN}}(\nu) = \phi^{\mathrm{ADN}}(\infty) \simeq \phi|_{\mathcal{K}_\delta}(x_0). \tag{3.17}$$

This is also confirmed by simulations (see Figure 3.2(a,b)). Hence, in the fast switching regime the external noise effectively rescales the selection strength by $(1-\gamma^2)/(1-\delta\gamma)$ relative to a constant environment where the carrying capacity is K_0. The fixation probability therefore will increase (relative to a constant environment) when $\delta < \gamma$ (i.e. if the switching asymmetry is less than the noise intensity), and decreases if $\delta > \gamma$.

In the intermediate switching regime ϕ exhibits rich behaviour as ν increases and ϕ interpolates between $\phi^{\mathrm{ADN}}(0)$ and $\phi^{\mathrm{ADN}}(\infty)$. Under large enough switching asymmetry, δ and noise intensity γ, ϕ is a non-monotonic function of ν in a non-trivial region $\gamma > \gamma_c(s)$, $\delta > \delta_c(\gamma, s)$ that can be found from (3.15) (see Figures 3.2(a,d) and 3.7(d)). This captures the qualitative dependence on ν, and that it has a maximum at $\nu^*_{\mathrm{ADN}} \sim s$. This optimal switching rate for the fixation of the slow growing species corresponds to $\mathcal{O}(1)$ switches prior to fixation (i.e. fixation and environmental switching occur on similar timescales), and the percentage difference, $\phi(\nu^*_{\mathrm{ADN}})/\max(\phi(0), \phi(\infty))$ can reach up to 30%.

Outside of this critical region, ϕ is a monotonic function of ν, increasing or decreasing with ν dependent on the value of s relative to a critical value $s_c(\gamma, \delta)$, the solution of the following transcendental equation, $\phi^{\mathrm{ADN}}(0) = \phi^{\mathrm{ADN}}(\infty)$:

$$(1-\delta)\left(\frac{z^{-x_0}-1}{1-z}\right) + (1+\delta)z^{a-1}\left(\frac{z^{-ax_0}-1}{1-z^a}\right) - 2z^{b-1}\left(\frac{z^{-bx_0}-1}{1-z^b}\right) = 0, \tag{3.18}$$

where $z = \exp(-sK_-)$, $a = (1+\gamma)/(1-\gamma)$, $b = (1+\gamma)/(1-\delta\gamma)$. When $s < s_c$, $\phi^{\mathrm{ADN}}(\nu)$ is an increasing function of ν, while it decreases if $s > s_c$. The numerical result of this equation is plotted in Figure 3.2(c), where we see that s_c decreases with δ and increases with γ. In the critical non-monotonic region, $\delta > \delta_c(\gamma, s)$, $\gamma > \gamma_c(s)$ this equation determines whether $\phi^{\mathrm{ADN}}(\nu)$ has a steeper increase at slow/intermediate switching ($s < s_c$) or fast/intermediate switching for $s > s_c$.

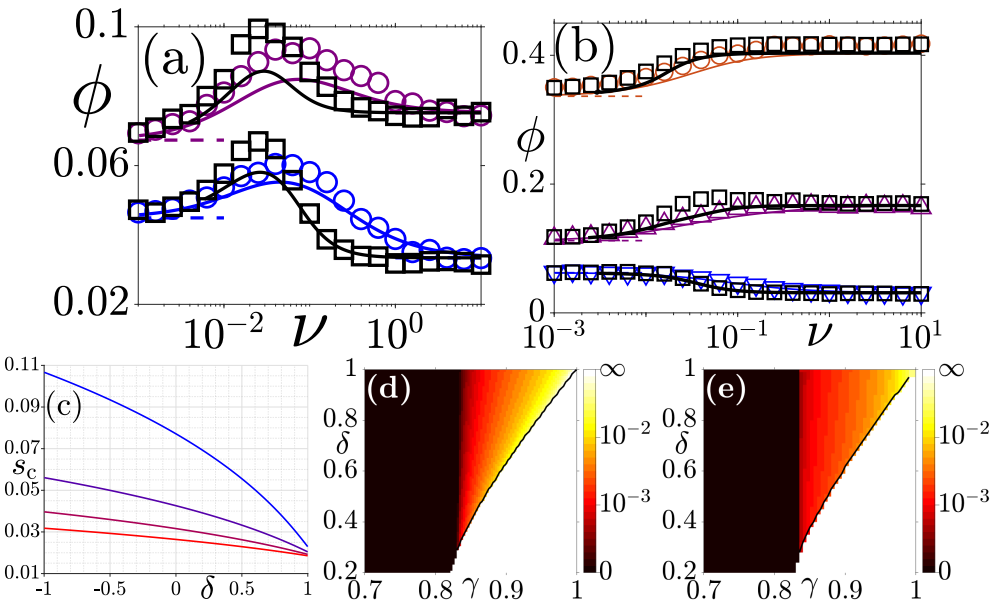

Figure 3.2: (a,b) Fixation probability for random/periodic switching (coloured/black): symbols are from simulations, solid lines are from (3.15) and (3.25) for random and periodic switching. Dashed lines show limiting cases for $\nu \to (0, \infty)$. (a) Parameters are $(s, K_0, \gamma, x_0) = (0.05, 250, 0.9, 0.6)$ and $\delta = [0.7, 0.8]$ (purple/blue). Here the fixation probability is a non-monotonic function of ν, and the value of ν that maximises ϕ is lower for periodic switching. (b) Parameters are $(s, K_0, x_0) = (0.05, 250, 0.6)$ and $(\gamma, \delta) = (0.9, -0.5)$ (orange), $(\gamma, \delta) = (0.9, 0.5)$ (purple) and $(\gamma, \delta) = (0.8, 0.6)$ (blue). Here the fixation probability is monotonic. (c) Critical selection intensity s_c as a function of δ for $\gamma = (0.6, 0.7, 0.8, 0.9)$ (red to blue) for $K_0 = 250$ and $x_0 = 0.6$. (d,e) Heatmaps of ν^*_{ADN} (c) and ν^*_{PN} (d) for $(K_0, s) = (250, 0.05)$: $\nu^* \to 0, \infty$ in the black and white areas respectively. In the red/yellow area, $\phi(\nu)$ is non-monotonic. ν^* increases with γ and decreases with δ. However we see that it is smaller for periodic noise (area is more red).

3.3.2 Comparison with Periodic Switching

When considering environmental variability, one should also consider periodic variations, firstly because other studies have found differences between the two cases (Hufton *et al.* (2018); Thattai & Van Oudenaarden (2004)). Secondly, Markovian switching is not entirely realistic: it assumes that the environmental process is memoryless, while environmental processes often have memory, with switches more likely to occur at certain moments in time. Periodic switching has this property taken to an extreme, with switches always occuring after a prescribed time interval. Environmental variability in real world falls between these two regimes, so by studying both one can infer what happens in the more realistic situations in-between (Hufton *et al.* (2018); Thattai & Van Oudenaarden (2004)). We consider periodic noise in the form of a periodic rectangular wave, defined by:

$$\begin{aligned} K(t) &= K_0(1+\gamma\xi_p(t+t_0)) \\ \xi_p(t) &= \sum_{j=-\infty}^{\infty}\left\{\text{rec}\left(\frac{t+\frac{1}{2\nu_+}+jT}{1/\nu_+}\right)-\text{rec}\left(\frac{t-\frac{1}{2\nu_-}+jT}{1/\nu_-}\right)\right\}, \end{aligned} \tag{3.19}$$

where K_0 and γ are defined as in (2.30), $T = (1/\nu_+) + (1/\nu_-) = 2/[(1-\delta^2)\nu]$ is the period of the wave and t_0 is a uniformly distributed random variable in $[0, T]$ to ensure that $K(t)$ is at stationarity (here, this means that at randomly selected time point t, the carrying capacity is at $K_\pm$ with probability $(1 \pm \delta)/2$). Hence this process spends *exactly* $1/\nu_\pm$ at $K_\pm$ (apart from the time until the first switch), whereas the random process spends *on average* $1/\nu_\pm$ at $K_\pm$. The form of (3.19) is the typical representation of a rectangular wave in signal processing. When performing the simulations, it is obviously not practical to perform this infinite sum since all but one of the terms will be zero. It is equivalent to finding $t' = t + t_0 \mod T$, then setting $\xi_p = 1$ if $t' \leq 1/\nu_+$ and $\xi_p = -1$ otherwise. This leads to the mean and variance of the noises ξ and ξ_p being the same when both processes are at stationarity, however the effect on the probability distribution for N, $\rho^{\text{PN}}(N)$, and the fixation probability, $\phi^{\text{PN}}(\nu)$, is different. A typical realisation is shown in Figure 3.3.

First we will consider the fast and slow switching regimes where it is possible to find approximations of the N-QSD that account for *both* internal and external

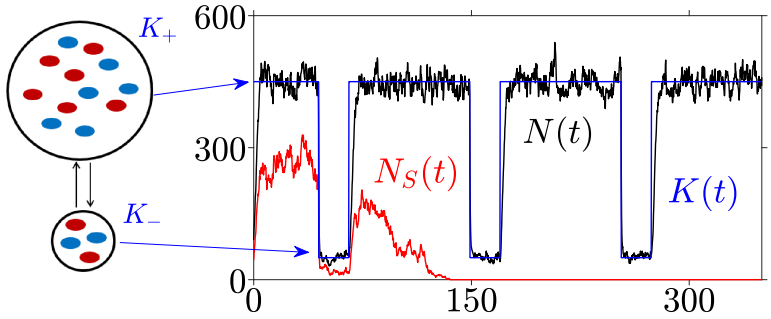

Figure 3.3: Asymmetric periodic noise switching between $K = K_+$ and $K = K_-$, spending $\nu_\pm^{-1}$ in either state (blue), along with typical realisations of N (black) and N_S (red) vs time. Parameters: $(s, K_0, \nu, \gamma, \delta, x_0) = (0.02, 250, 0.03, 0.8, 0.6, 0.5)$. After a switch the total population size is of order $K_\pm$ in a time of order 1, fluctuating around the carrying capacity until another switch occurs.

fluctuations. The approximation in the slow switching regime when $\nu \ll 1$ has the same form as for random switching for the same reasons: the system only experiences one environment $\xi = \pm 1$ with probability $\frac{1}{2}(1 \pm \delta)$ (because the noise is always started at stationarity) so the probability distribution will be the weighted sum of (2.28) with $K = K_\pm$:

$$\rho^{\mathrm{PN}}_{\nu\to 0,\delta}(N) = \sum_{\xi=\pm 1} P_{K(\xi)}(N|\xi)P(\xi) \simeq \left(\frac{1+\delta}{2}\right)\frac{K_+^{N+1}e^{-K_+}}{(N+1)!} + \left(\frac{1-\delta}{2}\right)\frac{K_-^{N+1}e^{-K_-}}{(N+1)!}. \tag{3.20}$$

This is the same as equation (3.13), and as such the fixation probability of the slow growing species is the same for both random and periodic noise in this limit (see Figures 3.4(a) and 3.2 (a,b)).

In the fast switching regime one can use the Kapitsa method (Assaf *et al.* (2008)), which involves separating the dynamics of N into fast and slow variables, then averaging the fast variables over the period of variation. Unlike the PDMP approximation for random switching, this approximation includes the effects of internal and external noise. The calculation for this was performed by a collaborator in our 2020 PRL paper (Taitelbaum *et al.* (2020)), in which the full

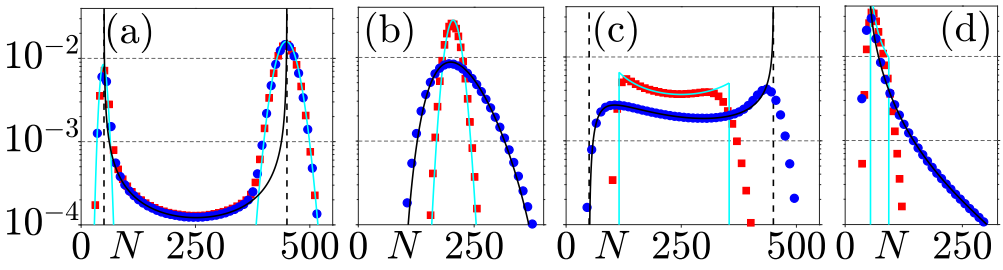

Figure 3.4: Comparison of the N-QSD in the random (blue) and periodic (red) switching cases for different values of ν (a) $\nu = 0.05$, (b) $\nu = 17.5$, (c) $\nu = 1.4$, (d) $\nu = 1$. Symbols are from simulations; solid black lines are from (2.39), those in cyan are from (3.20) in (a) and (3.21) in (b); vertical dashed lines in (a,c) show $N = K_{\pm}$; horizontal dashed lines are eyeguides. Here $(K_0, \gamma) = (250, 0.8)$, $\delta = 0.7$ in (a)-(c) and $\delta = -0.5$ in (d).

details can be found. Here I quote the result:

$$\rho^{\mathrm{PN}}_{\nu\gg 1,\delta}(N) \simeq P_{\nu,\delta} \exp\left[N - N\ln\left(N/\mathcal{K}_\delta\right) - \frac{K_0}{72\nu^2}\left(\frac{\gamma}{1-\gamma^2}\right)^2\left(\frac{2N-\mathcal{K}_\delta}{K_0}\right)^3\right], \tag{3.21}$$

where $P_{\nu,\delta}$ is a normalization constant. In the fast switching limit $\nu \to \infty$ we see that this is peaked around $N = \mathcal{K}_\delta$, as in the random switching case (see Figure 3.4 (b)), but the distribution is much narrower and sharper for periodic switching. In fact one can use the saddle point approximation to show that the variance is of order $\mathcal{K}_\delta$, for all $\nu >> 1$, whereas the PDMP for random switching predicts a variance of order K_0^2/ν for $1 \ll \nu \ll K_0$ (see Appendix B.1.2). Thus the fixation probabilities both tend to the same value, i.e. $\phi^{\mathrm{PN}}(\infty) \simeq \phi^{\mathrm{ADN}}(\infty). \simeq \phi|_{\mathcal{K}_\delta}(x_0)$. However the rates of convergence to these values differs for the two forms of noise (due to the difference in variance of the probability distributions), this is discussed in more detail in Section 3.3.3.

In the intermediate switching regime, one can use a similar method to O'Dwyer & Chisholm (2014) to find the probability distribution for N, treating N as a continuous process as for the PDMP. This calculation was again performed by a

collaborator on our 2020 PRL paper, and was found to give:

$$\rho^{\mathrm{PN}}_{\nu,\delta}(N) = C_{\nu,\delta}\left[\frac{1}{K_+ - N} + \frac{1}{N - K_-}\right], \quad \text{where} \tag{3.22}$$

$$C^{-1} = \ln\left[\frac{(K_+ - N_{\min})\,(N_{\max} - K_-)}{(K_+ - N_{\max})\,(N_{\min} - K_-)}\right], \tag{3.23}$$

$$N_{\min} = \frac{K_0(1-\gamma^2)}{1-\gamma+2\gamma\frac{1-\mathrm{e}^{-1/\nu_-}}{1-\mathrm{e}^{-T}}} \quad \text{and} \quad N_{\max} = \frac{K_0(1-\gamma^2)}{1-\gamma+2\gamma\frac{\mathrm{e}^{-1/\nu_+}-\mathrm{e}^{-T}}{1-\mathrm{e}^{-T}}}. \tag{3.24}$$

The support of the function in this case is $[N_{\min}, N_{\max}]$. Hence ν and δ do not affect the functional form of the probability distribution, their only influence is on the boundaries of the support (and therefore the normalisation constant). In Figure 3.4 (c,d) we see that this does a reasonable job of approximating the N-QSD, and similarly to the PDMP it fails to capture the 'leakage' of probability outside the support. Similarly to random noise, the fixation probability may be a non-monotonic function of ν (see Figure 3.2(a), and we can use the probability distribution of N calculated above to write a formula for the fixation probability, analogous to (3.15):

$$\phi^{\mathrm{PN}}(\nu) \simeq \int_{N_{\min}}^{N_{\max}} \rho^{\mathrm{PN}}_{\nu/s,\delta}(N)\phi|_N(x_0)dN. \tag{3.25}$$

Again we see that this does a good job of capturing the qualitative dependence of ϕ on the parameters of the system (see Figure 3.2 (a,b)), and we use this formula to find ν^*_{PN} (the optimal switching rate for the slow growing species to fixate) which is presented in Figure 3.2 (e). We see that the position of the optimum is at lower switching rates for periodic switching, and this is caused by the fact that the probability distribution for N is narrower for smaller values of ν i.e. the transition from the wide, bimodal distribution for small ν to the narrow, unimodal distribution for large ν happens earlier.

Above, I have investigated the effect of varying ν and s whilst keeping the other parameters fixed, but it is also interesting to vary the switching asymmetry, δ, or the noise intensity, γ, whilst keeping the other parameters fixed. First, note that increasing δ means that one spends more time at $\xi = 1$ where the mean fixation time is larger and the fixation probability is smaller, hence ϕ is a

decreasing function of δ while the mean fixation time is an increasing function (see Figure 3.5).

In ecology, there is a great interest in studying how environmental variations can effect species diversity. This led to the debate on the Intermediate disturbance hypothesis (Brockhurst *et al.* (2007); Fox (2013); Petraitis *et al.* (1989)), which looks at the evolutionary effects of the frequency and amplitude of external disturbances. In this broad context, and without direct relevance for the IDH, it is interesting to now study how ϕ depends on amplitude of the noise, γ, keeping ν fixed as a parameter. It is found that the effect of varying γ is different dependent on the asymmetry of the noise, δ: when $\delta > 0$ Figure 3.5 shows that the fixation probability and mean fixation time (MFT) are non-monotonic in γ, while for $\delta \leq 0$, ϕ is monotonically increasing and the MFT is monotonically decreasing. Hence, noise may (slightly) prolong species coexistence, but make conditions less favourable for the slow growing species. For ϕ, this can be understood analytically in the fast and slow switching regimes.

When $\nu/s \gg 1$ (Figure 3.5(c)) the N-QSD for both periodic and random switching is peaked roughly around $\mathcal{K}_\delta = K_0(1-\gamma^2)/(1-\delta\gamma)$, which sets the fixation probability as (3.10) evaluated at $\mathcal{K}_\delta$. Hence when $\gamma < \delta$, $\mathcal{K}_\delta > K_0$, and $\phi|_{\mathcal{K}_\delta} < \phi|_{K_0}$, while the opposite is true for $\gamma > \delta$. For simplicity, we work in the realm of the diffusion approximation, $s \ll K_0^{-1/2} \ll 1$. When $\nu \ll 1$ (Figure 3.5(a)) one can use (3.16) with the leading order contribution of (3.10) (i.e $\phi|_K \approx \mathrm{e}^{-Ks(1-x_0)}$) to write:

$$\phi(\gamma) \approx \frac{1}{2}\mathrm{e}^{-K_0 s(1-x_0)}\left[(1-\delta)\mathrm{e}^{\gamma K_0 s(1-x_0)} + (1+\delta)\mathrm{e}^{-\gamma K_0 s(1-x_0)}\right]. \tag{3.26}$$

Writing $y = \mathrm{e}^{\gamma K_0 s(1-x_0)}$ and setting $\phi(\gamma) = \phi|_{K_0}$ allows us to ascertain when the external noise promotes the slow growing species with respect to a constant environment, yielding the quadratic equation for the point where $\phi(\gamma)$ is the same that for a constant environment with $K = K_0$: $(1-\delta)y^2 - 2y + (1+\delta) = 0$. This has solutions $y = 1$, corresponding to the trivial solution $\gamma = 0$, and $y = (1+\delta)/(1-\delta)$, corresponding to $\gamma = \gamma^* = (K_0 s(1-x_0))^{-1}\ln\left[(1+\delta)/(1-\delta)\right]$, which is only physically realistic if $\delta > 0$. Furthermore, note that differentiating (3.26) with

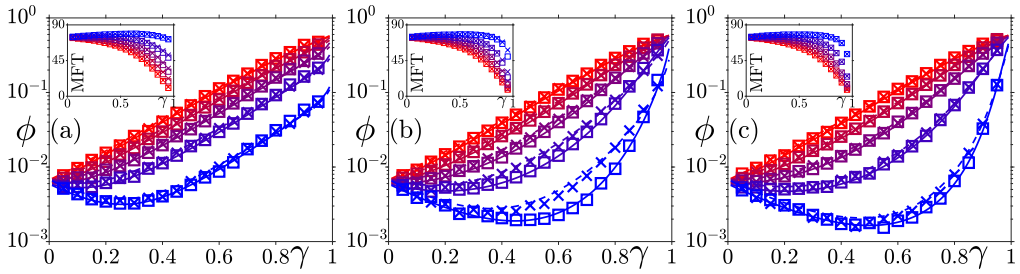

Figure 3.5: Dependence of ϕ (main panels) and Mean Fixation Time (insets) on γ and δ for $(K_0, s, x_0) = (250, 0.05, 0.6)$ for $\nu = (0.01, 0.1, 1)$ in (a,b,c). In all panels, x-axis shows γ and results for $\delta = (-0.8, -0.4, 0, 0.4, 0.8)$ are shown by red to blue. Squares/crosses represent simulation results for periodic/random variation. Solid/dashed lines in main panels are theoretical results from (3.25)/(3.15) for periodic/random variation. See text

respect to γ yields:

$$\frac{d}{d\gamma}\phi(\gamma) \approx \frac{1}{2}\mathrm{e}^{-K_0 s(1-x_0)} K_0 s(1-x_0)\left[(1-\delta)\mathrm{e}^{\gamma K_0 s(1-x_0)} - (1+\delta)\mathrm{e}^{-\gamma K_0 s(1-x_0)}\right]. \tag{3.27}$$

The term outside the bracket is always greater than zero, and expanding the term inside the bracket around $\gamma = 0$ yields:

$$\frac{d}{d\gamma}\phi(\gamma) \approx \mathrm{e}^{-K_0 s(1-x_0)} K_0 s(1-x_0)\left[-\delta + \gamma K_0 s(1-x_0)\right]. \tag{3.28}$$

Hence if $\delta > 0$, $\phi(\gamma)$ initially decreases, then increases, with $\phi(\gamma) = \phi|_{K_0}$ when $\gamma \approx \gamma^*$. Furthermore, for larger values of the switching asymmetry, δ, larger values of noise intensity γ are needed to increase the fixation probability relative to the constant environment.

3.3.3 Fast Switching Regime

In the fast switching regime $\nu/s \gg 1$, the fixation probabilities in both periodic and random switching cases tend to the same limit, however the rate at which they approach this limit is different. This is explained by calculating the next to leading order term of the fixation probability, achieved by performing a saddle point expansion of $\phi^{\alpha}(\nu)$, with $\phi|_N(x_0) = \exp\left[-N(1-x_0)\ln(1-s)\right]$ (i.e. the

leading order contribution of (3.9) - valid when $K_0^{-1} \ll s \ll K_0^{-1/2}$), and the PDMP approximation of the probability distribution for the random switching case, and the Kapitsa method approximation for fast switching in the periodic switching case, i.e.

$$\phi^{\mathrm{ADN}}(\nu) \simeq \mathcal{Z}_{\nu,\delta} \int_{K_-}^{K_+} \frac{1}{N^2} \left[\frac{K_+}{N} - 1\right]^{\nu_+ - 1} \left[1 - \frac{K_-}{N}\right]^{\nu_- - 1} \phi|_N(x_0) dN \quad \text{and} \tag{3.29}$$

$$\phi^{\mathrm{PN}}(\nu) \simeq P_{\nu,\delta} \int_{K_-}^{K_+} \exp\left[N - N\ln\left(N/\mathcal{K}_\delta\right) - \frac{K_0}{72\nu^2}\left(\frac{\gamma}{1-\gamma^2}\right)^2 \left(\frac{2N - \mathcal{K}_\delta}{K_0}\right)^3\right] \phi|_N(x_0) dN. \tag{3.30}$$

Where $\mathcal{Z}_{\nu,\delta}$ and $\mathcal{P}_{\nu,\delta}$ are normalisation constants which also have to be approximated. Full details are in Appendix B.1.1, where we find that:

$$\ln\left(\frac{\phi^\alpha(\nu)}{\phi(\infty)}\right) \simeq \begin{cases} \mathcal{A}^{\mathrm{ADN}}(s/\nu) & (\alpha = \mathrm{ADN}) \\ \mathcal{A}^{\mathrm{PN}}(s/\nu)^2 & (\alpha = \mathrm{PN}), \end{cases} \tag{3.31}$$

where $\phi(\infty) = \mathrm{e}^{m/2}$, $m = 2\mathcal{K}_\delta(1-x_0)\ln(1-s)$, $\mathcal{A}^{\mathrm{ADN}} = m(4+m)(1-\delta^2)(\gamma/(1-\delta\gamma))^2/16$ and $\mathcal{A}^{\mathrm{PN}} = \mathcal{K}_\delta(1-(1+m/\mathcal{K}_\delta)^3)(\gamma/(1-\delta\gamma))^2/72$. Hence when $K_0 s \gg 1$, the fixation probability of the slow growing species exhibits markedly different behaviours under random and periodic switching: it converges to $\phi(\infty)$ much faster in the case of periodic than for random switching (see Figure 3.6). This can be understood by noting that the N-QSD is much broader for random compared to periodic switching, with the variances scaling as ν^{-1} and ν^{-2} respectively (see Appendix B.1.2). N therefore attains smaller values under random switching, increasing ϕ^{ADN} with respect to ϕ^{PN} when $s > s_c$. Furthermore, when $\nu/s \gg 1$ the fixation probability is determined by the mean $\langle N\rangle \simeq \mathcal{K}_\delta$ of the N-QSD. The rate of convergence stems from the deviations of the mean $\langle N\rangle$ from $\mathcal{K}_\delta$, which decrease as ν^{-1} for random and ν^{-2} for periodic switching (see Appendix B.1.2). This also means that the fact that $\rho^{\mathrm{PDMP}}_{\nu,\delta}(N)$ is not a good approximation of the variance for DMN is not important for calculating the fixation probability, since this is determined by the mean. Also, the ratio $\phi^{\mathrm{ADN}}/\phi^{\mathrm{PN}}$ has a sharp peak at a non-trivial intermediate ν.

It should be noted here that other approximation methods are possible. For example in Hufton *et al.* (2019), the authors develop an approximation method

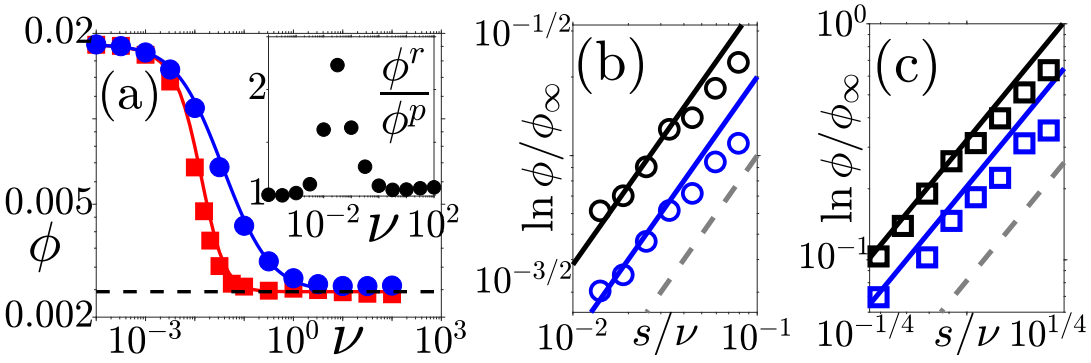

Figure 3.6: Fixation probability for random/periodic switching (circles/squares): symbols are from simulations, in (a) solid lines are from (3.15) and (3.25) for random and periodic switching respectively. In (b,c) solid lines are from (3.31). Parameters are $(s, K_0, \gamma, x_0) = (0.025, 800, 0.7, 0.5)$. (a) $\phi(\nu)$ with $\delta = 0.2$, dashed line shows $\phi(\infty)$. Inset: $\phi^{\mathrm{ADN}}/\phi^{\mathrm{PN}}$ for $\delta = 0.2$. (b,c) $\ln(\phi/\phi(\infty))$ vs s/ν for random (b) and periodic (c) switching with $\delta = 0.2$ (black) and $\delta = 0$ (blue). Dashed grey lines are eyeguides $\propto s/\nu$ in (b) and $(s/\nu)^2$ in (c).

that combines a system-size expansion with an expansion in the environmental switching parameter for systems with fast environmental switching. However, in the model presented in this Chapter, the population size is coupled to the environment via the carrying capacity. This means that there is no fixed large system size parameter for the first expansion, so their technique is not applicable here.

3.4 Public Good Games

Turning our attention to the case of the *public goods game*, defined by the same reactions (3.1) with $b > 0$ which supposes that the slow growing strain produces a public good available to the entire population, we find that similar qualitative results are observed in this more intricate case of *eco-evolutionary dynamics*. Here, the population composition now affects the population size: the global growth rate is multiplied by a factor of $g(x) = 1 + bx$, coupling the population size with the population composition leading to eco-evolutionary feedback: when there are more of the slow growing species the population size increases, reducing

the effect of demographic noise and on average reducing fraction of slow growers. This in turn reduces the total population size, making demographic noise more important, which can lead to an increase in the density of slow growers, increasing population size *etc.*.

It should be noted that this a simplification of the true biological process. Public goods that increase growth rates have been observed as molecules that are produced by some strains in a nutrient-starved environment that bind to otherwise inaccessible environmental molecules and are transported into the cell for use, for example the production of the iron scavenging molecule pyoverdine in *P. aeruginosa* (Becker *et al.* (2018); Buckling *et al.* (2007); Diggle *et al.* (2007); Griffin *et al.* (2004)). The concentration of these molecules will depend on the population composition, and should be modelled as an additional 'species' in the birth-death formulation. Furthermore, the amount of resources should also be included as another independent 'species', whose dynamics depends on the amount of public good and biotic individuals in the system. This would increase the dimension of the system, in both a stochastic and deterministic setting, by 2 (see Becker *et al.* (2018) for a deterministic model). Hence, the solutions are only available through numerical simulation of the stochastic process (or differential equations if using ODEs). In the model used in this section, the linear dependence of the global growth rate on the fraction of co-operators captures the phenomenological effect of public good production without increasing the dimensionality of the system, allowing us to find analytical results for the effect of the rate of public good production on the fixation probability of slow growing species. Using a different functional dependence of g on x, *e.g.* quadratic (peaked at some $0 < x < 1$) or sigmoidal (slow increase until some critical $0 < x < 1$, then fast saturation thereafter), would also be an interesting avenue of further research.

In the constant carrying capacity case, i.e. without external noise, the dynamics of the model is well described in terms of a population of effective size, by introducing a parameter $0 \leq q \leq b$ and replacing $g(x)$ by $1+q$ in (3.4). Using the same method as for the pure resource competition case, this decouples the mean field equations for N and x, and one finds that the PDMP approximation

now yields

$$\rho^{\mathrm{PDMP}}_{\nu,\delta,q}(N) = \frac{\mathcal{Z}_{\nu,\delta,q}}{N^2}\left[\frac{(1+q)K_+}{N} - 1\right]^{\frac{\nu_+}{1+q}-1}\left[1 - \frac{(1+q)K_-}{N}\right]^{\frac{\nu_-}{1+q}-1}, \tag{3.32}$$

for the probability distribution of N, where $\mathcal{Z}_{\nu,\delta,q}$ is a normalisation constant. The parameter q is found by matching the simulation results for the fixation probability of the slow growing species in the fast switching limit ($\nu/s \gg 1$), with $\phi|_{(1+q)\mathcal{K}_\delta}(x_0)$ (3.10). Results in Figure 3.7(a) show that q increases linearly with b, while it also exhibits a weak dependence on s and δ. From (3.32) we see that the effect of increasing b is to effectively increase the carrying capacities $K_\pm \to (1+q)K_\pm$ and reduce the switching rates $\nu_\pm \to \nu_\pm/(1+q)$. Replacing $1+bx$ with this effective parameter also allows us to find a closed formula for the fixation probability of the slow growing species in the same way as for the pure resource competition case ($b = 0$): averaging the expression for the fixation probability in a constant environment (3.10) (here denoted $\phi|_{K_0}(s, x_0)$ for reasons which will become clear) over the effective probability distribution (3.32) with the rescaled switching rate $\nu \to \nu/s$. Furthermore by changing the variable of integration $N' = N/(1+q)$ we find that this is equivalent to rescaling the selection strength to $s_{\mathrm{eff}} = (1+q)s$ in the model without public good:

$$\phi^{\mathrm{ADN}}(\nu, q) = \int_{(1+q)K_-}^{(1+q)K_+} \phi|_N(s, x_0)\rho^{\mathrm{PDMP}}_{\nu/s,\delta,q}(N)dN = \int_{K_-}^{K_+} \phi|_{N'}(s_{\mathrm{eff}}, x_0)\rho^{\mathrm{PDMP}}_{\nu/s_{\mathrm{eff}},\delta,0}(N')dN'. \tag{3.33}$$

Comparisons with numerical simulations show that this is a very good approximation when $\nu/s \ll 1$ and $\nu/s \gg 1$. Hence in these regimes increasing the public good benefit b is equivalent to rescaling the selection strength $s \to s_{\mathrm{eff}}$, and the fixation probability is an exponentially decreasing function of b.

In the intermediate switching regime, (3.33) gives a reasonable qualitative description of ϕ^{ADN}. With this and Figure 3.7 (d) we can understand how raising b at fixed s changes the phase diagram for $\phi^{\mathrm{ADN}}(\nu)$ in terms of γ & δ: As b is increased s_{eff} increases, squashing the triangular region (in which the fixation probability is non-monotonic), since γ_c increases under the effect of $s \to s_{\mathrm{eff}} = (1+q)s$. In Figure 3.7(b) where $\delta < \delta_c$ and $\phi^{\mathrm{ADN}}(\nu)$ is monotonically increasing for $b = 0$, increasing b moves (δ, γ) into the triangular region ($\gamma > \gamma_c, \delta > \delta_c$) and

$\phi^{\mathrm{ADN}}(\nu, q)$ varies non-monotonically with ν. In Figure 3.7(c) where $\delta > \delta_c$ and $\gamma > \gamma_c$ and therefore $\phi^{\mathrm{ADN}}(\nu)$ is a non-monotonic function for $b = 0$, increasing b increases γ_c, eventually attaining a value such that $\gamma < \gamma_c$, and $\phi^{\mathrm{ADN}}(\nu, q)$ becomes a monotonically decreasing function of ν. These are nice examples of the complex behaviour that eco-evolutionary feedback can generate and similar behaviour is also observed in the case of periodic switching: with the rescalings $K_\pm \to (1+q)K_\pm$ and $\nu_\pm \to \nu_\pm/(1+q)$ in (3.25) we obtain:

$$\phi^{\mathrm{PN}}(\nu, q) = \int_{N_{\min}(q)}^{N_{\max}(q)} \phi|_N(s, x_0)\rho^{\mathrm{PN}}_{\nu/s,\delta,q}(N)dN. \tag{3.34}$$

However, in this case this does not amount to a rescaling of s, due to the dependence of the support of $\rho^{\mathrm{PN}}_{\nu/s,\delta,q}(N)$ on the switching rate ν (see (3.22)). However in Figure 3.7(e,f) we see that this is good approximation of ϕ in the regimes $\nu/s \gg 1$ and $\nu/s \ll 1$. The intermediate switching regime is also characterised by a transition from either monotonically increasing to non-monotonic (see Figure 3.7(e)), or non-monotonic to monotonically decreasing (see Figure 3.7(f)).

3.5 Summary and Discussion

This chapter has built on the work of Wienand *et al.* (2017, 2018), analysing the effects of a randomly switching carrying capacity on the outcome of the two-species Prisoners Dilemma in a population of fluctuating size. Specifically I found that asymmetric switching (i.e. spending more time in one state that the other) can result in a non-trivial dependence of ϕ on the switching rate, ν. This occurs when the noise intensity, γ and asymmetry, δ are large, and when the selection strength s is not too large or too small. Furthermore, when the switching asymmetry is positive ($\delta > 0$), one also observes a non-monotonic dependence of ϕ on the noise intensity, γ, with larger intensities needed to increase the fixation probability of cooperators relative to a static environment as the external noise becomes more asymmetric.

These results are interesting when viewed in light of the Intermediate Disturbance Hypothesis (Begon *et al.* (2006); Brockhurst (2007); Brockhurst *et al.*

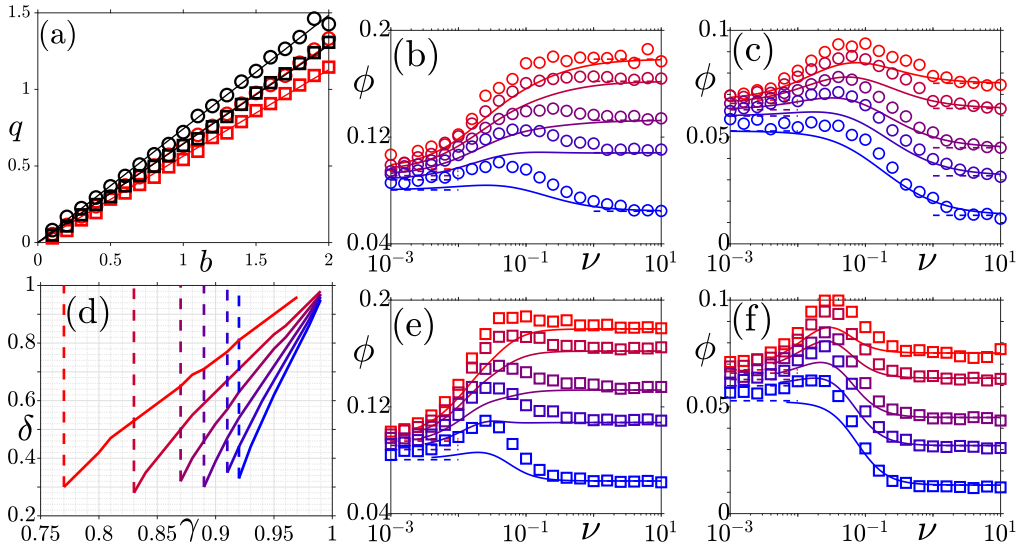

Figure 3.7: (a) Effective parameter q versus b for $\delta = -0.5, 0.5$ (black, red) and $s = 0.02, 0.05$ (squares, circles). Dependence of q on b is approximately linear while q depends weakly on δ and s (solid lines are eyeguides). (b,c,e,f) ϕ versus ν for $(K_0, \gamma, s, \delta, x_0) = (250, 0.9, 0.04, 0.6, 0.6)$ in (b,e) and $(250, 0.9, 0.05, 0.7, 0.6)$ in (c,f). Here (b,c) and (e,f) show results for random and periodic switching respectively. In (b,c,e,f) $b = (0, 0.1, 0.3, 0.5, 1)$ from red to blue. Open symbols are simulation results and solid lines are from (3.33) in (b,e) and (3.34) in (c,f). In (b,e), ϕ is an increasing function of ν for small b, and varies non-monotonically with ν for intermediate b. In (c,f) ϕ is a non-monotonic function of ν at low b and becomes a decreasing function of ν as b increases. (d) Triangular-like region in parameter space in which $\phi^{\rm ADN}(\nu)$ has a non-trivial maximum at $\nu = \nu^*$ for $s = 0.04, 0.05, 0.06, 0.07, 0.08, 0.09$ (red to blue), obtained from (3.15). This region, defined by $\gamma > \gamma_c(s)$, $\delta > \delta_c(\gamma, s)$ is enclosed by the dashed and solid lines. Compare with 3.2(d). Also, given that in the random noise case, (3.33) predicts a rescaling of s, this figure explains the behaviour observed in (b,c).

(2007); Buckling *et al.* (2000); Connell (1978); Grime (1973); Lampert & Sommer (2007); Petraitis *et al.* (1989)), which states that cooperative traits are most favoured by intermediate rates of disturbance in a community. Too slow and the cheats have enough time to exploit the cooperators, too fast and there is not enough time for the benefits of cooperation to be felt. Furthermore, the IDH also says the larger disturbances will promote cooperative behaviour more. However, the IDH has been criticised because the evidence for disturbances providing a benefit to cooperators is not widely observed (Fox (2013) for an overview). Strictly speaking, the IDH refers to situations where multiple species coexist for a long time, and describes the effect of noise on the *proportion* of cooperative strains in the system. Here, we are interested in the fixation probability of slow growing / co-operative strains, but the model could be extended so as to avoid fixation and test the IDH: First, one could specify that the selection strength s also follows DMN process, being neutral on average but favouring different strains depending on the environment. In some, but not all, cases this has been shown to lead to a super-linear dependence of the fixation time on the population size. Hence for very large K_0 one could consider the average proportion of cooperators before fixation. Second, a better adjustment would be to include mutation between the strains. This would avoid the fixation scenario entirely and thus be a much better test of the IDH. Finally, another interesting extension would be a meta-population of connected patches following their own DMN process (with the same statistics). In the public good scenario, this would be an interesting test of Simpson's Paradox (Blyth (1972); Chater *et al.* (2008); Chuang *et al.* (2009); Cremer *et al.* (2011, 2012, 2019); Hauert *et al.* (2002); Hense *et al.* (2019); Melbinger *et al.* (2015); Okasha (2006)), where the fraction of cooperators decreases within each patch but increases overall, due to patches with a larger fraction of co-operators increasing their total population size by a larger amount. Hence we could ascertain if this paradox is still observed in systems with environmental noise, and what effects the statistics of the noise have on the outcome.

Another interesting result is the qualitative difference between periodic and random switching on the fixation probability of cooperators. When there is an optimal switching rate, it is lower for periodic switching and reaches a higher value. Furthermore, in the fast switching regime, while the fixation probability

tends to the same value, the lowest order correction to the fixation probability is of order ν^{-1} for random switching but ν^{-2} for periodic. Hence for $\nu \gg 1$ cooperators are more favoured in random switching environment, due to the fact that the random nature of switching means that system could spend a time longer than ν_-^{-1} at K_-, allowing the system to reach smaller population sizes (as evidenced by the larger variance in population size), increasing the fixation probability of cooperators.

Chapter 4

Rock-Paper-Scissors Games in a Static Environment: Comparison of Different Models

The remainder of this thesis will focus on three species models where the fitness of individuals varies cyclically with the population composition: species 1 outcompetes species 2, species 2 outcompetes 3, and species 3 outcompetes species 1. These so-called 'Rock-Paper-Scissors' models are the paradigmatic model of cyclic dominance in microbiology and ecology, having been observed in *Uta stanisburiana* lizards (Sinervo & Lively (1996); Sinervo *et al.* (2000); Zamudio & Sinervo (2000)), bacterial communities (Hibbing *et al.* (2010); Kerr *et al.* (2002); Kirkup & Riley (2004); Nahum *et al.* (2011)), and plant and coral reef communities (Cameron *et al.* (2009); Jackson & Buss (1975); Taylor & Aarssen (1990)). There is large body of work already addressing different forms of cyclic competition, with different features depending on the precise aspects of cyclic competition under investigation. Here the main focus will be on the well mixed (*i.e.* no spatial structure) setting.

In this chapter I will first review two commonly used models of cyclic competition: firstly the 'chemical cyclic Lotka-Volterra model' (cCLV), the simplest form of cyclic competition with three dominance-replacement reactions and fixed population size, this will be used in Chapter 6 where I will investigate the effects of a randomly switching reaction rate. Secondly, the May-Leonard model of

cyclic competition (MLM) defined with the same dominance-replacement reactions as the cCLV, supplemented with 3 dominance-removal reactions and three birth reactions, hence this model allows for fluctuating population size. Finally I will introduce a game-theoretic generalisation of this model, the birth-death cyclic Lotka-Volterra model (BDCLV). This models cyclic competition via composition dependent birth rates, which vary according to a payoff matrix. Death rates are logistic, thus allowing for a fluctuating total population size around the carrying capacity (that, in contrast to the MLM can be exceeded). In Chapter 5 this model will be used when investigating the effects of dichotomously switching carrying capacity.

4.1 The chemical Cyclic Lotka-Volterra model (cCLV)

The chemical cyclic Lotka Volterra model (cCLV) is defined by three pairwise reactions involving the simultaneous death and birth of individuals of different species, therefore conserving the total population size N. Hence, in the cCLV, species i is the predator of species $i+1$ and the prey of species $i-1$: an i-individual kills and replaces an $(i+1)$-individual with one of its offspring, while it is killed and replaced by individual of type $i-1$ according to the following "pairwise chemical reactions", with $N_3 = N - N_1 - N_2$:

$$\begin{aligned} [N_1, N_2, N_3] &\xrightarrow{W_{21}} [N_1 + 1, N_2 - 1, N_3] \\ [N_1, N_2, N_3] &\xrightarrow{W_{32}} [N_1, N_2 + 1, N_3 - 1] \\ [N_1, N_2, N_3] &\xrightarrow{W_{13}} [N_1 - 1, N_2, N_3 + 1], \end{aligned} \tag{4.1}$$

with transition rates (Berr *et al.* (2009); Reichenbach *et al.* (2006); West *et al.* (2018)):

$$W_{i+1,i} = k_i \, \frac{N_i N_{i+1}}{N} = k_i x_i x_{i+1} \, N, \quad \text{where } k_i \geq 0 \text{ and } i, j \in \{1, 2, 3\}. \tag{4.2}$$

From these we see that this is a zero-sum game: when the total gains of all players are added up and the total losses subtracted, the total is zero. In each reaction,

one individual of type $i+1$ dies and is immediately replaced by one of type i (with cyclic ordering of species: $1-1=3$ and $3+1=1$), and the total population size is fixed. This form of cyclic competition has been extensively studied in well mixed (Berr *et al.* (2009); Broom & Rychtár (2013); Dobrinevski & Frey (2012); Hofbauer *et al.* (1998); Ifti & Bergersen (2003); Nowak (2006a); Reichenbach *et al.* (2006, 2008); Smith (1982)), spatial (Frachebourg *et al.* (1996a); Frean & Abraham (2001); He *et al.* (2010); Mitarai *et al.* (2016); Ni *et al.* (2010); Szabó & Szolnoki (2002); Tainaka (1989, 1993, 1994)) and network (Sato *et al.* (1997); Szabó *et al.* (2004); Szolnoki & Szabó (2004)) settings, and I will now review the key properties for this thesis in the well mixed case. We can write the master equation:

$$\begin{aligned}\frac{dP(\vec{N},t)}{dt} &= (\mathbb{E}_1^-\mathbb{E}_2^+ - 1)[W_{21}(\vec{N})P(\vec{N},t)] \\ &+ (\mathbb{E}_2^-\mathbb{E}_3^+ - 1)[W_{32}(\vec{N})P(\vec{N},t)] \\ &+ (\mathbb{E}_3^-\mathbb{E}_1^+ - 1)[W_{13}(\vec{N})P(\vec{N},t)],\end{aligned} \tag{4.3}$$

from which one can use Sec. 2.1.1 to find that the cCLV mean field equations for the x_i's are given by:

$$\frac{dx_i}{dt} = \frac{W_{i+1,i} - W_{i,i-1}}{N} = x_i\left(k_i x_{i+1} - k_{i-1}x_{i-1}\right), \quad i = 1,2,3. \tag{4.4}$$

These mean field equations describe the dynamics when the population size is infinitely large ($N \to \infty$) where demographic fluctuations are ignored. These rate equations (4.4) are characterised by three absorbing fixed points $\vec{x} = \vec{e}_i$, $i \in \{1,2,3\}$, which are saddles and correspond to the survival of one species and the extinction of the other two. The trivial fixed point $[0,0,0]^T$ is not relevant here, since the total population size is always N, so this state can only be attained if we start with $N = 0$. Furthermore, they also admit a non-trivial fixed point associated with the coexistence of the three species with densities given by:

$$\vec{x^*} = \frac{1}{k_1+k_2+k_3}\left(k_2, k_3, k_1\right), \tag{4.5}$$

which is a neutrally stable centre (i.e. has complex complementary eigenvalues with zero real part). In addition to the total population size being constant, the

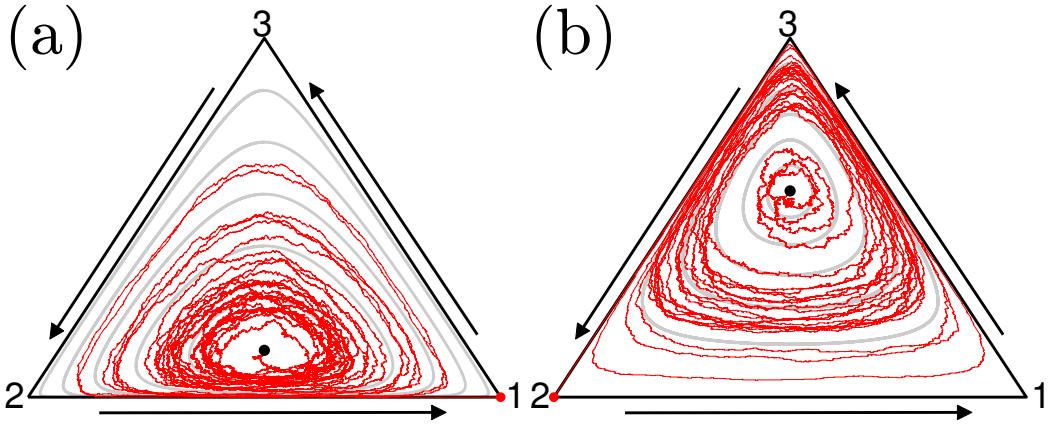

Figure 4.1: Stochastic orbits (thin red) and deterministic trajectories (grey) of the cCLV with $N = 1000$, $k_2 = k_3 = 1$ and $k_1 = 0.3$ (a), $k_1 = 5.7$ (b). Black dot shows coexistence fixed point $\vec{x}^*$, red dot shows final species that fixates the population and arrows indicate direction of travel. Note that the most likely species to fixate depends on the location of $\vec{x}^*$, and is here given by the lowest k_i according to the 'law of the weakest': species 1 is the most likely to prevail in (a) while 2 and 3 are both as likely in (b). See text.

rate equations (4.4) also admit another conserved quantity:

$$\mathcal{R} = x_1^{k_2} x_2^{k_3} x_3^{k_1}. \tag{4.6}$$

The non-trivial constant of motion $\mathcal{R}(t) = \mathcal{R}(0)$ governs the deterministic cCLV dynamics, characterised by regular oscillations associated with nested closed orbits surrounding $\vec{x}^*$ in the phase space simplex S_3 (Hofbauer *et al.* (1998), and trajectories flowing according to $1 \to 3 \to 2 \to 1$ (see Figure 4.1).

Given that the coexistence fixed point $\vec{x}^*$ is a centre and the orbits surrounding it (defined by conservation of (4.6)) are neutrally stable, the presence of demographic fluctuations change the dynamics predicted by (4.4) when $N < \infty$. In a finite population the cCLV dynamics is characterised by stochastic trajectories that follow the deterministic orbits of (4.4) for a short transient while performing a random walk between them until the boundary of S_3 is reached (see Figure 4.1). Hence, internal noise leads to the extinction of two species after a characteristic time that depends on N, while individuals of the third species survive (in this model, once the boundary is reached the fate of the system is known since

only one dominance-replacement reaction remains) (Reichenbach *et al.* (2006)). Hence the fixation probability ϕ_i^{cCLV} of species i is defined as the probability that individuals of species i take over, given initial densities $\vec{x}(0) = \vec{x^*}$ i.e.

$$\phi_i^{\text{cCLV}} = \lim_{t\to\infty} P(N_i(t) = N), \tag{4.7}$$

where the dependence on $\vec{x}(0)$ is dropped, since when N is not too small and $\vec{x^*}$ is sufficiently far from the boundary, ϕ_i^{cCLV} is independent of the initial condition. When the reactions rates k_i are equal, all species have the same fixation probability $\phi_i^{\text{cCLV}} = 1/3$, however, when the rates k_i are not equal the fixation probability depends non-trivially on the population size N.

In sufficiently large but finite populations, it was shown in Berr *et al.* (2009) that the fixation probabilities follow the 'law of the weakest' (LOW). This says that the species i that has the largest fixation probability is the one with the lowest dominance-replacement rate, k_i, the 'weakest species':

$$\phi_i^{\text{cCLV}} > \phi_j^{\text{cCLV}} \quad \text{if} \quad k_i < k_j \quad \text{for} \quad i \neq j \in \{1, 2, 3\}. \tag{4.8}$$

the LOW becomes a 'zero-one' law in the limit of very large populations (typically $N > 10^4$). Hence it predicts that the weakest species fixates the population with probability 1, at the expense of the others that go extinct. Hence when N is very large but finite the fixation probabilities follow:

$$\phi_i^{\text{cCLV}} = 1, \quad \phi_j^{\text{cCLV}} \to 0 \quad \text{if} \quad k_i < k_j \quad \text{for} \quad i \neq j \in \{1, 2, 3\}. \tag{4.9}$$

This was derived in Berr *et al.* (2009) by studying the effect of demographic fluctuations on the outermost deterministic orbit set by (4.6). The outermost orbit is defined as the one orbit for which the minimum distance to the boundary is $1/N$. If two species have the same reaction rate that is less than the other (e.g. $k_1 = k_2 < k_3$) the zero-one version of the LOW predicts that $\phi_3^{\text{cCLV}} \to 0$ and $\phi_{1,2}^{\text{cCLV}} = 1/2$ (see Figure 4.2). The LOW can be intuitively explained as follows: if species i has a high k_i, then it consumes the predator of its own predator, $i+1$ at a high rate. Hence it indirectly helps its predator $i-1$. Thus the species that benefits the most from this is the one has the lowest k_i, therefore consuming its predator's predator at the lowest rate.

In small population sizes a very different scenario emerges. Here the fixation probabilities follow the law of stay out (LOSO): the most likely species to fixate is one that predates on the species with the highest dominance-removal rate (the strongest species):

$$\phi_i^{\text{cCLV}} > \phi_{i+1,i-1}^{\text{cCLV}} \quad \text{if} \quad k_{i+1} > k_i, k_{i-1} \quad \text{for} \quad i \in \{1,2,3\}. \tag{4.10}$$

Unlike (4.9) this is a non-strict law, determining which is the *most likely* species to fixate for a given set of k_is, but never assigns a probability of 1 for any species. When $N = 3$ the LOSO explicitly yields $\phi_i^{\text{cCLV}} = r_i = k_{i+1}/(\sum_{i=1}^{3} k_i)$ (See Appendix C.5). The r_is are the rescaled reaction rates so that their sum is 1, in which the LOW and LOSO in S_3 can be conveniently visualised (see Figure 4.2). The LOSO can be explained as follows: a species is guaranteed to go extinct once all of its prey are dead. The species that is the most likely to do this is one with the highest k_i. In this case, $i+1$ is the first to go extinct, leaving $i-1$ and i remaining. Hence $i-1$ (the predator of the species with the highest k_i) then goes on to fixate the population.

In Berr *et al.* (2009) the authors carried out a detailed analysis of the fixation probabilities, and found that they follow the LOSO when $3 < N \lesssim 20$, while they are predominantly determined by the LOW when $N > 100$, with asymptotic zero-one behaviour when $N \gtrsim 10^4$. When $20 \lesssim N \lesssim 100$ the fixation probability interpolates between the LOSO and the LOW. These laws are both specific to three species cyclic competition, and are not observed in cyclic competition models of more than three species, where the situation is more complicated (see Durney *et al.* (2011); Knebel *et al.* (2013)). However, versions of the LOW have been found in other three species systems, such as the two-dimensional cCLV with mutation (Tainaka (1993)).

Another quantity of interest is the mean fixation time, t_{fix}, the mean time it takes for a species to fixate the population. This has been studied in Dobrinevski & Frey (2012); Reichenbach *et al.* (2006) where the presence of the conserved quantity $\mathcal{R}$ enables analytical techniques to show that it scales linearly with population size,

$$t_{\text{fix}} \sim N. \tag{4.11}$$

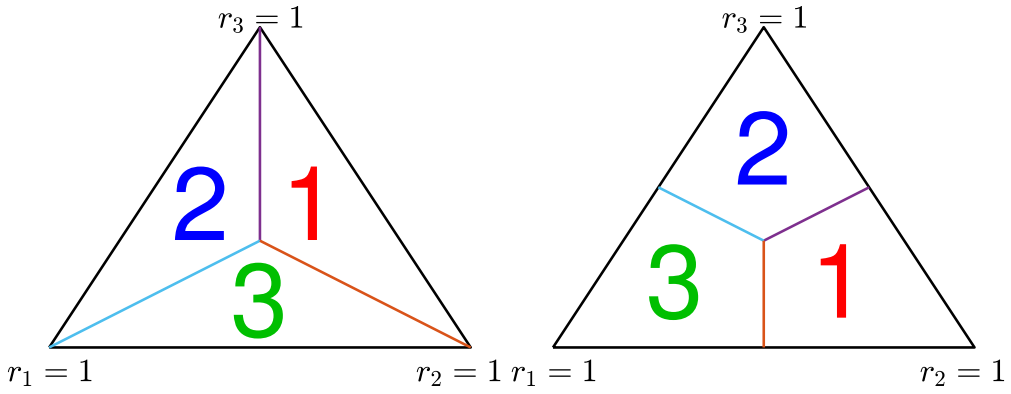

Figure 4.2: Law of the weakest (a) and law of stay out (b) in the simplex S_3 spanned by $r_i = k_i/(\sum_{i=1}^{3} k_i)$, divided into three regions where the most likely species to fixate is labelled. On the lines separating these regions, both adjacent species are equally likely to fixate. (a) Law of the weakest (LOW): In the large population sizes the most likely species to fixate is that with the lowest r_i. The LOW becomes asymptotically a zero-one law. (b) Law of stay out (LOSO) when all species initially coexist with the same density: For small population sizes no species is guaranteed to survive, but the most likely is the one which predates on the species with the largest r_i.

4.2 The May-Leonard Model (MLM)

Another common formulation of cyclic competition is the 'May-Leonard Model' (MLM), first introduced as a deterministic system in May & Leonard (1975). Since then it has been formulated as a stochastic process (Szolnoki *et al.* (2014)) as follows. Letting S_i denote an individual of species i there are nine reactions:

$$S_iS_{i+1} \xrightarrow{k} S_iS_i, \quad S_iS_{i+1} \xrightarrow{\sigma} S_i, \quad S_i \xrightarrow{b} S_iS_i, \quad i \in \{1,2,3\}, \tag{4.12}$$

where the indices are ordered cyclically (i.e. $S_{3+1} = S_1$ and $S_{1-1} = S_3$). The first reaction is the dominance-replacement reaction introduced for the cCLV, where in this case the rates for different species are equal. The second is a dominance-removal reaction, another form of cyclic dominance where the weaker species is killed and not replaced. The final reaction corresponds to birth of species i, and its rate is proportional to $\left(1 - \sum_{i=1}^{3} N_i/K\right)$, where K is the carrying capacity of the system. Thus, rather than having separate birth and death reactions for each species, the logistic growth is included in the birth rate: if the total population size is at the carrying capacity, $(\sum_{i=1}^{3} N_i = K)$ the birth transition rates for all species are zero, and the total population size never goes above K. The reason for this is that this model is typically formulated in a spatial system, where each node has a maximal number of occupants. With the birth rates set like this, no modifications need to be made between the well mixed and spatial setting. As you can see this is a more general model of cyclic competition, and coincides with the cCLV when $b = \sigma = 0$.

In the limit of $K \to \infty$, the mean field equations for the population densities N_i/K can be written as:

$$\frac{dx_i}{dt} = x_i\left[1 - x_i - (1-k)x_{i+1} - (1+k+\sigma)x_{i-1}\right]. \tag{4.13}$$

Where without loss of generality we specify $b = 1$[1]. These coincide with those of May & Leonard (1975) with different parameter labels. Using these results, we can deduce that in addition to the trivial unstable extinction state $[0,0,0]^{\mathrm{T}}$ this

[1] if $0 < b \neq 1$ we can rescale time as $t \to bt$ and the other rates $k \to k/b$, $\sigma \to \sigma/b$ to find the same mean field equations.

system of equations has steady states $\vec{e}_i$, $i \in \{1,2,3\}$ corresponding to the extinction of all but one species which are saddles (with eigenvalues $(-1, k, -(k+\sigma))$), and a coexistence steady state $\vec{x^*} = [1,1,1]^{\mathrm{T}}/(3+\sigma)$, whose stability depends on the parameter σ: the eigenvalues are -1 and $\frac{1}{2}(\sigma \pm i\sqrt{3}(\sigma+2k))/(3+\sigma)$ so it is a neutrally stable centre when $\sigma = 0$. In this case the dynamics is characterised by a family of neutrally stable orbits along which, as in the cCLV, the quantity $\mathcal{R}(t) = x_1 x_2 x_3$ is conserved. Trajectories approach one of these asymptotically, due to the presence of empty spaces, the density of which decreases over time (May & Leonard (1975)). When $\sigma > 0$ the coexistence fixed point is unstable, and trajectories are attracted to a heteroclinic cycle between the fixation fixed points $\vec{e}_i$, spending progressively longer times in their vicinity but never reaching them (May & Leonard (1975); Postlethwaite & Rucklidge (2017)). The time taken to complete each cycle is a factor of $\frac{\sigma+k}{k}$ longer than the last (Postlethwaite & Rucklidge (2019)). It has also been shown that the heteroclinic cycles become degenerate when $k = 0$, in the sense that the eigenvalues of the fixation fixed points are $(-1, 0, -\sigma)$, so they are neither stable nor unstable, but a small change in the parameter k would lead to either stability or instability May & Leonard (1975).

A further consideration is the presence of mutations, since there is evidence that these occur in the two biological applications of these models: *E. coli* bacteria are known to mutate (Kerr *et al.* (2002)), and *U. stansburiana* lizards can undergo throat colour transformations (Sinervo *et al.* (2000)). The above reactions (4.12) are therefore supplemented with six further mutation reactions:

$$S_i \xrightarrow{\mu} \begin{cases} S_{i-1} \\ S_{i+1} \end{cases} \qquad \text{for} \quad i \in \{1,2,3\} \tag{4.14}$$

and the mean field equations become

$$\frac{dx_i}{dt} = x_i\left[1 - x_i - (1-k)x_{i+1} - (1+k+\sigma)x_{i-1}\right] + \mu\left(x_{i-1} + x_{i+1} - 2x_i\right). \tag{4.15}$$

This has a dramatic effect on the stability of the coexistence fixed point due to a supercritical Hopf bifurcation when $\mu = \mu_{\mathrm{H}} = \frac{\sigma}{6(3+\sigma)}$ (Mobilia (2010); Mobilia *et al.* (2016); Szczesny *et al.* (2013, 2014); Szolnoki *et al.* (2014)). The coexistence fixed point is a stable focus when $\mu > \mu_{\mathrm{H}}$, while it is unstable when $\mu < \mu_{\mathrm{H}}$ where

the dynamics is characterised by a stable limit cycle with frequency $\omega_{\mathrm{H}} = \frac{\sqrt{3}(\sigma+2k)}{2(3+\sigma)}$ (Mobilia (2010); Szczesny *et al.* (2013); Szolnoki *et al.* (2014)). It should also be noted that it was shown in Toupo & Strogatz (2015) that stable limit cycles can also be observed in the deterministic dynamics when a subset of the reactions (4.14) are added to the MLM. Here the value of μ for which the Hopf bifurcation happens depends inversely on the number possible mutation pathways.

In finite systems, $K < \infty$, demographic fluctuations cause deviations from these trajectories, and fixation of one species is guaranteed when there are no mutations. In this case, as for the cCLV the fixation probabilities are characterised by the LOW in large finite populations, and the LOSO in small populations. The time to fixation has been shown via simulations to scale logarithmically with the carrying capacity K (Rulands *et al.* (2013)).

4.3 Rock-Paper-Scissors Games with Spatial Structure

While it is not the focus of thesis, it is worth giving a brief overview of cyclic competition with spatial structure due to the interesting dynamics this can lead to. This is because in many biological applications (*e.g.* biofilms) each individual interacts with its neighbours, rather than the whole population. This locality of interactions and the ability of individuals to move become important factors in determining the outcome of rock-paper scissors models, in some cases leading to pattern formation and long-time coexistence of all three species. Unless specified, in the following I consider the cases without mutations.

The simplest form of spatial structure is a 1-D lattice, where each individual interacts with its two adjacent neighbours. In this case, when the individuals are immobile, fixation occurs in a time that scales algebraically with N, with the weaker species prevailing in large systems (Frachebourg *et al.* (1996a,b); He *et al.* (2010); Provata *et al.* (1999)). However, mobility of individuals in the form of pair exchange (two neighbours swap places: $S_iS_j \xrightarrow{\gamma_e} S_jS_i$, for $i \neq j \in \{1,2,3\}$) leads to a stable coexistence state when γ_e is sufficiently large (Venkat & Pleimling (2010)).

On regular (i.e. all individuals have the same number of neighbours) 2-D square lattices, the result is primarily dependent on the form of cyclic competition being considered and the presence of mobility. This can take two forms: pair exchange (defined above) and hopping, where an individual moves into an adjacent empty space with rate γ_{h} (i.e. $S_i\emptyset \xrightarrow{\gamma_{\mathrm{h}}} \emptyset S_i$, for $i \in \{1,2,3\}$, $\emptyset$ representing an empty lattice site). In the MLM ($\sigma, b > 0$) the outcome is highly dependent on the presence and type of mobility. If the populations are immobile, the dynamics is characterised by clusters similar to the cCLV (see below). However the presence of mobility has a profound effect on the system dynamics: when the rates of pair exchange and hopping are equal, the diffusion is linear (Dobramysl *et al.* (2018)). When the dominance-reproduction rate $k = 0$, low mobility promotes species coexistence through the spontaneous formation of spiral waves. The spirals grow in size with increasing mobility, until they reach a critical threshold, effectively outgrowing the system size leading to a loss in biodiversity (Reichenbach *et al.* (2007a,b, 2008)). When $k \neq 0$ the result is more complicated, and mobility can lead to spiral waves of various stabilities (Reichenbach & Frey (2008)). When the presence of mutations was considered in Mobilia *et al.* (2016) and the lattice was extended to a metapopulation model (i.e. each node on a lattice is now a well mixed patch with carrying capacity N, intra-species reactions occur within a patch and mobility occurs between adjacent patches), the authors found four phases dependent on a variable c, which is a complicated function of the system parameters (eq. (6) of Mobilia *et al.* (2016)). These four phases characterise the different types of stability of spiral waves, which are also observed when $\gamma_{\mathrm{e}} \neq \gamma_{\mathrm{h}}$ and the diffusion is non-linear (although the situation is slightly different, see Szczesny *et al.* (2013, 2014)). Further characterisation of the spiral waves in spatial rock-paper-scissors games can also be found in Hasan *et al.* (2019); Postlethwaite & Rucklidge (2017, 2019).

In the cCLV, when the dominance-replacement rates k_i are of the same order the dynamics is characterised by clusters of the same species that invade clusters of their prey and are in turn invaded by clusters of their predator. Hence the species coexist in a long-lived quasi-stationary state, but they do not form coherent patterns (He *et al.* (2010); Peltomäki & Alava (2008)). However, spiral patterns similar to those observed in the spatially extended MLM and plane

waves are observed in off-lattice (i.e. continuous-space) simulations when the interaction range and total species density is large enough (Avelino *et al.* (2018); Ni *et al.* (2010)). In this case, the effect of mobility is dependent on the interaction range: beyond a critical interaction range mobility always jeopardises coexistence. However below this, and above a critically small interaction range (so small that the individuals in effect do not interact) coexistence is promoted by an intermediate value of mobility. These features are also observed in off-lattice MLM models (Ni *et al.* (2010)).

Finally, RPS games have also been studied on random and complex networks, which are particularly relevant for behavioural sciences. This is an even further departure from the focus of this thesis, but I will briefly note that cCLV dynamics on small-world networks (i.e. low connectivity between individuals) is characterised by limit cycles and noisy oscillations of the species densities (see e.g. Sato *et al.* (1997); Szabó *et al.* (2004); Szolnoki & Szabó (2004); Tainaka (1994)), while more general reviews for the interested reader can be found in Perc & Szolnoki (2010); Szabó & Fath (2007); Szolnoki *et al.* (2014).

4.4 The Birth-Death Cyclic Lotka-Volterra Model (BDCLV)

In this section I will describe a new formulation of cyclic competition. This is motivated by the desire for a model in which the total population size can fluctuate in time (unlike the cCLV where the total population size is fixed) in a logistic but unbounded manner (unlike the MLM which has a maximum total population size). In contrast to the cCLV and MLM here there are no dominance-replacement or dominance-removal reactions. Instead there are three birth and three death reactions, with the cyclic competition entering via the birth rates. As we will see this allows for a fluctuating total population size around a carrying capacity, which can be exceeded. Using game-theoretic formulation, the underpinning cyclic competition is described in terms of the payoff matrix (Broom & Rychtár (2013); Claussen & Traulsen (2008); Dobramysl *et al.* (2018); Galla (2011); Hofbauer *et al.* (1998); Mobilia (2010); Nowak (2006a); Smith (1982); Szabó & Fath

(2007); Toupo & Strogatz (2015)):

$$\mathcal{P} = \begin{array}{c|ccc} \text{Species} & 1 & 2 & 3 \\ \hline 1 & 0 & r_1 & -r_3(1+\epsilon) \\ 2 & -r_1(1+\epsilon) & 0 & r_2 \\ 3 & r_3 & -r_2(1+\epsilon) & 0 \end{array}$$

Here, $0 < r_i = \mathcal{O}(1)$, $\sum_{i=1}^{3} r_i = 1$, and $\epsilon > -1$. According to $\mathcal{P}$, intraspecies interactions do not provide a payoff, while an individual of species i gains a payoff r_i against an $(i+1)$ individual and suffers a negative payoff of $-r_{i-1}(1+\epsilon)$ against an $(i-1)$ individual, where the indices are, as before, ordered cyclically. With a slight change in terminology to the cCLV and MLM, species $(i+1)$ is referred to as the 'weak opponent' of species i and $(i-1)$ as the 'strong opponent'. When $\epsilon \neq 0$, $\mathcal{P}$ describes the general non-zero-sum RPS game where the payoff that i receives against $(i+1)$ differs from what $(i+1)$ loses (Claussen & Traulsen (2008); Dobramysl *et al.* (2018); Galla (2011); He *et al.* (2011); May & Leonard (1975); Mobilia (2010); Mobilia *et al.* (2016); Postlethwaite & Rucklidge (2017); Reichenbach *et al.* (2007a,b, 2008); Szczesny *et al.* (2013, 2014); Szolnoki *et al.* (2014); Yang *et al.* (2017)).

As for the cCLV and MLM, it is convenient to discuss the dynamics in terms of the species densities $x_i = N_i/N$, where $N = \sum_{i=1}^{3} N_i$, that span the phase space simplex S_3. The expected payoff for species i, Π_i, and the average population payoff, $\bar{\Pi}$, are:

$$\Pi_i = (\mathcal{P}\vec{x})_i = r_i x_{i+1} - r_{i-1}(1+\epsilon)x_{i-1}, \tag{4.16}$$

$$\bar{\Pi} = \vec{x} \cdot \mathcal{P}\vec{x} = -\epsilon \sum_{i=1}^{3} r_i x_i x_{i+1}, \tag{4.17}$$

where $\vec{x} = (x_1, x_2, x_3)^{\mathrm{T}}$. As is common in evolutionary game theory, the fitness of each species f_i are defined as a linear function of the expected payoff Π_i[1] (Broom

[1]Non-linear dependence is also sometimes used, as in the Fermi Process (Blume *et al.* (1993); Claussen & Traulsen (2008); Hauert & Szabó (2005); Szabó & Hauert (2002); Szabó & Tőke (1998); Traulsen *et al.* (2006)). However note that features of RPS models are robust to changes in the microscopic update details (Claussen & Traulsen (2008)).

& Rychtár (2013); Hofbauer *et al.* (1998); Nowak (2006a); Szabó & Fath (2007)):

$$f_i = 1 + s\Pi_i \quad \text{and} \tag{4.18}$$

$$\bar{f} = \sum_{i=1}^{3} x_i f_i = 1 + s\bar{\Pi} \quad \text{(average fitness)}, \tag{4.19}$$

where $s \geq 0$ is a parameter measuring the contribution to the fitness arising from $\mathcal{P}$ i.e. the strength of the cyclic interactions. When $s \ll 1$ (weak selection) species have similar fitnesses, regardless of the composition, whereas the cyclic dominance dominates when $s = \mathcal{O}(1)$ (strong selection). When $\epsilon = 0$ the average fitness $\bar{f} = 1$.

The reactions in the BDCLV are defined as:

$$N_i \xrightarrow{T_i^+} N_i + 1 \quad \text{and} \quad N_i \xrightarrow{T_i^-} N_i - 1, \quad \text{with} \quad i \in \{1, 2, 3\}. \tag{4.20}$$

where the first set of reactions corresponds to the birth of an individual of species i and the others are associated with the death of an i-individual. These reactions occur with transition rates:

$$T_i^+ = f_i N_i = (1 + s\Pi_i)N_i = (1 + \{\alpha_i x_{i+1} - \alpha_{i-1}(1+\epsilon)x_{i-1}\})N_i \quad \text{and} \tag{4.21}$$

$$T_i^- = \frac{N}{K} N_i, \tag{4.22}$$

where $N = \sum_{i=1}^{3} N_i$ is the total population size, K is the carrying capacity, $\sum_{i=1}^{3} r_i = 1$ and $\alpha_i = s r_i$. The birth rates, T_i^+ are as usual the per-capita fitnesses multiplied by the relevant population size, and the death rates are dependent on the total population density and relevant population size. Also note that I consider $0 \leq s \leq 1/(1+\epsilon)$ to ensure that $T_i^+ \geq 0$. It is worth noting that this is not the only formulation of the transition rates. Another possibility would be to define T_i^- as above but rescale the birth rate by the average fitness (as in Chapter 3), $T_i^+ = f_i N_i / \bar{f}$. When $\epsilon = 0$ this would coincide with (4.21), but a difference would arise when $\epsilon \neq 0$ and $\bar{f} = 1 - \epsilon \sum_{i=1}^{3} \alpha_i x_i x_{i+1}$. In this case, the mean field rate equations (4.37) would be rescaled by the non-linear term $1/\bar{f}$, and would no longer coincide with replicator equations of the general rock-paper-scissors game

(Broom & Rychtár (2013); Hofbauer *et al.* (1998)), agreeing only to leading order in $s\epsilon$.

The master equation describing the probability $P(\vec{N},t)$ find the population in state $\vec{N}=(N_1,N_2,N_3)^{\mathrm{T}}$ at time t is given by (Gardiner (1985); Van Kampen (1992)):

$$\frac{dP(\vec{N},t)}{dt}=\sum_{i=1}^{3}\left(\mathbb{E}_i^{-}-1\right)\left[T_i^{+}P(\vec{N},t)\right]+\sum_{i=1}^{3}\left(\mathbb{E}_i^{+}-1\right)\left[T_i^{-}P(\vec{N},t)\right], \tag{4.23}$$

where $\mathbb{E}_i^{\pm}$ are shift operators, associated with (4.21), such that $\mathbb{E}_1^{\pm}h(N_1,N_2,N_3,t)=h(N_1\pm1,N_2,N_3,t)$ etc, for any $h(\vec{N},t)$. We also specify that $P(\vec{N},t)=0$ whenever any $N_i<0$. The process is characterised by a first stage when all three species coexist, then a second stage where two species compete. This is in contrast to the cCLV and MLM where the species that will fixate the population is known once the first species has died out. Finally, the third stage is characterised by the one remaining species fluctuating around the carrying capacity K according to the logistic birth-death process (see Section 2.2). The population will finally collapse into the only absorbing state $\vec{N}=\vec{0}$. However, as discussed in Section 2.2 the time-scale for this scales exponentially with K, so I will focus on the first two stages. First I will consider the case $\epsilon=0$ (zero-sum BDCLV) in the next section (Section 4.4.1), then the case $\epsilon\neq0$, $|\epsilon|\ll1$ in Section 4.4.2 (close-to-zero-sum BDCLV).

In presenting the results, I will focus on the general case where the r_is are unequal[1], unless otherwise stated. All subsequent figures have been obtained with initial fraction 1/3 of each species $\vec{x}_0=(1/3,1/3,1/3)^{\mathrm{T}}=\vec{x}_c$, and I consider two parameter sets: $\vec{r}\equiv(r_1,r_2,r_3)=\vec{r}^{(1)}\equiv(1,5,5)/11$ and $\vec{r}=\vec{r}^{(2)}\equiv(3,1,1)/5$. These choices suffice to reveal most of the generic properties of the system. When I study how $\phi_{i,i+1}$, ϕ_i and $\widetilde{\phi}_i$ depend on sK, in Figures 4.5 and 4.6 I consider $K\in\varkappa\equiv\{1000,450,250,90,50\}$ and $s=1$ for $K=1000$, $s\in\{10^{-k/4},k=0\ldots3\}$ for $K=450$, $s\in\{10^{-(2+k)/4},k=0\ldots9\}$ for $K=250$, $s\in\{10^{-k/4},k=0\ldots8\}$ for $K=90$, and $s\in\{10^{-(9+k)/4},k=0\ldots3\}$ for $K=50$. In all figures (except Figures 4.3 and 4.4), simulation results have been sampled over 10^4-10^5 realizations.

[1]The overall fixation probabilities are trivially 1/3 when the rates are equal

4.4.1 Zero-Sum BDCLV

When $\epsilon = 0$, $\mathcal{P}$ corresponds to the zero-sum rock-paper-scissors game, as in the cCLV, where i gains exactly what $(i+1)$ loses (Berr *et al.* (2009); Dobramysl *et al.* (2018); Dobrinevski & Frey (2012); Frean & Abraham (2001); He *et al.* (2010); Hofbauer *et al.* (1998); Ifti & Bergersen (2003); Knebel *et al.* (2013); May & Leonard (1975); Nowak (2006a); Perc & Szolnoki (2010); Reichenbach *et al.* (2006); Smith (1982); Szabó & Szolnoki (2002); Tainaka (1989, 1993, 1994); Venkat & Pleimling (2010); West *et al.* (2018)). The average payoff and fitness are given by $\bar{\Pi} = 0$ and $\bar{f} = 1$, and the mean field equations (where demographic fluctuations are ignored) can be found by using the results of Sec. 2.1.2:

$$\frac{d}{dt}N = N\left(1 - \frac{N}{K}\right), \tag{4.24}$$

$$\frac{d}{dt}x_i = s\Pi_i x_i = x_i\left(\alpha_i x_{i+1} - \alpha_{i-1}x_{i-1}\right). \tag{4.25}$$

These equations are decoupled, and from (4.24) we see that the total population size follows the logistic equation, and $N(t) \to K$ in a time of order $\mathcal{O}(1)$, while (4.25) show that the population composition changes due to cyclic dominance on a time scale of $1/s$ so that when $s << 1$ there is timescale separation: N rapidly approaches K while the population composition evolves much slower. When time is rescaled ($t \to st$), the rate equations (4.25) coincide with the celebrated replicator equations of the zero-sum RPS game (Broom & Rychtár (2013); Hofbauer *et al.* (1998); Nowak (2006a); Smith (1982); Szabó & Fath (2007)). As for the cCLV (Section 4.1) these are characterised by the neutrally stable fixed point $\vec{x}^* = (r_2, r_3, r_1)^{\mathrm{T}}$ and three unstable saddle points $\{\vec{e}_i\}_{i=1}^3$, with the additional unstable extinction state $\vec{0}$. They also conserve $x_1 + x_2 + x_3 = 1$ and $\mathcal{R}$ (4.6), so the deterministic trajectories in the phase space S_3 are neutrally stable orbits around $\vec{x}^*$, along which $\mathcal{R}$ is constant.

In finite populations, trajectories are noisy oscillations around $\vec{x}^*$ performing a random walk between the deterministic orbits until the boundary, ∂S_3 is hit (see Figures 4.3 and 4.4). This first stage of dynamics (Stage 1) where three species coexist is followed by Stage 2, where in contrast to the cCLV the fate of the system is still not known: the two surviving species (say i and $i+1$) compete

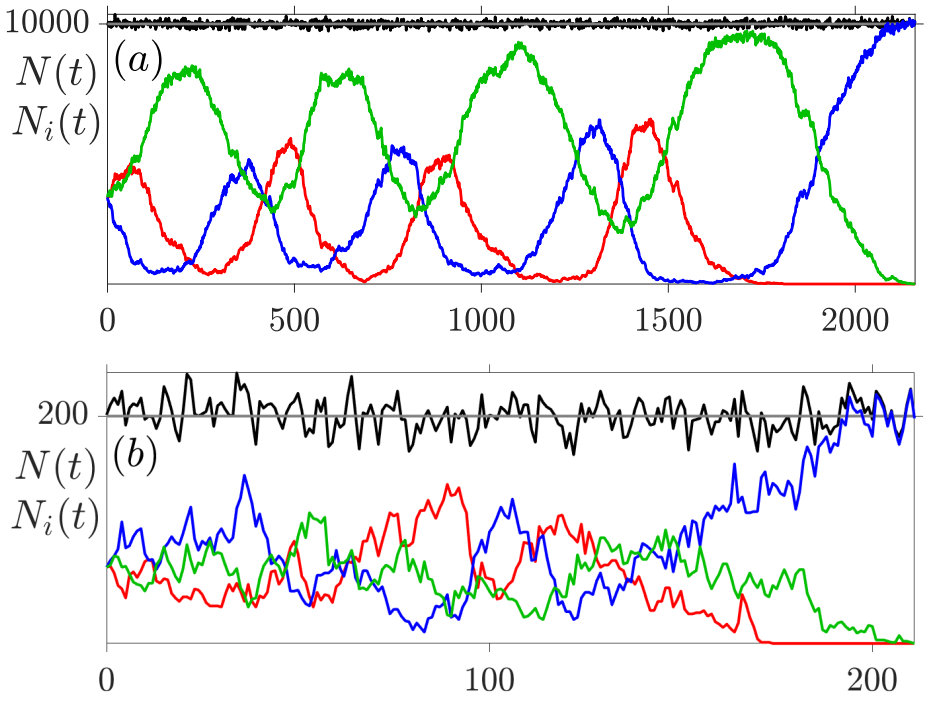

Figure 4.3: Sample paths of $N(t)$ (black) and $N_i(t)$ ($i = 1, 2, 3$ shown by red, blue green respectively) in the BDCLV with constant carrying capacity $K = 10^4$ (a) and $K = 200$ (b) indicated by solid grey lines. Parameters are $(s, r_1, r_2, r_3) = (0.1, 0.6, 0.2, 0.2)$. $N(t)$ quickly fluctuates around K, while N_i evolve on a much slower timescale.

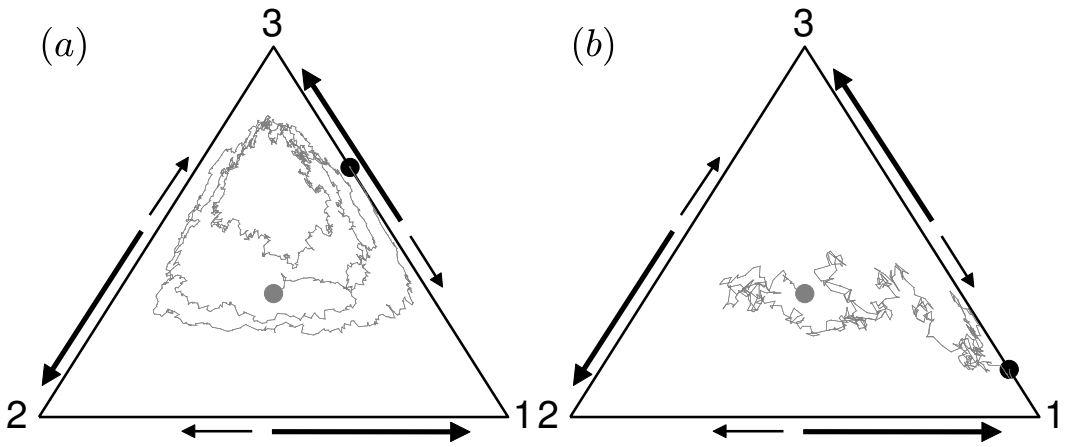

Figure 4.4: Stochastic orbits in S_3 of the constant-K BDCLV of, with $(s, r_1, r_2, r_3) = (1/10, 3/5, 1/5, 1/5)$ and illustration of Stages 1 and 2 dynamics, see text. Initially all species have the same density 1/3 (gray dot), and (a) $K = 10^4$, (b) $K = 200$. (a) In Stage 1, when $sK \gg 1$, erratic trajectories approach ∂S_3 from the outermost orbit (deterministic orbit at a distance $1/K$ from ∂S_3, see text). (b) When $sK \lesssim 10$, in Stage 1, stochastic trajectories reach ∂S_3 without settling onto the outermost orbit. Stage 2: Once on an edge of ∂S_3 (black dot), a competition (shown as arrows) takes place between species i and its weak opponent $i + 1$, with the former (long arrows) more likely to win than the latter (short arrows), see text.

along the $(i, i+1)$ edge of S_3 until one fixates the system (see Fig. 4.4). This affects the fixation probabilities: the LOW and LOSO are still applicable, but in different situations to the cCLV, as I will now discuss.

In order to do this, first note that after a short transient $N(t) \approx K$, suggesting a relationship with models of cyclic competition that preserve total population size. Replacing the three birth and three death reactions with six dominance-replacement reactions where an individual of type i replaces one of type j with rate $T_{ji} = T_i^+ T_j^- / K$ and $i \neq j$, we define the Moran CLV (MCLV). This is further formalised in Appendix C.1, where it is shown that the fixation properties are the same in the MCLV and BDCLV for $K \gg 1$. Furthermore, in Appendix C.2 it is shown that with a suitable rescaling of time, the drift and diffusion terms of the Fokker-Plank equations for the MCLV and cCLV can be mapped onto each other. Thus, before the extinction of the first species (Stage 1), the dynamics of the BDCLV is similar to the dynamics of the cCLV with population of size $\mathcal{O}(sK)$. In Stage 2, the absorption properties of the BDCLV when $K \gg 1$ can are the same as those for the MCLV (see Appendix C.1).

A further complication is that unlike the cCLV, the fate of the system is not known once the first species dies out. Hence to calculate the fixation probability of species i, $\widetilde{\phi}_i$, we need to find the probability it survives Stage 1, as either the stronger ($\phi_{i,i+1}$) or weaker ($\phi_{i-1,i}$) remaining species (survival probabilities). Then, in Stage 2 we need to find the probability that it wins the remaining two player competition game, ϕ_i when it is the stronger species, and $1 - \phi_{i-1}$ when it is the weaker (absorption probabilities). The relationship between the cyclic selection strength s and carrying capacity K allows us to identify three regimes:

(i) *quasi-neutrality*, when $sK \ll 1$ and $K \gg 1$: here the selection strength is too weak to have an effect on the dynamics, so they are completely driven by demographic fluctuations.

(ii) *weak selection*, when $sK \approx 10$, $s \ll 1$ and $K \gg 1$: here the selection intensity is weak and comparable to that of the demographic fluctuations.

(iii) *strong selection*, when $sK \gg 1$, $s = \mathcal{O}(1)$ and $K \gg 1$: here the selection intensity is much stronger than that of the demographic fluctuations.

Stage 1: Survival probabilities in the BDCLV

Using the fact that the Stage 1 dynamics of the BDCLV and cCLV with $N = sK$ are similar, the survival probabilities in the BDCLV, $\phi_{i,i+1}$ are therefore similar to the fixation probabilities of species i in the cCLV (ϕ_i^{cCLV}), and one can use the LOSO and LOW to determine $\phi_{i,i+1}$ in regimes (ii) and (iii):

(i) When $sK \ll 1$ and $K \gg 1$ the system is in quasi-neutrality, and since we always start with an equal fraction of each species we find that $\phi_{i,i+1} \approx 1/3$ $\forall i$.

(ii) When $sK \approx 10$, $s \ll 1$ and $K \gg 1$ the selection intensity is weak and comparable to that of the demographic fluctuations. We use the relationship with cCLV to infer that $\phi_{i,i+1}$ is given by the fixation probability of i in the cCLV with $N = sK \approx 10$. i.e. in this regime the survival probabilities follow the *law of stay out*:

$$\begin{aligned} &\phi_{i-1,i} > \phi_{i,i+1}, \phi_{i+1,i-1} \quad \text{if} \quad r_i > r_{i\pm1} \\ &\phi_{i,i+1} \approx \phi_{i+1,i-1} > \phi_{i-1,i} \quad \text{if} \quad r_{i+1} = r_{i-1} > r_i. \end{aligned} \tag{4.26}$$

Hence, when $r_i > r_{i\pm1}$ the $(i-1,i)$ edge is the most likely to be hit first, as confirmed by Fig. 4.5(b), and when $r_i < r_{i-1} = r_{i+1}$ the edges $(i, i+1)$ and $(i+1, i-1)$ are the mostly likely to be hit first see Fig. 4.5(a).

(iii) When $sK \gg 1$, $s = \mathcal{O}(1)$ and $K \gg 1$ the dynamics is governed by cyclic dominance: an edge of S_3 is hit from the outermost orbit, see Fig. 4.4(a). Using the relationship between the BDCLV and cCLV, we have $\phi_{i,i+1}$ is given by the fixation probability of species i in the cCLV with $N = sK$ and the survival probabilities obey the *law of the weakest*:

$$\begin{aligned} &\phi_{i,i+1} > \phi_{i+1,i-1}, \phi_{i-1,i} \text{ if} \quad r_i < r_{i\pm1}, \\ &\phi_{i,i+1} \approx \phi_{i+1,i-1} > \phi_{i-1,i} \text{ if} \quad r_i = r_{i+1} < r_{i-1}. \end{aligned} \tag{4.27}$$

When $sK \gtrsim 10^3$, the LOW becomes asymptotically a zero-one law: $\phi_{i,i+1} \to 1, \phi_{i-1,i} \to 0$ and $\phi_{i+1,i-1} \to 0$ if $r_i < r_{i\pm1}$, and $\phi_{i,i+1} = \phi_{i+1,i-1} \to 1/2, \phi_{i-1,i+1} \to 0$ if $r_i = r_{i+1} < r_{i-1}$. Accordingly, when $sK \gg 1$ and

$r_i < r_{i\pm1}$ species i and $i+1$ are most likely to survive and species $i-1$ the most likely to die out in Stage 1, in agreement with Fig. 4.5 (a). Similarly, when $r_i > r_{i-1} = r_{i+1}$, species i is the most likely to die out first, see Fig. 4.5 (b).

These relations (4.26) and (4.27) explain that $\phi_{i,i+1}$ is a function of sK, and can exhibit non-monotonic behaviour: In Figure 4.5(a), where $r_1 < r_2 = r_3$ (4.26) give that $\phi_{1,2} \approx \phi_{2,3} > \phi_{3,1}$ in regime (ii), while (4.27) predicts that $\phi_{1,2} > \phi_{2,3}, \phi_{3,1}$ in regime (iii). Hence $\phi_{1,2}$ and $\phi_{3,1}$ increase and decrease respectively from regime (i) to (iii), while $\phi_{2,3}$ increases from regime (i) to (ii), then decreases from (ii) to (ii). Similarly in Figure 4.5(b), where $r_1 > r_2 = r_3$ (4.26) give that $\phi_{1,2} \approx \phi_{2,3} < \phi_{3,1}$ in regime (ii), while (4.27) predicts that $\phi_{1,2} < \phi_{2,3} = \phi_{3,1}$ in regime (iii). Hence $\phi_{1,2}$ decreases from regime (i) to (iii), while $\phi_{2,3}$ decreases from regime (i) to (ii), then increases from (ii) to (ii). The non-monotonicity of $\phi_{3,1}$ can be seen by noting that due to the behaviour of the other two survival probabilities, $\phi_{3,1}$ must increase from regime (i) to (ii) and then decrease from (ii) to (iii).

Stage 2: Absorption probabilities in the constant-K BDCLV

At start of Stage 2, species i competes against $i+1$ (weak opponent), along the edge $(i, i+1)$ where their fitnesses are $f_i = 1 + \alpha_i(1 - x_i)$ and $f_{i+1} = 1 - \alpha_i x_i$. Stage 2 ends with the absorption of either i or $i+1$, respectively with probability ϕ_i and $1 - \phi_i$.

(i) At quasi neutrality, species i's selective advantage is negligible since $f_i - f_{i+1} = \alpha_i \ll 1$. In regime (i), species i and $i+1$ have therefore almost the same absorption probability $\phi_i \approx 1/2$.

(iii) Under strong selection, species i has an important selective advantage over species $i+1$: $f_i - f_{i+1} = \mathcal{O}(1)$. In regime (iii), species i is almost certain to be absorbed as in Stage 2 of the cCLV dynamics, and therefore $\phi_i \approx 1$ as predicted by the LOW.

(ii) Under weak selection, ϕ_i is non-trivial and can be obtained from the fixation probability $\phi_i|_K$ of species i in the MCLV with $N = K$ (see Appendix

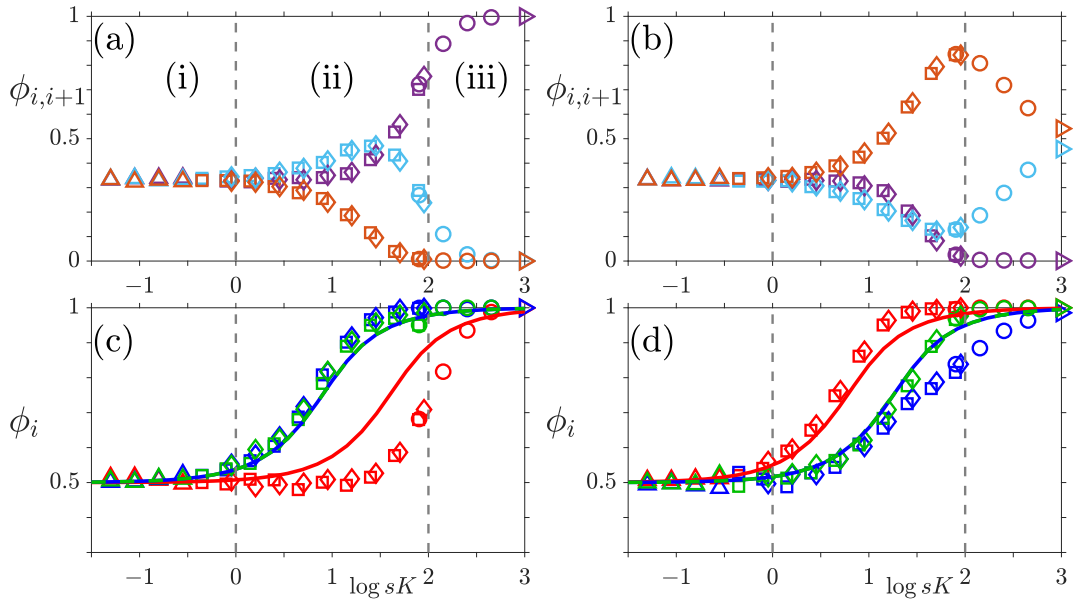

Figure 4.5: (a,b) Constant-K BDCLV survival probabilities simulation results ($\Diamond$): $\phi_{1,2}$ (purple), $\phi_{2,3}$ (light blue) and $\phi_{3,1}$ (orange) vs. sK for values of $s \in (10^{-3}, 1)$ and $K \in \varkappa$ in regimes (i)-(iii) separated by dashed lines, see text. Non-monotonicity arises across regimes (ii) and (iii) and can be explained in terms of the LOSO (regime (ii)) and LOW (regime (iii)), see text. (a) $\vec{r} = \vec{r}^{(1)}$; species 1 and 3 are the most likely to die out in regime (ii) and (iii), respectively. (b) $\vec{r} = \vec{r}^{(2)}$; species 2 and 1 are the most likely to die out in regime (ii) and (iii), respectively. (c,d) Constant-K BDCLV absorption probabilities ϕ_i vs. sK: ϕ_1 (red), ϕ_2 (blue) and ϕ_3 (green) vs. sK for $K = (1000, 450, 250, 50, 20)$, with (c) $\vec{r} = \vec{r}^{(1)}$ and (d) $\vec{r} = \vec{r}^{(2)}$. The solid line is given by (4.31) and coincide for species 2 and 3. In all panels $K = 1000$ ($\triangleright$), 450 ($\circ$), 250, ($\diamond$), 90 ($\square$), 50 ($\triangle$), $\epsilon = 0$, $\vec{x}_0 = \vec{x}_c$.

C.1 and 2.1.1). When the Stage 2 dynamics starts with a fraction $\hat{x}_i$ of individuals of species i, $\phi_i|_K$ under weak selection is obtained from (2.18), with $A(x_i) = \alpha_i x_i(1-x_i)$ and $B(x) = \frac{A(x)}{K\alpha_i}\left[2+\alpha_i\left(1-2x_i\right)\right]$ to give:

$$\phi_i(\hat{x}_i)|_K = \frac{\left(2+\alpha_i\right)^{K+1} - \left[2+\alpha_i\left(1-2\hat{x}_i\right)\right]^{K+1}}{\left(2+\alpha_i\right)^{K+1} - \left(2-\alpha_i\right)^{K+1}}. \tag{4.28}$$

When $s \ll 1$, we retrieve the familiar exponential expression:

$$\phi_i(\hat{x}_i)|_K \simeq \frac{1-e^{-\alpha_i K \hat{x}_i}}{1-e^{-\alpha_i K}}. \tag{4.29}$$

A difficulty arises from $\hat{x}_i$ being a random variable depending on the outcome of Stage 1: $\hat{x}_i$ is distributed according to the probability density $P_{(i,i+1)}(\hat{x}_i)$. The absorption probability is thus obtained by averaging (4.29) over $P_{(i,i+1)}$:

$$\phi_i \simeq \phi_i|_K = \int_0^1 P_{(i,i+1)}(\hat{x}_i)\ \phi_i(\hat{x}_i)|_K\ d\hat{x}_i. \tag{4.30}$$

In practice, $P_{(i,i+1)}(\hat{x}_i)$ is obtained from stochastic simulations, see Appendix C.3. Analytical progress can be made by noticing that in regime (ii) where $s \ll 1$ and $sK \lesssim 10$, each pair $i, i+1$ has approximately the same survival probability at the end of Stage 1 ($\phi_{i,i+1} \approx 1/3$, see Figure 4.5 (a,b)), and the initial distribution along $(i, i+1)$ can be assumed to be uniform, i.e. $P_{i,i+1}(\hat{x}_i) \approx 1$, see Appendix C.3. Substituting in Eq. (4.30), we obtain the approximation ($s \ll 1, sK \lesssim 10$):

$$\phi_i \simeq \phi_i|_K \approx \frac{e^{-\alpha_i K} + \alpha_i K - 1}{\alpha_i K(1-e^{-\alpha_i K})}, \tag{4.31}$$

which is an S-shaped function of $\alpha_i K$ that correctly predicts the behaviours $\phi_i \to 1/2$ when $\alpha_i K \ll 1$ (regime (i)) and $\phi_i \to 1$ when $\alpha_i K \gg 1$ (regime (iii)), see Figure 4.5 (c,d). Comparison with simulation results of Figure 4.5 (c,d) confirm that ϕ_i is sigmoid function of sK and Eq. (4.31) provides a good approximation of ϕ_i when the assumption $P_{(i,i+1)} \approx 1$ holds, see Appendix C.3

Total fixation probabilities in the constant-K BDCLV

Species i's total fixation probability $\widetilde{\phi}_i$ consists of two contributions: $\phi_{i,i+1}\phi_i$ and $\phi_{i-1,i}(1-\phi_{i-1})$. The first one counts the probability for i to fixate after hitting the edge $(i, i+1)$, with a probability $\phi_{i,i+1}$, and prevailing against $i+1$ (weak opponent) with a probability ϕ_i. We also need to consider that, after reaching the edge $(i-1, i)$ with a probability $\phi_{i-1,i}$, species i has a probability $1-\phi_{i-1}$ to win against $i-1$ (strong opponent), which yields $\phi_{i-1,i}(1-\phi_{i-1})$. With these two contributions, we obtain

$$\widetilde{\phi}_i = \phi_{i,i+1}\phi_i + \phi_{i-1,i}(1-\phi_{i-1}), \tag{4.32}$$

which is also a function of sK, see Figure 4.6 (a,b). Of particular interest is the situation where the selection intensity is weak, $s \ll 1$, in which case (4.32) can be simplified by noting $\phi_{i,i+1} \approx \phi_{i-1,i} \simeq 1/3$ and using the result $\phi_i \simeq \phi_i|_K$, given by (4.31), for the absorption probability in the MCLV with $N = K$, yielding

$$\widetilde{\phi}_i \simeq \frac{1}{3}\left(1+\phi_i-\phi_{i-1}\right) \approx \frac{1}{3}\left(1+\phi_i|_K-\phi_{i-1}|_K\right). \tag{4.33}$$

Using the properties of the survival and absorption probabilities $\phi_{i,i+1}$ and ϕ_i discussed above, we can infer those of $\widetilde{\phi}_i$ in the regimes (i)-(iii):

(i) At quasi-neutrality, all species have the same fixation probability to first order: $\widetilde{\phi}_i = 1/3 + \mathcal{O}(sK)$. An estimate of the subleading correction is obtained by noticing $\phi_i|_K \simeq \frac{1}{2}(1+\alpha_i K/6)$ when $\alpha_i K \ll 1$. This, together with Eq. (4.33), gives

$$\widetilde{\phi}_i \simeq \frac{1}{3}\left(1+\frac{sK}{12}(r_i-r_{i-1})\right). \tag{4.34}$$

This result allows us to understand which are the species (slightly) favoured by selection: When $r_1 < r_2, r_3$, Eq. (4.34) predicts that $\widetilde{\phi}_1$ is less than $1/3$ and decreases with sK, while $\widetilde{\phi}_2 > 1/3$ and increases with sK, and $\widetilde{\phi}_3 = 1/3 + \mathcal{O}(s^2)$. These predictions agree with the simulation results of Figure 4.6 (a) in regime (i).

(iii) Under strong selection, the total fixation probability obeys the LOW, as in the cCLV. The species overall fixation probabilities are therefore ordered as follows:

$$\begin{aligned} &\widetilde{\phi}_i > \widetilde{\phi}_{i+1}, \widetilde{\phi}_{i-1} \quad \text{if} \quad r_i < r_{i\pm1}, \quad \text{and} \\ &\widetilde{\phi}_i \approx \widetilde{\phi}_{i+1} > \widetilde{\phi}_{i-1} \quad \text{if} \quad r_i = r_{i+1} < r_{i-1}, \end{aligned} \tag{4.35}$$

with $\widetilde{\phi}_i \approx \phi_{i,i+1} \overset{sK\gg1}{\longrightarrow} 1$, $1/2$ or 0. These predictions agree with the simulations results of Figure 4.6 (a,b).

(ii) Under weak selection, $\widetilde{\phi}_i$ can vary non-monotonically with sK, see Figure 4.6 (a,b). This behavior can be understood by noticing that near the boundary of regimes (i)-(ii), we have $\phi_i \approx 1/3$ that increases with sK if $r_i > r_{i-1}$ and decreases when $r_i < r_{i-1}$, see Eq. (4.34) and Figure 4.6 (a,b). As sK approaches the boundary of regimes (ii)-(iii), the dynamics is increasingly governed by the LOW with $\widetilde{\phi}_i \approx \phi_{i,i+1} \overset{sK\gg1}{\longrightarrow} 1$, $1/2$ or 0. This can lead to a non-monotonic dependence on sK: For instance, if $r_1 < r_2, r_3$, $\widetilde{\phi}_1$ decreases and $\widetilde{\phi}_2$ increases about the value $1/3$ near the (i)-(ii) boundary, and then respectively increases and decreases as sK approaches the boundary (ii)-(iii), and through regime (iii) where $\widetilde{\phi}_1 \to 1$ while $\widetilde{\phi}_2 \to 0$, see Figure 4.6 (a).

The main features of the survival, absorption and overall fixation probabilities in the constant-K BDCLV are summarized in the chart of Figure 4.6 (c).

Mean Fixation Time

The mean fixation time T_F is the average time taken for one species to take over the population. Similarly to the fixation probability, this quantity consists of one contribution from Stage 1, referred to as the *mean extinction time*, T_1, and the *mean absorption time*, T_2, arising from Stage 2. T_1 and T_2 are studied in detail in Appendix C.4, the main result of which is that when $\vec{x}_0 = \vec{x}_c$, the overall mean fixation time $T_F = \mathcal{O}(K)$. Since $N(t) \approx K$ after a short transient, this means that species coexistence is lost in a mean time scaling with system size.

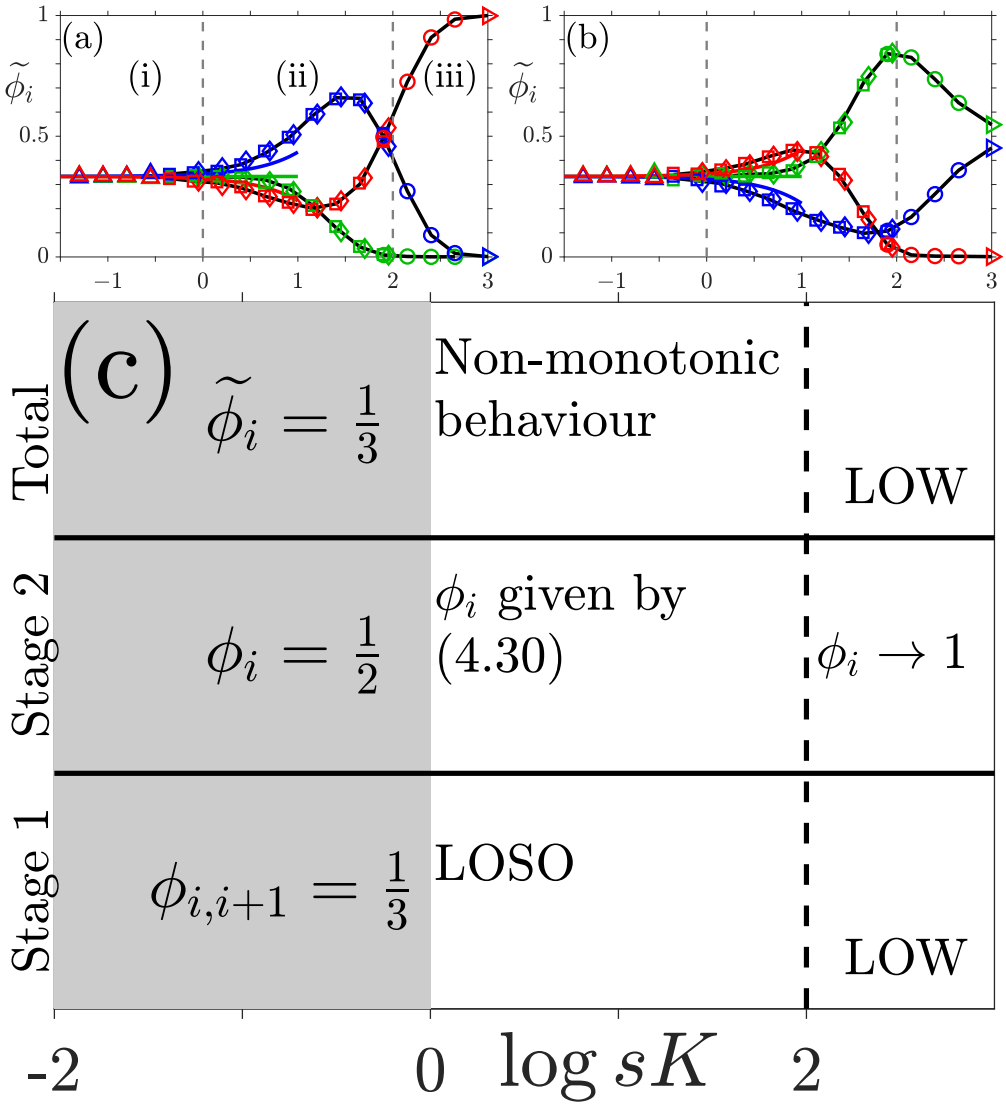

Figure 4.6: (a,b) Total fixation probabilities $\widetilde{\phi}_1$ (red), $\widetilde{\phi}_2$ (blue), $\widetilde{\phi}_3$ (green) vs. sK for values of $s \in (10^{-3}, 1)$ and $K \in \varkappa$ with symbols as in Figure 4.5, see text. Regimes (i)-(iii), from left to right, are indicatively separated by dashed gray lines. (a) $\vec{r} = \vec{r}^{(1)}$; (b) $\vec{r} = \vec{r}^{(2)}$. The solid black lines show the predictions of (4.32) using (4.30), with $\phi_{i,i+1}$ and $P_{(i,i+1)}$ inferred from simulations. Predictions from (4.34) are shown as solid colored line. $\widetilde{\phi}_i$ can display a non-monotonic dependence on sK across regimes (ii)-(iii), see text. (c) Chart summarizing the outcome of Stage 1, Stage 2 and the overall fixation probability $\widetilde{\phi}_i$ as function of sK in regimes (i)-(iii), from left to right. In all panels: $\vec{x}_0 = \vec{x}_c$ and $\epsilon = 0$.

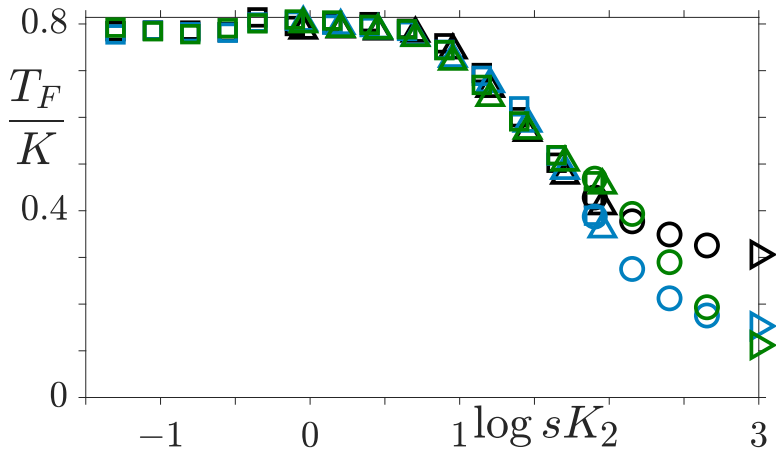

Figure 4.7: Mean fixation time T_F in the constant-K BDCLV: T_F/K vs. sK for values of $s \in (10^{-3}, 1)$ and $K \in \varkappa$ showing that $T_F = \mathcal{O}(K)$ across all regimes with subleading prefactors in regime (iii) shorter than in (i) and (ii). Colours and symbols refer to simulation results for: $\vec{r} = \vec{r}^{(1)}$ (green), $\vec{r} = \vec{r}^{(2)}$ (blue), and equal r_i (black) with $K = 1000$ ($\triangleright$), 450 ($\circ$), 250, ($\triangle$), 90 ($\square$), $\epsilon = 0$, $\vec{x}_0 = \vec{x}_c$.

4.4.2 Close-to-Zero-Sum BDCLV

The general non-zero-sum rock-paper-scissors game refers to the payoff matrix (4.16) with $\epsilon \neq 0$ and non-zero average fitness $\bar{f} = 1 - \epsilon \sum_{i=1}^{3} \alpha_i x_i x_{i+1}$. In this case the mean field description from the birth death process (4.20) - (4.22) is given by (using the results of Section 2.1.2):

$$\frac{d}{dt}N = N\left(\bar{f} - \frac{N}{K}\right) \tag{4.36}$$

$$\frac{d}{dt}x_i = x_i\left[\alpha_i x_{i+1} - (1+\epsilon)\alpha_{i-1}x_{i-1} + 1 - \bar{f}\right]. \tag{4.37}$$

Hence in this model the evolution of N is coupled with the x_is whose mean field dynamics is characterised by heteroclinic cycles (as in the MLM with $\sigma > 0$) when $\epsilon > 0$, and a stable coexistence fixed point when $\epsilon < 0$ (as in the MLM with $\sigma < 0$ i.e. the dominance removal reaction in (4.12) going in the opposite direction) Broom & Rychtár (2013); Dobramysl *et al.* (2018); Hofbauer *et al.* (1998); May & Leonard (1975); Smith (1982); Szabó & Fath (2007); Szczesny *et al.* (2014).

Here I will briefly discuss the case of close-to-zero-sum BDCLV when $|\epsilon| \ll 1$. Hence the approximation $\bar{f} \approx 1$ is used and we therefore assume that there is timescale separation between N and x_i. This assumption is backed up by simulation results which show that the fixation properties are qualitatively the same as in the zero-sum BDCLV (see Figure 4.8). This suggests that the fixation properties of the close-to-zero-sum BDCLV can be obtained from those of the zero-sum BDCLV by rescaling the selection intensity as $s \to s\,(1 + \beta\epsilon + \mathcal{O}(\epsilon^2))$. Since the fixation properties of the BDCLV vary little with the selection strength at quasi-neutrality and under strong selection, I focus on regime (ii) of weak selection in order to determine the parameter β. Here $s \ll 1$ and $sK \approx 10$ and we assume that the survival probabilities, $\phi_{i,j} \approx 1/3$, and the initial distribution in Stage 2, $P_{(i,j)}(\hat{x}_i) \approx 1$. Using (2.18), with $A(x_i) = \alpha_i x_i(1 - x_i)(1 + \epsilon x_i)$ and $B(x) = \frac{A(x)}{K\alpha_i(1+\epsilon x_i)}\left[2 + \alpha_i\left(1 - (2+\epsilon)x_i\right)\right]$ to give the absorption probability of species i with initial fraction $\hat{x}_i$ of species i:

$$\phi_i|_K(\hat{x}_i) = \frac{(2+\alpha_i)^{Kh(\epsilon,\alpha_i)+1} - \{2 + \alpha_i(1 - (2+\epsilon)\hat{x}_i)\}^{Kh(\epsilon,\alpha_i)+1}}{(2+\alpha_i)^{Kh(\epsilon,\alpha_i)+1} - (2 - \alpha_i(1+\epsilon))^{Kh(\epsilon,\alpha_i)+1}} \tag{4.38}$$

$$\text{where} \qquad h(\epsilon, \alpha_i) \equiv \frac{1 + \epsilon(1 + 1/\alpha_i)}{(1 + \epsilon/2)^2}. \tag{4.39}$$

When $|\epsilon| \ll 1$, this expression simplifies in the weak selection regime ($s \ll 1$) where it takes the form

$$\phi_i|_K(\hat{x}_i) \simeq \frac{1 - e^{-K\alpha_i(1+\epsilon/2)\hat{x}_i}}{1 - e^{-K\alpha_i(1+\epsilon/2)}}. \tag{4.40}$$

The absorption probability in regime (ii) is then found by averaging this over $P_{i,i+1} \approx 1$, yielding:

$$\phi_i \simeq \frac{e^{-\alpha_i(1+\frac{\epsilon}{2})K} + \alpha_i(1+\frac{\epsilon}{2})K - 1}{\alpha_i(1+\frac{\epsilon}{2})K(1 - e^{-\alpha_i(1+\frac{\epsilon}{2})K})}, \tag{4.41}$$

which coincides with (4.31) upon rescaling $s \to s\,(1 + \epsilon/2)$. This is confirmed in Figure 4.8(a) where it is found that this scaling holds across all regimes (i) - (iii). A similar argument is used for the total fixation time. Since T_1 varies little with s in regime (ii) the mean fixation time T_F and mean absorption time T_2 can be obtained from those for the zero-sum BDCLV with $s \to s(1 + \epsilon/2)$. From Figure

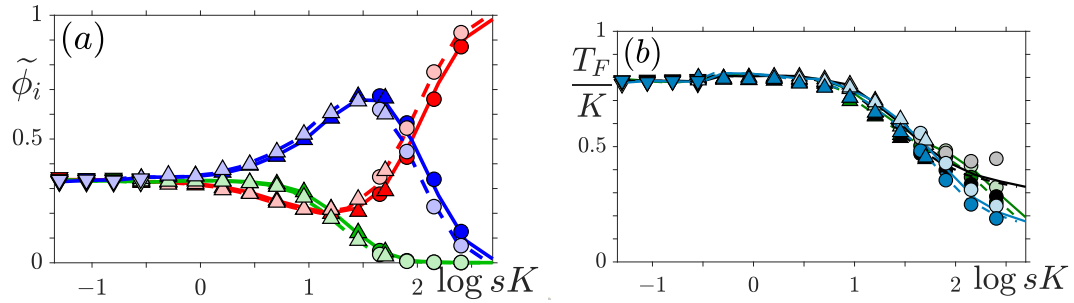

Figure 4.8: (a) $\widetilde{\phi}_i$ vs. sK in the close-to-zero-sum RPS game with constant carrying capacity $K = 450$ (circles), 90 (upward triangles), 50 (downward triangles), $\vec{r} = \vec{r}(1)$, $\epsilon = -0.2$ (light symbols) and $\epsilon = 0.2$ (dark symbols). Lines show stochastic simulation results for the BDCLV ($\epsilon = 0$, see Figure 4.6) with rescaled selection intensity $s \to s(1 + \epsilon/2)$ with $\epsilon = 0.2$ (solid) and $\epsilon = -0.2$ (dashed). Dark symbols / solid lines and light symbols / dashed lines collapse, demonstrating $\widetilde{\phi}_i^{\epsilon}(s) \simeq \widetilde{\phi}_i^{\mathrm{BDCLV}}(s(1 + \epsilon/2))$, see text. (b) Rescaled mean fixation time T_F/K vs. sK in the close-to-zero-sum game ($|\epsilon| \ll 1$) and constant K for values of $s \in (10^{-3}, 1)$ and $K = 450$ (circles), 90 (upward triangles), 50 (downward triangles). Symbols are from stochastic simulations for $\epsilon = -0.2$ (light) and $\epsilon = 0.2$ (dark). Lines are from the constant-K BDCLV obtained with the same carrying capacity but a rescaled selection intensity $s(1 + \epsilon/2)$. Solid lines are for $\epsilon = 0.2$, dashed lines are for $\epsilon = -0.2$. $\vec{r} = (1, 1, 1)/3$ (black), $\vec{r} = \vec{r}(1)$ (green), $\vec{r} = \vec{r}(2)$ (blue). In both panels $\vec{x}_0 = \vec{x}_c$.

4.8(b) we see that this works well in regimes (i) and (ii), but breaks down in regime (iii) where $sK \gg 1$, overestimating T_F when $\epsilon > 0$ and underestimating when $\epsilon < 0$, due to the changes in stability of the interior fixed point compared to the case for $\epsilon = 0$.

4.5 Summary

In this section I have introduced three ways of modelling cyclic competition. The cCLV assumes constant population size and will be used in Chapter 6 when I investigate the effects of a randomly switching reaction rate, and the MLM is a more general model of cyclic competition where the total population is not fixed,

but is bounded from above. This model leads to particularly intriguing behaviour when considered in a spatial setting, with spiral waves of varying degrees of stability observed depending on the type and strength of mobility used by the individuals. In both these models, the fixation probabilities follow the 'law of the weakest' in large populations, and the 'law of stay out' when the population size is small. The mean fixation time in well mixed settings scales linearly with N in the cCLV while it is of order $\ln N$ in the MLM. The final model, the BDCLV, is a new model of cyclic competition, formulated as a game-theoretic birth-death process, allowing for a fluctuating total population size that is unbounded above. In the zero sum case, the fixation probabilities are dependent on sK, with three regimes characterised by (i) quasi-neutrality, (ii) weak selection and (iii) strong selection, and those for the close-to-zero-sum case $|\epsilon| \ll 1$ can be well approximated by rescaling $s \to s(1 + \epsilon/2)$ in the zero-sum case. In the next chapter, I will present the effects of a randomly switching carrying capacity on the BDCLV, where it will be seen that when the carrying capacities are such that the system switches between different regimes, novel fixation scenarios arise.

Chapter 5

Cyclic Competition in Populations of Fluctuating Size

This Chapter will present the coupled effect of environmental and internal noise on the fixation properties of a three species rock-paper-scissors game (as in Section 4.4) in a population of fluctuating size, where the resources continuously vary between states of scarcity and abundance. Unlike the two-species competition model considered in Chapter 3, here the relative size of the species birth rates change cyclically with the population composition so, while all three species coexist, no individual species is always the fastest growing. Once the first species has died out, the two remaining species compete until one fixates the population. This stage of the population evolution is similar to Chapter 3, where one species has a fitness advantage over the other. Hence the fixation statistics are dependent on these two stages of population evolution: Which species are most likely to survive the initial cyclic phase and, once this is over, which species are then more likely to win the subsequent two-player competition? Given that we have seen in Section 4.4 that the strength of these cyclic interactions compared to neutral drift increases with the system size, a randomly switching carrying capacity will lead to different species being favoured for survival to the end of the first stage, following the 'LOW' or 'LOSO' dependent on the population size (see Figures 4.2 and 4.5(a,b)). Furthermore, the outcome of the second stage is clearly dependent on the first and (as we have seen in Chapter 3) the outcome of

two species competition models can be greatly affected by a fluctuating environment. The combination of these results in complex fixation scenarios the result of which is not obvious *a priori*. In this Chapter, a combination of numerical and theoretical techniques will be used to understand:

1. Under what conditions do the fixation rules established in Section 4.4 hold and when do new fixation scenarios occur?

2. Does environmental noise promote or inhibit species coexistence?

Again, for simplicity, we assume that environmental variability is modelled by letting the carrying capacity follow a symmetric dichotomous Markov noise process, switching randomly between a high and low value representing rich and sparse resources, spending on average the same time at each (see Section 2.2.1). The general model and its basic properties are introduced in Section 5.1, then in Section 5.2 the effects on the survival, absorption and fixation probabilities, and the mean fixation time for the zero-sum BDCLV (i.e. $\epsilon = 0$) are presented, explained and compared with their counterparts of Section 4.4.1, obtained when the population is subject to a constant carrying capacity. In general, it is found that random switching effectively levels the field of the competition: The species that is least/most like to fixate in a constant environment has an increased/decreased fixation probability in a fluctuating one. Furthermore, when the variance of the noise is large enough new fixation scenarios can occur: the most likely species to survive is different to that expected without external noise. In Section 5.3 the results for the close-to-zero-sum BDCLV (i.e. $|\epsilon| \ll 0$) with a randomly switching carrying capacity are presented and compared with those of Section 4.4.2 without external noise. Similarly to the case in a constant environment it is found that the fixation statistics can be well approximated by those for the zero-sum BDCLV with rescaled selection intensity.

5.1 Model Definition

Proceeding as in Section 4.4.1, and using the same notations, the birth-death cyclic Lotka-Volterra model with randomly switching carrying capacity (switching-

K BDCLV) is defined by the birth death reactions:

$$N_i \xrightarrow{T_i^+} N_i + 1 \quad \text{and} \quad N_i \xrightarrow{T_i^-(\xi(t))} N_i - 1, \quad \text{with} \quad i \in \{1, 2, 3\} \tag{5.1}$$

with rates

$$T_i^+ = f_i N_i = (1 + s\Pi_i)N_i = (1 + \{\alpha_i x_{i+1} - \alpha_{i-1}(1+\epsilon)x_{i-1}\})N_i \quad \text{and} \tag{5.2}$$

$$T_i^-(\xi(t)) = \frac{N}{K(t)} N_i, \tag{5.3}$$

where Π_i accounts for cyclic competition and is defined as in Sec. 4.4, $0 < s < 1$ is the selection strength, measuring the strength of this cyclic competition compared with neutral drift, $|\epsilon| \ll 1$ characterises the stability of the interior fixed point and therefore the type of cyclic competition ($\epsilon = 0$: zero-sum game with neutrally stable interior fixed point, otherwise, a non-zero-sum game with stable ($\epsilon < 0$) or unstable ($\epsilon > 0$) interior fixed point, see Section 4.4), and the death rates vary in time with the carrying capacity, following a symmetric dichotomous Markov process that switches between a high (K_+) and low (K_-) value according to:

$$K(t) = K_0\,(1 + \gamma\xi(t)) \quad \text{and} \quad \xi \xrightarrow{\nu} -\xi, \tag{5.4}$$

where $K_0 = \frac{K_+ + K_-}{2}$ and $\gamma = \frac{K_+ - K_-}{K_+ + K_-}$ measures the intensity of the environmental noise. Using the results of Sec. 2.2.1 we find that the mean and variance of $K(t)$ are $\langle K(t)\rangle = K_0$ and $\mathrm{var}(K(t)) = (\gamma K_0)^2$ and can write $K_\pm = (1 \pm \gamma)K_0$. We specify that $\gamma = \mathcal{O}(1)$ and $K_0 \gg 1$ so that the environmental variability $\mathrm{var}(K) \gg 1$ is large and the population size itself is large enough to ensure that demographic fluctuations alone are not the main source of randomness. Note that when I say 'compared to the case to case without external noise' I mean compared with the model introduced in Section 4.4 with $K = K_0$ and the other parameters the same.

As we have seen in Section 4.4, when all forms of noise are ignored the total population size $N = N_1 + N_2 + N_3$ follows a logistic-like equation. The inclusion of external noise results in the carrying capacity being dependent on the environmental state:

$$\frac{dN}{dt} = N\left(\bar{f} - \frac{N}{\mathcal{K}}(1 - \gamma\xi(t))\right), \tag{5.5}$$

where $\mathcal{K} = (1-\gamma^2)K_0$ is the harmonic mean of $K_\pm$. Since $|\epsilon| \ll 1$ we use the approximation $\bar{f} \approx 1$ as in Section 4.4.2 (although note that in the zero-sum case $\bar{f} = 1$ and this case (5.5) is a logistic equation when $\gamma = 0$, while N obeys a stochastic differential equation defining a PDMP when $\gamma > 0$). The mean field equations for the species densities, x_i, are the same as for the constant K case (see (4.37)), so again there is a timescale separation when $s \ll 1$: N evolves faster than the x_i's, settling into its N-QSD in a time $t = \mathcal{O}(1)$, while the x_i's change on a timescale $t = \mathcal{O}(1/s)$ (see Figure 5.1). The results of Section 2.2.1 can be used to find the approximation of the N-QSD, the marginal stationary distribution of the PDMP (*i.e.* independent of the environmental state variable ξ):

$$p_\nu(N) = \frac{\mathcal{Z}}{N^2}\left[\frac{(K_+ - N)(N - K_-)}{N^2}\right]^{\nu-1}, \tag{5.6}$$

where $\mathcal{Z}$ is a normalisation constant. In this symmetric case the distribution is bimodal with peaks at $K_\pm$ if $\nu < 1$, and is unimodal with peak at $N^* = K_0(1+\nu)\left(1 - \sqrt{1 - 4\nu(1-\gamma^2)/(1+\nu^2)}\right)/2$ when $\nu > 1$. In the limit $\nu \to \infty$ $N^* \to \mathcal{K}$, as expected from the self averaging of $\xi(t)$ when $\nu \gg 1$. See Fig. 5.2 where one can see that the $p_\nu(N)$ captures the position of the peaks well, but not the width around them. Again, this is because the PDMP ignores all internal noise, and has compact support $[K_-, K_+]$. As for the two species competition model, a next order approximation that takes into account internal noise can be found by performing a linear noise expansion around the PDMP (see A.1.2 for details), but is not necessary for my purposes, the lowest order approximation $p_\nu(N)$ is sufficient to characterise the fixation properties.

In presenting the results, I use the same parameter sets for $\vec{r}$ as in Section 4.4: $\vec{r} \equiv (r_1, r_2, r_3) = \vec{r}^{(1)} \equiv (1, 5, 5)/11$ and $\vec{r} = \vec{r}^{(2)} \equiv (3, 1, 1)/5$, with initial fraction $1/3$ of each species $\vec{x}_0 = (1/3, 1/3, 1/3)^{\mathrm{T}} = \vec{x}_c$. In all figures (except Figure 5.1, simulation results have been sampled over $10^4 - 10^5$ realizations.

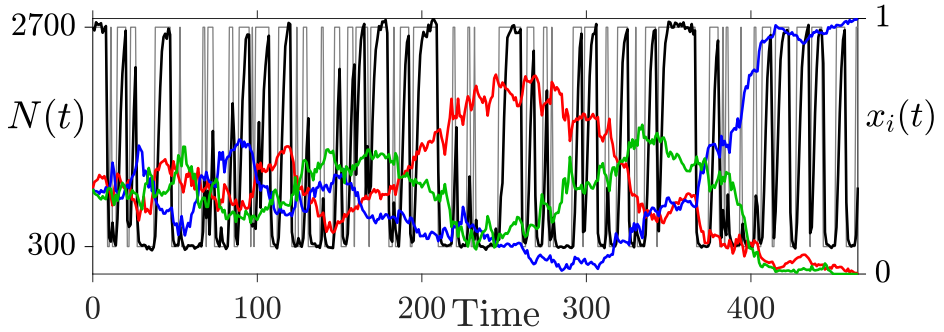

Figure 5.1: (c) Sample paths of $N(t)$ (black), densities $x_i(t) = N_i(t)/N(t)$ (colored), and typical evolution of the randomly switching $K(t)$ (gray). Parameters are: $(s, r_1, r_2, r_3, \nu, K_+, K_-) = (1/20, 1/3, 1/3, 1/3, 1/4, 2700, 300)$. $N(t)$ quickly settles into its (quasi) stationary state while x_i vary much more slowly until fixation occurs in a time $\sim \mathcal{O}(K_0)$, see Section 5.2.4. Colours are $x_1(t)$ in red, $x_2(t)$ in blue, and $x_3(t)$ in green, $\epsilon = 0$. Initially, all species have the same density 1/3.

5.2 Fixation Statistics in the zero-sum switching-K BDCLV

First I present the results for the zero-sum case, $\epsilon = 0$. As in the constant-K BDCLV, the total fixation probability $\widetilde{\phi}_i$ depends on the Stage 1 survival and Stage 2 absorption probabilities. Here, the effect of the environmental randomness on these quantities is analysed, by distinguishing again the regimes of (i) quasi-neutrality, where $s \ll 1$ and $sK_0 \ll 1$; (ii) weak selection, where $s \ll 1$ and $sK_0 \approx 10$; and (iii) strong selection, where $s = \mathcal{O}(1)$ and $sK_0 \gg 1$.

Similarly, the mean fixation time T_F depends on the mean extinction and absorption times, T_1 and T_2 characterizing Stages 1 and 2, respectively. This allows us it to be shown that the mean fixation time $T_F = T_1 + T_2 = \mathcal{O}(\langle N \rangle) = \mathcal{O}(K_0)$ scales linearly with the average population size when $\vec{x}_0 = \vec{x}_c$. This is similar to the constant K BDCLV, hence we ask, how does random switching alter the cyclic competition and possibly change the species coexistence time?

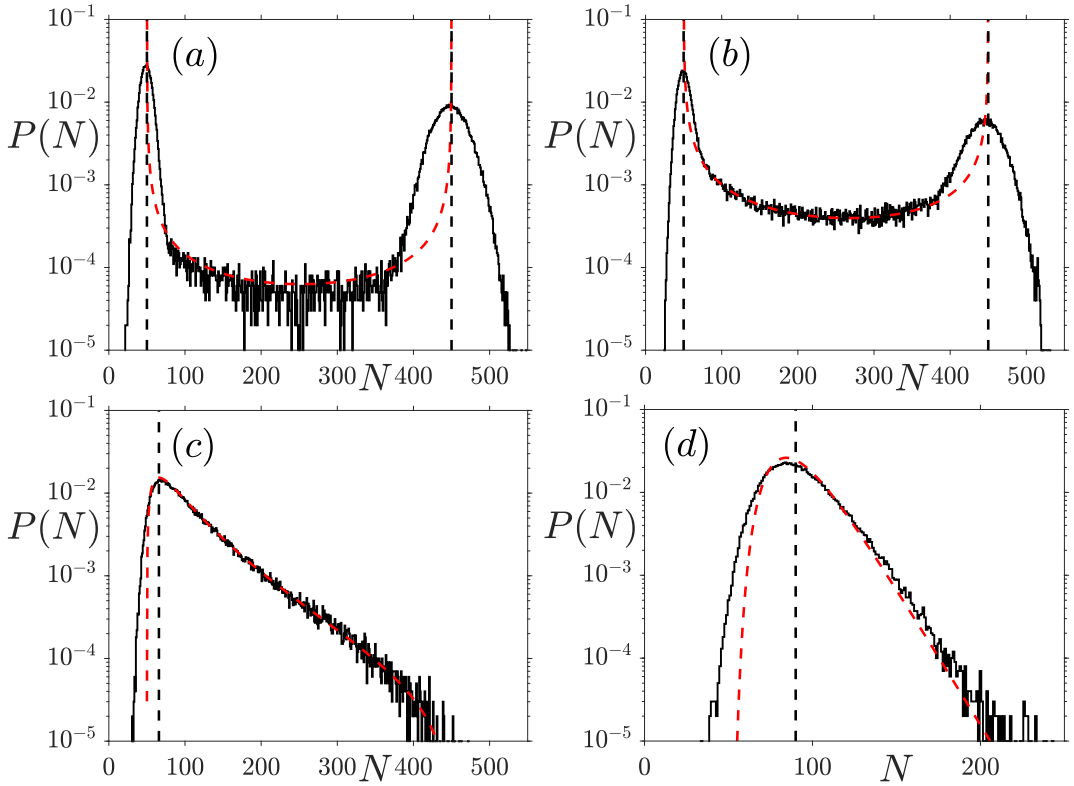

Figure 5.2: N-QSD and $p^*_\nu(N)$ for (a) $\nu = 0.01$, (b) $\nu = 0.1$, (c) $\nu = 2$, (d) $\nu = 10$. Parameters are $(s, K_+, K_-) = (0.02, 450, 50)$. Solid lines are histograms from stochastic simulations and colored dashed lines are PDMP predictions from (5.6), see text. Black dashed lines indicate $N = K_\pm$ in (a) and (b), $N = N^*$ in (c), and $N = \mathcal{K}$ in (d), see text.

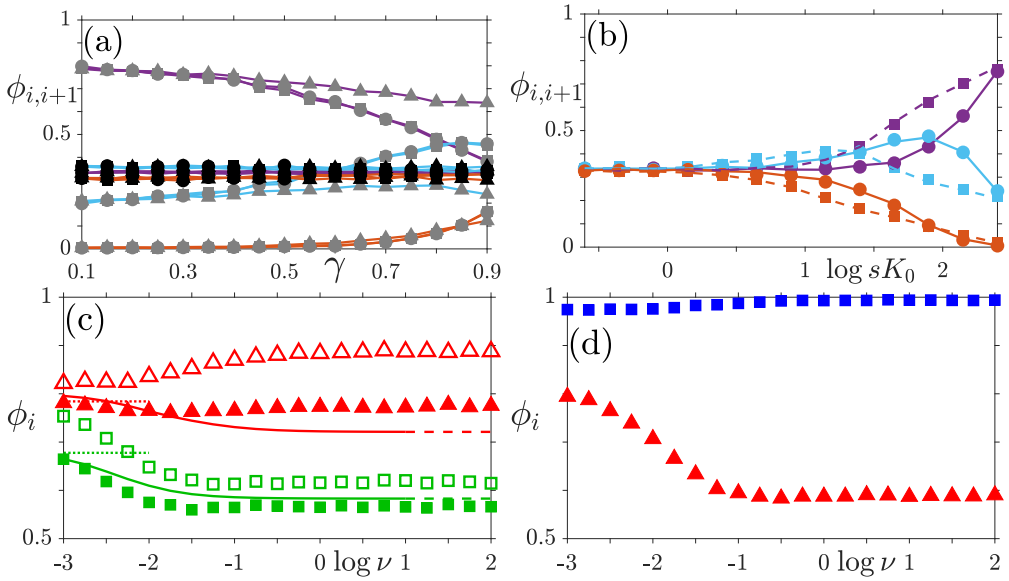

Figure 5.3: (a) Stage 1 survival probability $\phi_{i,i+1}$ vs. γ for $K_0 = 250$ kept fixed ($K_+ \in [275, 475]$ and $K_- \in [25, 225]$). and $s = 0.01$ (black), $s = 0.4$ (gray). Simulation results for $\nu = 10$ (circles), $\nu = 1.2$ (squares) and $\nu = 0.001$ (triangles). (b) $\phi_{i,i+1}$ vs. sK_0 for $K_0 = 250, \gamma = 0.8$ and $s \in \{10^{-k/4}, k = 0, \ldots, 12\}$ kept fixed, with $\nu = 2$ (circles) and $\nu = 0.001$ (squares); lines are $\phi_{i,i+1}|_{(1-\gamma^2)K_0}$ (solid) and $\frac{1}{2}(\phi_{i,i+1}|_{(1+\gamma)K_0} + \phi_{i,j}|_{(1-\gamma)K_0})$ (dashed) are from the constant-K_0 BDCLV. In panels (a,b) $\vec{r} = \vec{r}^{(1)}$, $\phi_{1,2}$ in purple, $\phi_{2,3}$ in light blue, $\phi_{3,1}$ in orange. (c) Stage 2 absorption probabilities ϕ_1 (red triangles) and ϕ_3 (green squares) vs. ν for $K_0 = 250$ and $\gamma = 0.8$ kept fixed and $\vec{r} = \vec{r}^{(2)}$. Symbols are from simulations for with $s = 0.1$ (open) and $s = 10^{-5/4} \approx 0.056$ (filled). Lines are from (5.11) (solid), (5.10) (dashed), (5.9) (dotted), and assume $P_{i,i+1} \approx 1$; they capture reasonably well the ν-dependence of ϕ_1 and ϕ_3 when $sK_0 \lesssim 10$, see text. (d) Same as in panel (c) for ϕ_1 (red triangles) and ϕ_2 (blue squares) vs. ν with $s = 10^{-1/4}$ and $\vec{r} = \vec{r}^{(1)}$. In all panels $\vec{x}_0 = \vec{x}_c$, $\epsilon = 0$.

5.2.1 Stage 1: Survival probabilities in the switching-K BDCLV

To analyze the survival probability $\phi_{i,i+1}$ in the switching-K BDCLV, it is convenient to consider this quantity in the limits $\nu \to \infty$ and $\nu \to 0$, where $\phi_{i,i+1}$ can be expressed in terms of $\phi_{i,i+1}|_K$, the survival probability in the constant-K BDCLV studied in Section 4.4.1.

When $\nu \to \infty$, many switches occur in Stage 1 and the EN self averages, $\xi \to \langle \xi \rangle = 0$ (Wienand *et al.* (2017, 2018)). The population thus rapidly settles in its N-QSD that is peaked at $N = (1-\gamma^2)K_0 = \mathcal{K}$ when $K_0 \gg 1$. Hence, the Stage 1 dynamics under fast switching is similar to the cCLV dynamics in a population of size $(1-\gamma^2)sK_0$ (see Appendix C.2). This yields $\phi_{i,i+1} \overset{\nu\to\infty}{=} \phi_{i,i+1}|_{(1-\gamma^2)K_0}$.

When $\nu \to 0$, there are no switches in Stage 1, and the extinction of the first species is equally likely to occur in each environmental state $\xi = \pm 1$ (with $K = (1 \pm \gamma)K_0$). This gives $\phi_{i,i+1} \overset{\nu\to 0}{=} \left(\phi_{i,i+1}|_{(1+\gamma)K_0} + \phi_{i,i+1}|_{(1-\gamma)K_0}\right)/2$.

The case of intermediate ν can be inferred from the above by noting that the average number of switches occurring in Stage 1 is $\mathcal{O}(\nu K_0)$ (average amount of time spent in Stage 1 is of order K_0, and the environment spends on average $1/\nu$ in each environmental state. Hence the average number of switches in Stage 1 is of order $K_0/(\nu^{-1}) = K_0\nu$ - see Appendix C.4.3 and Figure C.5). As the population experiences a large number of switches in Stage 1 when $\nu = \mathcal{O}(1)$ and $K_0 \gg 1$, the EN effectively self-averages, $\xi(t) \simeq \langle \xi \rangle = 0$, and therefore

$$\phi_{i,i+1} \overset{\nu=\mathcal{O}(1)}{\approx} \phi_{i,i+1}|_{(1-\gamma^2)K_0}. \tag{5.7}$$

When $\nu \ll 1/K_0$, there are very few or no switches after a time of order $\mathcal{O}(K_0)$ prior to extinction the first species, and therefore

$$\phi_{i,i+1} \overset{\nu\ll 1/K_0}{\approx} \frac{1}{2}\left(\phi_{i,i+1}|_{(1+\gamma)K_0} + \phi_{i,i+1}|_{(1-\gamma)K_0}\right). \tag{5.8}$$

Eq. (5.7) implies that for any $\nu = \mathcal{O}(1)$, the survival probability of species $i, i+1$, i.e the probability that species $i-1$ dies out first, is given by the survival probability in the constant-K BDCLV with $K = K_0$ (same average carrying capacity) and a rescaled selection intensity $(1-\gamma^2)s$. The effect of random switching is therefore to effectively reduce the selection intensity by a factor

$1-\gamma^2 = 1-(\mathrm{var}(K(t))/K_0^2)$ proportional to the variance of the carrying capacity. The sK_0-dependence of $\phi_{i,i+1}$ can thus readily be obtained from Figure 4.5 (a,b) by rescaling $s \to (1-\gamma^2)s$ as shown in Figure 5.3 (a,b). Hence, when there is enough environmental variability (γ large enough) the survival scenarios differ from those of the constant-K BDCLV and depend on the switching rate:

1. When $\nu \gg 1/K_0$ (*i.e.* if the average time before a switch, ν^{-1}, is much less than mean extinction time, $T_1 \sim K_0$ - see Appendix C.4), switching reduces the selection by a factor $1-\gamma^2$, see Figure 5.3 (b). Hence, there is a critical γ^*, estimated as $\gamma^* \approx (1-50/sK_0)^{1/2}$, such that $\phi_{i,i+1}$ obeys the LOSO when $\gamma > \gamma^*$ and $sK_0 \gg 1$, while the LOW still applies when $\gamma < \gamma^*$. Therefore, when $\gamma > \gamma^*$, all species have a finite chance to survive Stage 1, with probabilities ordered according to the LOSO, ($\phi_{1,2} \approx \phi_{2,3} > \phi_{3,1}$ with $\gamma^* \approx 0.7$, in Figure 5.3 (a)). Figure 5.3 (a), also shows that the exact value ν has little influence on $\phi_{i,i+1}$ provided that $\nu K_0 \gg 1$ (circles and squares almost coincide).

2. When $\nu \ll 1/K_0$ (*i.e.* if the average time before a switch, ν^{-1}, is much greater than mean extinction time, $T_1 \sim K_0$ - see Appendix C.4), we have $\phi_{i,i+1} \approx (\phi_{i,i+1}|_{K_+} + \phi_{i,i+1}|_{K_-})/2$. Hence, if $sK_0 \gg 1$ and $\gamma > \hat{\gamma}$, where $\hat{\gamma} \approx 1 - 50/sK_0$, $\phi_{i,i+1}|_{K_+}$ follows the LOW whereas $\phi_{i,i+1}|_{K_-}$ obeys the LOSO, and the $\phi_{i,i+1}$'s therefore interpolate between LOW and LOSO values: For $\gamma > \hat{\gamma}$, the survival probabilities under strong selection and slow switching deviate markedly from the purely LOW values of $\phi_{i,i+1}|_{K_0}$ which asymptotically approach 0, 1 or 1/2 (see triangles in Figure 5.3 (a) where $\hat{\gamma} \approx 0.5$).

3. When $s \ll 1$ and $sK_0 \approx 10$ in regime (ii), changing γ has little effect on the survival probabilities: the survival probabilities $\phi_{i,i+1} \approx 1/3$, and remain ordered according to the LOSO (see black symbols in Figure 5.3 (a)).

These results show that environmental variability leads to new survival scenarios in the BDCLV under strong selection: When there is enough variability, all species have a finite probability to survive even when $sK_0 \gg 1$. The departure from the pure LOW survival scenario is most marked in the generic case of a

finite switching rate ($\nu \gg 1/K_0$). With respect to the constant-K BDCLV, the general effect of random switching in Stage 1 is therefore to "level the field" by hindering the onset of the zero-one LOW.

5.2.2 Stage 2: Absorption probabilities in the switching-K BDCLV

Stage 2 consists of the competition between types i and $i+1$ along the edge $(i, i+1)$ of S_3. This starts with an initial fraction $\hat{x}_i$ of i individuals and ends up with the absorption of one of the species with probabilities ϕ_i (for species i) and $1-\phi_i$ (for $i+1$). Again $\hat{x}_i$ is randomly distributed according to a probability density $P_{(i,i+1)}$ resulting from Stage 1, see Appendix C.3[1]. Since $\phi_i \approx 1/2$ at quasi-neutrality and $\phi_i \approx 1$ under strong selection, see Figure 5.3 (c,d), Stage 2 dynamics is nontrivial in regime (ii). To analyze the stage 2 dynamics under weak selection $s \ll 1$ and $K_0 \gg 1$, it is again useful to consider the limits $\nu \to 0$ and $\nu \to \infty$:

1. When $\nu \to 0$, there are no switches in Stage 2 and absorption is equally likely to occur in the static environment $K = K_-$ or $K = K_+$. Hence, if the fraction $\hat{x}_i$ is known, one has $\phi_i(\hat{x}_i) \overset{\nu\to 0}{=} \phi_i^{(0)}(\hat{x}_i) = \frac{1}{2}\left(\phi_i(\hat{x}_i)|_{K_-} + \phi_i(\hat{x}_i)|_{K_+}\right)$, where $\phi_i(\hat{x}_i)|_K = (1-e^{-\alpha_i K \hat{x}_i})/(1-e^{-\alpha_i K})$, see (4.29). Since $\hat{x}_i$ is randomly distributed, one needs to integrate over $P_{(i,i+1)}$: $\phi_i \overset{\nu\to 0}{=} \phi_i^{(0)} = \int_0^1 \phi_i^{(0)}(\hat{x}_i) P_{(i,i+1)}(\hat{x}_i)\, d\hat{x}_i$. In general, $P_{(i,i+1)}$ is obtained from stochastic simulations and has been found to be mostly independent of ν, see Figure C.2 (c,d). When $s \ll 1$ with $sK_0 \lesssim 10$, one can again assume $P_{(i,i+1)} \approx 1$ (uniform distribution), which allows us to obtain

$$\phi_i \overset{\nu\to 0}{=} \phi_i^{(0)} \simeq \frac{1}{2}\left(\phi_i|_{K_-} + \phi_i|_{K_+}\right), \quad \text{where} \tag{5.9}$$

$\phi_i|_K \equiv (e^{-\alpha_i K} + \alpha_i K - 1)/(\alpha_i K(1-e^{-\alpha_i K}))$, see (4.31).

[1]The probability density function of $\hat{x}_i$ is generally different in the constant-K and switching-K BDCLV, see Figure C.2. Yet, for the sake of simplicity, with a slight abuse of notation, these two quantities are denoted by $P_{i,i+1}(\hat{x}_i)$.

2. When $\nu \to \infty$, the DMN self averages ($\xi \to \langle \xi \rangle = 0$) (Wienand *et al.* (2017, 2018)), and the absorption occurs subject to the effective $K(t) = \mathcal{K}$, see (5.5). Hence, when $\hat{x}_i$ is known, $\phi_i(\hat{x}_i) \overset{\nu\to\infty}{=} \phi_i^{(\infty)}(\hat{x}_i) = \phi_i(\hat{x}_i)|_{\mathcal{K}}$, whose integration over $P_{(i,i+1)}$ gives the absorption probability: $\phi_i \overset{\nu\to\infty}{\equiv} \phi_i^{(\infty)} = \int_0^1 \phi_i^{(\infty)}(\hat{x}_i)\ P_{(i,i+1)}(\hat{x}_i)\ d\hat{x}_i$. When $s \ll 1$ with $sK_0 \lesssim 10$, and $P_{(i,i+1)} \approx 1$, we have

$$\phi_i \overset{\nu\to\infty}{=} \phi_i^{(\infty)} \simeq \phi_i|_{\mathcal{K}} = \frac{e^{-\alpha_i \mathcal{K}} + \alpha_i \mathcal{K} - 1}{\alpha_i \mathcal{K}(1 - e^{-\alpha_i \mathcal{K}})}. \tag{5.10}$$

3. When the switching rate ν is finite and $s \ll 1$, with $sK_0 \approx 10$, the probability ϕ_i can be computed as in Wienand *et al.* (2017) and Chapter 3 by exploiting the time scale separation between N and x_i, and by approximating the N-QSD by the PDMP marginal stationary probability density (5.6). In this framework, ϕ_i can be computed by averaging $\phi_i(\hat{x}_i)|_N = (1 - e^{-\alpha_i N \hat{x}_i})/(1 - e^{-\alpha_i N})$ over the rescaled PDMP probability (5.6) (Wienand *et al.* (2017, 2018)):

$$\phi_i(\hat{x}_i) \simeq \phi_i^{(\nu)}(\hat{x}_i) = \int_{K_-}^{K_+} \phi_i(\hat{x}_i)|_N\ p_{\nu/\alpha_i}(N)\ dN,$$

where p^*_{ν/α_i} is given by (5.6) with a rescaled switching rate $\nu \to \nu/\alpha_i$ due to an average number $\mathcal{O}(\nu/\alpha_i)$ of switches occurring in Stage 2, see Wienand *et al.* (2018) and Appendix C.4.3. As above, the absorption probability is obtained by formally integrating over $P_{(i,i+1)}$, i.e. $\phi_i \simeq \phi_i^{(\nu)} \equiv \int_0^1 \phi_i^{(\nu)}(\hat{x}_i)\ P_{(i,i+1)}(x_i)\ d\hat{x}_i$. Under weak selection, one can approximate $P_{(i,i+1)} \approx 1$, see Appendix C.3, and, using (4.30) and (4.31), we obtain

$$\phi_i \simeq \phi_i^{(\nu)} \approx \int_{K_-}^{K_+} \left\{ \frac{e^{-N\alpha_i} + \alpha_i N - 1}{\alpha_i N\,(1 - e^{-\alpha_i N})} \right\}\ p_{\nu/\alpha_i}(N)\ dN. \tag{5.11}$$

The uniform approximation of $P_{(i,i+1)} \approx 1$ is legitimate when $sK_0 \approx 10$, and has broader range applicability than in the constant-K case, see Appendix C.3 and Figure C.2. Hence, Eq. (5.11), along with (5.9) and (5.10), captures the ν-dependence of ϕ_i over a broad range of values ν when $s \ll 1$. In fact, simulation results of Figure 5.3 (c,d) show that the ϕ_i's generally have a non-trivial ν-dependence. When $s \ll 1$ and $sK_0 \approx 10$, this is satisfactorily captured

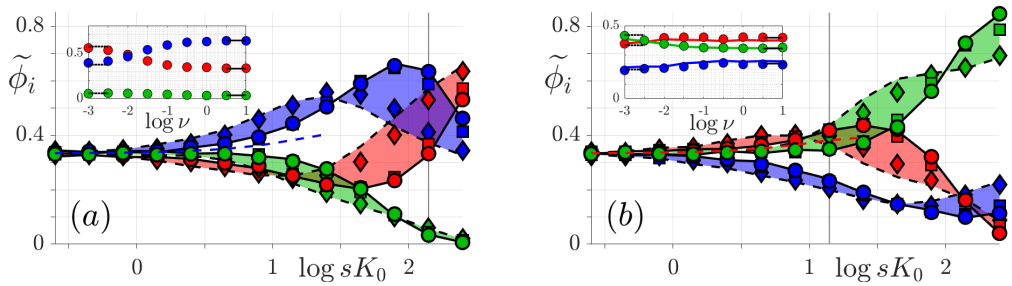

Figure 5.4: Total fixation probabilities $\widetilde{\phi}_i$ vs. sK_0 for values of $s \in (10^{-3}, 1)$ and with $K_0 = 250$ and $\gamma = 0.8$ kept fixed, see text. (a) $\vec{r} = \vec{r}^{(1)}$; (b) $\vec{r} = \vec{r}^{(2)}$. Shaded areas and symbols are from stochastic simulations with $\nu = 10$ ($\circ$), $\nu = 0.1$ ($\square$), $\nu = 10^{-5/2}$ ($\diamond$). Solid and dashed black lines show respectively $\widetilde{\phi}_i|_{\mathcal{K}}$ and $(\widetilde{\phi}_i|_{K_-} + \widetilde{\phi}_i|_{K_+})/2$ in both panels and insets, see text. Vertical light gray lines indicate $\widetilde{\phi}_i$ for $s = 10^{-1/4}$ (a) and $s = 10^{-5/4}$ (b). $\widetilde{\phi}_i$ increases with ν when the solid black line is above the dashed black line, otherwise $\widetilde{\phi}_i$ decreases with ν, see text. Dashed colored lines show $\widetilde{\phi}_2$ in (a) and $\widetilde{\phi}_1$ in (b) obtained from $\widetilde{\phi}_i \approx (1 + \phi_i - \phi_{i-1})/3$, with (5.11) and $\nu = 10$. Insets: $\widetilde{\phi}_i$ vs. ν for $s = 10^{-1/4}$ (a) and $s = 10^{-5/4}$ (b); symbols are from stochastic simulations and solid lines in inset (b) are predictions of (4.32) obtained using (5.11), with $\phi_{i,i+1}, \phi_{i-1,i}$ inferred from simulations. Fixation scenario changes at $\nu = \nu^*(s)$ with $\nu^* \approx 10^{-2}$ in (a) and $\nu^* \approx 10^{-5/2}$ in (b), see text. In all panels and insets: species 1 in red, species 2 in blue, species 3 in green; $\vec{x}_0 = \vec{x}_c$, $\epsilon = 0$.

by (5.9)-(5.11), with $\phi_i^{(\nu)} \approx \phi_i^{(0)}$ when $\nu \ll 1$, and $\phi_i^{(\nu)} \approx \phi_i^{(\infty)}$ when $\nu \gg 1$, see Figure 5.3 (c, filled symbols). Clearly, the assumption $P_{(i,j)} \approx 1$ and the timescale separation break down when $s = \mathcal{O}(1)$ (Wienand *et al.* (2018)), and the approximations (5.9)-(5.11) are then no longer valid.

5.2.3 Overall fixation probabilities in the switching-K BDCLV

The overall fixation probability $\widetilde{\phi}_i$ is obtained from the survival and absorption probabilities according to $\widetilde{\phi}_i = \phi_{i,i+1}\phi_i + \phi_{i-1,i}(1 - \phi_{i-1})$, see Eq. (4.32).

In order to study the influence of the environmental variability on $\widetilde{\phi}_i$, it is again useful to consider the limiting cases of fast/slow switching. In fact, as

shown in Figure 5.4, when $\nu \to \infty, 0$, the overall fixation probability is given by $\widetilde{\phi}_i \to \widetilde{\phi}_i^{(\infty)}$ when $\nu \to \infty$ and $\widetilde{\phi}_i \to \widetilde{\phi}_i^{(0)}$ when $\nu \to 0$, with

$$\widetilde{\phi}_i^{(\infty)} \equiv \widetilde{\phi}_i|_{\mathcal{K}} = \widetilde{\phi}_i|_{(1-\gamma^2)K_0} \tag{5.12}$$

$$\widetilde{\phi}_i^{(0)} \equiv \frac{1}{2}\left(\widetilde{\phi}_i|_{(1+\gamma)K_0} + \widetilde{\phi}_i|_{(1-\gamma)K_0}\right), \tag{5.13}$$

where $\widetilde{\phi}_i|_K$ is the overall fixation probability in the BDCLV with constant carrying capacity K, see Figure 4.6 (a,b). These results stem from the outcomes of Stage 2 when $\alpha_i K_0 \ll 1$ and from Stage 1 when $\alpha_i K_0 \gg 1$:

1. When $sK_0 \ll 1$, in regime (i) and about the boundary of regimes (i)-(ii): $\phi_{i,i+1} \approx 1/3$ for all species and $P_{(i,i+1)} \approx 1$, see Appendix C.3. The overall fixation probabilities are thus given by $\widetilde{\phi}_i \approx (1+\phi_i-\phi_{i-1})/3$, where $\phi_i \approx \phi_i^{(\infty)}$ if $\nu/s \gg 1$ and $\phi_i \approx \phi_i^{(0)}$ if $\nu/s \ll 1$, yielding (to leading order in sK_0)

$$\widetilde{\phi}_i \approx \widetilde{\phi}_i|_\kappa = \frac{1}{3}\left[1 + \frac{s\kappa}{12}(r_i - r_{i-1})\right], \tag{5.14}$$

   where $\kappa = (1-\gamma^2)K_0$ if $\nu/s \gg 1$ and $\kappa = K_0$ if $\nu/s \ll 1$. In agreement with Figure 5.4, Eq. (5.14) predicts that $\widetilde{\phi}_i$ is greater than $1/3$ and increases with sK_0 (at ν fixed) if $r_i > r_{i-1}$, whereas $\widetilde{\phi}_i$ is less than $1/3$ and is a decreasing function of sK_0 (at ν constant) when $r_i < r_{i-1}$.

2. When $\alpha_i K_0 \gg 1$, about the boundary of regimes (ii)-(iii) and in regime (iii): Selection strongly favors species i on edge $(i, i+1)$ in Stage 2, and the fixation probability is determined by the outcome of Stage 1: $\widetilde{\phi}_i \approx \widetilde{\phi}_i^{(\infty)}$ if $\nu \gg 1/K_0$ and $\widetilde{\phi}_i \approx \widetilde{\phi}_i^{(0)}$ when $\nu \ll 1/K_0$.

Hence, in regime (i) and about the boundary of regimes (i)-(ii) and (ii)-(iii), as well as in regime (iii) we have $\widetilde{\phi}_i \to \widetilde{\phi}_i^{(\infty)}$ when $\nu \to \infty$ and $\widetilde{\phi}_i \to \widetilde{\phi}_i^{(0)}$ when $\nu \to 0$. We have found that the fixation probabilities of the species surviving Stage 1 vary monotonically with ν, whereas the fixation probability of the species most likely to die out first varies little with ν, see the insets of Figure 5.4. Therefore, as corroborated by Figure 5.4, for finite switching rates, we have

$$\min\left(\widetilde{\phi}_i^{(0)}, \widetilde{\phi}_i^{(\infty)}\right) < \widetilde{\phi}_i < \max\left(\widetilde{\phi}_i^{(0)}, \widetilde{\phi}_i^{(\infty)}\right). \tag{5.15}$$

Taking into account the average number of switches arising in Stages 1 and 2, see C.4.3, we have $\widetilde{\phi}_i \approx \widetilde{\phi}_i^{(\infty)}$ when $\nu \gg \max(s, 1/K_0)$ and $\widetilde{\phi}_i \approx \widetilde{\phi}_i^{(0)}$ if $\nu \ll \min(s, 1/K_0)$, see Figure 5.4.

According to Eqs. (5.12)-(5.15), the fixation probabilities under random switching can be inferred from $\widetilde{\phi}_i|_K$ obtained in the constant-K BDCLV with a suitable value of K:

1. Under fast switching, $\widetilde{\phi}_i$ coincides with $\widetilde{\phi}_i|_{(1-\gamma^2)K_0}$. Since $\widetilde{\phi}_i|_K$ is a function of sK, when the average carrying capacity K_0 is kept fixed, $\widetilde{\phi}$ is thus given by $\widetilde{\phi}_i|_{K_0}$ subject to a rescaled selection intensity $(1-\gamma^2)s$. Hence, when $\nu \gg \max(s, 1/K_0)$ and K_0 is kept fixed, the effect of random switching is to reduce the selection intensity by a factor $1 - \mathrm{var}(K(t))/K_0^2$.

2. Under slow switching, $\widetilde{\phi}_i$ is given by the arithmetic average of $\widetilde{\phi}_i|_{K_+}$ and $\widetilde{\phi}_i|_{K_-}$. When the average carrying capacity K_0 is kept fixed, $\widetilde{\phi}$ is thus given by the average of $\widetilde{\phi}|_{K_0}$ subject to a selection intensity $(1+\gamma)s$ and $(1-\gamma)s$.

These predictions agree with the results of Figure 5.4, and imply that the sK_0-dependence of $\widetilde{\phi}_i$ can be readily obtained from Figure 4.6 (a,b).

At this point, we can discuss the effect of random switching on $\widetilde{\phi}_i$ by comparison with $\widetilde{\phi}_i|_{K_0}$ in the constant-K BDCLV, when K_0 is kept fixed:

- *Random switching "levels the field" of competition and balances the effect of selection*: The species that is the least likely to fixate has a higher fixation probability under random switching than under a constant $K = K_0$, compare Figures 4.6 (a,b) and 5.4 (see also Figure 5.5). The DMN therefore balances the selection pressure that favours the fixation of the other species, and hence levels the competition.

- *Random switching effectively reduces the selection intensity under fast switching*: When $\nu \gg \max(s, 1/K_0)$, we have seen $\widetilde{\phi}_i = \widetilde{\phi}_i|_{K_0}$ subject to a rescaled selection intensity $(1-\gamma^2)s = (1 - \mathrm{var}(K(t))/K_0^2)s$. Fast random switching therefore reduces the selection intensity proportionally to the variance of K. Hence, under strong selection and fast switching, a zero-one LOW law appears in the switching-K BDCLV only in a population whose average

size is $1/(1-\gamma^2)$ times greater than in the constant-K BDCLV. This means that when K has a large variance (large γ) the onset of the zero-one LOW, with $\widetilde{\phi}_i \to 0, 1/2, 1$, in the fast switching-$K$ BDCLV arises when $sK_0 \gg 1$ and K_0 is at least one order of magnitude larger than in the constant-K BDCLV (*e.g.*, $K_0 \gtrsim 10^4$ instead of $K_0 \gtrsim 10^3$ when $\gamma = 0.8$), see also Figure 5.5.

- *Random switching can yield new fixation scenarios*: Which species is the most likely to fixate can vary with ν and γ, at s and K_0 fixed, and does not generally obey a simple law (neither LOW nor LOSO). When the environmental variance is large enough ($\gamma \gtrsim \gamma^*$) the shaded areas of Figure 5.4 can overlap. This occurs when the fixation probabilities of the two most likely species to prevail cross, see insets of Figure 5.4. This yields different fixation scenarios below/above a critical switching rate $\nu^*(s)$: one of these species is the best off at low switching rate, while the other is the best to fare under fast switching. These crossings therefore signal a stark departure from the LOW/LOSO laws. For a crossing between $\widetilde{\phi}_i$ and $\widetilde{\phi}_{i+1}$ to be possible, one, say $\widetilde{\phi}_i$, should decrease and the other increase with ν, i.e. $\widetilde{\phi}_i^{(\infty)} < \widetilde{\phi}_i^{(0)}$ and $\widetilde{\phi}_{i+1}^{(\infty)} > \widetilde{\phi}_{i+1}^{(0)}$. Thus, if $\widetilde{\phi}_i^{(0)} > \widetilde{\phi}_{i+1}^{(0)}$ and $\widetilde{\phi}_i^{(\infty)} < \widetilde{\phi}_{i+1}^{(\infty)}$, there is a critical switching rate $\nu = \nu^*(s)$ where $\widetilde{\phi}_i = \widetilde{\phi}_{i+1}$. The crossing conditions can be determined using (5.12) and (5.13). A new fixation scenario emerges when the switching rate varies across ν^*: $\widetilde{\phi}_{i+1} > \widetilde{\phi}_i$ when $\nu > \nu^*$, while $\widetilde{\phi}_{i+1} \leq \widetilde{\phi}_i$ when $\nu \leq \nu^*$. Intuitively, crossings are possible when the variance of K is large ($\gamma \gtrsim \gamma^*$), ensuring that Stage 1 ends up with comparable probabilities of hitting two edges of S_3, and the two most likely species to fixate have a different ν-dependence arising from Stage 2, see Figure 5.3 (c,d). In the inset of Figure 5.4 (a), $\widetilde{\phi}_1$ decreases and $\widetilde{\phi}_2$ increases with ν; they intersect at $\nu = \nu^* \approx 0.01$ for $s = 10^{-1/4}$: Species 1 is the most likely to fixate at $\nu < \nu^*$ and species 2 the most likely to prevail at $\nu > \nu^*$, and we have $\widetilde{\phi}_1 > \widetilde{\phi}_2 \gg \widetilde{\phi}_3$ for $\nu < \nu^*$ and $\widetilde{\phi}_2 \gg \widetilde{\phi}_1 > \widetilde{\phi}_3$ when $\nu > \nu^*$. This is to be contrasted with Figure 4.6 (a), where the LOW yields $\widetilde{\phi}_1|_{K_0} \gg \widetilde{\phi}_2|_{K_0} \gg \widetilde{\phi}_3|_{K_0}$. The inset of Figure 5.4 (b), shows another

example of a fixation scenario that depends on ν, with $\widetilde{\phi}_3 > \widetilde{\phi}_1 > \widetilde{\phi}_2$ when $\nu < \nu^* \approx 0.03$ and $\widetilde{\phi}_1 \gtrsim \widetilde{\phi}_3 > \widetilde{\phi}_2$ when $\nu > \nu^*$.

The main effect of the random switching of K is therefore to balance the influence of selection and to "level the field" of cyclic dominance according to (5.12)-(5.15). This is particularly important under strong selection and large K variability, when random switching hinders the LOW by effectively promoting the fixation of the species that are less likely to prevail under constant $K = K_0$. This can result in new fixation scenarios in which the most likely species to win varies with the variance and rate of change of the carrying capacity.

To rationalize further how environmental variability affects the fixation probabilities, we compute the ratio of the fixation probability under switching K and that in the constant environment with $K = K_0$:

$$\rho_i \equiv \frac{\widetilde{\phi}_i}{\widetilde{\phi}_i|_{K_0}}, \tag{5.16}$$

which describes the effect of environmental noise on the fixation probability: we say that random switching enhances the fixation of species i when $\rho_i > 1$, whereas it hinders species i's fixation when $\rho_i < 1$ and environmental variability has no influence if $\rho_i \approx 1$. Using (5.12) and (5.13), we have $\rho_i \to \rho_i^{(\infty)} \equiv \widetilde{\phi}_i|_{(1-\gamma^2)K_0}/\widetilde{\phi}_i|_{K_0}$ and $\rho_i \to \rho_i^{(0)} \equiv (\widetilde{\phi}_i|_{K_-} + \widetilde{\phi}_i|_{K_+})/(2\widetilde{\phi}_i|_{K_0})$ for fast and slow switching, respectively. Simulation results of Figure 5.5 show that ρ_i varies non-monotonically across regime (i)-(iii), with a weak dependence on the switching rate ν, and ρ_i lying between $\rho_i^{(0)}$ and $\rho_i^{(\infty)}$ for intermediate ν.

It is clear in Figure 5.5 that, when there is enough environmental variance (large γ), the main effect of random switching arises at the boundary of regimes (ii)-(iii) and in regime (iii): In this case, the DMN balances the strong selection pressure yielding $\widetilde{\phi}_i < 1$ and $\rho_i < 1$ when $\widetilde{\phi}_i|_{K_0} \approx 1$ (for $r_i < r_{i\pm1}$), and $\widetilde{\phi}_i > 0$ and $\rho_i > 1$ when $\widetilde{\phi}_i|_{K_0} \approx 0$ (for $r_i > r_{i\pm1}$). This signals a systematic deviation from the asymptotic zero-one law predicted by the LOW in the constant-K BDCLV. The LOW and the zero-one LOW still arise in the switching-K BDCLV with $s = \mathcal{O}(1)$, but they set in for much larger values of K_0 than in the constant-K BDCLV (for $K_0 = 10^3 - 10^4$), see insets of Figure 5.5. This demonstrates

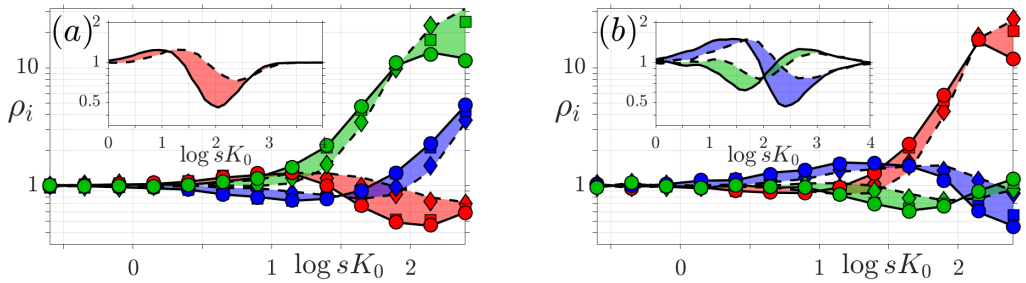

Figure 5.5: ρ_i vs. sK_0 for values of $s \in (10^{-3}, 1)$ and with $K_0 = 250$ and $\gamma = 0.8$ kept fixed, see text. (a) $\vec{r} = \vec{r}^{(1)}$; (b) $\vec{r} = \vec{r}^{(2)}$. Shaded areas and symbols are from stochastic simulations with $\nu = 10$ ($\circ$), $\nu = 0.1$ ($\square$), $\nu = 10^{-5/2}$ ($\diamond$); lines show $\rho_i^{(\infty)}$ (fast switching, solid) and $\rho_i^{(0)}$ (slow switching, dashed), see text. Insets: (a) $\rho_1^{(\infty)}$ (solid) and $\rho_1^{(0)}$ (dashed) vs. sK_0; (b) $\rho_2^{(\infty)}$ and $\rho_3^{(\infty)}$ (solid), $\rho_2^{(0)}$ and $\rho_3^{(0)}$ (dashed) vs. sK_0 with $\gamma = 0.8$ and $K_0 = 10000$ fixed and s varies between $1/K_0$ and 1. When $sK_0 = 10^3 - 10^4$, $\rho_i \to 1$. In both panels and insets: species 1 in red, species 2 in blue, and species 3 in green; $\vec{x}_0 = \vec{x}_c$; $\epsilon = 0$.

again that environmental variability acts to "level the field" of cyclic competition among the species by hindering the onset of the zero-one LOW.

From Eq. (5.14), when $sK_0 \ll 1$, to leading order, we find

$$\rho_i = 1 - s(K_0 - \kappa)\left(\frac{r_i - r_{i-1}}{12}\right), \tag{5.17}$$

with $\kappa = (1-\gamma^2)K_0$ if $\nu/s \gg 1$ and $\kappa = K_0$ if $\nu/s \ll 1$. When $sK_0 \ll 1$ and $\nu/s \gg 1$, we thus have have $\rho_i \approx 1 - s\gamma^2(r_i - r_{i-1})/12$ when $\nu/s \gg 1$ and $\rho_i = 1 + \mathcal{O}(s^2)$ when $\nu/s \ll 1$. This means that in regime (i), and at the boundary of regimes (i)-(ii), when the switching is fast enough ($\nu \gg s$), $\rho_i > 1$ if $r_i < r_{i-1}$ and $\rho_i < 1$ if $r_i > r_{i-1}$, which is in agreement with the results of Figure 5.5. Accordingly, whether a fast switching environment promotes/hinders species i under weak selection depends only on its growth rate relative to that of its strong opponent. In Figure 5.5, we notice a non-monotonic dependence of ρ_i on sK_0 resulting from a different influence of environmental variability under weak and strong selection: In Figure 5.5, the fixation probability of a species that is promoted/hindered under weak selection is hindered/promoted under strong selection.

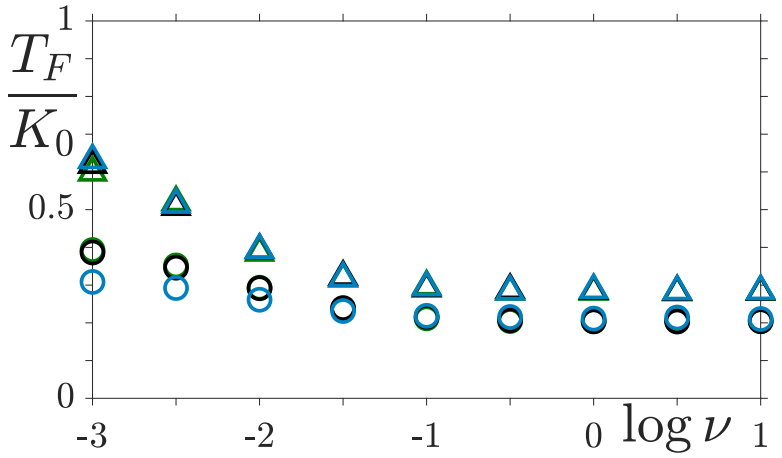

Figure 5.6: T_F/K_0 vs. ν for $r_1 = 1/11(\text{green}), 1/3(\text{black}), 3/5(\text{blue})$ and $r_2 = r_3 = (1-r_1)/2$, with $s = 10^{-1/2}$ (circles) and $s = 10^{-3/2}$ (triangles), showing $T_F = \mathcal{O}(K_0)$ over a broad range of values ν, see text. Parameters are: $K_0 = 250, \gamma = 0.8$ ($K_- = 50, K_+ = 450$) and $\vec{x}_0 = \vec{x}_c$; $\epsilon = 0$.

5.2.4 Mean Fixation time in the switching-K BDCLV

As for the constant-K BDCLV, the mean fixation time T_F is the average time taken for one species to take over the population. Similarly to the fixation probability, this quantity consists of one contribution from Stage 1, referred to as the *mean extinction time*, T_1, and the *mean absorption time*, T_2, arising from Stage 2. T_1 and T_2 are studied in detail in Appendix C.4, the main result of which is that when $\vec{x}_0 = \vec{x}_c$, the overall mean fixation time $T_F = \mathcal{O}(\langle N \rangle) = \mathcal{O}(K_0)$. This again means that species coexistence is lost in a mean time scaling with system size, with subleading prefactors that vary slowly with ν and s, see Figure 5.6. Hence while random switching balances the effect of selection to make competition more egalitarian, it does not prolong species coexistence.

5.3 Fixation properties of the close-to-zero-sum switching-K BDCLV

Here I will briefly discuss the effect of environmental variability on the close-zero-sum BDCLV, defined as (5.1) - (5.4) with $|\epsilon| \ll 1$. As in Section 4.4.2,

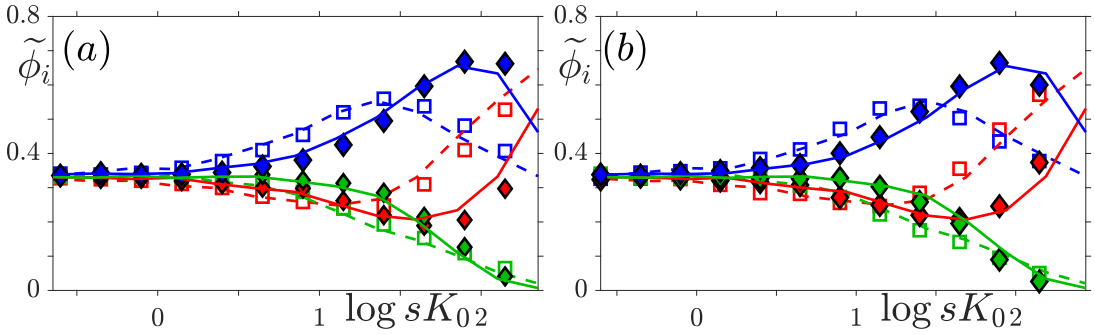

Figure 5.7: (a) $\widetilde{\phi}_i$ vs. sK_0 when K switches between $K_- = 50$ and $K_+ = 450$ ($K_0 = 250, \gamma = 0.8$), with $s \in (10^{-3}, 1)$. Symbols are stochastic simulation results for $\epsilon = -0.2$ and and $\nu = 10$ (filled diamonds) and $\nu = 0.001$ (open squares). Lines are stochastic simulation results from the BDCLV with same switching carrying capacity, $\nu = 10$ (solid) and $\nu = 0.001$ (dashed) and rescaled selection intensity $s \to s(1 + \epsilon/2)$, see text and Figure 5.4. (b) Same as in panel (a) with $\epsilon > 0$: Symbols are stochastic simulation results for $\epsilon = 0.2$; solid ($\nu = 10$) and dashed ($\nu = 0.001$) lines are results from the BDCLV with same switching carrying capacity and selection intensity $s \to s(1 + \epsilon/2)$. In all panels: red denotes species 1, blue species 2, and green species 3; $\vec{r} = \vec{r}^{(1)}$ and $\vec{x}_0 = \vec{x}_c$.

we use the approximation $\bar{f} \approx 1$ and assume that there is timescale separation between N and x_i. Then, proceeding as in Section 4.4.2 and focusing on the weak selection regime where $s \ll 1$ and $sK \approx 10$, we can assume that $\phi_{i,i+1} \approx 1/3$ and $P_{(i,i+1)} \approx 1$, and find that ϕ_i is given by (5.11) with the same carrying capacity and rescaled selection intensity $s \to s(1 + \epsilon/2)$. With the same arguments as in Section 4.4.2, the overall fixation probabilities across regimes (i) - (iii) are approximately the same as in the zero-sum switching-K BDCLV with rescaled selection intensity $s \to s(1 + \epsilon/2)$. This is confirmed by the simulation results in Figures 5.7, where we present $\widetilde{\phi}_i$ for fast and slow switching rates. As in the zero-sum BDCLV, results for intermediate ν lie between the data shown in Figure 5.7.

The mean fixation time of the close-to-zero-sum rock-paper-scissors game under weak selection can be obtained with a similar argument for the fixation probabilities. In fact, the mean absorption time T_2 and the mean fixation time $T_F = T_1 + T_2$ (T_1 varies little with s in regime (ii), see Figure C.3(a)) under weak

selection can be obtained from their values in the BDCLV with a rescaled selection intensity $s \to s(1 + (\epsilon/2))$, as shown in Figure 5.8 (a,b). This confirms that the effect of $0 < \epsilon \ll 1$ on the fixation properties simply boils down to increasing the selection intensity by a factor $1 + (\epsilon/2)$ with respect to the BDCLV when sK_0 are in regimes (i) and (ii). When $sK_0 \gg 1$ (regime (iii)), the above argument breaks down and rescaling the selection intensity of the BDCLV's mean fixation time is no longer a good approximation: As for the close-to-zero-sum constant-K BDCLV, under strong selection, the actual T_F is systematically overestimated and underestimated by the $s \to s(1 + (\epsilon/2))$ rescaling when $\epsilon > 0$ and $\epsilon < 0$ (compare Figure 5.8 with Figure 4.8(b)). This is not surprising when you consider that $\epsilon > 0$ (resp. < 0) corresponds to the case where the interior fixed point is now unstable (stable).

Hence, from these observations we can draw the same conclusion as in Section 4.4.2: The fixation statistics for *close-to*-zero-sum rock-paper-scissors games, $|\epsilon| \ll 1$ subject to a randomly switching carrying capacity, are well described by those of the zero-sum case with a fluctuating carrying capacity, with selection rescaled as $s \to (1 + \epsilon/2)s$.

5.4 Summary

This Chapter has shown that external noise in the form of a randomly switching carrying capacity has a marked effect on the outcome of Rock-Paper-Scissors games, here formulated as the BDCLV introduced in Section 4.4. This is because the outcome of the cyclic competition is driven demographic fluctuations which depend on the population size. This varies with the carrying capacity, hence internal noise is coupled to environmental noise: In general, the main results are: Firstly, random switching 'levels the field' of competition and balances the effect of selection. When the average carrying capacity is kept constant, the species that is least likely to prevail has a higher probability to fixate under random switching than in a static environment. In particular, when the rate of switching is very large, the effect of the environmental noise is to effectively reduce the selection intensity by a factor that increases with the variance of the carrying capacity. Thus, when the carrying capacity has a large variance, the

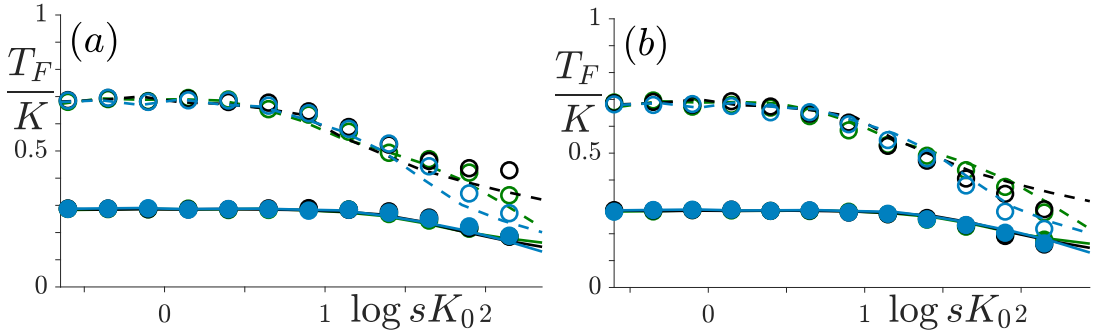

Figure 5.8: (a) T_F/K_0 vs. sK_0 when K switches between $K_- = 50$ and $K_+ = 450$ with $s \in (10^{-3}, 1)$, and $\nu = 10$ (closed symbols) and $\nu = 0.001$ (open symbols). Symbols are from stochastic simulations obtained for $\epsilon = -0.2$; solid ($\nu = 10$) and dashed ($\nu = 0.001$) lines are from the switching-K BDCLV obtained with the same $K(t)$ but selection intensity $s(1+\epsilon/2) = 0.9s$. (b) Same as in panel (a) with $\epsilon > 0$: Symbols are stochastic simulation results for $\epsilon = 0.2$; solid ($\nu = 10$) and dashed ($\nu = 0.001$) lines are results from the BDCLV with same switching carrying capacity and selection intensity $s \to s(1+\epsilon/2) = 1.1s$. In both panels: $\vec{r} = (1,1,1)/3$ (black), $\vec{r} = (1,5,5)/11$ (green), $\vec{r} = (3,2,2)/5$ (blue); $\vec{r} = \vec{r}^{(1)}$ and $\vec{x}_0 = \vec{x}_c$. $\vec{r} = \vec{r}^{(1)}$ and $\vec{x}_0 = \vec{x}_c$.

'law of the weakest' becomes a zero-one only when the average population size is much larger than in the case without external noise. Additionally, external noise can produce new fixation scenarios, not obeying the LOSO or LOW, that are not observed in the case without environmental randomness. This is due the absorption probabilities in Stage 2 depending on the switching rate, leading to one species being favoured below a critical ν and the other for fast switching. Fixation still occurs after a mean time that scales linearly with the average population size, with a subleading prefactor that depends on the switching rate. Hence, while environmental switching makes cyclic competition more even, it does not prolong species coexistence. Finally, as for the case without external noise, the fixation probabilities of close-to-zero-sum games can be found by rescaling the selection intensity.

Chapter 6

cCLV with a Variable Predation Rate

The final example of external noise that I will consider will be the effect of a variable reaction rate on the cCLV model introduced in Section 4.1. This is the simplest model of cyclic competition, with three dominance-replacement reactions constituting a zero-sum game where the total population size is fixed. Here the external noise affects one of the dominance-replacement rates: one of them switches between two values while the other two are assumed constant. This corresponds to the case where environmental variability corresponds to more or less favourable conditions for one of the species with the other two unaffected. As for the previous Chapter, I will be interested in the effect of external noise on the fixation probability of each species ϕ_i and the mean extinction time t_{ext} (In this Chapter, this is defined as the time it takes for the first species to die out, since once this happens the fate of the system is known). In particular, when does external noise causes a departure from the previously established 'LOW' for large populations, 'LOSO' for small populations and the linear dependence of the mean extinction time on N?

In Section 6.1 I will introduce the model and its basic properties, then the effect of noise in large populations will be analysed in detail Section 6.2. Section 6.3 gives a special case when the effect of noise can be worked out exactly when $N = 3$. A summary of the effect of random switching in terms of the population size, N, switching rate, ν, and external noise intensity, Δ, is then presented in

Section 6.4, and a description of the extension to the case where all three rates varying time with markedly different time-scales in presented in Section 6.5.

6.1 Model Definition

As in Section 4.1, we consider a well-mixed population of size N, with N_1 individuals of species 1, N_2 of type 2 and N_3 of type 3. The population size (and therefore strength of demographic noise) is kept fixed, but its composition changes in time due to cyclic competition between the species: 1 dominates 2, 2 dominates 3 and 3 dominates 1 according to the reaction scheme:

$$\begin{aligned} [N_1, N_2, N_3] &\xrightarrow{k_1} [N_1 + 1, N_2 - 1, N_3] \\ [N_1, N_2, N_3] &\xrightarrow{k_2} [N_1, N_2 + 1, N_3 - 1] \\ [N_1, N_2, N_3] &\xrightarrow{k_3} [N_1 - 1, N_2, N_3 + 1]. \end{aligned} \tag{6.1}$$

These are dominance-replacement reactions, where when two species interact, the weaker (according to the cyclic competition) dies and is instantaneously replaced by an offspring of the stronger. For example when individuals of species 1 and 2 interact, 1 kills 2 and replaces it with a species 1 offspring with rate k_1. I will assume that external noise affects the rate that 1 replaces 2, switching between two values according to a symmetric dichotomous Markov process,

$$k_1 = k_1(\xi(t)) = k + \Delta\xi = \begin{cases} k^+ = k + \Delta & \text{if} \quad \xi = +1 \\ k^- = k - \Delta & \text{if} \quad \xi = -1, \end{cases} \tag{6.2}$$

where $0 < \Delta < k$ is the intensity of the environmental noise and ξ varies in time according to:

$$\xi \xrightarrow{\nu} -\xi \quad (\xi \in \{-1, +1\}) \,. \tag{6.3}$$

To illustrate the most interesting effects of the noise, I will assume that species 1 is the strongest in the fixed environment *i.e.* $k > k_2, k_3$. Hence the states $\xi = \{+1, -1\}$ correspond to times when the environment is more/less favourable to species 1 than in the constant environment. This model will be abbreviated as 'CLVDN'

As discussed in Section 4.1, in a constant environment the mean field equations are characterised by a neutrally stable coexistence fixed point at $\vec{x}^* = (k_2, k_3, k_1)/(k_1 + k_2 + k_3)$, with orbits characterised by the conservation of $\mathcal{R} = x_1^{k_1} x_2^{k_3} x_3^{k_1}$ (where $x_1 = N_1/N$ *etc.*). In finite populations, stochastic trajectories follow the deterministic orbits for a small transient, performing a random walk between them until the boundary of the state space S_3 is hit. The fixation probabilities are characterised by the 'LOW' in large populations ($N \gtrsim 100$) (which becomes a zero-one law asymptotically), and the 'LOSO' when $N \lesssim 20$. It has also been shown that the mean fixation time scales with N (see Section 4.1 for a description of these laws).

With external noise in the form of a variable rate k_1, the process forms a piecewise deterministic Markov process when the population size $N \to \infty$, with the mean fractions of each species evolving according to:

$$\begin{aligned} \frac{dx_1}{dt} &= x_1\left[(k+\Delta\xi)x_2 - k_3 x_3\right], \\ \frac{dx_2}{dt} &= x_2\left[k_2 x_3 - (k+\Delta\xi)x_1\right], \\ \frac{dx_3}{dt} &= x_3\left[k_3 x_1 - k_2 x_2\right]. \end{aligned} \tag{6.4}$$

Hence each environment is characterised by its own coexistence fixed point, $\vec{x}^*_{\pm 1} = (k_2, k_3, k^{\pm})/(k_2 + k_3 + k^{\pm})$, and conserved quantity $\mathcal{R}^{\pm} = x_1^{k_2} x_2^{k_3} x_3^{k^{\pm}}$ (see Figure 6.1). Thus, when the environment switches (after an average time of ν^{-1}), the location of the fixed point changes from $\vec{x}^*_{\xi}$ to $\vec{x}^*_{-\xi}$. The dynamics then settle onto a new set of orbits that can be closer to the boundaries of the phase space, the amplitude and period of the oscillations change and the densities can suddenly be very close to 0 or 1. (see Figure 6.2). As for the case without external noise, demographic fluctuations in finite populations cause the extinction of two species and the fixation of the system by the remaining species.

I will now discuss the effect of a switching rate on the fixation probabilities in large populations, focusing on the different switching regimes as characterised by the rate ν.

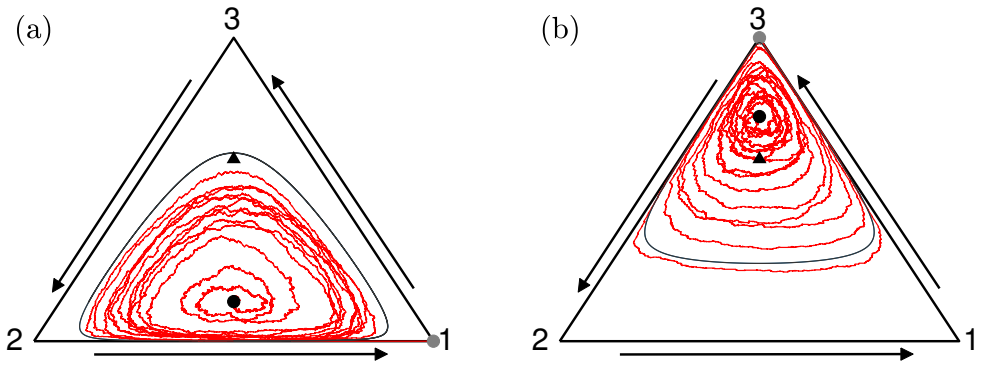

Figure 6.1: Stochastic orbits (red) of the CLVDN with $\nu = 0$ (i.e. the system only experiences one environment), $k = 3$ and $\Delta = 2.7$: Orbits surrounding (a) $\vec{x}^*_{-1}$ (circle) in the state $\xi = -1$, and $\vec{x}^*_{+1}$ (circle) in the state $\xi = +1$ in (b). Black solid lines indicate the 'outermost orbit' in each state $\xi = \pm 1$ (Berr *et al.* (2009)) (see Section 6.2.3) : It passes at a distance $1/N$ from the absorbing edge 12 in (a) and from either of the absorbing edges 13 and 23 (b). The coexistence state $\vec{x}^*$ is shown as a reference (triangle). Other parameters are $k_2 = k_3 = 1$ and $N = 1000$.

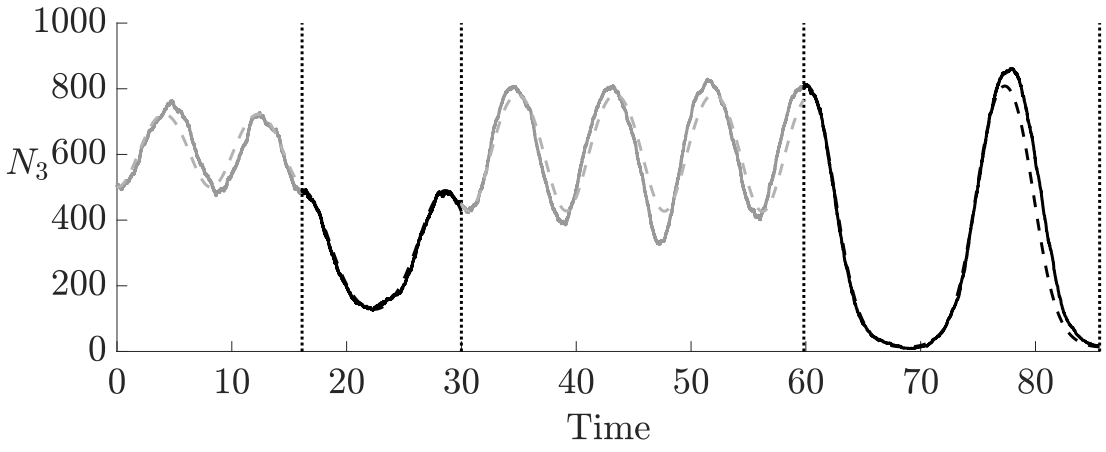

Figure 6.2: Solid: Time series of $N_3(t)$ in the CLVDN in a population of size $N = 1000$ (single simulation realization). Dashed: PDMP sample path for $x_3(t)N$, with $x_3(t)$ obtained from (6.4). Vertical dotted black lines indicate the points in time when the environment switches. Light gray indicates the evolution in the environmental state $\xi = +1$ and dark gray corresponds to $\xi = -1$. Other parameters are: $k_1 = 2, k_2 = k_3 = 1, \Delta = 1.2$ and $\nu = 0.05$.

6.2 Effect of Noise on Fixation Statistics in Large Populations

Determining the effect of external noise on the fixation probability is an intriguing puzzle, the result of which is not obvious *a-priori*. In this Section I will discuss the effect of external noise in large populations, in which the fixation probabilities follow the 'LOW' in a constant environment (see (4.8))). I will show that different scenarios emerge above and below a critical environmental intensity $\Delta^* \equiv k - k_{\min}$, where $k_{\min} = \min\{k_2, k_3\}$. Here, because $k > k_2, k_3$, the LOW predicts that $\phi_1 \to 0$ when $N \gg 1$, the LOW is no longer valid when the fixation probability of species 1 no longer vanishes in a large population.

In order to understand the results, in the subsequent subsections extensive computer simulations are reported with $k_2 = k_3 = 1$ and $k > 1$. Hence in these examples the critical intensity is $\Delta^* = k - 1 > 0$, with $k^- > 1$ when $\Delta < \Delta^*$ and $k^- < 1$ when $\Delta > \Delta^*$, while $k^+ > 1$ for al values of Δ. Hence when $\Delta < \Delta^*$ species 2 and 3 are the weakest in both environments, but when $\Delta > \Delta^*$ species 2 and 3 are the weakest in one environment and 1 is in the other. The simulations were performed using the Gillespie algorithm (Gillespie (1977)) with averages for ϕ and t_{ext} taken over 10000 runs for each parameter set, with simulations started at the fixed point in the absence of external noise $\vec{x}^* = (1, 1, k)/(k + 2)$. The population size $N \sim 10^3$ is large enough so that in the absence of noise the LOW holds, where $(k_1, k_2, k_3) = (k, 1, 1)$ predicting that $(\phi_1, \phi_2, \phi_3) \xrightarrow{N \gg 1} (0, 1/2, 1/2)$.

The simulation results of Figures 6.3(a,b), 6.4(a,b) and 6.5(a,b) confirm that t_{ext} scales with the population size N in all regimes. This can be explained as in the cCLV: extinction in the CLVDN results from a random walk between the nested neutrally stable orbits in the phase space S_3 driven by demographic noise, see Figure 6.1. In the CLVDN the erratic trajectories depend on the environment, changing with Δ and k. however it still takes $\sim N^2$ infinitesimal steps occurring at time increment $\sim 1/N$ to reach the edge of S_3 starting from the interior of the phase space. Hence the mean extinction time scales with N, *i.e.* $t_{\text{ext}} \sim N$, as verified in Figures 6.3(a), 6.4(a) and 6.5(a).

Since t_{ext} scales with the population size, and as the average time between two random switches is ν^{-1}, the average number of environmental switches before

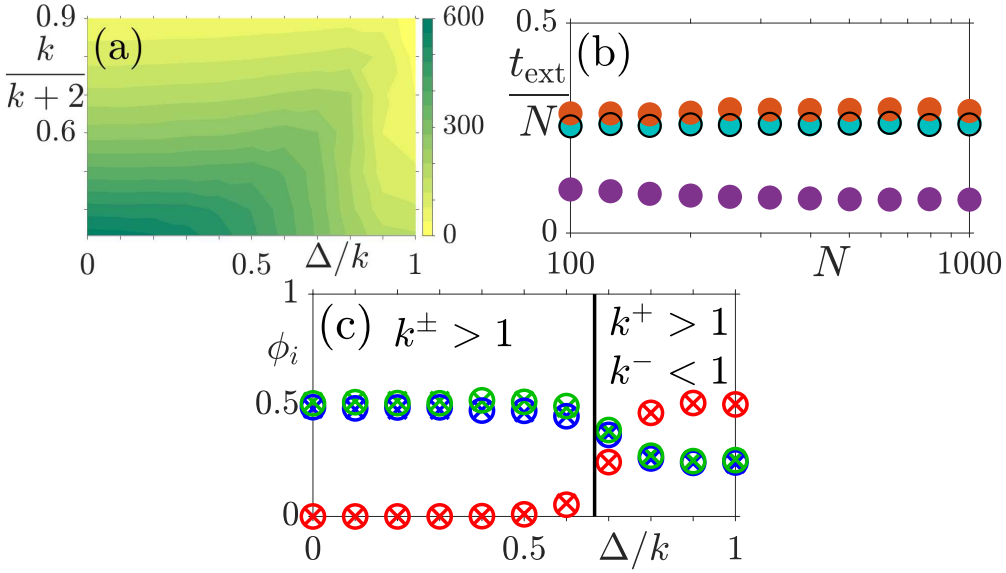

Figure 6.3: t_{ext} and ϕ_i of the CLVDN in the slow-switching regime. (a) Heatmap of t_{ext} as function of $k/(k+2)$ and Δ/k for $(N, \nu) = (1000, 10^{-4})$: t_{ext} increases when Δ is raised from 0 to $\Delta^* = k - 1$ and decreases after. (b) t_{ext} vs N for $k = 3$, $N\nu = 0.1$ ($10^{-4} \leq \nu \leq 10^{-3}$), $\Delta = (0.5, 2, 2.7)$ represented by blue, orange and purple circles respectively. Open symbols show results for $\Delta = 0$. t_{ext} scales (approximately) linearly with the population size and is largest when $\Delta = k - 1$ (see text). (c) $\phi_i, i \in \{1, 2, 3\}$ vs. Δ/k with $(N, \nu) = (1000, 10^{-4})$ and $(N, \nu) = (2000, 5 \times 10^{-5})$ represented by crosses and circles respectively. Colour code: species 1 is in red, 2 in blue, and 3 in green. As an eyeguide, there is a vertical line at Δ^*/k.

extinction is of order $N\nu$. Thus I will discuss three regimes: (a) the slow switching regime where $N\nu \ll 1$ (Section 6.2.1), (b) the fast switching regime where $N\nu \gg 1$ (Section 6.2.2), and (c) the intermediate switching regime where $N\nu \sim \mathcal{O}(1)$ (Section 6.2.3). These situations correspond to the dichotomous noise having (a) long correlation time, (b) short correlation time, and (c) a finite correlation time, when compared to the mean extinction time t_{ext}.

6.2.1 Slow-switching regime $N\nu \ll 1$

In this regime, $t_{\text{ext}} \ll 1/\nu$, and the external noise has a long correlation time $1/\nu \gg N \gg 1$. Hence, only very few or no switches occur prior to extinction. This means that in this regime the population is as likely to be locked into either of the environmental states $\xi = \pm 1$ (since $\langle \xi \rangle = 0$) until one species takes over and the others go extinct after a time of order $t_{\text{ext}} \sim N$. This can be used to determine the fixation probabilities:

- When $\Delta < \Delta^*$ and N is sufficiently large, the *LOW is followed* because $k^{\pm} > 1$: 2 and 3 are the 'weakest' species and therefore the most likely to survive in a large population, i.e. $\phi_2 \approx \phi_3 > \phi_1$ (Berr *et al.* (2009)). When $N \gg 1$, the LOW takes its zero-one form and thus species 2 or 3 is certain to be the sole species to survive whereas 1 goes extinct: $(\phi_1, \phi_2, \phi_3) \xrightarrow{N \gg 1} (0, 1/2, 1/2)$, as shown in Figure 6.3(c).

- When $\Delta > \Delta^*$, the LOW *is not valid* because $k^- < 1$ and $k^+ > 1$: When $\xi = -1$, $k_1 = k^- < 1$ and 1 is the weakest species, whereas when $\xi = +1$, $k_1 = k^+ > 1$ and 1 is the strongest species. Since the population is as likely to be locked in either state $\xi = \pm 1$, in half of the realizations species 1 is the most likely to survive and in the others it is the least likely to survive. When $N \gg 1$, in the former case species 1 is certain to be the sole surviving species whereas in the latter situation it is guaranteed to go extinct while species 2 and 3 have the same probability to survive. Hence, when $N \gg 1$ we find $(\phi_1, \phi_2, \phi_3) \xrightarrow{N \gg 1} (1/2, 1/4, 1/4)$, which is in good agreement with the results of Figure 6.3(c). So even though the LOW is valid in either environmental state, the fact that a realization is effectively locked in the state it starts in leads the LOW to not being valid overall.

- When $\Delta = \Delta^* = k - 1$, we have $k^- = k_2 = k_3 = 1$ and $k^+ > 1$. Hence, all species are as likely to survive when $\xi = -1$ (*i.e.* $\phi_i = 1/3 \ \forall i$), while 1 is the strongest species and therefore the least likely to survive when $\xi = +1$. When $N \gg 1$, this means that species 1 is certain to go extinct in the environmental state $\xi = +1$ and the other two species survive with probability 1/2 each. Taking into account that the system is equally likely

to stay in either state $\xi = \pm 1$, we find $(\phi_1, \phi_2, \phi_3) \xrightarrow{N\gg 1} (1/6, 5/12, 5/12)$, as confirmed by Figure 6.3(c).

Furthermore, in Figure 6.3(c) the results for different values of (N, ν) are identical when $N\nu$ is kept constant. One can proceed similarly if the rates are all different, say $k > k_2 > k_3$ and finds that $(\phi_1, \phi_2, \phi_3) \xrightarrow{N\gg 1} (0, 0, 1)$ when $\Delta < \Delta^* = k - k_3$, and $(\phi_1, \phi_2, \phi_3) \xrightarrow{N\gg 1} (1/2, 0, 1/2)$ when $\Delta > \Delta^*$. These results indicate a transition occurring at $\Delta = \Delta^*$, and that external noise alters the fixation probabilities when $\Delta > \Delta^*$: if the external noise is sufficiently strong, $\Delta > \Delta^*$, no species is guaranteed to survive and the LOW is no longer valid.

The results of the fixation probabilities can qualitatively explain the dependence of t_{ext} on Δ and k by noting that when $\Delta > 0$ and k increase, $\vec{x}^*_{+1}$ moves toward the absorbing boundaries of species 2 and 3 while $\vec{x}^*_{-1}$ moves toward the absorbing boundary of species 1, see Figure 6.1. When $\Delta < \Delta^*$ and $N \gg 1$, the system attains either the absorbing state of species 2 or 3 which takes longer from the orbits surrounding $\vec{x}^*_{-1}$ than from those around $\vec{x}^*_{+1}$. Hence, when $\Delta < \Delta^*$, t_{ext} increases as Δ increases (with k fixed) because $\vec{x}^*_{-1}$ moves closer to the center of S_3. However, when $\Delta < \Delta^*$ is kept fixed, t_{ext} decreases when k increases and approaches the edges of S_3. When $\Delta > \Delta^*$ and $N \gg 1$, there is a finite probability to reach any of the three absorbing states and this takes approximately the same time from any of the orbits surrounding $\vec{x}^*_{\pm 1}$ which decreases as k and Δ increase (since $\vec{x}^*_{\pm 1}$ approach the boundaries of S_3). Hence, t_{ext} decreases when k and Δ increase and $\Delta > \Delta^*$. t_{ext} is maximal when $(\Delta, k) = (k - 1, 1)$, and it is minimal when $\Delta \to k \gg 1$.

6.2.2 Fast-switching regime $N\nu \gg 1$

In this regime, the environment varies rapidly with respect to the time scale of the population evolution. Hence, $k_1(\xi)$ switches many times ($\sim N\nu \gg 1$ times, on average) before extinction occurs, and thus self-averages: $k_1(\xi) \to k_1(\langle\xi\rangle) = k$ (Bena (2006); Horsthemke & Lefever (1984); Wienand *et al.* (2017)). In this regime, the CLVDN is approximately identical to the cCLV with reaction rates $(k_1, k_2, k_3) = (k, 1, 1)$ and therefore

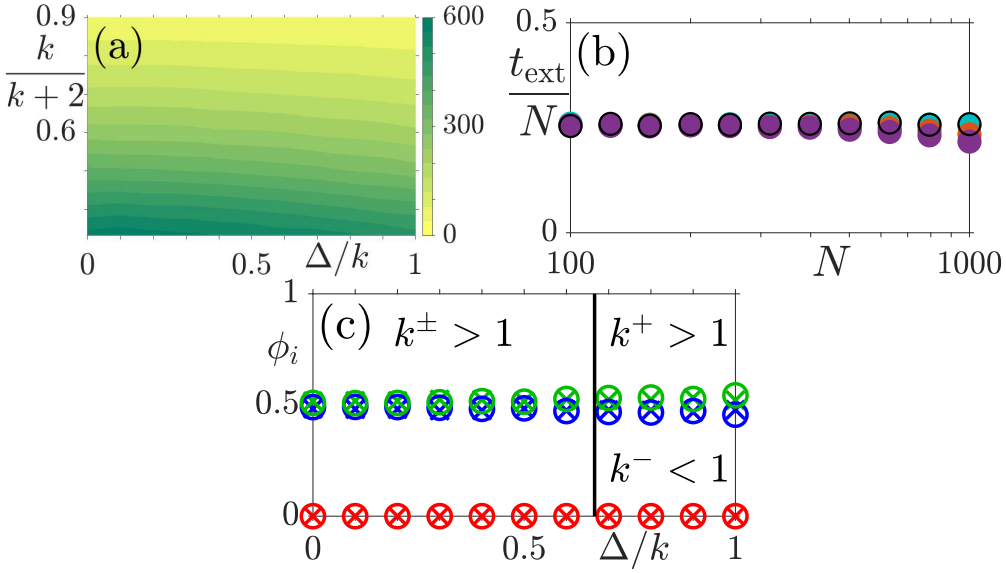

Figure 6.4: t_{ext} and ϕ_i of the CLVDN as in Figure 6.3 but in the fast-switching regime. (a) Heatmap of t_{ext} as function of $k/(k+2)$ and Δ/k for $(N, \nu) = (1000, 100)$. (b) t_{ext} vs N for $k = 3$, $N\nu = 10^5$ ($100 \leq \nu \leq 1000$), $\Delta = (0.5, 2, 2.7)$ represented by blue, orange and purple circles respectively. Open symbols show results for $\Delta = 0$. t_{ext} scales (approximately) linearly with the population size and is almost independent of Δ. (c) $\phi_i, i \in \{1, 2, 3\}$ vs. Δ/k with $(N, \nu) = (1000, 100)$ and $(N, \nu) = (2000, 50)$. Same colour code, symbols and vertical line as in Figure 6.3(c).

- The *LOW holds* (when $N > 20$ (Berr *et al.* (2009)), see also below) for all values of Δ: species A is the strongest and therefore the least likely to survive, and we have $(\phi_1, \phi_2, \phi_3) \xrightarrow{N\gg 1} (0, 1/2, 1/2)$ when $N \gg 1$, see Figure 6.4(c).

- Figures 6.4(a,b) show that, in this regime, t_{ext} is independent of Δ due to the self-averaging, but it decays when k increases and $\vec{x}^*$ moves closer to the 2 and 3 absorbing boundaries, see Figure 6.1(c). $t_{\text{ext}} \sim N$ is maximal when $k \approx 1$, and all species coexist with densities oscillating about the same values in the transient prior to extinction.

Again, notice that in Figure 6.4(c) the results for different values of (N, ν) are identical when $N\nu$ is kept constant. In Figure 6.4(c) we notice that ϕ_3 is slightly greater than ϕ_2 for all values of Δ. This small effect stems from the influence of the LOSO which says that in small population (without external noise), species 3 is more likely to survive than species 1 and 2 since here $k > k_2, k_3$ ($\Delta^* > 0$) and $\xi \to \langle \xi \rangle = 0$ self averages.

One can proceed similarly if the rates are all different, say $k > k_2 > k_3$, in which case, according to the zero-one LOW, we have $(\phi_1, \phi_2, \phi_3) \xrightarrow{N\gg 1} (0, 0, 1)$.

6.2.3 Intermediate-switching regime $N\nu \sim \mathcal{O}(1)$

In this regime, the population composition and the environment vary on comparable time scales. On average, there are therefore a finite number of switches occurring prior to extinction, and the environmental noise does not self-average. A markedly different fixation behaviour is therefore expected in this regime, where the external noise has a finite positive correlation time, than in the other regimes. For large but finite N, in Figure 6.5(c), the following is found:

- When $\Delta < \Delta^*$, species 1 is the strongest species and thus the least likely to survive according to the LOW, with $\phi_1 \approx 0$, whereas $\phi_2 \approx \phi_3 \approx 1/2$ when $\Delta \approx 0$. However, ϕ_3 increases and ϕ_2 decreases when Δ is raised from 0 to Δ^*.

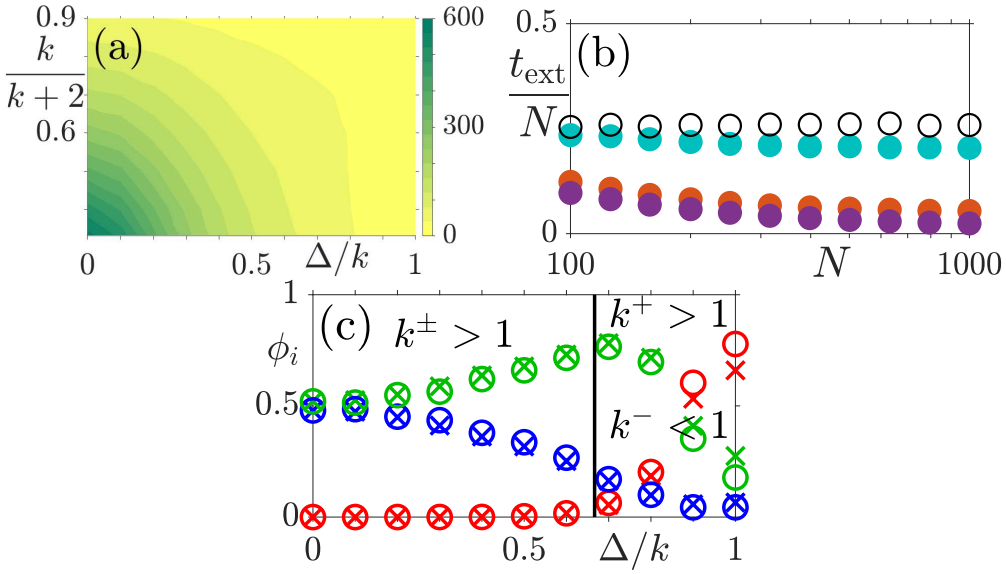

Figure 6.5: t_{ext} and ϕ_i of the CLVDN as in Figure 6.3 in the intermediate-switching regime. (a) Heatmap of t_{ext} as function of $k/(k+2)$ and Δ/k for $(N, \nu) = (1000, 0.05)$. (b) t_{ext} vs N for $k = 3$, $N\nu = 50$ $(0.5 \leq \nu \leq 0.05)$, $\Delta = (0.5, 2, 2.7)$ represented by blue, orange and purple circles respectively. Open symbols show results for $\Delta = 0$. t_{ext} scales approximately linearly with the population size and decreases as Δ increases (see text). (c) $\phi_i, i \in \{1, 2, 3\}$ vs. Δ/k with $(N, \nu) = (1000, 0.05)$ and $N = (2000, 0.025)$. Same colour code, symbols and vertical line as in Figure 6.3

- When $\Delta > \Delta^*$, both ϕ_2 and ϕ_3 decrease when Δ is raised, while ϕ_1 increases with Δ. Hence, when $\Delta \approx k$, species 1 is the most likely to be the surviving one whereas species 2 is the most likely to go extinct: $\phi_1 > \phi_3 > \phi_2$. Therefore, under strong external noise, the species that is the strongest without environmental randomness (species 1) is the most likely to prevail. In this case, the LOW is not valid since these results are in *stark contrast with the predictions of the LOW* for the cCLV with reaction rates $(k_1, k_2, k_3) = (k, 1, 1)$ and $k > 1$.

- Surprisingly, the fixation probability ϕ_3 exhibits an intriguing non-monotonic dependence on Δ and species 3 is most likely to be the surviving one when $\Delta \approx \Delta^*$, which is explained below. The results for different values of (N, ν) are identical when $N\nu$ is kept constant.

- t_{ext} decreases when k increases because $\vec{x}^*$ moves towards the absorbing boundaries of 2 and 3. Additionally t_{ext} decreases as Δ increases, as a result of the environmental switching changing the parts of the phase space that are more prone to extinction, as explained below.

To explain the intriguing behaviour of ϕ_i reported in Figure 6.5(c), the arguments used in Berr *et al.* (2009) can be adapted to discuss the fixation probabilities in the cCLV. For this, the authors of Berr *et al.* (2009) used the so-called 'outermost orbit' as the deterministic orbit that lies at a distance $1/N$, i.e. one dominance-replacement reaction away, from the closest edge of S_3. In the cCLV, extinction arises once on the outermost orbit when a chance fluctuation pushes the trajectory along the edge of S_3 that drives it toward the absorbing state of the weakest species, yielding the LOW. Within a piecewise deterministic Markov process picture, we can adapt this argument to the CLVDN dynamics by considering two types of outermost orbits obtained from $\mathcal{R}^{\pm}$: the orbit that surrounds $\vec{x}^*_{-1}$ (formed by the points satisfying $\mathcal{R}^-(t) = \mathcal{R}^-(0)$) and is associated with the environmental state $\xi = -1$, and that is at a distance $1/N$ from the 23 and 31 edges of S_3 when $\Delta < \Delta^*$, or the 12 edge of S_3 when $\Delta > \Delta^*$, as shown in Figures 6.1(a) (see also Figure 6.6). The other outermost orbit (formed by the

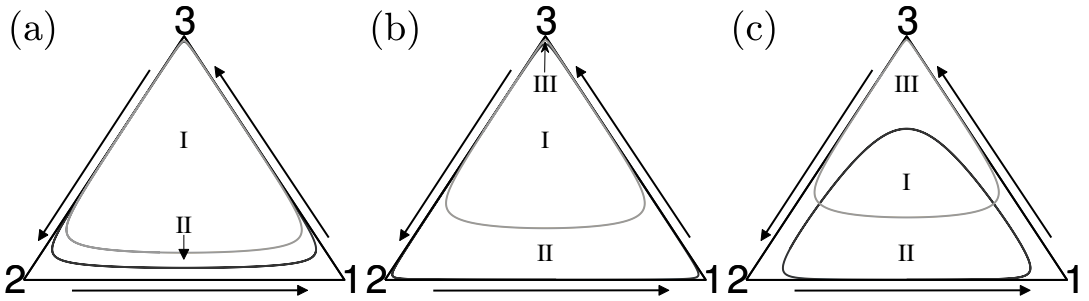

Figure 6.6: Outermost orbits for $N = 1000$, $(k, k_2, k_3) = (3, 1, 1)$ with $\Delta = 0.5$ (a), $\Delta = 2$(b) and $\Delta = 2.7$(c). The orbits in the environmental state $\xi = +1$ ($k_1 = k + \Delta$) are in gray; those in the state $\xi = -1$ ($k_1 = k - \Delta$) are in black. Region I: area of S_3 where the switching of k_1 leaves the trajectory within an outermost orbit. Regions II/III show the areas where where extinction is very likely, see text. In (a) and (b) the area in Region III (only species 1 survives) is very small and Region II (species 3 sole surviving species) increases with Δ up to $\Delta \approx \Delta^*$. When $\Delta > \Delta^*$, as in (c), the area in Region II/III decreases/increases when Δ is increased.

points satisfying $\mathcal{R}^+(t) = \mathcal{R}^+(0)$) surrounds $\vec{x}^*_{+1}$ and is associated with the environmental state $\xi = +1$, as shown in Figure 6.1(b); it is at a distance $1/N$ from the 31 and 23 edges of S_3. When $\Delta < \Delta^*$, these two types of outermost orbits overlap greatly, see Figure 6.6(a,b) where they are approximately equal except when the density of species 3 is small, whereas there is only a partial overlap when $\Delta > \Delta^*$ as shown in Figure 6.6(c). These considerations help shed light on the Δ-dependence of the fixation probabilities.

In fact, when $N \gg 1$, a typical CLVDN trajectory in S_3 performs a random walk around $\vec{x}^*_{\pm 1}$ by approximately moving along the nested deterministic orbits and moving from one to another, see Figures 6.1 and 6.2. When the environment switches, the orbit on which the trajectory is instantly changes, as does the coexistence fixed point. This results in a trajectory on an orbit that is either closer or further to the absorbing boundary of S_3. As in the cCLV, if after a switch the trajectory lands outside the outermost orbit of the actual environmental state, internal fluctuations are likely to drive it to extinction into the closest absorbing state (if no other switches occur prior to extinction). This picture can be ratio-

nalized by considering the Regions I-III shown in Fig 6.6: Region II denotes the area within the $\xi = -1$ outermost orbit that lies outside the $\xi = +1$ outermost orbit. Region III is defined similarly for the part of within the $\xi = +1$ outermost orbit, while Region I is the area contained within both outermost orbits. The dynamics in each of these regions is the following:

- When there is a switch $\xi = -1 \to \xi = +1$, the trajectories lying within Region II are outside the system's outermost orbit and are very likely to flow along the 13 edge and reach the species 3 absorbing state ($\phi_3 = 1$).
- Similarly, when a switch from $\xi = +1 \to \xi = -1$ occurs, the trajectories within Region III are outside the actual outermost orbit and therefore flow along the 23 and 12 edges to attain the species 1 absorbing state ($\phi_1 = 1$).
- All trajectories within Region I remain within the outermost orbit independently of the environmental state and their dynamics is essentially the same as in the cCLV and dominated by internal noise. The LOW applies within Region I and in the case of Figure 6.5(c) lead to the species 2 or 3 absorbing state with probability 1/2 ($\phi_2 = \phi_3 = 1/2$).

As a consequence, the area in Region I indicates the influence of the external noise in departing from the cCLV/LOW scenario, while the areas of Region II and III are associated with the probability of species 3 and 1 being the sole surviving species. When Δ is small (weak external noise), Regions I and II cover respectively a large and small part of S_3 while Region III is negligible, corresponding to $\phi_1 \approx 0$, see Fig 6.6(a). Since Region II/I slightly increases/decreases when Δ increases, ϕ_3 increases with Δ up to $\Delta = \Delta^*$, see Fig 6.6(b). When $\Delta \gtrsim \Delta^*$, $\vec{x}^*_{\pm 1}$ are well separated and all Regions I-III have a finite area corresponding to finite probabilities ϕ_i. When Δ is increased further, the area of Region III grows and that within Region I and II shrink, see Fig 6.6(c). Hence, ϕ_1 increases while ϕ_2 and ϕ_3 decrease with Δ when $\Delta > \Delta^*$, and species 1 is the most likely to be the surviving one when the amplitude of the external noise is strong enough (for $\Delta \gtrsim 2.4$ in Figure 6.5(c)). This analysis explains the features of ϕ_i displayed in Figure 6.5(c) and in particular, the non-monotonic Δ-dependence of ϕ_3.

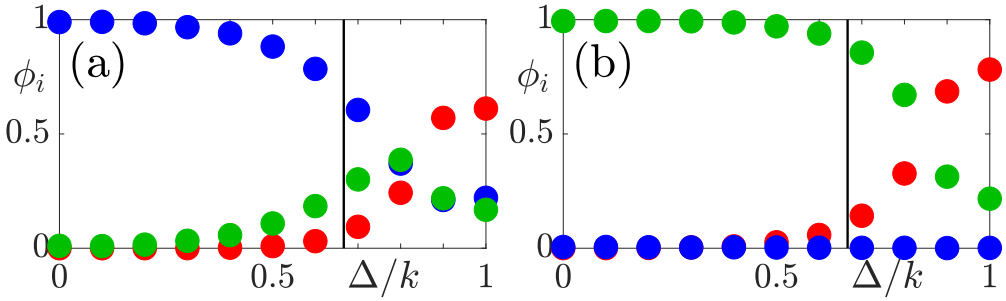

Figure 6.7: Survival probabilities for the CLVDN when $k_2 \neq k_3$. The effect on the fixation probabilities is the same as in the case for $k_2 = k_3$, with differences due to the expected behaviour in the absence of external noise. Parameters are: $k_1 = 3$, $N = 1000$, $\nu = 0.05$. Species (1, 2, 3) represented by (red, blue, green) circles respectively. (a) $k_2 = 1 < k_3 = 2$: B is the weakest species in the absence of external noise so is initially the most likely species to survive. The qualitative behaviour of the fixation probabilities is the same as for $k_2 = k_3$, except the peak of ϕ_3 has moved to the right. (b) $k_2 = 2 > k_3 = 1$: 3 is the weakest species in the absence of external noise, so starts of as the most likely species to survive.

This can also explain the monotonic decrease of the t_{ext} for fixed k: as Δ increases, the fraction of the phase space contained in Regions II and III increases, so a larger amount of the phase space is more prone to extinction, reducing the expected time to extinction.

When $k_2 \neq k_3$, the results are similar: Figure 6.7 shows the results for (a) $k_2 < k_3$ and (b) $k_2 > k_3$. In the first case species 2 is the most likely species to survive without external noise (EN), and as the intensity Δ of the EN is increased ϕ_2 decreases, while ϕ_1 increases after $\Delta = \Delta^*$ and ϕ_3 increases then decreases. The only difference with Figure 6.5(c) is that ϕ_3 reaches its peak slightly after $\Delta = \Delta^*$. When $k_2 > k_3$, species 3 is the surviving one with probability 1 in the absence of EN, so $\phi_3 \approx 1$ when $\Delta \approx 0$ and then ϕ_3 is reduced as the EN intensity Δ increases, with most of the variation occurring after $\Delta = \Delta^*$, when ϕ_1 increases ($\phi_2 \approx 0$ for all values of Δ). Thus the non-monotonic dependence of ϕ_3 on Δ is a robust non-trivial joint effect of internal and environmental noise.

6.3 Deviation from the 'LOSO' in Small Populations

In the cCLV, the fixation probabilities obey the law of stay out (LOSO see (4.10)) in small systems, typically for $3 \leq N \lesssim 20$ (Berr *et al.* (2009)). It has also been found that the LOSO quantitatively influences ϕ_i in populations of greater size (Berr *et al.* (2009)). Here, the CLVDN fixation probabilities in small populations are studied in order to understand how external noise alters the LOSO. In particular, given $(k_1, k_2, k_3) = (k + \Delta\xi(t), k_2, k_3)$, I ask *whether the ϕ_i's satisfy the LOSO relations in a small population when* $\Delta > 0$. When it is the case, we say that the LOSO is followed, otherwise the LOSO is not valid when $\Delta > 0$.

To address this question, first consider a population of size $N = 3$. Proceeding as described in Appendix C.5.2, it is found that

$$\phi_1 = \frac{(\gamma+\nu)\,k_2}{\gamma^2 - \Delta^2 - \nu^2}, \quad \phi_2 = \frac{(\gamma+\nu)\,k_3}{\gamma^2 - \Delta^2 - \nu^2}, \quad \phi_3 = \frac{k(\gamma+\nu) - \Delta^2}{\gamma^2 - \Delta^2 - \nu^2}, \tag{6.5}$$

where $\gamma = k + k_2 + k_3 + \nu$. Clearly, in the absence of external noise ($\Delta = 0$) one recovers the LOSO according to which $\phi_3 > \phi_1, \phi_2$ when, as in this section, $k > k_2, k_3$. However, it is clear from (6.5) that when $\Delta > 0$, it is only when $(\gamma + \nu)(k - \max(k_2, k_3)) > \Delta^2$, that $\phi_3 > \phi_1, \phi_2$. Hence, even when $N = 3$, the LOSO is followed only at sufficiently low Δ and/or at high enough ν, but is generally not valid. The results (6.5) indicate that determining which of species $1, 2$ or 3 is the species to be the most likely to survive in small systems of size $3 \leq N \lesssim 20$ depends non trivially on (Δ, ν) and on the k_is. Hence, the LOSO is generally not valid for small systems in the presence of environmental noise, and there is no simple general "law" to predict which species is most likely to survive in small populations when $\Delta > 0$. An exception arises in the fast-switching regime, $N\nu \gg 1$, when the noise self-averages and one recovers the LOSO for $3 \leq N \lesssim 20$. It has also to be noticed that for such small systems, the initial condition becomes relevant. What is more important here, is that it is confirmed that, as for the cCLV, coherent large-system scenarios emerge also in the CLVDN when $N \gtrsim 100$. Hence, small-size effects are marginal in systems of size $N \geq 1000$ that we have considered in sections 6.2.1, 6.2.2 and 6.2.3.

6.4 Summary of Fixation Behaviour in the CLVDN: Dependence on N, ν and Δ and Comparison with Chapter 5

I now summarize the CLVDN fixation behaviour as a function of the population size N, which controls the demographic noise, and of the external noise parameters ν and Δ. It is always found that the (unconditional) mean extinction time scales linearly with the population size, i.e. $t_{\text{ext}} \sim N$, independently of the initial condition (when it is well separated from the absorbing boundaries), see Figures 6.3(a,b), 6.4(a,b), 6.5(a,b), however the MET is shortened when the 12 reaction rate k increases, and has a different dependence on the intensity Δ of the external noise depending on the switching rate of the noise ν.

The species fixation probabilities depend greatly on (N, Δ, ν) and on the average number of switches, of order $N\nu$, occurring prior to extinction. Except under fast switching, when the external noise self-averages and the law of the weakest holds, non-LOW scenarios emerge both below and above the critical EN intensity $\Delta^* = k - k_{\text{min}}$. In fact, when $k > k_2, k_3$ and $N \gg 1$, it is found that:

- When $\Delta < \Delta^*$: Species 1 is almost certain to go extinct for all values of $\Delta < \Delta^*$. The LOW holds only in slow switching regime where $N\nu \ll 1$. In the intermediate-switching regime, $N\nu \sim \mathcal{O}(1)$, ϕ_2 decreases and ϕ_3 grows when Δ increases and no species is guaranteed to survive according to a non-LOW scenario, see Figure 6.8(a).

- When $\Delta > \Delta^*$: Under slow switching, no species is guaranteed to survive and $\phi_1 \to 1/2$ when the intensity of the EN is high ($\Delta \to k$). Under intermediate-switching, ϕ_1 increases while ϕ_2 and ϕ_3 decrease when Δ increases according to a non-LOW scenario. Hence, species 1 is the most likely to be the surviving one under external noise of high intensity ($\Delta \approx k$) and switching rate $\nu \sim \mathcal{O}(1/N)$, see Figures 6.5(b), 6.7 and Figure 6.8(b).

- When $\Delta = \Delta^*$: the main influence of the external noise occurs in the intermediate-switching regime, as illustrated Figure 6.8(c) where ϕ_3 is much greater than in the CLV when $N\nu \sim \mathcal{O}(1)$. This figure also shows that

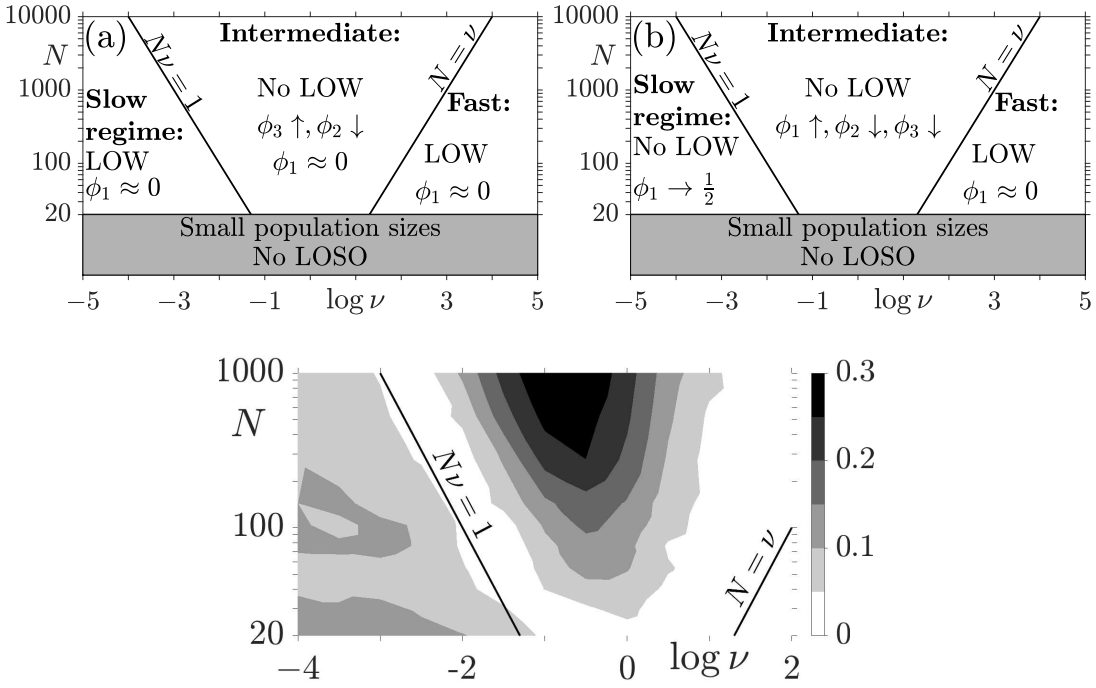

Figure 6.8: Summary of the CLVDN fixation probabilities when $k > k_2, k_3$ in $N - \nu$ diagrams showing ϕ_i when $\Delta < \Delta^*$ (a) and $\Delta > \Delta^*$ (b). The upward/downward arrows indicate whether ϕ_i increases/decreases when Δ is increased. The lines $N = \nu$ and $N\nu = 1$ indicatively separate the slow/intermediate/fast switching regimes. The shaded regions indicate the regime of small populations. (c) Heatmap of the absolute value of $\phi_3|_{\Delta=\Delta^*} - \phi_3|_{\Delta=0}$ for $k = 3, k_2 = k_3 = 1$ as function of ν and N. The gray area to the left of the line indicating $N\nu = 1$ shows the slow switching region, where $\phi_3|_{\Delta=\Delta^*} < \phi_3|_{\Delta=0}$, while the white region to the right of the $N = \nu$ line shows the fast switching regime $\phi_3|_{\Delta=\Delta^*} \approx \phi_3|_{\Delta=0}$. Between these two lines is the intermediate switching regime, where $\phi_3|_{\Delta=\Delta^*} > \phi_3|_{\Delta=0}$ and the magnitude of $\phi_3|_{\Delta=\Delta^*} - \phi_3|_{\Delta=0}$ that increases with N.

$\phi_3|_{\Delta=\Delta^*} < \phi_3|_{\Delta=0}$ in the slow switching regime (left-hand light gray area), and $\phi_3|_{\Delta=\Delta^*} \approx \phi_3|_{\Delta=0}$ in the fast switching regime (right-hand white area).

While I have focused on $k > k_2, k_3$, the above results also hold for $k = k_2 = k_3$ when $\Delta^* = 0$, in which case the scenarios summarized in Figure 6.8(b) for $\Delta > \Delta^*$ arise. In populations of small size, $3 \leq N \lesssim 20$, the fixation probabilities depend in an intricate way of (N, Δ, ν) and generally do not follow neither the LOSO nor the LOW.

Furthermore, these results are also interesting to compare with those of Chapter 5. While we see that in both cases there are conditions for the LOW and LOSO to be broken, the fixation scenarios are richer and more complex in Chapter 5, where the demographic and environmental noise are coupled. In both cases, for small switching rates the fixation probabilities are found by finding the average of those in each environmental state, while those for fast switching rates are found by considering the case without external noise and $\xi(t) = \langle \xi \rangle = 0$. For the model discussed in this Chapter this is the same the case for zero noise intensity, $\Delta = 0$. However in Chapter 5 fast switching results in a rescaling of the selection strength by a factor of $(1 - \gamma^2)$, *i.e.* *different* to the case with zero noise intensity, $\gamma = 0$. This is due to the way that the noise affects each model: here, rapid switching between k^+ and k^- results in an effective rate k, and the intensity of demographic fluctuations is the same in each environment, due to the population size being fixed. In Chapter 5, the noise affects the carrying capacity, and hence the strength of the demographic fluctuations, and rapid switching results in an effective carrying capacity of $\mathcal{K} = (1 - \gamma^2)K_0$, or effectively the same carrying capacity, K_0 with a rescaled selection $s(1-\gamma^2)$. For intermediate switching rates, the deviation from the LOW in this Chapter results from parts of the phase space S_3 being more prone to extinction (*i.e.* reaching an absorbing boundary of S_3) after a switch (Regions II and III in Figure 6.6), while in Chapter 5 this is not the case. There the deviation from the LOW stems from the coupling of N with the external noise. The randomly switching carrying capacity results in a total population size probability distribution, with the LOW and LOSO favoured at different values of N. Furthermore, at intermediate ν the outcome of Stage 2 in the previous Chapter is not guaranteed, and is itself affected by external noise.

These results suggest that it would be interesting to combine these models to find the effect of noise operating on both the carrying capacity and one of the reaction rates, *i.e.* reactions (5.1) - (5.4), with the rate r_1 following the process defined by (6.2) and (6.3) (but different environmental noise processes for the carrying capacity and rate). If the rate switches very slowly, then the fixation probability could be found by considering the results of Chapter 5, finding the average of those for $r_1 = r(1 \pm \Delta)$, while those for a fast switching rate could also be found from those of Chapter 5, with $r_1 = \langle r_1(t) \rangle = r$. Similarly, if the carrying capacity switches very slowly, the result could be inferred from the results of this Chapter, averaging the results over those for $N = K_\pm$, while the fast switching case could be found from the results of this Chapter with $N = K_0(1 - \gamma^2)$. The most interesting case would be when both processes have an intermediate switching rate, the implications of which are not obvious *a-priori*.

6.5 Fixation Probabilities with Three Randomly Switching Reaction Rates

For simplicity, above I focused on the case where only one reaction rate k_1 randomly switches. However it is also possible that all reaction rates are subject to environmental variability. In general, each k_i, with $i \in \{1, 2, 3\}$ would be affected by different environmental factors, leading to the CLVDN (6.1) with

$$k_1 = k + \Delta_1 \xi_1, \quad k_2 = \bar{k} + \Delta_2 \xi_2, \quad k_3 = \underline{k} + \Delta_3 \xi_3, \tag{6.6}$$

where $\xi_i \in \{-1, +1\}$ and $i \in \{1, 2, 3\}$ are independent dichotomous noise variables, such that $\xi_i \xrightarrow{\nu_i} -\xi_i$, each with a distinct switching rate ν_i and intensities $0 < \Delta_1 < k$, $0 < \Delta_2 < \bar{k}$, $0 < \Delta_3 < \underline{k}$. Each ξ_i in (6.6) has the same properties as ξ defined by (6.3), *i.e.*, $\langle \xi_i \rangle = 0$. The CLVDN with (6.6) spans a large-dimensional parameter space that is difficult to scrutinize.

Here, for the sake of concreteness, I show that the results obtained so far can be of direct relevance for the general model (6.1) with noisy rates (6.6) when these fluctuate on markedly different timescales. Here, I assume $\nu_2 \gg \nu_1 \gg \nu_3$, with $N\nu_1 \sim \mathcal{O}(1)$, and I set $\bar{k} = \underline{k} = 1$. This corresponds to the situation where

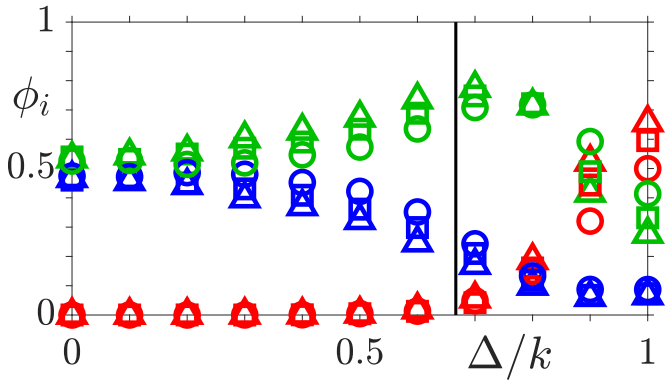

Figure 6.9: Survival probabilities for the three species switching case, with $k_1 = 3$, $N = 1000$, $\nu_1 = 0.05$, $\nu_2 = 100$ and $\nu_3 = 10^{-4}$, Δ_2 is kept constant at 0.8 and different values Δ_3 are shown with different markers. The vertical line indicates Δ^*/k. When Δ_3 increases, the peak of ϕ_3 moves towards higher values of Δ_1, see text.

species 2 and 3 are subject external factors changing with high and low frequency, respectively, while the growth rate of species 1 changes with factors varying on the same times scale $\mathcal{O}(1/N)$ on which the population composition changes. Since k_2 switches fast ($\nu_2 \gg 1/N$) and k_3 switches slowly ($\nu_3 \ll 1/N$), from Section 6.2, we expect ξ_2 to self-average and thus simply consider that $k_2 = 1$, while $k_3 = 1 + \Delta_3$ (when $\xi_3 = +1$) or $k_3 = 1 - \Delta_3$ (when $\xi_3 = -1$), each with a probability 1/2. By denoting here $k^\pm = k \pm \Delta_1$ and $\Delta^* = k - 1 > 0$, we can thus make contact with the results of Section 6.2.3.

When $\Delta_1 < \Delta^*$, we have $k^\pm > 1$ and the survival behaviour is similar to that of Section 6.2.3 as shown by Figure 6.9 which is qualitatively very similar to Figure 6.5(b): ϕ_3 and ϕ_2 respectively increases and decreases with Δ_1 while $\phi_1 \approx 0$. Hence, as in Sec. 6.2.3, species C is the most likely to be the surviving one under external noise of low intensity while 1 is the "strongest" species and therefore the most likely to go extinct. When $\Delta_1 > \Delta^*$, $k^+ > 1$ and $k^- < 1$ which also yields the same qualitative behaviour as in Figure 6.5(c): ϕ_1 and ϕ_2 increase and decreases with Δ_1 while ϕ_3 varies non-monotonically with Δ_1. For the same reason explained in Section 6.2.3, species 1 becomes the most likely to survive under strong external noise. A noticeable, yet marginal, difference

between Figures 6.5(c) and 6.9 is the fact that the ϕ_3 is maximum for $\Delta_1 \gtrsim \Delta^*$ in Figure 6.9 instead of $\Delta_1 \approx \Delta^*$. In Figure 6.9 the peak of ϕ_3 moves towards higher values of Δ_1 because 1 is the "weakest" species under strong EN in the environmental states $\xi_1 = \xi_3 = -1$ when $\Delta_1 > \Delta^* + \Delta_3$.

6.6 Conclusion

In this Chapter, I have shown that even in a simpler model of three species cyclic competition with fixed population size, the interplay of internal and external noise can still cause deviations from the behaviour expected in a constant environment. These results have focused on the case where the species with the variable rate is the strongest in a constant environment, but can be adapted to the case where all rates are equal, by noting that in this case $\Delta^* = 0$.

In a large population, when the switching rate is not too high and the external noise is of sufficiently high intensity, the law of the weakest no longer holds, with no species guaranteed to survive and new fixation scenarios emerging. The most interesting results are under intermediate switching, where the environment and population evolve on similar time-scales. Here, the fixation probability of the predator of the species that switches varies non-monotonically with noise intensity Δ, attaining its maximum when $\Delta \approx \Delta^*$. When the noise intensity is greater than Δ^*, the fixation probability of the species with the variable rate increases, becoming the most likely to survive when $\Delta \approx k$. Hence, in direct contradiction to the 'LOW', the strongest species can be the most likely to fixate the population. These results also extend to the case where all three rates switching on markedly different timescales, however it would be interesting to investigate the case where all three rates switch at an intermediate rate.

Furthermore, I have also found exact results for the effect of external noise on the 'LOSO', where $N = 3$. This is achieved using a first-step analysis, and shows again that under external noise where the rate is not too high and of sufficient intensity, the 'LOSO' again fails to hold and there is no simple law that describes that fixation properties.

Chapter 7

Conclusion

The results of this thesis have added to the extensive body of work that suggests that environmental noise plays an important role in the fate of some biological systems, in particular microbial communities. Here I have focused on two and three species systems where fixation of one species is certain: mutations between species are not considered, and creation of an individual needs a 'parent' of the same species. Hence, once a species has died out, it cannot recover. The majority of this thesis has focused on environmental noise in the form of a randomly switching carrying capacity. In this way, the total population size is coupled to the environmental noise. The total population size itself controls the strength of the demographic fluctuations and the resulting evolutionary dynamics of the population composition. Hence a key feature is that the demographic noise is coupled to the external noise. We find that, in general, coloured environmental noise can have a marked effect on the species fixation probabilities, especially on the probability that the least favoured species will take over the population, and a small effect on the time it takes for fixation to occur.

The results of Chapters 5 and 6 show that symmetric dichotomous Markov noise can have a drastic effect on the fixation probabilities in models of three species cyclic competition, where new fixation scenarios that do not follow the previously established 'law of stay out' or 'law of the weakest' can arise. When the carrying capacity of the system varies in time (Chapter 5), we find that external noise makes the competition more egalitarian, but does not prolong species coexistence. When the population size is fixed and one of the rates varies in time

(Chapter 6), we find that the result of the competition is highly dependent on the rate and intensity of switching, with the LOW and LOSO broken when the noise intensity is sufficiently high and the switching rate not too large. It would be interesting to extend these analyses, considering other forms of coloured noise, *e.g.* asymmetric dichotomous Markov noise or periodic noise, which we have seen can lead to different fixation scenarios to symmetric Markov noise; or continuous noise processes, like the Ornstein-Uhlenbeck process (see Appendix A.2), in order to ascertain whether the effect on the fixation statistics is characteristic of all coloured noise processes, or if they change between processes with discrete or continuous state spaces. Furthermore, it would be interesting to consider a meta-population of connected patches of well-mixed cyclic competition systems with external noise, to see if the characteristic spiral patterns are robust to environmental variation.

The results of Chapter 3 show that a dichotomously switching carrying capacity has a drastic effect on the fixation probability of co-operative species in the Prisoner's Dilemma, and that the type of switching: periodic or random, is also an important consideration. A characteristic of both periodic and random switching is the possibility of the fixation probability of the slow growing species being maximised at an intermediate switching rate. This is the most interesting and unexpected result, and can be explained as follows. First, note that an environmental switch changes the fixed point for the mean field equation for the total population size, N. When a switch occurs the stochastic system quickly approaches the new fixed point then fluctuates rapidly around it. When the switching is very slow this means that N spends most of its time (before one of the species fixates) around either K_+ or K_-, depending on the initial condition. Similarly, for very fast switching the noise self averages and N fluctuates rapidly around $\mathcal{K}_\delta$. Thus in both these limits there is a timescale separation between the dynamics of N and x, and the formulas (3.15) and (3.25) give good approximations for the fixation probability. On the other hand, for intermediate switching rates, N doesn't have time to settle around one of the equilibrium points $K_\pm$ before a switch, and the switching is not fast enough for the external noise to self average. Thus N actually spends a lot of time travelling between $K_\pm$, and the

timescale separation between N and x is lost. This leads to the aforementioned formulae being less accurate, and the unexpected behaviour of ϕ.

To extend this model, it would again be interesting to compare these results with continuous noise processes, to see if the dependence of ϕ on the correlation time and intensity of noise is different for continuous state-space noise processes. Another possibility would be to analyse a meta-population model with external noise in order to investigate Simpson's Paradox (Blyth (1972); Chater *et al.* (2008); Chuang *et al.* (2009); Cremer *et al.* (2011, 2012, 2019); Hauert *et al.* (2002); Hense *et al.* (2019); Melbinger *et al.* (2015); Okasha (2006)), upon which the effect of external noise has not been determined. Here, interconnected patches of populations evolve according to the Prisoner's Dilemma. The fraction of co-operators decreases within each patch but paradoxically increases for the whole system, due to those patches with more cooperators growing to larger sizes. Hence it would be interesting to see how the type and statistics of external noise affects this paradox. Alternatively, the model could be extended by allowing mutations between the two species, analysing the effect of noise on the average number of cooperative individuals, rather than the fixation probability. This simple extension of the model would allow one to investigate the 'Intermediate Disturbance Hypothesis' (Begon *et al.* (2006); Brockhurst (2007); Brockhurst *et al.* (2007); Buckling *et al.* (2000); Connell (1978); Fox (2013); Grime (1973); Lampert & Sommer (2007); Petraitis *et al.* (1989)). This states that external disturbances at an intermediate rates and large intensity will lead to a higher fraction of co-operators. It has, however, proved controversial, as most empirical studies do not show this relationship (Fox (2013)). In Chapter 3 it was observed that the fixation probability of the slow growing species can be maximal at an intermediate switching rate for large enough noise intensity and asymmetry, suggesting that in a version of this model extended by allowing mutations, a higher fraction of co-operators might be maintained in a randomly switching environment when the noise asymmetry and intensity are large enough, but not otherwise. This would have implications in the formation and maintenance of biofilms, and the phenomenon of anti-microbial resistance, both of which are pressing issues in today's world.

Appendix A

Single Species Logistic Growth with Noise in the Carrying Capacity

A.1 Dichotomous Markov Noise

When demographic noise is neglected, by assuming that the fluctuating population size is always large, and the only source of noise stems from the randomly switching carrying capacity, we have seen that the N-QSD, $P(N)$, can be described in terms of the marginal stationary probability density of the underlying PDMP. Without the normalisation constant, we have (Horsthemke & Lefever (1984); Wienand *et al.* (2018)):

$$\rho_{\nu,\delta}^{\mathrm{PDMP}}(N) \propto \frac{1}{N^2}\left[\left(\frac{K_+}{N}-1\right)^{\nu_+-1}\left(1-\frac{K_-}{N}\right)^{\nu_--1}\right], \tag{A.1}$$

where the dependence on γ, δ and ν is given by $K_\pm = (1 \pm \gamma)K_0$ and $\nu_\pm = (1\mp\delta)\nu$. Clearly, $\rho_{\nu,\delta}^{\mathrm{PDMP}}(N)$ has support $[K_-, K_+]$ and accounts for environmental noise, but ignores all demographic fluctuations. The expression of $\rho_{\nu,\delta}^{\mathrm{PDMP}}(N)$ gives a suitable description of $P(N)$ in the intermediate switching regime where interesting phenomena arise.

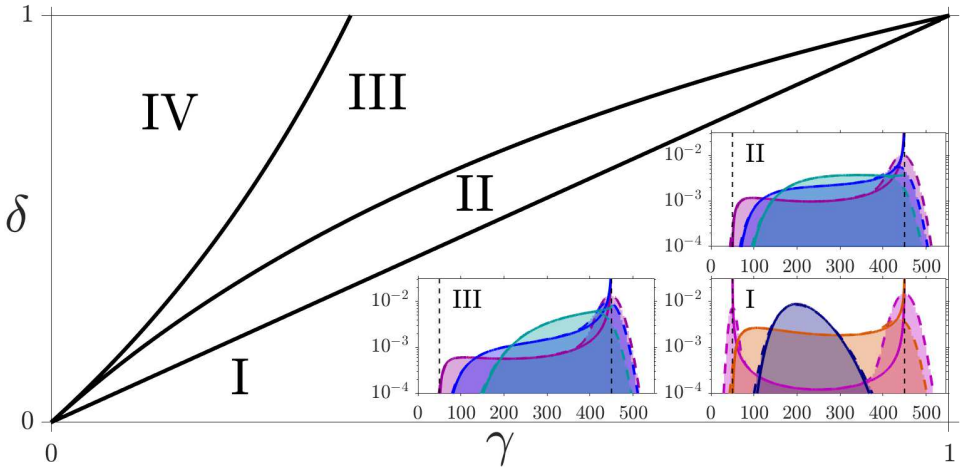

Figure A.1: Phase diagram for the N-QSD, $P^{\mathrm{ADN}}(N)$, and its approximations $\rho^{\mathrm{PDMP}}_{\nu,\delta}(N)$ and $\rho^{\mathrm{LNA}}_{\nu,\delta}(N)$ (insets), see Eq. (A.5). We distinguish four regions described in the text: In addition to a peak about K_+, the N-QSD has always a local maximum $K_- < N^* < K_+$ in the intermediate switching regime in I; in regime II and III, the N-QSD and $\rho^{\mathrm{PDMP}}_{\nu,\delta}(N)$ have a peak about K_+ and, depending on ν, possibly another peak at some values $K_- < N^* < K_+$, see insets; the N-QSD and $\rho^{\mathrm{PDMP}}_{\nu,\delta}(N)$ have one single peak about K_+ in IV. Insets illustrate the form of $P(N)$, $\rho^{\mathrm{PDMP}}_{\nu,\delta}(N)$ and $\rho^{\mathrm{LNA}}_{\nu,\delta}(N)$ in regions I-III. In the insets, solid lines are from the $\rho^{\mathrm{PDMP}}_{\nu,\delta}(N)$, given by Eq. (A.1), dashed lines are from $\rho^{\mathrm{LNA}}_{\nu,\delta}(N)$, given by Eq. (A.5), solid areas are from computer simulations, and the vertical dashed lines are eyeguides showing $N = K_\pm$. Parameters are: $(K_0, \gamma, s, x_0) = (250, 0.8, 0.05, 0.5)$ and (inset I) $\delta = 0.7$, $\nu = (0.05, 1.4, 17.5)$ (pink, orange, blue); (inset II) $\delta = 0.85$, $\nu = (1, 3, 6.5)$ (purple, blue, green); (inset III) $\delta = 0.92$, $\nu = (1, 3, 12)$ (purple, blue, green). In inset I, N^* is in the intermediate regime for $\nu = 1.4$ (orange). In inset II, N^* is in the intermediate regime for $\nu = 1$ (purple) and $\nu = 6.5$ (green). In inset III, N^* is in the intermediate regime for $\nu = 1$ (purple). We notice that the LNA excellently agrees with simulation results for the N-QSD: $P(N)$ and $\rho^{\mathrm{LNA}}_{\nu,\delta}(N)$ are almost indistinguishable in each inset.

A.1.1 Phase Diagram for $\rho^{\mathrm{PDMP}}_{\nu,\delta}(N)$ with asymmetric dichotomous Markov noise

The N-QSD, $P(N)$, and its PDMP approximation $\rho^{\mathrm{PDMP}}_{\nu,\delta}(N)$ are bimodal, with peaks about $K_\pm$, when $\nu < 1$, and unimodal when $\nu > 1$ with a peak N^* that is the smaller solution to

$$N^2 - (\nu(1-\gamma\delta)+1)\,K_0 N + (1-\gamma^2)K_0^2\nu = 0, \tag{A.2}$$

with $N^* \to \mathcal{K}_\delta$ as $\nu \to \infty$ (Horsthemke & Lefever (1984); Wienand *et al.* (2017, 2018)). In addition, two other regimes can arise under *asymmetric* switching at *intermediate* rate when $1/(1+|\delta|) < \nu < 1/(1-|\delta|)$. Here, the N-QSD has a different form not found when $\delta = 0$: When $\delta < 0$ and $1/(1-\delta) < \nu < 1/(1+\delta)$, $\rho^{\mathrm{PDMP}}_{\nu,\delta}(N)$ and $P(N)$ have a peak at $N \simeq K_-$. When $\delta > 0$ and $1/(1+\delta) < \nu < 1/(1-\delta)$, $\rho^{\mathrm{PDMP}}_{\nu,\delta}(N)$ and $P(N)$ have a peak at $N \simeq K_+$ and, depending on δ, γ and ν, also a peak at N^*. The condition for the existence of such a peak at $K_- < N^* < K_+$ can be inferred from the PDMP approximation (A.1) by noting that (A.2) has real roots when

$$(1-\gamma\delta)^2\nu^2 - 2(1+\gamma(\delta-2\gamma))\nu + 1 > 0. \tag{A.3}$$

We thus distinguish four regions, I-IV, in the (δ, γ) - space, see Fig. A.1:

I: $\delta < \gamma$, where N^* exists for all intermediate ν.

II: $\gamma < \delta < \frac{2\gamma}{1+\gamma}$, where N^* exists for all intermediate ν that lie outside the interval between the two solutions of (A.3), here denoted by $\nu_{1,2}$ (with $\nu_2 \geq \nu_1$).

III: $\frac{2\gamma}{1+\gamma} < \delta < \frac{2\gamma}{1-\gamma}$, where N^* only exists if $\frac{1}{1+\delta} < \nu < \nu_1$.

IV: $\delta > \frac{2\gamma}{1-\gamma}$ - where N^* does not exist.

Simulation results of Figure 3.4 and A.1 confirm that the above analysis correctly reflects the properties of $P(N)$.

A.1.2 Linear Noise Approximation: Combined effect of Internal and External noise on the population size

While the PDMP is a good approximation of the true N-QSD, capturing the position of the peaks in the distribution, it fails to capture the width of the around them and the 'leakage' of probability outside $[K_-, K_+]$. This is because the PDMP approximation necessarily ignores all demographic noise. We can include this by performing the linear noise approximation (LNA) around the PDMP to account for the joint effects of internal and external noise on the N-QSD. Full details can be found in Hufton *et al.* (2016); Wienand *et al.* (2018) but here I give an outline of the major steps and assumptions.

First, one must assume that $K_+, K_- \gg 1$, so that $\Omega \equiv \langle K \rangle$ (which I use as the system's 'large parameter') is large and of the same order as $K_\pm$. We then work with the more convenient variable $n = N/\Omega$, which decomposes as $n(t) = \psi(t) + \eta(t)/\Omega$. The first term $\psi(t) = \lim_{\Omega\to\infty} N/\Omega$ obeys the SDE $\dot{\psi} = \psi(1 - \frac{\psi}{1+\xi\gamma})$, defining the corresponding PDMP, and $\eta(t)$ accounts for the fluctuations of n around ψ.

We are then interested in the stationary joint probability density $\pi(\eta, \psi, \xi)$ of the complementary Markov process $\{n(t), \xi(t)\}$. This is decomposed as $\pi(\eta, \psi, \xi) = \pi(\eta|\psi, \xi)\pi(\psi, \xi)$, where the second term is the stationary joint pdf of the PDMP, obtained from:

$$\rho^{\mathrm{PDMP}}_{\nu,\delta}(N, \xi) \propto \begin{cases} \frac{1+\delta}{N^2}\left[\frac{K_+}{N} - 1\right]^{\nu_+ - 1}\left[1 - \frac{K_-}{N}\right]^{\nu_-}, & (\xi = +1) \\ \frac{1-\delta}{N^2}\left[\frac{K_+}{N} - 1\right]^{\nu_+}\left[1 - \frac{K_-}{N}\right]^{\nu_- - 1}, & (\xi = -1) \end{cases} \tag{A.4}$$

and the first term accounts for the demographic fluctuations around ψ in environmental state ξ. We make a further simplification by supposing that the demographic fluctuations are approximately the same in both states, writing $\pi(\eta|\psi, \pm\xi) = \pi(\eta|\psi)$. This allows us to write an SDE for $\pi(\eta|\psi)$, showing that it is a Gaussian distribution with zero mean and variance ψ. With this one can

define the quasi-stationary marginal LNA probability density of $N(t)$ as:

$$\begin{aligned} P^{\mathrm{LNA}}_{\nu,\delta}(N) &= \sum_{\xi=\pm 1} \int\int \pi(\eta|\psi)\pi(\psi,\xi)\delta\left(n-\psi-\frac{\eta}{\psi}\right)d\psi d\eta \\ &\propto \int_{K_-}^{K_+} \frac{e^{\frac{-(N-\widetilde{N})^2}{2\widetilde{N}}}}{\widetilde{N}^{1/2}} \Bigg\{ \frac{(1+\delta)}{\widetilde{N}^2}\left[\frac{K_+}{\widetilde{N}}-1\right]^{\nu_+-1}\left[1-\frac{K_-}{\widetilde{N}}\right]^{\nu_-} \\ &+ \frac{(1-\delta)}{\widetilde{N}^2}\left[\frac{K_+}{\widetilde{N}}-1\right]^{\nu_+}\left[1-\frac{K_-}{\widetilde{N}}\right]^{\nu_--1}\Bigg\} d\widetilde{N}, \end{aligned} \tag{A.5}$$

where $\delta\left(n-\psi-\frac{\eta}{\psi}\right)$ in the first line is the Dirac-delta function. From Figure A.1 we see that this is an excellent approximation of the N-QSD: it accurately predicts all the details of the population probability density $P(N)$ obtained from stochastic simulations.

A.2 Ornstein - Uhlenbeck Noise

While it is not the main focus of this thesis, it is important not to restrict ourselves to discrete noise sources because real-world environmental variables like temperature, moisture, pH level *etc.* do not abruptly switch but rather vary continuously in time. The simplest continuous-state-space but coloured stochastic process that the carrying capacity could follow is the Ornstein-Uhlenbeck process, defined by the equation for $K(t)$ and the stochastic differential equation (SDE):

$$K(t) = K_{\mathrm{OU}}(1+\xi_{\mathrm{OU}}(t)) \quad \text{where} \tag{A.6}$$

$$d\xi_{\mathrm{OU}} = -\frac{\xi_{\mathrm{OU}}}{\tau}dt + \sqrt{\frac{2\sigma^2}{\tau}}dW, \tag{A.7}$$

where τ is the correlation time (to be compared with $1/(2\nu)$ for dichotomous noise), σ is the noise intensity and dW is an interval of the Wiener process. The autocorrelation function of the zero-mean OU process ξ_{OU} has been shown to be (Reimann (1995)) $\sigma^2 \mathrm{e}^{-|t-t'|/\tau}$. It is also straightforward to show that the mean and variance of $K(t)$ are K_{OU} and $(\sigma K_{\mathrm{OU}})^2$.

As mentioned in Chapter 1, using OU noise to drive the carrying capacity has an important limitation: it is an unbounded process so can go negative leading to unphysical results. This can be avoided by either adding a reflecting barrier at

$K = 0$, or by changing (A.6) to $K(t) = |K_{\rm OU}(1 + \xi_{\rm OU}(t))|$. These will both affect the resulting distribution for K (and hence the effect of the noise), but this can be mitigated by choosing σ small enough so that the chance of going below zero (before an arbitrary time) is small.

Unlike periodic and random dichotomous noise, approximations for the probability distribution of N subject to OU noise, $\rho_\tau^{\rm OU}(N)$, can only be found in the long and short correlation time limits. When the correlation time is long, $\tau \to \infty$, the carrying capacity is approximately fixed and so the total population size tends to the initial value $K(0)$, drawn from a Gaussian distribution with mean $K_{\rm OU}$ and variance $(\sigma K_{\rm OU})^2$. We write:

$$\rho_{\tau\to\infty}^{\rm OU}(N) \simeq \frac{1}{\sigma K_{\rm OU}\sqrt{2\pi}} \exp\left[-\frac{1}{2}\left(\frac{N - K_{\rm OU}}{\sigma K_{\rm OU}}\right)^2\right] \tag{A.8}$$

In the short correlation time limit, $\tau \to 0$, we separate the dynamics into fast and slow variables and use the WKB method to average the effect of the noise over the period of variation. For this to be valid, we need $\tau \ll 1$, so that the dynamics of the noise is much faster than that of N, and $K_{\rm OU} \gg 1$, so that it can be used as a large parameter. Full details can be found in, for example, Roberts *et al.* (2015) but here we show the main steps. Starting with the Fokker-Planck equation in terms of $\xi_{\rm OU}$ and $n = N/K_{\rm OU}$:

$$\begin{aligned}\frac{dP(n,\xi_{\rm OU})}{dt} &= -\frac{d}{dn}\left[n\left(1 - \frac{n}{1+\xi_{\rm OU}}\right)P(n,\xi_{\rm OU})\right] \\ &+ \frac{1}{2K_{\rm OU}}\frac{d^2}{dn^2}\left[n\left(1 + \frac{n}{1+\xi_{\rm OU}}\right)P(n,\xi_{\rm OU})\right] \\ &- \frac{d}{d\xi_{\rm OU}}\left[-\frac{\xi_{\rm OU}}{\tau}P(n,\xi_{\rm OU})\right] + \frac{1}{2}\frac{d^2}{d\xi_{\rm OU}^2}\left[\frac{2\sigma^2}{\tau}P(n,\xi_{\rm OU})\right],\end{aligned} \tag{A.9}$$

where the first two terms on the right hand side account for the drift and diffusion due to births and deaths, and the second two terms account for the change in the environmental variable ξ, we use the ansatz for the quasi-stationary distribution $\pi(n,\xi_{\rm OU}) \approx \exp\left[-K_{\rm OU}S(n,\xi_{\rm OU})\right]$ to find the effective Hamiltonian:

$$\mathcal{H}(n,p_n) = n(1-n)p_n + p_n^2 n\left[1 + n + \epsilon n^3\right], \tag{A.10}$$

where $p_n = dS/dn$ and $\epsilon = 2K_{\mathrm{OU}}\sigma^2\tau$. We then set this equal to zero to find an expression for p_n and use the fact that $S(n) = \int_0^n p_n(z)dz$ to find the QSD:

$$\pi(n) \simeq \exp\left[-K_{\mathrm{OU}} \int_0^n \frac{-2\,(1-z)}{1+z+\epsilon z^3} dz\right]. \tag{A.11}$$

This is still a work in progress and, while not all details are known yet, below I outline how I plan to compute the fixation probability.

The fixation probability of the slow growing species can then be found in the long correlation time limit by averaging (3.10) over the population size density (A.8):

$$\phi^{\mathrm{OU}}(\tau \to \infty) \simeq \int_0^\infty \rho^{\mathrm{OU}}_{\tau\to\infty}(N)\phi|_N(x_0)dN, \tag{A.12}$$

Simulation results for ϕ and the mean fixation time T_F are presented in Figure A.2. These preliminary results suggest that there are similarities and differences with two-state noise presented in Chapter 3. Firstly, for large enough noise intensity (σ, which should be compared with γ in Chapter 3) the fixation probability can be peaked at a finite intermediate correlation time (see Figure 3.2), and the mean fixation time is of order $1/s$ and a decreasing increasing function of the correlation time (see Figure S3(a) of Taitelbaum *et al.* (2020)). However, in this case the mean fixation time always decreases with increasing noise intensity (compared with possible non-monotonic behaviour in insets of Figure 3.5). Additionally the biggest difference is that the fixation probability is an increasing function of σ, whereas in Figure 3.5 it was shown that this is not always the case in dichotomous noise. This can be explained by noting that here σ defines the width of the distribution for N, so for larger values of σ the process can attain lower values of N, increasing the fixation probability.

A disadvantage of using OU noise is that the simulations take a lot longer to run, so I do not yet have a complete picture of its effects. This is because the fastest way to simulate the process is to approximate the OU process as a birth-death process. In the short correlation time limit the rates for this process are very large compared to the birth-death rates for the species, so most of the simulation time is taken up with the carrying capacity changing, rather than the evolution of the species. Preliminary work for a forthcoming publication has been done, and will be completed shortly. In particular, we plan to ascertain

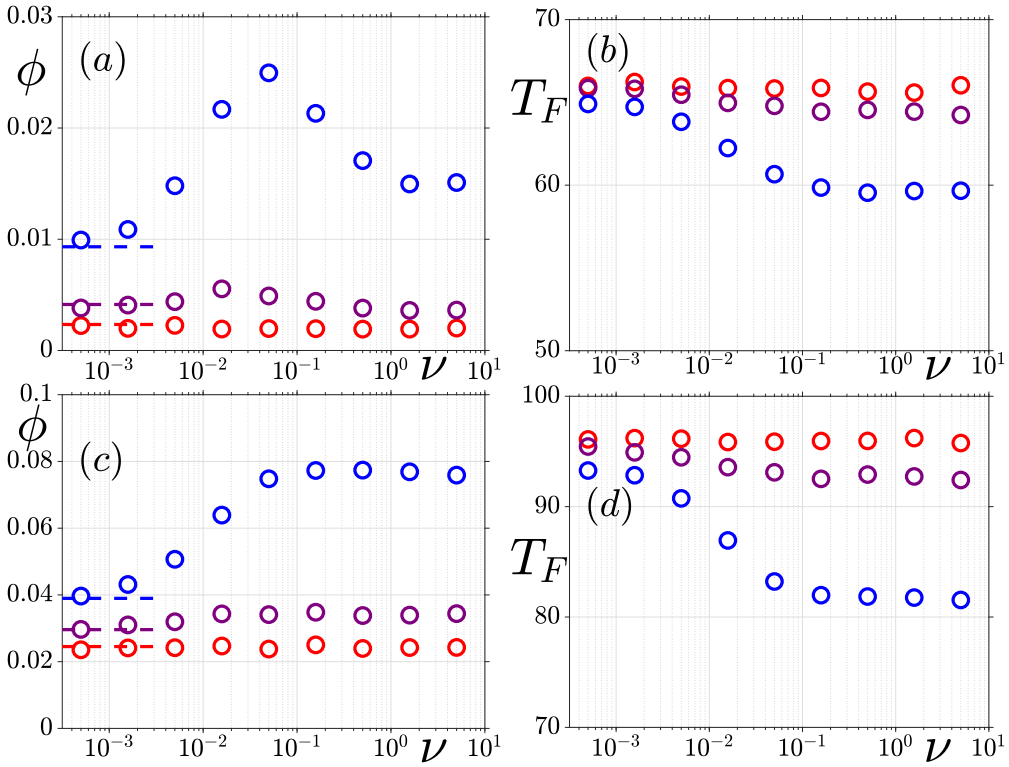

Figure A.2: Fixation probability (a,c) and mean fixation time (b,d) for the 2 species competition model (3.1) with the carrying capacity following the Ornstein-Uhlenbeck process (A.6). In all panels, $(b, K_{\mathrm{OU}}, x_0) = (0, 250, 0.5)$ and $\sigma = (0.1, 0.2, 0.3)$ (red, purple, blue), while $s = 0.05$ in (a,b) and $s = 0.03$ in (c,d). Results are plotted against $\nu = 1/(2\tau)$ for easier comparison with DMN and PN. Dashed lines in (a,c) are from (A.12) (see text).

the similarities and differences between continuous and discrete state space noise, and see if there is a way to approximate continuous noise with discrete noise in the case of small correlation times.

Appendix B

Fast Switching Limit: Large ν approximations for Two Species Competition

B.1 Saddle-Point Approximation

The saddle-point approximation is a standard approximation method, used to approximate integrals of exponential functions that are sharply peaked at a single value. We write:

$$\int_{-\infty}^{\infty} \exp[f(x)]dx \simeq \frac{\exp[f(x^*)]}{\sqrt{f''(x^*)}}, \tag{B.1}$$

where x^* is the maximum of $f(x)$ and the dash denotes differentiation w.r.t. x. I will now show how we use this to approximate the fixation probability and variance in the fast switching limit of dichotomous Markov noise. These are valid in the fast switching regime, $\nu/s \gg 1$. Similar calculations can be performed for periodic noise, and were performed by a collaborator in (Taitelbaum *et al.* (2020)). Details can be found in the supplementary material of that paper.

B.1.1 Fixation Probability

To perform the saddle-point approximation of ϕ^{ADN}, we rewrite (3.15) in terms of the total population density $y = N/K_0$. Accounting for the normalisation

constant, the fixation probability can be written:

$$\phi^{\mathrm{ADN}}(\nu) = \frac{\int_{1-\gamma}^{1+\gamma} \rho^{\mathrm{PDMP}}_{\nu/s,\delta}(y) \exp\left[K_0 y(1-x_0)\ln(1-s)\right] dy}{\int_{1-\gamma}^{1+\gamma} \rho^{\mathrm{PDMP}}_{\nu/s,\delta}(y) dy} \tag{B.2}$$

$$= \frac{\int_{1-\gamma}^{1+\gamma} \exp\left[f^{\mathrm{ADN}}_{\mathrm{num}}(y)\right] dy}{\int_{1-\gamma}^{1+\gamma} \exp\left[f^{\mathrm{ADN}}_{\mathrm{den}}(y)\right] dy}, \tag{B.3}$$

where $f^{\mathrm{ADN}}_{\mathrm{den}}(y) = \ln \rho^{\mathrm{PDMP}}_{\nu/s,\delta}(y)$ and $f^{\mathrm{ADN}}_{\mathrm{num}}(y) = \ln \rho^{\mathrm{PDMP}}_{\nu/s,\delta}(y) + K_0 y(1-x_0)\ln(1-s)$. Evaluating both the integrals separately using the saddle point approximation, we find:

$$\phi(\nu) \simeq \sqrt{\kappa^{\mathrm{ADN}}_1/\kappa^{\mathrm{ADN}}_2} \exp\left[f^{\mathrm{ADN}}_{\mathrm{num}}(y_2) - f^{\mathrm{ADN}}_{\mathrm{den}}(y_1)\right], \tag{B.4}$$

where y_1 and y_2 are the positions of the saddle points of the denominator and numerator respectively, satisfying, $(d/dy)f^{\mathrm{ADN}}_{\mathrm{den}}(y_1) = 0$ and $(d/dy)f^{\mathrm{ADN}}_{\mathrm{num}}(y_2) = 0$. Additionally, $\kappa^{\mathrm{ADN}}_1 = (d^2/dy^2)f^{\mathrm{ADN}}_{\mathrm{den}}(y_1)$ and $\kappa^{\mathrm{ADN}}_2 = (d^2/dy^2)f^{\mathrm{ADN}}_{\mathrm{num}}(y_2)$ are the curvatures at the saddle-point of the denominator and numerator respectively.

For the denominator, we can write:

$$f^{\mathrm{ADN}}_{\mathrm{den}}(y) = \ln \rho^{\mathrm{PDMP}}_{\nu/s,\delta}(y) = -2\frac{\nu}{s}\ln y + \left[(1-\delta)\frac{\nu}{s} - 1\right]\ln(1+\gamma-y) + \left[(1+\delta)\frac{\nu}{s} - 1\right]\ln(y-1+\gamma), \tag{B.5}$$

and the saddle point is found at:

$$y_1 \simeq \frac{(1-\gamma^2)}{(1-\delta\gamma)}\left[1 + \frac{\gamma(\delta-\gamma)}{(1-\delta\gamma)^2\nu/s}\left(1 + \frac{(1-2\gamma^2+\delta\gamma)}{(1-\delta\gamma)^2\nu/s}\right)\right]. \tag{B.6}$$

Hence we find:

$$f^{\mathrm{ADN}}_{\mathrm{den}}(y_1) \simeq (\nu/s)\left\{(1+\delta)\ln\left[\frac{\gamma(1+\delta)(1-\gamma)}{(1-\delta\gamma)}\right] + (1-\delta)\ln\left[\frac{\gamma(1-\delta)(1+\gamma)}{(1-\delta\gamma)}\right] - 2\ln\left[\frac{1-\gamma^2}{1-\delta\gamma}\right]\right\} + \ln\left[\frac{(1-\delta\gamma)^2}{\gamma^2(1-\delta^2)(1-\gamma^2)}\right] + \frac{(\delta-\gamma)^2}{(1-\delta^2)(1-\delta\gamma)^2\nu/s}, \tag{B.7}$$

$$\kappa^{\mathrm{ADN}}_1 \simeq \frac{-2(1-\delta\gamma)^4\nu/s}{\gamma^2(1-\delta^2)(1-\gamma^2)^2} + \frac{2(1-\delta\gamma)^2(1+6\delta\gamma-2\delta^3\gamma-5\gamma^2-3\delta^2(1-\gamma^2))}{(1-\delta^2)^2(1-\gamma^2)^2\gamma^2}. \tag{B.8}$$

For the numerator, we write $f_{\text{num}}^{\text{ADN}}(y) = f_{\text{den}}^{\text{ADN}}(y) + K_0 y(1-x_0)\ln(1-s)$, and find the saddle point at:

$$y_2 \simeq \frac{(1-\gamma^2)}{(1-\delta\gamma)}\left\{1+\frac{\gamma\left[2\left(1-\delta\gamma\right)\left(\delta-\gamma\right)+b\gamma\left(1-\gamma^2\right)\left(1-\delta^2\right)\right]}{2\left(1-\delta\gamma\right)^3\nu/s}\left[1+\frac{2-2\gamma^2\left(2+\delta^2-2\delta\gamma\right)-b\gamma\left(1-\gamma\right)^2\left(2\delta-3\gamma+\delta^2\gamma\right)}{2\left(1-\delta\gamma\right)^3\nu/s}\right]\right\}, \tag{B.9}$$

where $b = K_0(1-x_0)\ln(1-s)$. As a result, we find:

$$\begin{aligned} f_{\text{num}}^{\text{ADN}}(y_2) &\simeq (\nu/s)\left\{(1+\delta)\ln\left[\frac{\gamma\left(1+\delta\right)\left(1-\gamma\right)}{\left(1-\delta\gamma\right)}\right]+(1-\delta)\ln\left[\frac{\gamma\left(1-\delta\right)\left(1+\gamma\right)}{\left(1-\delta\gamma\right)}\right]\right. \\ &- \left.2\ln\left[\frac{1-\gamma^2}{1-\delta\gamma}\right]\right\}+\ln\left[\frac{\left(1-\delta\gamma\right)^2}{\gamma^2\left(1-\delta^2\right)\left(1-\gamma^2\right)}\right]+\frac{b\left(1-\gamma^2\right)}{1-\delta\gamma} \\ &+ \frac{\left[2\left(\delta-\gamma\right)\left(1-\delta\gamma\right)+b\gamma\left(1-\gamma^2\right)\left(1-\delta^2\right)\right]^2}{4\left(1-\delta^2\right)\left(1-\delta\gamma\right)^4\nu/s}, \end{aligned} \tag{B.10}$$

$$\begin{aligned} \kappa_2^{\text{ADN}} &\simeq -\frac{-2\left(1-\delta\gamma\right)^4\nu/s}{\left(1-\delta^2\right)\gamma^2\left(1-\gamma^2\right)^2}-\frac{2\left(1-\delta\gamma\right)}{\left(1-\delta^2\right)^2\left(1-\gamma^2\right)^2\gamma^2}\left[\left(5-3b\right)\gamma^2+\right. \\ &3b\gamma^4+\delta^2\left(3+\left(3+4b\right)\gamma^2-4b\gamma^4\right)-\delta^4\gamma^2\left(2+b\left(1-\gamma^2\right)\right)+ \\ &\left.\delta^3\gamma\left(-1+3\gamma^2-2b\left(1-\gamma^2\right)\right)+\delta\gamma\left(2b\left(1-\gamma^2\right)-5\left(1+\gamma^2\right)\right)-1\right]. \end{aligned} \tag{B.11}$$

Putting these together, we find that for fast random switching,

$$\ln\left(\frac{\phi^{\text{ADN}}}{\phi(\infty)}\right) \simeq \mathcal{A}^{\text{ADN}}(\nu/s)^{-1}, \tag{B.12}$$

where

$$\mathcal{A}^{\text{ADN}} = (1-x_0)\ln(1-s)\mathcal{K}_\delta\frac{\gamma^2(1-\delta^2)}{2(1-\delta\gamma^2)}\left(1+\frac{\mathcal{K}_\delta(1-x_0)\ln(1-s)}{2}\right). \tag{B.13}$$

While in the (Taitelbaum *et al.* (2020)) our collaborator found that (using $\rho^{\text{PN}}_{\nu\gg 1,\delta}(N)$ (3.21) found using the Kapitsa method):

$$\ln\left(\frac{\phi^{\text{PN}}}{\phi(\infty)}\right) \simeq \mathcal{A}^{\text{PN}}(\nu/s)^{-2}, \tag{B.14}$$

where

$$\mathcal{A}^{\mathrm{PN}} = \frac{\mathcal{K}_\delta}{72}\left\{1-\left[1+2(1-x_0)\ln(1-s)\right]^3\right\}\left(\frac{\gamma}{1-\delta\gamma}\right)^2. \tag{B.15}$$

From the above, we see that while the saddle-point approximation predicts the same fixation probability in the fast switching limit, $\phi^{\mathrm{ADN}}_{\nu\to\infty} = \phi^{\mathrm{PN}}_{\nu\to\infty} \simeq \phi(\infty) = \exp[\mathcal{K}_\delta(1-x_0)\ln(1-s)]$, the approach to this value is much faster for periodic compared to random switching.

B.1.2 Variance of Total Population Size and Validity of Piecewise-Deterministic Approximations

The saddle-point approximation can also be used to find the mean and variance of the N-QSD approximations for random and periodic switching, allowing us to ascertain the validity of the approximations (3.12) and (3.22), the piecewise-deterministic (i.e. not including demographic noise) approximations for random and periodic switching respectively. In the limit $\nu \to \infty$, the approximations that include demographic noise, the LNA (A.5) (random switching) and Kapitsa method (3.21) (periodic switching) both reduce to a Gaussian of mean and variance $\mathcal{K}_\delta$. i.e.:

$$P^{\alpha}_{\nu\to\infty}(N) \propto \frac{1}{\sqrt{\mathcal{K}_\delta}}\exp\left[\frac{-(N-\mathcal{K}_\delta)^2}{\mathcal{K}_\delta}\right] \quad \text{for} \quad \alpha = \mathrm{ADN},\ \mathrm{PN}. \tag{B.16}$$

This is because in this limit the population size distribution is affected only by demographic noise: the rate of environmental switching is much faster than the reactions in the underlying process, hence the agents feel the average effect of the noise, which is the same for both random and periodic switching. The variance of the piecewise-deterministic approximations (3.12) and (3.22) can be found by performing saddle-point approximations to leading order in $1/\nu$ to find:

$$\begin{aligned}
\sigma^2_{\mathrm{PN}} &= \int_{N_{\min}}^{N_{\max}} (N-\langle N\rangle)^2\,\rho^{\mathrm{PN}}_{\nu,\delta}(N)dN = \frac{1}{12}\left(\frac{\gamma}{1-\gamma\delta}\right)^2\frac{\mathcal{K}^2_\delta}{\nu^2},\\
\sigma^2_{\mathrm{ADN}} &= \int_{K_-}^{K_+} (N-\langle N\rangle)^2\rho^{\mathrm{PDMP}}_{\nu,\delta}(N)dN = \frac{1}{2}\left(\frac{\gamma}{1-\gamma\delta}\right)^2\left(1-\delta^2\right)\ \frac{\mathcal{K}^2_\delta}{\nu},
\end{aligned} \tag{B.17}$$

where the means are also found from a saddle-point calculation to leading order in $1/\nu$:

$$\begin{aligned}\langle N\rangle_{\mathrm{PN}} &= \int_{N_{\min}}^{N_{\max}} N\rho_{\nu,\delta}^{\mathrm{PN}}(N)dN = \mathcal{K}_\delta\left[1+\frac{\gamma^2}{12(1-\gamma\delta)^2\nu^2}\right],\\ \langle N\rangle_{\mathrm{ADN}} &= \int_{K_-}^{K_+} N\ \rho_{\nu,\delta}^{\mathrm{PDMP}}(N)dN = \mathcal{K}_\delta\left[1+\frac{\gamma^2(1-\delta^2)}{2\nu(1-\delta\gamma)^2}\right].\end{aligned} \tag{B.18}$$

Hence when $\nu \gg 1$, (B.17) shows that the variance of N-QSD for periodic noise is of order ν^{-2}, while that of random noise is of order ν^{-1}. Hence the width of the N-QSD under random switching is much larger than in the periodic case, allowing the total population size to reach smaller values of N. This is because under random switching there will be periods where the carrying capacity is at K_- for a longer time than $1/\nu_-$, and leads to a larger fixation probability when $s > s_{\mathrm{c}}$. Furthermore, it is the convergence of the means (B.18) to $\mathcal{K}_\delta$ at different rates that leads to the different rates of convergence to $\phi(\infty)$.

From (B.17) we also note that $\sigma^2_{\mathrm{PN}} > \mathcal{K}_\delta$ when $1 \ll \nu \ll \sqrt{\mathcal{K}_\delta}$ and $\sigma^2_{\mathrm{ADN}} > \mathcal{K}_\delta$ when $1 \ll \nu \ll \mathcal{K}_\delta$. These are the cases where the variance caused by environmental noise is much larger than demographic noise, so these approximations are valid when $\nu \ll \sqrt{\mathcal{K}_\delta}$ (periodic) and $\nu \ll \mathcal{K}_\delta$ (random).

Appendix C

Extra Information for Cyclic Competition Models in Chapters 4, 5 and 6

This Section contains extra details for Chapters 4, 5 and 6. Section C.1 defines the Moran-CLV, which is used to calculate the absorption probabilities and mean absorption time of the BDCLV (Stage 2). Section C.2 details the links between the BDCLV, MCLV and cCLV, in order to justify the use of the cCLV fixation probabilities and mean fixation time when calculating the BDCLV survival probabilities and mean extinction time (Stage 1). Section C.3 gives details of the initial probability distribution of the population composition in the BDCLV at the start of Stage 2. This is used when calculating the absorption probabilities. Section C.4 shows how the mean extinction (Stage 1) and absorption (Stage 2) times are calculated in the BDCLV. Section C.5 shows how the 'law of stay out' is derived for the cCLV 4.1 and the CLVDN 6.

C.1 The Moran-CLV (MCLV)

Here I will outline the main features of the MCLV. The purpose of this is to use the fact that it is a good approximation of the BDCLV but is less complex to analyse, due to the total population being fixed. It is therefore used to make theoretical predictions about the BDCLV that would otherwise be inaccessible.

The MCLV is defined by six pairwise reactions each of which corresponds to the *simultaneous* birth of an individual of species i and the death of an individual of species $j \neq i \in \{1,2,3\}$ (Antal & Scheuring (2006); Blythe & McKane (2007); Ewens (2004); Moran *et al.* (1962); Nowak (2006a)). This occurs with a rate T_{ji}. If the state of the system consisting of N_1 individuals of type 1, N_2 of species 2, and $N_3 = K - N_1 - N_2$ of the third type is denoted by $[N_1, N_2, N_3]$, the six reactions of the MCLV are (Claussen & Traulsen (2008); Galla (2011); Mobilia (2010)):

$$[N_1,N_2,N_3] \xrightarrow{T_{12}} [N_1-1,N_2+1,N_3];\ [N_1,N_2,N_3] \xrightarrow{T_{21}} [N_1+1,N_2-1,N_3]$$

$$[N_1,N_2,N_3] \xrightarrow{T_{31}} [N_1+1,N_2,N_3-1];\ [N_1,N_2,N_3] \xrightarrow{T_{13}} [N_1-1,N_2,N_3+1]$$

$$[N_1,N_2,N_3] \xrightarrow{T_{23}} [N_1,N_2-1,N_3+1];\ [N_1,N_2,N_3] \xrightarrow{T_{32}} [N_1,N_2+1,N_3-1],$$

with the transition rates (Claussen & Traulsen (2008); Mobilia (2010)):

$$T_{ji} = f_i x_i x_j\ N = (1+s\Pi_i)\ x_i x_j\ N = (1+\{\alpha_i x_{i+1} - \alpha_{i-1}x_{i-1}\})\ x_i x_j\ N, \quad \text{(C.1)}$$

where f_i and Π_i are given by (4.18) and (4.16) and $\alpha_i = sr_i$. To make sure $T_{ji} > 0$ we use the same assumptions for s and r_i: that $0 \leq s \leq 1$, $0 < r_i < 1$ and $\sum_{i=1}^{3} r_i = 1$. Here the transition rates can be expressed in terms of those of the BDCLV for a population of constant size $N = K$: using (4.21), (4.22) with $N = K$, we have $T_{ji} = T_i^+ T_j^- / K$. Using (2.12) we find that the mean field rate equations are:

$$\frac{d}{dt}x_i = \frac{1}{N}\sum_{j=1;j\neq i}^{3}(T_{ji} - T_{ij}) = s\Pi_i x_i = x_i\left(\alpha_i x_{i+1} - \alpha_{i-1}x_{i-1}\right). \quad \text{(C.2)}$$

These coincide with the mean field rate equations for the BDCLV (4.25). Therefore the dynamics of the population composition of the MCLV and BDCLV coincide in the mean field limit $K \to \infty$: both are characterised by a neutrally stable coexistence fixed point $\vec{x}^* = (r_2, r_3, r_1)$ and constant of motion $\mathcal{R} = x_1^{r_2} x_2^{r_3} x_3^{r_1}$.

Since in the BDCLV dynamics the population size obeys a logistic equation, after a short transient $N(t) \approx K$, see (4.24) and Figure 4.3 This establishes a

useful relationship between the BDCLV and MCLV: Except for a short transient (on a timescale $t \sim \mathcal{O}(1)$), corresponding to the so-called exponential phase of the logistic equation, the evolution of the BDCLV is similar to the dynamics of the MCLV in a population of constant size $N = K$. The BDCLV and MCLV relation is particularly useful to determine the absorption/fixation properties of the former in terms of the well-studied fixation properties of latter. In Figure C.1 it is shown that the survival and absorption probabilities $\phi_{i,j}$ and ϕ_i in the BDCLV are almost indistinguishable from those obtained in the MCLV (with $N = K$). Since the overall fixation probabilities $\widetilde{\phi}_i = \phi_{i,i+1}\phi_i + \phi_{i-1,i}(1-\phi_i)$, see (4.32), we can consider that the absorption and total fixation probabilities in the BDCLV and those of the MCLV with $N = K \gg 1$ coincide. Similarly, the mean extinction and absorption times T_1 and T_2 in the BDCLV with and MCLV with $N = K \gg 1$ are indistinguishable, see the insets of Figure C.1 and below.

To study the absorption/fixation properties of the BDCLV and MCLV, it is useful to write down the two-dimensional forward Fokker-Planck equation (FPE) obeyed by the probability density $P_{\text{MCLV}} \equiv P_{\text{MCLV}}(\vec{x}, t)$ of the latter. Using standard methods, (see *e.g.* Claussen & Traulsen (2008); Gardiner (1985); Mobilia (2010); Reichenbach *et al.* (2006); Van Kampen (1992)) we have the forward FPE:

$$\begin{aligned} &[\partial_t - \mathcal{G}_{\text{fMCLV}}(\vec{x})]\ P_{\text{MCLV}}(\vec{x}, t) = 0, \quad \text{where} \\ &\mathcal{G}_{\text{fMCLV}}(\vec{x}) \equiv -\sum_{i=1}^{2} \partial_i A_i^{\text{MCLV}}(\vec{x}) + \frac{1}{2}\sum_{i,j=1}^{2} \partial_i \partial_j B_{ij}^{\text{MCLV}}(\vec{x}), \end{aligned} \tag{C.3}$$

is the forward FPE generator, with $\partial_i \equiv \partial/\partial x_i$ [1], defined by

$$\begin{aligned} &A_i^{\text{MCLV}}(\vec{x}) \equiv \sum_{j=1, j\neq i}^{3} (T_{ji} - T_{ij}), \quad B_{ii}^{\text{MCLV}}(\vec{x}) \equiv \sum_{j=1, j\neq i}^{3} \left(\frac{T_{ji} + T_{ij}}{K}\right), \\ &\text{and} \quad B_{12}^{\text{MCLV}}(\vec{x}) = B_{21}^{\text{MCLV}}(\vec{x}) \equiv -\left(\frac{T_{12} + T_{21}}{K}\right). \end{aligned} \tag{C.4}$$

Within the linear noise approximation (Gardiner (1985); Van Kampen (1992)), upon linearising A_i^{MCLV} about the coexistence fixed point $\vec{x}^*$ and by evaluating

[1] In Eq. (C.3), the indices $i, j \in \{1, 2\}$ since $x_3 = 1 - x_1 - x_2$ and, as usual in the diffusion theory, we have rescaled the time $t \to t/N$.

$B_{ij}^{\mathrm{MCLV}}(\vec{x})$ at $\vec{x}^*$, in the variables $\vec{y} = \mathbf{S}\vec{x} = \frac{\sqrt{3}}{2}\begin{pmatrix} \frac{(r_1+r_2)\omega_0^{\mathrm{MCLV}}}{r_1 r_2} & \frac{\omega_0^{\mathrm{MCLV}}}{r_1} \\ 0 & 1 \end{pmatrix}\vec{x}$, the forward FPE reads (Mobilia (2010); Reichenbach *et al.* (2006))

$$\begin{aligned} \partial_t P_{\mathrm{MCLV}}(\vec{y},t) &= -\omega_0^{\mathrm{MCLV}}\left[y_1\partial_{y_1} - y_2\partial_{y_2}\right] P_{\mathrm{MCLV}}(\vec{y},t) \\ &+ D^{\mathrm{MCLV}}\left[\partial_{y_1}^2 + \partial_{y_2}^2\right] P_{\mathrm{MCLV}}(\vec{y},t), \end{aligned} \tag{C.5}$$

where $\omega_0^{\mathrm{MCLV}} = s\sqrt{r_1 r_2(1-r_1-r_2)}$ and $D^{\mathrm{MCLV}} = 3[r_1+r_2-4r_1r_2-(r_1-r_2)^2]/(4N)$. To study the fixation properties of the MCLV, the FPEs (C.3) and (C.5) have to be supplemented with absorbing boundaries at the corners of S_3 (Berr *et al.* (2009); Reichenbach *et al.* (2006); West *et al.* (2018)).

C.2 Link Between the BDCLV, MCLV and cCLV

Before elucidating the link between the three models, it is first useful to proceed as above and consider the two-dimensional forward Fokker-Planck equation (FPE) obeyed by the cCLV probability density $P_{\mathrm{cCLV}} \equiv P_{\mathrm{cCLV}}(\vec{x},t)$ (with $t \to t/N$):

$$\begin{aligned} &\left[\partial_t - \mathcal{G}_{\mathrm{cCLV}}(\vec{x})\right]\ P_{\mathrm{cCLV}}(\vec{x},t) = 0, \quad \text{where} \\ &\mathcal{G}_{\mathrm{cCLV}}(\vec{x}) \equiv -\sum_{i=1}^{2}\partial_i A_i^{\mathrm{cCLV}}(\vec{x}) + \frac{1}{2}\sum_{i,j=1}^{2}\partial_i\partial_j B_{ij}^{\mathrm{cCLV}}(\vec{x}), \end{aligned} \tag{C.6}$$

with $A_i^{\mathrm{cCLV}}(\vec{x}) \equiv W_{i+1,i} - W_{i,i-1}$, $B_{ii}^{\mathrm{cCLV}}(\vec{x}) \equiv (W_{i+1,i} + W_{i,i-1})/K$ where $i \in \{1,2\}$, and $B_{12}^{\mathrm{cCLV}}(\vec{x}) = B_{21}^{\mathrm{cCLV}}(\vec{x}) \equiv -(W_{12}+W_{21})/K$. It is worth noting that the drift terms of the cCLV and MCLV are simply related by $A_i^{\mathrm{cCLV}} = sA_i^{\mathrm{MCLV}}/(k_1+k_2+k_3)$. In the case of symmetric rates, $k_1 = k_2 = k_3 = 1$, within the linear noise approximation, this forward FPE in the variables $\vec{y} = \mathbf{S}\vec{x}$ reads:

$$\begin{aligned} \partial_t P_{\mathrm{cCLV}}(\vec{y},t) &= -\omega_0^{\mathrm{cCLV}}\left[y_1\partial_{y_1} - y_2\partial_{y_2}\right] P_{\mathrm{cCLV}}(\vec{y},t) \\ &+ D^{\mathrm{cCLV}}\left[\partial_{y_1}^2 + \partial_{y_2}^2\right] P_{\mathrm{cCLV}}(\vec{y},t), \end{aligned} \tag{C.7}$$

where $\omega_0^{\mathrm{cCLV}} = 1/\sqrt{3}$ and $D^{\mathrm{cCLV}} = 1/(12N)$ (Reichenbach *et al.* (2006)). This FPE is similar to (C.5). The comparison with the MCLV with equal rates $r_i = 1/3$ is particularly illuminating: $\omega_0^{\mathrm{MCLV}} = s\omega_0^{\mathrm{cCLV}}/3$ and $D^{\mathrm{MCLV}} = 2D^{\mathrm{cCLV}}$. Hence,

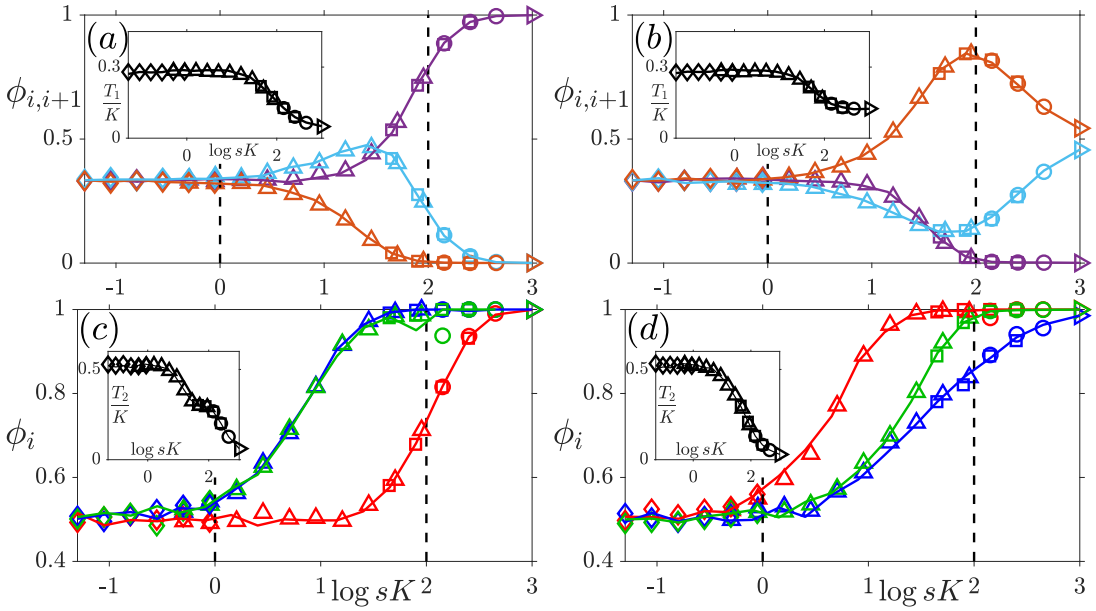

Figure C.1: Comparison of the fixation properties vs. sK in the BDCLV (solid lines) with constant carrying capacity K and in the MCLV (symbols) with a constant population size $N = K \in \{1000\ (\triangleright), 450\ (\circ), 250\ (\diamond), 90\ (\square), 50\ (\triangle)\}$, with $\vec{r} = \vec{r}^{(1)}$ in (a,c) and $\vec{r} = \vec{r}^{(2)}$ in (b,d) and different values of selection intensity: $s \in \{10^{-j/4}, j \in J_K^{\mathrm{MCLV}}\}$ with $J_{1000}^{\mathrm{MCLV}} = \{0\}$, $J_{450}^{\mathrm{MCLV}} = \{0, \ldots, 3\}$, $J_{250}^{\mathrm{MCLV}} = \{0, \ldots, 4\}$, $J_{90}^{\mathrm{MCLV}} = \{0, \ldots, 10\}$, $J_{50}^{\mathrm{MCLV}} = \{7, \ldots, 12\}$ for the MCLV and $s \in \{10^{-j/4}, j \in J_K^{\mathrm{BDCLV}}\}$ with $J_{1000}^{\mathrm{BDCLV}} = \{1\}$, $J_{450}^{\mathrm{BDCLV}} = \{0, \ldots, 12\}$, $J_{90}^{\mathrm{BDCLV}} = \{10, 11, 12\}$, $J_{50}^{\mathrm{BDCLV}} = \{12\}$ for the BDCLV. (a,b) Stage 1 survival probabilities $\phi_{1,2}$ (purple), $\phi_{2,3}$ (light blue) and $\phi_{3,1}$ (orange) vs. sK: BCLV results (lines) match perfectly with those obtained for the MCLV (symbols). Insets: Rescaled mean extinction times T_1/K vs. sK for the BDCLV (solid lines) and MCLV (symbols) virtually coincide, see text. (c,d) Stage 2 conditional fixation probabilities ϕ_1 (red), ϕ_2 (blue) and ϕ_3 (green) vs. sK: BCLV results (lines) agree perfectly with those obtained for the MCLV (symbols). Insets: Rescaled mean absorption times T_2/K vs. sK for the BDCLV (solid lines) and MCLV (symbols) almost coincide, see text. In all panels: $\vec{x}_0 = \vec{x}_c$, $\epsilon = 0$; regimes (i)-(iii), from left to right, are indicatively separated by dashed lines. Simulation results for the fixation probabilities of in the constant-K BDCLV and MCLV with $N = K$ are almost indistinguishable, see text.

upon a suitable rescaling of the timescale, the MCLV and cCLV deterministic drift and diffusive terms (about $\vec{x}^*$) can be mapped onto each other.

With this, we are now in a position to establish a link between the Stage 1 dynamics in all three models. We have seen that the cCLV survival/fixation probabilities are set in Stage 1 by the outermost orbit and follow the LOW in large populations. The MCLV and cCLV obey the same mean-field equations (up to time rescaling), with the same constant of motion $\mathcal{R}$ and fixed points, see (4.4) and (C.2), and as such they admit the same outermost orbits. Furthermore, with the same timescale, the diffusion constant in the MCLV is $1/(Ns)$ and $1/N$ in the cCLV. The survival probabilities $\phi_{i,i+1}^{\mathrm{MCLV}}$ of a population evolving with the MCLV are therefore expected to correspond to those of the cCLV in a population of effective size $\mathcal{O}(Ns)$, with rates related according to $r_i = k_i/(k_1+k_2+k_3)$. We have also seen that in the BDCLV the population size rapidly fluctuates about K, i.e. $N(t) \simeq K$, see (4.24) and Figure 4.3, and its survival probabilities are the same as in the MCLV with $N = K \gg 1$ (see Figure C.1). The survival probabilities $\phi_{i,i+1}$ in the BDCLV are therefore the same as those, $\phi_{i,i+1}^{\mathrm{cCLV}}|_{Ks}$, in the cCLV with a population of size $\mathcal{O}(Ks)$: $\phi_{i,i+1} \approx \phi_{i,i+1}^{\mathrm{MCLV}}|_K \approx \phi_{i,i+1}^{\mathrm{cCLV}}|_{Ks} = \phi_i^{\mathrm{cCLV}}|_{Ks}$. We therefore expect that the survival probabilities of the BDCLV obey the LOW when $Ks \gtrsim 100$, whereas they obey the LOSO when $Ks = \mathcal{O}(10)$, see Figure 4.2. This is confirmed by the results discussed in Section 4.4.1, see Figure 4.5(a,b). It has also been previously established in (Dobrinevski & Frey (2012); Reichenbach *et al.* (2006)) that the mean extinction time in the cCLV scales with K to leading order and can be obtained within a linear noise approximation about $\vec{x}^*$. We can proceed similarly with the MCLV, and since the linear noise approximation about $\vec{x}^*$ of the cCLV and MCLV is similar, see Eqs. (C.7) and (C.4), we can obtain the mean extinction time T_1^{MCLV} by solving the radial diffusion equation $\partial_t\ P_{\mathrm{MCLV}}(r,t) = D^{\mathrm{MCLV}}\ [r^{-1}\partial_r + \partial_r^2]\ P_{\mathrm{MCLV}}(r,\theta,t)$, with absorbing boundary on ∂S_3 and $D^{\mathrm{MCLV}} = 2D^{\mathrm{cCLV}}$. This yields $T_1^{\mathrm{MCLV}} \simeq \frac{3}{2}R^2N \approx 0.3K$ (where $R = \frac{1}{2\sqrt{3}}\left(1+\frac{1}{\sqrt{3}}\right)$ (Reichenbach *et al.* (2006))) when $r_i = r = 1/3$ (symmetric rates). A similar relation, with a different expression of R, holds when the rates r_i are asymmetric. Since $N(t) \simeq K$ in the BDCLV (after a time $t = \mathcal{O}(1)$), we readily obtain its mean extinction time: $T_1 \simeq \frac{3}{2}R^2K \approx 0.3K$ to leading order in $K \gg 1$, when $r_i = 1/3$. The insets of Figure C.1 confirm that T_1 in BDCLV is

almost indistinguishable from T_1^{MCLV} obtained in the MCLV with $N = K \gg 1$. This result also holds when the dynamics towards extinction is driven by diffusion (weak demographic noise). This is certainly the case when $\vec{x}_0 = \vec{x}^*$ and also when $\vec{x}_0 \neq \vec{x}^*$ and $s \ll 1$. In fact, under weak selection, the deterministic drift arising when $\vec{x}_0 \neq \vec{x}^*$ is weak and extinction is driven by weak demographic fluctuations when $s \ll 1$. we therefore find $T_1 \simeq \frac{3}{2}R^2 N \approx 0.3N$ when $r_i = r = 1/3$ and when $s \ll 1$ and $sK = \mathcal{O}(1)$, as reported in Figure C.3(a)

C.3 Initial Composition in Stage 2

The stage 2 dynamics of the BDCLV and MCLV, as well as their fixation properties, depend on the population composition at the end of Stage 1 which coincides with the inception of Stage 2. In Sections 4.4.1 and 5.2.2, we have seen that the initial fraction $\hat{x}_i$ of i individuals along the edge $(i, i+1)$ of S_3 is given by the probability density $P_{(i,i+1)}(\hat{x}_i)$ which can be approximated by a uniform distribution $P_{(i,i+1)}(\hat{x}_i) \approx 1$ when $sK \lesssim 10$ (constant K) and $sK_0 \lesssim 10$ (switching K), yielding an average initial fraction $\mu_i = \int_0^1 \hat{x}_i P_{(i,i+1)}(\hat{x}_i)\, d\hat{x}_i \approx 1/2$ of i individuals along $(i, i+1)$, see Figure C.2. The same holds true also when $|\epsilon| \ll 1$, see Section 4.4.2.

This is no longer the case under strong selection, when the $P_{(i,i+1)}$'s are skewed and far from being uniform, see the lower insets of Figure C.2. When $K \gg 1$ is constant and the LOW holds, the extinction of the first species in Stage 1 occurs from the outermost orbit as in the cCLV (Berr *et al.* (2009); West *et al.* (2018), see also Section 4.1), and μ_i can be estimated as follows: Along the outermost orbit that is closest ($x_{i-1} = 1/K$) to the edge $(i, i+1)$ in the BDCLV, from the rate equations (4.25) we have $x_i/x_{i+1} = r_{i+1}/r_{i-1}$ yielding $\mu_i = r_{i+1}/(r_{i+1} + r_{i-1})$. The results of Figure C.2 (a,b) for $sK \gg 1$ are in satisfying agreement with this prediction.

The results reported in Figure C.2 (c,d) show that the averages μ_i's are closer to 1/2 in regime (ii) than in the constant-K BDCLV. This stems from the environmental variability operating to balance the effect of selection and implies that $P_{(i,i+1)} \approx 1$ is a better approximation in the regime (ii) when K is randomly switching than when it is constant. In the lower insets of Figure C.2 (c,d), we

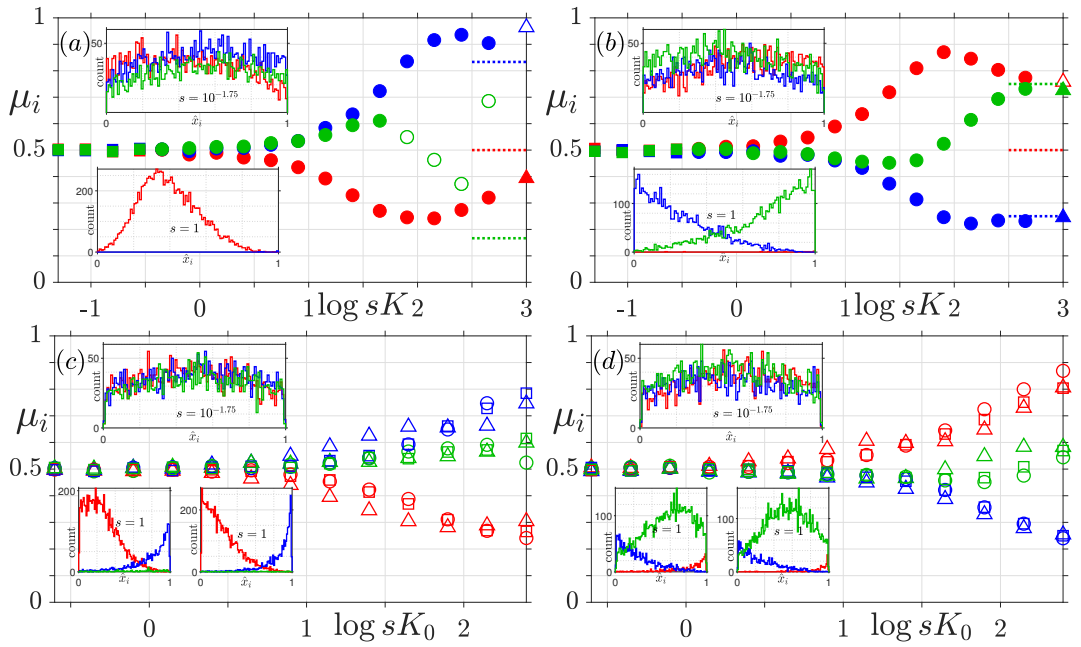

Figure C.2: Population composition at the inception of Stage 2 vs. sK (a,b) and sK_0 (c,d) with $\vec{r} = \vec{r}^{(1)}$ in (a,c) and $\vec{r} = \vec{r}^{(2)}$ in (b,d). In all panels: $\mu_i = \int_0^1 \hat{x}_i P_{(i,i+1)}(\hat{x}_i)\, d\hat{x}_i$ is the mean value of $\hat{x}_i$ for species $i = 1$ (red), 2 (blue), 3 (green), with $\vec{x}_0 = \vec{x}_c$ and $\epsilon = 0$. (a,b) μ_i vs. sK in the BDCLV with $K = 1000\ (\triangle), 450\ (\circ), 50\ (\square)$ and $s \in (10^{-3}, 1)$. (Empty symbols denote data arising from small survival probability $\phi_{i,i+1} < 0.01$ that would require additional sampling). When $sK \lesssim 10$, $\mu_i \approx 1/2$ and $P_{(i,i+1)} \approx 1$ is approximately uniform. When $sK \gg 1$, the dynamics is dominated by the LOW and $\mu_i \approx r_{i+1}/(r_{i+1} + r_{i-1})$ shown as dotted lines, see text. Upper insets: Histograms corresponding to $P_{(i,i+1)}(\hat{x}_i)$ with $s = 10^{-7/4}$ and $K = 250$, is approximately uniform, corresponding to $P_{(i,i+1)} \approx 1$, along the three edges. Lower insets: Same with $s = 1$ and $K = 1000$, showing that $P_{(i,i+1)}$ is no longer uniform when $sK \gg 1$. (c,d) μ_i vs. sK_0 in the switching-K BDCLV with $K_0 = 250$ and $\gamma = 0.8$ kept fixed and s varies with $\nu = 10\ (\square)$, $\nu = 1\ (\circ)$ and $\nu = 0.001\ (\triangle)$. Insets: (Upper) Histograms corresponding to $P_{(i,i+1)}(\hat{x}_i)$ with $s = 10^{-7/4}$, $\nu = 0.1$ and $K_0 = 250, \gamma = 0.8$ for $i = 1, 2, 3$. (Lower) Same with $s = 1$, $K_0 = 250, \gamma = 0.8$, $\nu = 0.1$ (left) and $\nu = 10$ (right).

find very similar probability densities $P_{(i,i+1)}$ for very different switching rates ($\mu = 0.1$ and $\mu = 10$), showing that in the switching-K BDCLV $P_{(i,i+1)}$ varies little with ν.

C.4 Mean Extinction and Absorption Time in the BDCLV and number of switches

We study the overall mean fixation time T_F, which is the average time after which one species takes over the entire population, in the constant-K and switching-K BDCLV. $T_F = T_1 + T_2$ consists of the *mean extinction time* T_1 and the *mean absorption time* T_2 arising from Stages 1 and 2, respectively. We also compute the average number of switches occurring in Stages 1 and 2 of the switching-K BDCLV.

C.4.1 Mean extinction, absorption and fixation times in the constant-K BDCLV

We first consider the case of the constant-K BDCLV and show that the overall mean fixation time $T_F = \mathcal{O}(K)$ across all regimes (i)-(iii), see Figure 4.7(a).

Stage 1: Mean extinction time T_1 in the constant-K BDCLV

The *mean extinction time* T_1 is the average time for one of the species to go extinct at the end of Stage 1. As explained in Section C.2, with the results obtained for the cCLV, we find $T_1 \simeq T_1^{\text{cCLV}}/2 \approx 0.3K$ when $s \ll 1$ (regimes (i,ii)) and for arbitrary s when all $r_i = 1/3$, see Figure C.3 (a). Deviations from $T_1 \approx 0.3K$, and a weak dependence on s and on the r_i's, are found near the boundary of regimes (ii)-(iii) and in regime (iii), where $T_1 \simeq \beta_c(s, \vec{r})K$, where β_c is a decreasing function of s when the r_i's are unequal, see Figure C.3 (a).

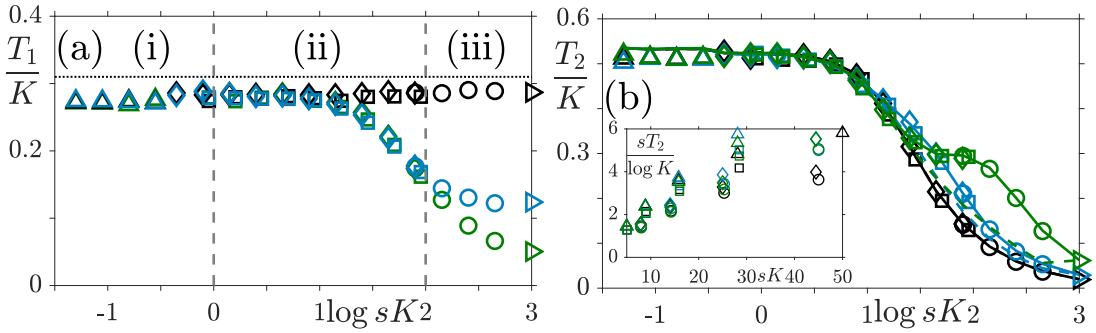

Figure C.3: Mean extinction and absorption times T_1 and T_2, in the constant-K BDCLV for $K \in \{1000\ (\triangleright), 450\ (\circ), 250\ (\diamond), 90\ (\square), 50\ (\triangle)\}$ and the same values of s as in Figures 4.5 and 4.6: (a) T_1/K vs. sK; showing $T_1 = \mathcal{O}(K)$ when $K \gg 1$ and $T_1 \approx 0.31K$ (dotted line) when $r_i = r$ and under weak selection ($sK \lesssim 10$) when $\vec{x}_c \neq \vec{x}^*$ (unequal r_i's), see text. (b) T_2/K vs. sK; solid and dashed lines show the respective predictions of $T_2|_K = \sum_i \phi_{i,i+1} T_2^{(i,i+1)}|_K$ and (C.10), see text. Inset: $sT_2/\log K = \mathcal{O}(1)$ when $s \ll 1$ and $sK \gg 1$, see text. In all panels: symbols are from stochastic simulations, $\vec{x}_0 = \vec{x}_c$, $\epsilon = 0$ and $\vec{r} = \vec{r}^{(1)}$ (green), $\vec{r} = \vec{r}^{(2)}$ (blue), and equal r_i (black).

Stage 2: Mean absorption time T_2 in the constant-K BDCLV

The stage 2 mean absorption time T_2 is given by

$$T_2 = \sum_{i=1}^{3} \phi_{i,i+1} T_2^{(i,i+1)}, \tag{C.8}$$

where the mean absorption time along the edge $(i, i+1)$ of S_3, denoted by $T_2^{(i,i+1)}$, is weighted by the probability $\phi_{i,i+1}$ that Stage 1 ends on that edge.

The expression of $T_2^{(i,i+1)}$ is obtained from the mean fixation time of the MCLV with $N = K$, here denoted by $T_2^{(i,i+1)}|_K$ with $T_2^{(i,i+1)} \simeq T_2^{(i,i+1)}|_K$, see Section C.2. For a given initial fraction $\hat{x}_i$ of i's at the start of Stage 2 is $(\hat{x}_i)$, $T_2^{(i,i+1)}(\hat{x}_i)|_K$ when $s \ll 1$ is obtained by solving $\mathcal{G}_{(i,i+1)}|_K(\hat{x}_i)\, T_2^{(i,i+1)}(\hat{x}_i)|_K = -1$, with $T_2^{(i,i+1)}|_K(0) = T_2^{(i,i+1)}|_K(1) = 0$ (see (C.3) and (2.19)). Since the exact population composition along the edge $(i, i+1)$ at the inception of Stage 2 is given by $P_{(i,i+1)}(\hat{x}_i)$, we

have:

$$T_2 \simeq \sum_{i=1}^{3} \phi_{i,i+1} T_2^{(i,i+1)}|_K = \sum_{i=1}^{3} \phi_{i,i+1} \int_0^1 P_{(i,i+1)}(\hat{x}_i)\ T_2^{(i,i+1)}(\hat{x}_i)|_K\ d\hat{x}_i. \quad \text{(C.9)}$$

with $T_2^{(i,i+1)}|_K \equiv \int_0^1 P_{(i,i+1)}(\hat{x}_i)\ T_2^{(i,i+1)}(\hat{x}_i)|_K\ d\hat{x}_i$. A simpler expression for T_2 is obtained when $s \ll 1$ and $sK \lesssim 10$ upon substituting $\phi_{i,i+1} \approx 1/3$ and $P_{(i,i+1)} \approx 1$ in (C.9):

$$T_2 \simeq \frac{1}{3} \sum_{i=1}^{3} \int_0^1 T_2^{(i,i+1)}(\hat{x}_i)|_K\ d\hat{x}_i. \quad \text{(C.10)}$$

While the expression of $T_2^{(i,i+1)}(\hat{x}_i)$ is not particularly illuminating, its asymptotic behavior is simple and allows us to determine the behavior of T_2: In the weak-selection regime (ii) where $s \ll 1$ and $sK \approx 10$, we obtain the classical result $T_2^{(i,i+1)}|_K = \mathcal{O}((\log K)/s)$ according to which T_2 scales as $1/s$ with a subleading prefactor $\sim \log K$ (Blythe & McKane (2007); Ewens (2004)), which is confirmed by the results of Figure C.3 (c).

On the other hand, since the mean fixation time in the neutral Moran model scales linearly with the population size (Blythe & McKane (2007); Crow & Kimura (2009); Ewens (2004)), we readily find $T_2 = \mathcal{O}(K)$ in the quasi-neutral regime (i). The mean fixation time in the Moran model with strong selection favouring species i against $i+1$ scales logarithmically with the population size (Antal & Scheuring (2006)), from which we infer that $T_2 = \mathcal{O}(\log K)$ in regime (iii).

Putting the asymptotic behaviors of T_1 and T_2 together, we find that to leading order in $N \simeq K \gg 1$ the overall mean fixation time $T_F = T_1 + T_2 = \mathcal{O}(K)$ scales linearly with the population size across the regimes (i)-(iii), with different subleading prefactors in each regime. We also notice that in regime (iii) $T_1 \gg T_2$: The extinction of a second species (Stage 2) occurs much faster than the death of a first species in Stage 1, see Figure 4.3 (a). In regime (i) $T_1/T_2 = \mathcal{O}(1)$ and $T_1/T_2 = \mathcal{O}(sK/\log K)$ in regime (ii), see Figure 4.3(b)

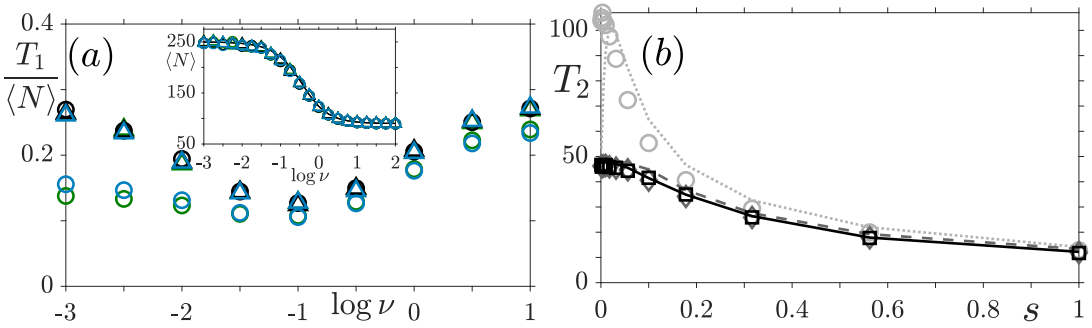

Figure C.4: (a) $T_1/\langle N\rangle$ vs. ν for $r_1 = 1/11(\text{green}), 1/3(\text{black}), 3/5(\text{blue})$ and $r_2 = r_3 = (1-r_1)/2$, with $s = 10^{-1/2}$ (circles) and $s = 10^{-3/2}$ (triangles). In agreement with (C.11), $T_1/\langle N\rangle = \beta_s = \mathcal{O}(1)$ and slowly varies with ν and s. Inset: $\langle N\rangle$ vs ν; solid lines are from the average over the marginal probability density (5.6) of the process defined by (5.5) and symbols are from stochastic simulations with $s = 10^{-1/2}$ (circles) and $s = 10^{-3/2}$ (triangles), showing $\langle N\rangle = \mathcal{O}(K_0)$, see text. (b) T_2 vs. s for $\nu = 10^{-3}$ (circles, light dotted gray), 10^{-1} (diamonds, dashed gray), 10 (squares, solid black) and $\vec{r} = (1/3, 1/3, 1/3)$. Symbols are from stochastic simulations and lines are from (C.12). T_2 scales as $1/s$ with subleading prefactor $\sim \log K_0$ when $s \ll 1$ and $sK_0 \approx 10$, see text. In both panels: $K_0 = 250, \gamma = 0.8$ ($K_- = 50, K_+ = 450$) and $\vec{x}_0 = \vec{x}_c$; $\epsilon = 0$.

C.4.2 Mean extinction, absorption and fixation times in the switching-K BDCLV

We study the effect of random switching on the mean extinction and absorption times, T_1 and T_2 characterizing Stages 1 and 2, respectively. This allows us to show that the mean fixation time $T_F = T_1 + T_2 = \mathcal{O}(\langle N \rangle) = \mathcal{O}(K_0)$ scales linearly with the average population size, and to compute the average number of switches occurring in Stages 1 and 2.

Stage 1: Mean extinction time in the switching-K BDCLV

Guided by the results of the constant-K BDCLV, where T_1 scales linearly with $N \approx K$ to leading order in $K_0 \gg 1$, we expect

$$T_1 = \beta_s \langle N \rangle \quad \text{with} \quad \beta_s = \beta_s(s, \vec{r}, \nu), \tag{C.11}$$

where $\langle N \rangle = \mathcal{O}(K_0)$ is the long-time average population size that is in principle obtained by averaging N over the N-QSD. In the inset of Figure C.4, this quantity is accurately computed in the realm of the piecewise deterministic Markov process approximation as $\langle N \rangle = \int_{K_-}^{K_+} N p_\nu^*(N) dN$, see the inset of Figure C.4 (a), and is shown to be independent of s and a decreasing function of ν. For fast/slow switching, we have $\langle N \rangle = (1 - \gamma^2) K_0$ when $\nu \to \infty$ and $\langle N \rangle = K_0$ when $\nu \to 0$ (Wienand *et al.* (2017, 2018)). Comparison with simulation results of Figure C.4 confirm that $T_1 / \langle N \rangle = \beta_s = \mathcal{O}(1)$ is a slowly varying function of ν and a weakly decreasing function of s. Since $\langle N \rangle = \mathcal{O}(K_0)$ when $\gamma = \mathcal{O}(1)$, we obtain $T_1 = \mathcal{O}(\langle N \rangle) = \mathcal{O}(K_0)$ to leading order in K_0.

Stage 2 mean absorption time and overall mean fixation time in the switching-K BDCLV

Proceeding as in Appendix C.4.1, the Stage 2 mean absorption time is given by $T_2 = \sum_{i=1}^{3} \phi_{i,i+1} T_2^{(i,i+1)}$. In the realm of the piecewise deterministic Markov process approximation, when $s \ll 1$ and $sK_0 \gg 1$, $T_2^{(i,i+1)}$ is obtained by averaging the constant-K_0 mean absorption time $T_2^{(i,i+1)}|_{K_0}$ along the edge $(i, i+1)$ over

the probability density function (5.6) (Wienand *et al.* (2017, 2018)):

$$T_2^{(i,i+1)} \simeq \int_0^1 \int_{K_-}^{K_+} P_{(i,i+1)}(\hat{x}_i)\; T_2^{(i,i+1)}(\hat{x}_i)|_{K_0}\; p^*_{\nu/\alpha_i}(N)\; d\hat{x}_i\; dN.$$

As in Section 5.2.2, the switching rate is rescaled $\nu \to \nu/\alpha_i$ due to the average number $\mathcal{O}(\nu/\alpha_i)$ of switches occurring in Stage 2 along the edge $(i, i+1)$ when $s \ll 1$ and $sK_0 \gg 1$ (Wienand *et al.* (2017, 2018)). The above equation can be simplified using $\phi_{i,i+1} \approx 1/3$ and $P_{(i,i+1)}(\hat{x}_i) \approx 1$ when $s \ll 1$ and $sK_0 \lesssim 10$ (see Appendix C.3)

$$T_2 \approx \frac{1}{3}\sum_{i=1}^{3} T_2^{(i,i+1)} \simeq \frac{1}{3}\sum_{i=1}^{3} \int_{K_-}^{K_+} T_2^{(i,i+1)}(\hat{x}_i)|_{K_0}\; p^*_{\nu/\alpha_i}(N)\; dN, \tag{C.12}$$

where $T_2^{(i,i+1)} \sim T_2^{(i,i+1)}|_{K_0}(\hat{x}_i)$ which scales as $1/\alpha_i$ with a prefactor $\sim \log K_0$ and a weak dependence on ν when $s \ll 1$ and $sK_0 \gg 1$ (Wienand *et al.* (2017)). This yields $T_2^{(i,i+1)} = \mathcal{O}((\log K_0)/s)$ in regime (ii): In agreement with the results of Figure C.4 (b), $T_2 = \mathcal{O}(1/s)$ with a subleading prefactor $\sim \log K_0$ when $s \ll 1$ and $sK_0 \lesssim 10$. As in the constant-K BDCLV, the quasi-neutral regime (i), where $sK_0 \ll 1$, $T_2 = \mathcal{O}(K_0)$, whereas under strong selection, $sK_0 \gg 1$, $T_2 = \mathcal{O}(\log K_0)$, see Figure C.4 (b).

Putting together the results for T_1 and T_2, we obtain the overall mean fixation time $T_F = T_1 + T_2 \sim \langle N \rangle$. Since $\langle N \rangle = \mathcal{O}(K_0)$, we have $T_F = \mathcal{O}(K_0)$ which, with subleading prefactors that vary slowly with ν and s, as illustrated by Figure 5.6.

C.4.3 Average number of switches in Stages 1 and 2 of the switching-K BDCLV

Since the average duration of Stage 1 in the the switching-K BDCLV is $T_1 = \beta_s \langle N \rangle = \mathcal{O}(K_0)$, see Eq. (C.11), the average number of switches occurring prior one of the species die out scales as $\mathcal{O}(\nu K_0)$, as shown in Figure C.5 (a), i.e. the average number of switches increases as νK_0, with a prefactor that depends on s via β_s which is a weakly decreasing function of s (i.e. the number of switches is greater for smaller values of s). Hence, for any non-vanishingly small switching rate $\nu \gg 1/K_0$ and $K_0 \gg 1$, a large number of switches occur during Stage 1

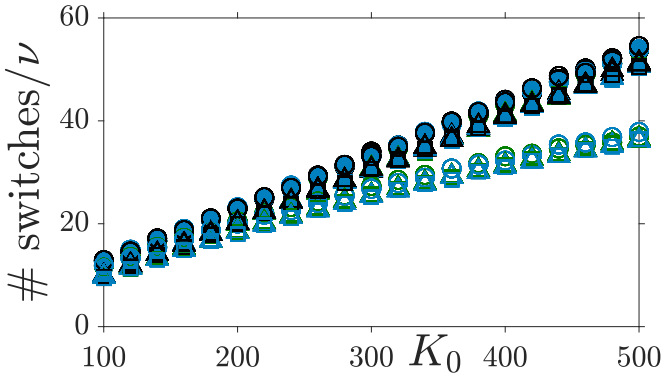

Figure C.5: Average number of switches in Stage 1 of the BDCLV for $\nu = 0.1$ (circles), 1 (triangles), 10 (squares). Selection intensity is $s = 10^{-3/2}$ (filled symbols) and $s = 10^{-1/2}$ (open symbols). Data for (average number of switches in Stage 1)$/\nu$ vs K_0 and different values of ν and $\vec{r}$ essentially collapse onto a curve (almost a line). Other parameters are: $\vec{r} = (1,1,1)/3$ (black), $\vec{r} = (1,5,5)/11$ (green), $\vec{r} = (3,2,2)/5$ (blue); $\vec{r} = \vec{r}^{(1)}$ and $\vec{x}_0 = \vec{x}_c$.

prior to the extinction of the first species and the DMN self averages, see Section 5.2.1.

In Wienand *et al.* (2017, 2018), it has been shown that that under weak selection the population experiences, on average, $\mathcal{O}(\nu/\alpha_i)$ switches during the two-species competition characterizing the Stage 2 dynamics along the edge $(i, i+1)$. This supports the rescaling $\nu \to \nu/\alpha_i$ in formula (5.11) which has been found to be actually valid when the selection intensity s is neither vanishingly small nor too large (Wienand *et al.* (2018)).

C.5 Fixation Probabilities in the cCLV and CLVDN when $N = 3$

The law of stay out ('LOSO' - see (4.10)) states that the most likely species to fixate the population is the one that predates on the species with the highest dominance-replacement rate. Here I will use a first-step analysis to derive an exact expression for the 'LOSO' when $N = 3$ in the cCLV when the environment is constant (see Section 4.1): I will show that $\phi_i = k_{i+1}/\left(\sum_{i=1}^{3} k_i\right)$. In the case

where k_1 varies in time according to a dichotomous Markov process (see Chapter 6), I will show that the fixation probability depends on the rates, k_i, the intensity of the noise Δ and the switching rate ν.

C.5.1 LOSO in the cCLV

When $N = 3$ in the cCLV with one individual of each species initially, the fate of the system is known after the first reaction has taken place. This is because two species then remain (say, i and $i + 1$), the only reaction that can happen is for the 'predator' i to replace the 'prey' $i + 1$ until only i remains and it has fixated the population.

If we consider species 1, it will fixate the population if the first reaction is species 2 replacing species 3. The probability that this occurs first is the rate at which this occurs, k_2, divided by the total rate of all reactions $\left(\sum_{i=1}^{3} k_i\right)$. Proceeding similarly for species 2 and 3 we have:

$$\phi_1 = \frac{k_2}{\sum_{i=1}^{3} k_i}, \quad \phi_2 = \frac{k_3}{\sum_{i=1}^{3} k_i}, \quad \phi_3 = \frac{k_1}{\sum_{i=1}^{3} k_i} \tag{C.13}$$

C.5.2 Fixation Properties in the CLVDN when $N = 3$

Again in the model described by (6.1) - (6.3) in Chapter 6 the fixation probability is completely determined by the first dominance replacement reaction to occur. Considering species 1, it will be the fixating species if the first dominance-replacement reaction to occur is species 2 replacing species 3. However, in contrast to the cCLV, here we also have to take into account that the environment may switch an arbitrary number of times before a dominance replacement reaction happens. Hence the probability that species 1 fixates the population is:

$$\begin{aligned} \phi_1 &= P(23 \text{ reaction first}) = P(23) + P(\text{switch then } 23) \\ &+ \quad P(2 \text{ switches then } 23) + \ldots, \end{aligned} \tag{C.14}$$

where $P(.)$ stands for "probability of (.)".

Considering first that initially $\xi = +1$ and according to (C.14), with $\gamma = k + k_2 + k_3 + \nu$ and $\alpha = \nu^2/(\gamma^2 - \Delta^2)$, we have :

$$\begin{aligned} P(1 \text{ fixates}|\text{ start with } \xi = +1) &= \frac{k_2}{\gamma + \Delta} + \frac{\nu}{\gamma + \Delta}\frac{k_2}{\gamma - \Delta} \\ &+ \frac{\nu^2}{(\gamma + \Delta)(\gamma - \Delta)}\frac{k_2}{\gamma + \Delta} + \dots \\ &= \sum_{n=0}^{\infty} \alpha^n \left(\frac{1}{\gamma + \Delta} + \frac{\nu}{\gamma^2 - \Delta^2} \right) k_2 \\ &= \frac{(\gamma - \Delta + \nu)\, k_2}{\gamma^2 - \Delta^2 - \nu^2}. \end{aligned} \tag{C.15}$$

The case of the initial state $\xi = -1$ is treated similarly and yields:

$$P(1 \text{ fixates}|\text{ start with } \xi = -1) = \frac{(\gamma + \Delta + \nu)\, k_2}{\gamma^2 - \Delta^2 - \nu^2}. \tag{C.16}$$

Since the population is initially as likely to be in either of the environmental states, we have

$$\begin{aligned} \phi_1 &= \frac{1}{2} P(1 \text{ fixates}|\text{ start in } \xi = +1) \\ &+ \frac{1}{2} P(1 \text{ fixates}|\text{ start in } \xi = -1) = \frac{(\gamma + \nu)\, k_2}{\gamma^2 - \Delta^2 - \nu^2}. \end{aligned} \tag{C.17}$$

Proceeding similarly for ϕ_2 and ϕ_3, we obtain (6.5).

Appendix D

Simulation Methods

In this thesis, theoretical predictions are backed up by simulations. Depending on the kind of environmental noise being studied, different simulation methods must be used. Here I will briefly explain the different simulation methods, and when they are applicable. Full algorithms can be found in the cited papers.

When considering dichotomous Markov noise (DMN), or no environmental noise, I use the well-known 'Gillespie algorithm' (Gillespie (1977)). This is an exact realisation of the Master equation, using two random numbers and the rate of each reaction (T_i^+, T_i^- and $\nu_\pm$) to determine the time that the next reaction takes place, and which one it is. This method is possible here because each reaction (species reactions and environmental switch) occurs randomly with a certain rate. DMN is the main focus of the thesis, hence this is the simulation method I use the most.

In Chapter 3 we compare this to periodic switching, and in this case we use a modified version of the 'Next Reaction Method' (Anderson (2007)), which is more suitable for systems with explicit time dependent rates. This differs from the Gillespie algorithm because for each reaction it keeps track of the next time each is due to occur, along with the global time (*i.e.* the current time of the system). To initialise, the 'internal reaction times' are set (for the species reactions these are drawn from an exponential random variable with rate $T_i^\pm$, for the environmental switches this is known exactly from ν, δ and ξ), and the 'global reaction time' is initialised to zero. Then at each iteration the reaction with the smallest next reaction time is selected and the global reaction time set to this internal time, the

populations are updated, and the internal reaction times for the species reactions that did not occur are updated according to:

$$\begin{aligned}\text{new internal time} &= \frac{\text{old reaction rate}}{\text{new reaction rate}}(\text{internal reaction time} - \text{new global time}) \\ &+ \text{new global time.}\end{aligned}$$

Finally, for the reaction that occurred the new internal reaction time is calculated as an exponential random variable with new reaction rate if it was a species reaction, or calculated from (ν, δ, ξ) if it was an environmental switch. In this situation this is also an exact realisation of the Master equation and while it has added advantage of only requiring one random variable to be generated in each time-step, you are required to keep track of all the internal firing times and the global time, rather than just the global time for the Gillespie Algorithm.

For the Ornstein-Uhlenbeck (OU) process briefly discussed in Appendix A.2, all the processes are random processes but there is the added complication that the OU process has a continuous sample space but the sample spaces for the species processes are discrete. Simulating these together is made more difficult by the dependence of the death rates on the OU process. To get around this, one approximates the OU process via a discrete birth death process that can be described with a Master equation. To this end, one defines the 'copy number' of the carrying capacity $k = K_{\text{OU}}(1 + \xi_{\text{OU}})$, where ξ_{OU} is the OU process with zero mean, correlation time τ and intensity σ as in (A.7), and $K_{\text{OU}} \gg 1$ is the mean value of the carrying capacity and a large number (Roberts *et al.* (2015)). The Master equation describing the probability of finding copy number k, P_k satisfies:

$$\frac{dP_k}{dt} = b_{k-1}P_{k-1} + d_{k+1}P_{k+1} - (b_k + d_k)P_k, \tag{D.1}$$

where the birth and death rates are

$$b_k = \frac{2K_{\text{OU}}^2\sigma^2 - k + K_{\text{OU}}}{2\tau} \quad \text{and} \tag{D.2}$$

$$d_k = \frac{2K_{\text{OU}}^2\sigma^2 + k - K_{\text{OU}}}{2\tau} \tag{D.3}$$

respectively. Using these birth and death rates, the stochastic differential equation (SDE) for the copy number k is:

$$dk = -\frac{(k - K_{\text{OU}})}{\tau} + \sqrt{\frac{2K_{\text{OU}}^2\sigma^2}{\tau}}dW, \tag{D.4}$$

where dW is an interval of the Wiener process. This is the same as the SDE for the carrying capacity $K(t)$ defined by (A.6) and (A.7) which can be found by noting that $dK = K_{\mathrm{OU}} d\xi_{\mathrm{OU}}$ and substituting $\xi = \frac{K - K_{\mathrm{OU}}}{K_{\mathrm{OU}}}$.

With this approximation of the full OU process, all the reactions being simulated are now birth death processes so one can, in principle, use the Gillespie algorithm or Next Reaction Method. However, because $K_{\mathrm{OU}} \gg 1$ the birth and death rates for the copy number are much larger than those for the species (of order K_{OU}^2/τ compared to order K_{OU}). So, between successive species reactions there will be of order K_{OU}/τ copy number reactions. When τ is large the speed of both algorithms is comparable, but when τ is of order $\mathcal{O}(1)$ it is faster to use the Next Reaction Method, because this requires only one random number per iteration (which is the slowest step in the algorithms).

Finally one must also recognise that the unboundedness of the OU process can lead to negative carrying capacities. This is obviously not physically realistic and is overcome by by specifying that the death rate of the copy number when $k = 1$, $d_1 = 0$. This effectively imposes a reflecting boundary at zero and has a negligible effect on the steady state distribution when $\sigma < 0.3$.

References

Acar, M., Mettetal, J.T. & Van Oudenaarden, A. (2008). Stochastic switching as a survival strategy in fluctuating environments. *Nature Genetics*, **40**, 471. 1, 33

Allesina, S. & Tang, S. (2012). Stability criteria for complex ecosystems. *Nature*, **483**, 205–208. 13

Anderson, D.F. (2007). A modified next reaction method for simulating chemical systems with time dependent propensities and delays. *The Journal of chemical physics*, **127**, 214107. 166

Antal, T. & Scheuring, I. (2006). Fixation of strategies for an evolutionary game in finite populations. *Bulletin of Mathematical Biology*, **68**, 1923–1944. 17, 18, 150, 159

Ashcroft, P., Altrock, P.M. & Galla, T. (2014). Fixation in finite populations evolving in fluctuating environments. *Journal of The Royal Society Interface*, **11**, 20140663. 1, 34

Assaf, M. & Meerson, B. (2010). Extinction of metastable stochastic populations. *Physical Review E*, **81**, 021116. 25

Assaf, M. & Mobilia, M. (2010). Large fluctuations and fixation in evolutionary games. *Journal of Statistical Mechanics: Theory and Experiment*, **2010**, P09009. 17

Assaf, M., Kamenev, A. & Meerson, B. (2008). Population extinction in a time-modulated environment. *Physical Review E*, **78**, 041123. 25, 46

Assaf, M., Mobilia, M. & Roberts, E. (2013a). Cooperation dilemma in finite populations under fluctuating environments. *Physical Review Letters*, **111**, 238101. 1, 3, 34

Assaf, M., Roberts, E., Luthey-Schulten, Z. & Goldenfeld, N. (2013b). Extrinsic noise driven phenotype switching in a self-regulating gene. *Physical Review Letters*, **111**, 058102. 1, 3

Avelino, P., Bazeia, D., Losano, L., Menezes, J. & de Oliveira, B. (2018). Spatial patterns and biodiversity in off-lattice simulations of a cyclic three-species Lotka-Volterra model. *EPL (Europhysics Letters)*, **121**, 48003. 70

Avery, S.V. (2006). Microbial cell individuality and the underlying sources of heterogeneity. *Nature Reviews Microbiology*, **4**, 577–587. 32

Balaban, N.Q., Merrin, J., Chait, R., Kowalik, L. & Leibler, S. (2004). Bacterial persistence as a phenotypic switch. *Science*, **305**, 1622–1625. 1

Balakrishnan, V. (1993). On a simple derivation of master equations for diffusion processes driven by white noise and dichotomic Markov noise. *Pramana*, **40**, 259. 27

Balakrishnan, V. (2003). Solvability of dichotomous flows, dichotomous diffusion, and generalizations. In *Noise in Complex Systems and Stochastic Dynamics*, vol. 5114, 40–46, International Society for Optics and Photonics. 27

Balakrishnan, V. & Van den Broeck, C. (2001). Solvability of the master equation for dichotomous flow. *Physical Review E*, **65**, 012101. 27

Balakrishnan, V., Van den Broeck, C. & Bena, I. (2001). Stochastically perturbed flows: Delayed and interrupted evolution. *Stochastics and Dynamics*, **1**, 537–551. 27

Becker, F., Wienand, K., Lechner, M., Frey, E. & Jung, H. (2018). Interactions mediated by a public good transiently increase cooperativity in growing Pseudomonas putida metapopulations. *Scientific Reports*, **8**, 1–13. 4, 53

Begon, M., Townsend, C.R. & Harper, J.L. (2006). *Ecology: From Individuals to Ecosystems*. Blackwell. 55, 135

Bena, I. (2006). Dichotomous Markov noise: Exact results for out-of-equilibrium systems. *International Journal of Modern Physics B*, **20**, 2825–2888. 2, 3, 27, 118

Bena, I., Van den Broeck, C., Kawai, R. & Lindenberg, K. (2002). Nonlinear response with dichotomous noise. *Physical Review E*, **66**, 045603. 27

Bena, I., Van den Broeck, C., Kawai, R. & Lindenberg, K. (2003). Drift by dichotomous Markov noise. *Physical Review E*, **68**, 041111. 27

Benaim, M., Schreiber, S.J., Tarres, P. *et al.* (2004). Generalized urn models of evolutionary processes. *The Annals of Applied Probability*, **14**, 1455–1478. 15

Berr, M., Reichenbach, T., Schottenloher, M. & Frey, E. (2009). Zero-one survival behavior of cyclically competing species. *Physical Review Letters*, **102**, 048102. 8, 60, 61, 63, 64, 74, 114, 117, 120, 122, 126, 152, 155

Biroli, G., Bunin, G. & Cammarota, C. (2018). Marginally stable equilibria in critical ecosystems. *New Journal of Physics*, **20**, 083051. 13

Bladon, A.J., Galla, T. & McKane, A.J. (2010). Evolutionary dynamics, intrinsic noise, and cycles of cooperation. *Physical Review E*, **81**, 066122. 36

Blume, L.E. *et al.* (1993). The statistical mechanics of strategic interaction. *Games and Economic Behavior*, **5**, 387–424. 71

Blyth, C.R. (1972). On Simpson's paradox and the sure-thing principle. *Journal of the American Statistical Association*, **67**, 364–366. 57, 135

Blythe, R.A. & McKane, A.J. (2007). Stochastic models of evolution in genetics, ecology and linguistics. *Journal of Statistical Mechanics: Theory and Experiment*, **2007**, P07018. 150, 159

Bressloff, P.C. (2017). Stochastic Liouville equation for particles driven by dichotomous environmental noise. *Physical Review E*, **95**, 012124. 27

Bressloff, P.C. & Lawley, S.D. (2017). Mean first passage times for piecewise deterministic Markov processes and the effects of critical points. *Journal of Statistical Mechanics: Theory and Experiment*, **2017**, 063202. 27

Brockhurst, M.A. (2007). Population bottlenecks promote cooperation in bacterial biofilms. *PLoS One*, **2**. 5, 6, 33, 55, 135

Brockhurst, M.A., Buckling, A. & Gardner, A. (2007). Cooperation peaks at intermediate disturbance. *Current Biology*, **17**, 761–765. 5, 6, 33, 49, 55, 135

Broom, M. & Rychtár, J. (2013). *Game-Theoretical Models in Biology*. CRC Press. 61, 70, 71, 73, 74, 85

Buckling, A., Kassen, R., Bell, G. & Rainey, P.B. (2000). Disturbance and diversity in experimental microcosms. *Nature*, **408**, 961–964. 57, 135

Buckling, A., Harrison, F., Vos, M., Brockhurst, M.A., Gardner, A., West, S.A. & Griffin, A. (2007). Siderophore-mediated cooperation and virulence in Pseudomonas aeruginosa. *FEMS Microbiology Ecology*, **62**, 135–141. 4, 53

Bunin, G. (2017). Ecological communities with Lotka-Volterra dynamics. *Physical Review E*, **95**, 042414. 13

Burns, J.G. & Dyer, A.G. (2008). Diversity of speed-accuracy strategies benefits social insects. *Current Biology*, **18**, R953–R954. 32

Cameron, D.D., White, A. & Antonovics, J. (2009). Parasite–grass–forb interactions and rock–paper–scissor dynamics: Predicting the effects of the parasitic plant Rhinanthus minor on host plant communities. *Journal of Ecology*, **97**, 1311–1319. 59

Caro-Astorga, J., Frenzel, E., Perkins, J.R., Álvarez-Mena, A., De Vicente, A., Ranea, J.A., Kuipers, O.P. & Romero, D. (2020). Biofilm formation displays intrinsic offensive and defensive features of Bacillus cereus. *NPJ Biofilms and Microbiomes*, **6**. 4

Casadesús, J. & Low, D. (2006). Epigenetic gene regulation in the bacterial world. *Microbiology and Molecular Biology Reviews*, **70**, 830–856. 32

Chater, N., Vlaev, I. & Grinberg, M. (2008). A new consequence of Simpson's paradox: Stable cooperation in one-shot prisoner's dilemma from populations of individualistic learners. *Journal of Experimental Psychology: General*, **137**, 403. 57, 135

Chesson, P.L. & Warner, R.R. (1981). Environmental variability promotes coexistence in lottery competitive systems. *The American Naturalist*, **117**, 923–943. 1

Chuang, J.S., Rivoire, O. & Leibler, S. (2009). Simpson's paradox in a synthetic microbial system. *Science*, **323**, 272–275. 57, 135

Claussen, J.C. & Traulsen, A. (2008). Cyclic dominance and biodiversity in well-mixed populations. *Physical Review Letters*, **100**, 058104. 70, 71, 150, 151

Coates, J., Park, B.R., Le, D., Şimşek, E., Chaudhry, W. & Kim, M. (2018). Antibiotic-induced population fluctuations and stochastic clearance of bacteria. *eLife*, **7**, e32976. 37

Cohen, D. (1966). Optimizing reproduction in a randomly varying environment. *Journal of Theoretical Biology*, **12**, 119–129. 32

Connell, J.H. (1978). Diversity in tropical rain forests and coral reefs. *Science*, **199**, 1302–1310. 57, 135

Cremer, J., Melbinger, A. & Frey, E. (2011). Evolutionary and population dynamics: A coupled approach. *Physical Review E*, **84**, 051921. 21, 57, 135

Cremer, J., Melbinger, A. & Frey, E. (2012). Growth dynamics and the evolution of cooperation in microbial populations. *Scientific Reports*, **2**, 281. 5, 21, 57, 135

Cremer, J., Melbinger, A., Wienand, K., Henriquez, T., Jung, H. & Frey, E. (2019). Cooperation in microbial populations: Theory and experimental model systems. *Journal of Molecular Biology*. 57, 135

Crow, J.F. & Kimura, M. (2009). *An Introduction to Population Genetics Theory*. Blackburn Press, New Jersey. 1, 159

Danino, M. & Shnerb, N.M. (2018). Fixation and absorption in a fluctuating environment. *Journal of Theoretical Biology*, **441**, 84–92. 1

Diggle, S.P., Griffin, A.S., Campbell, G.S. & West, S.A. (2007). Cooperation and conflict in quorum-sensing bacterial populations. *Nature*, **450**, 411–414. 4, 53

Dobramysl, U. & Täuber, U.C. (2013). Environmental versus demographic variability in two-species predator-prey models. *Physical Review Letters*, **110**, 048105. 1

Dobramysl, U., Mobilia, M., Pleimling, M. & Täuber, U.C. (2018). Stochastic population dynamics in spatially extended predator–prey systems. *Journal of Physics A: Mathematical and Theoretical*, **51**, 063001. 69, 70, 71, 74, 85

Dobrinevski, A. & Frey, E. (2012). Extinction in neutrally stable stochastic Lotka-Volterra models. *Physical Review E*, **85**, 051903. 61, 64, 74, 154

Doebeli, M. & Knowlton, N. (1998). The evolution of interspecific mutualisms. *Proceedings of the National Academy of Sciences*, **95**, 8676–8680. 5

Doebeli, M., Ispolatov, Y. & Simon, B. (2017). Point of view: Towards a mechanistic foundation of evolutionary theory. *eLife*, **6**, e23804. 15

Doering, C. & Horsthemke, W. (1985). A comparison between transitions induced by random and periodic fluctuations. *Journal of Statistical Physics*, **38**, 763–783. 27

Doering, C.R., Sargsyan, K.V. & Sander, L.M. (2005). Extinction times for birth-death processes: Exact results, continuum asymptotics, and the failure of the Fokker–Planck approximation. *Multiscale Modeling & Simulation*, **3**, 283–299. 25

Donohue, I., Petchey, O.L., Montoya, J.M., Jackson, A.L., McNally, L., Viana, M., Healy, K., Lurgi, M., O'Connor, N.E. & Emmerson, M.C. (2013). On the dimensionality of ecological stability. *Ecology Letters*, **16**, 421–429. 13

Dubnau, D. & Losick, R. (2006). Bistability in bacteria. *Molecular Microbiology*, **61**, 564–572. 32

Durney, C., Case, S., Pleimling, M. & Zia, R. (2011). Saddles, arrows, and spirals: Deterministic trajectories in cyclic competition of four species. *Physical Review E*, **83**, 051108. 64

Durrett, R. & Levin, S. (1994). The importance of being discrete (and spatial). *Theoretical Population Biology*, **46**, 363–394. 5

Ewens, W.J. (2004). *Mathematical Population Genetics*. Springer Science, New York. 1, 4, 15, 17, 150, 159

Fox, J.W. (2013). The Intermediate Disturbance Hypothesis should be abandoned. *Trends in Ecology & Evolution*, **28**, 86–92. 49, 57, 135

Frachebourg, L., Krapivsky, P. & Ben-Naim, E. (1996a). Segregation in a one-dimensional model of interacting species. *Physical Review Letters*, **77**, 2125. 61, 68

Frachebourg, L., Krapivsky, P.L. & Ben-Naim, E. (1996b). Spatial organization in cyclic Lotka-Volterra systems. *Physical Review E*, **54**, 6186. 68

Frank, S.A. (1998). *Foundations of social evolution*, vol. 2. Princeton University Press. 5

Frean, M. & Abraham, E.R. (2001). Rock–scissors–paper and the survival of the weakest. *Proceedings of the Royal Society of London. Series B: Biological Sciences*, **268**, 1323–1327. 8, 61, 74

Frey, E. (2010). Evolutionary game theory: Theoretical concepts and applications to microbial communities. *Physica A: Statistical Mechanics and its Applications*, **389**, 4265–4298. 8

Fudenberg, D., Imhof, L., Nowak, M.A. & Taylor, C. (2004). Stochastic evolution as a generalized Moran process. *Unpublished manuscript*. 15

Galbraith, J.K. (2008). *The predator state: How conservatives abandoned the free market and why liberals should too*. Simon and Schuster. 12

Galla, T. (2011). Imitation, internal absorption and the reversal of local drift in stochastic evolutionary games. *Journal of Theoretical Biology*, **269**, 46–56. 70, 71, 150

Galla, T. (2018). Dynamically evolved community size and stability of random Lotka-Volterra ecosystems (a). *EPL (Europhysics Letters)*, **123**, 48004. 13

Gardiner, C.W. (1985). *Handbook of Stochastic Methods*, vol. 3. springer Berlin. 1, 4, 17, 20, 73, 151

Gillespie, D.T. (1977). Exact stochastic simulation of coupled chemical reactions. *The Journal of Physical Chemistry*, **81**, 2340–2361. 115, 166

Gravel, D., Massol, F. & Leibold, M.A. (2016). Stability and complexity in model meta-ecosystems. *Nature Communications*, **7**, 1–8. 13

Griffin, A.S., West, S.A. & Buckling, A. (2004). Cooperation and competition in pathogenic bacteria. *Nature*, **430**, 1024–1027. 4, 53

Grime, J.P. (1973). Competitive exclusion in herbaceous vegetation. *Nature*, **242**, 344–347. 57, 135

Hamilton, W.D. (1995). Narrow roads of gene land: The collected papers of W.D. Hamilton, Volume 1: Evolution of Social Behaviour. 5

Hänggi, P. & Jung, P. (1995). Colored noise in dynamical systems. *Advances in Chemical Physics*, **89**, 239–326. 27

Hasan, C.R., Osinga, H.M., Postlethwaite, C.M. & Rucklidge, A.M. (2019). Stability of periodic travelling waves in a rock-paper-scissors model. *arXiv preprint arXiv:1911.10447*. 69

Hassell, M.P., Comins, H.N. & May, R.M. (1994). Species coexistence and self-organizing spatial dynamics. *Nature*, **370**, 290–292. 5

Hauert, C. & Doebeli, M. (2004). Spatial structure often inhibits the evolution of cooperation in the snowdrift game. *Nature*, **428**, 643–646. 5

Hauert, C. & Szabó, G. (2005). Game theory and physics. *American Journal of Physics*, **73**, 405–414. 71

Hauert, C., De Monte, S., Hofbauer, J. & Sigmund, K. (2002). Volunteering as Red Queen mechanism for cooperation in public goods games. *Science*, **296**, 1129–1132. 57, 135

He, Q., Mobilia, M. & Täuber, U.C. (2010). Spatial rock-paper-scissors models with inhomogeneous reaction rates. *Physical Review E*, **82**, 051909. 1, 8, 61, 68, 69, 74

He, Q., Mobilia, M. & Täuber, U.C. (2011). Coexistence in the two-dimensional May-Leonard model with random rates. *The European Physical Journal B*, **82**, 97–105. 71

Hense, B.A., McIntosh, M., Müller, J. & Schuster, M. (2019). Homogeneous and heterogeneous response of quorum-sensing bacteria in an evolutionary context. *arXiv preprint arXiv:1905.00334*. 57, 135

Hibbing, M.E., Fuqua, C., Parsek, M.R. & Peterson, S.B. (2010). Bacterial competition: Surviving and thriving in the microbial jungle. *Nature Reviews Microbiology*, **8**, 15–25. 6, 7, 59

Hidalgo, J., Suweis, S. & Maritan, A. (2017). Species coexistence in a neutral dynamics with environmental noise. *Journal of Theoretical Biology*, **413**, 1–10. 1, 34

Hofbauer, J. & Sigmund, K. (2003). Evolutionary game dynamics. *Bulletin of the American Mathematical Society*, **40**, 479–519. 4

Hofbauer, J., Sigmund, K. *et al.* (1998). *Evolutionary Games and Population Dynamics*. Cambridge University Press. 4, 15, 61, 62, 70, 72, 73, 74, 85

Horsthemke, W. & Lefever, R. (1984). *Noise-Induced Transitions: Theory and Applications in Physics, Chemistry and Biology*. Springer. 27, 28, 29, 118, 136, 138

Hufton, P.G., Lin, Y.T., Galla, T. & McKane, A.J. (2016). Intrinsic noise in systems with switching environments. *Physical Review E*, **93**, 052119. 1, 139

Hufton, P.G., Lin, Y.T. & Galla, T. (2018). Phenotypic switching of populations of cells in a stochastic environment. *Journal of Statistical Mechanics: Theory and Experiment*, **2018**, 023501. 1, 33, 45

Hufton, P.G., Lin, Y.T. & Galla, T. (2019). Model reduction methods for population dynamics with fast-switching environments: Reduced master equations, stochastic differential equations, and applications. *Physical Review E*, **99**, 032122. 51

HumonComics (2012). Humon Comics, Animal Lives. `http://humoncomics.com/side-blotched-lizard`, accessed: 5th May 2020. 7

Ifti, M. & Bergersen, B. (2003). Survival and extinction in cyclic and neutral three-species systems. *The European Physical Journal E*, **10**, 241–248. 8, 61, 74

Ives, A.R. & Carpenter, S.R. (2007). Stability and diversity of ecosystems. *Science*, **317**, 58–62. 13

Jackson, J. & Buss, L. (1975). Alleopathy and spatial competition among coral reef invertebrates. *Proceedings of the National Academy of Sciences*, **72**, 5160–5163. 59

Kaern, M., Elston, T.C., Blake, W.J. & Collins, J.J. (2005). Stochasticity in gene expression: From theories to phenotypes. *Nature Reviews Genetics*, **6**, 451–464. 32

Kaufmann, B.B. & van Oudenaarden, A. (2007). Stochastic gene expression: From single molecules to the proteome. *Current Opinion in Genetics & Development*, **17**, 107–112. 32

Kermack, W.O. & McKendrick, A.G. (1927). A contribution to the mathematical theory of epidemics. *Proceedings of the Royal Society of London. Series A, Containing papers of a mathematical and physical character*, **115**, 700–721. 12

Kermack, W.O. & McKendrick, A.G. (1932). Contributions to the mathematical theory of epidemics. II.–The problem of endemicity. *Proceedings of the Royal Society of London. Series A, containing papers of a mathematical and physical character*, **138**, 55–83. 12

Kermack, W.O. & McKendrick, A.G. (1933). Contributions to the mathematical theory of epidemics. III.–Further studies of the problem of endemicity. *Proceedings of the Royal Society of London. Series A, Containing Papers of a Mathematical and Physical Character*, **141**, 94–122. 12

Kerr, B., Riley, M.A., Feldman, M.W. & Bohannan, B.J. (2002). Local dispersal promotes biodiversity in a real-life game of rock–paper–scissors. *Nature*, **418**, 171–174. 6, 59, 67

Killingback, T., Doebeli, M. & Knowlton, N. (1999). Variable investment, the continuous prisoner's dilemma, and the origin of cooperation. *Proceedings of the Royal Society of London. Series B: Biological Sciences*, **266**, 1723–1728. 5

Kimura, M. (1957). Some problems of stochastic processes in genetics. *The Annals of Mathematical Statistics*, 882–901. 15

Kirkup, B.C. & Riley, M.A. (2004). Antibiotic-mediated antagonism leads to a bacterial game of rock–paper–scissors in vivo. *Nature*, **428**, 412–414. 6, 59

Knebel, J., Krüger, T., Weber, M.F. & Frey, E. (2013). Coexistence and survival in conservative Lotka-Volterra networks. *Physical Review Letters*, **110**, 168106. 64, 74

Kussell, E. & Leibler, S. (2005). Phenotypic diversity, population growth, and information in fluctuating environments. *Science*, **309**, 2075–2078. 1, 32

Kussell, E., Kishony, R., Balaban, N.Q. & Leibler, S. (2005). Bacterial persistence: A model of survival in changing environments. *Genetics*, **169**, 1807–1814. 2, 32

Lachmann, M. & Jablonka, E. (1996). The inheritance of phenotypes: An adaptation to fluctuating environments. *Journal of Theoretical Biology*, **181**, 1–9. 32

Lampert, W. & Sommer, U. (2007). *Limnoecology: The ecology of lakes and streams*. Oxford University Press. 57, 135

Lieberman, E., Hauert, C. & Nowak, M.A. (2005). Evolutionary dynamics on graphs. *Nature*, **433**, 312–316. 5

Loreau, M. & De Mazancourt, C. (2013). Biodiversity and ecosystem stability: A synthesis of underlying mechanisms. *Ecology Letters*, **16**, 106–115. 13

Lotka, A.J. (1926). Elements of physical biology. *Science Progress in the Twentieth Century (1919-1933)*, **21**, 341–343. 12

Maheshri, N. & OShea, E.K. (2007). Living with noisy genes: How cells function reliably with inherent variability in gene expression. *Annual Review of Biophysics and Biomolecular Structure*, **36**, 413–434. 32

Marrec, L. & Bitbol, A.F. (2020). Resist or perish: Fate of a microbial population subjected to a periodic presence of antimicrobial. *PLoS Computational Biology*, **16**, e1007798. 37

Masoliver, J., Lindenberg, K. & West, B.J. (1986a). First-passage times for non-Markovian processes: Correlated impacts on a free process. *Physical Review A*, **34**, 1481. 27

Masoliver, J., Lindenberg, K. & West, B.J. (1986b). First-passage times for non-Markovian processes: Correlated impacts on bound processes. *Physical Review A*, **34**, 2351. 27

May, R.M. (1971). Stability in multispecies community models. *Mathematical Biosciences*, **12**, 59–79. 13

May, R.M. (1972). Will a large complex system be stable? *Nature*, **238**, 413–414. 13

May, R.M. (1974). *Stability and Complexity in Model Ecosystems*. Princeton University Press. 2, 13

May, R.M. (2006). Network structure and the biology of populations. *Trends in Ecology & Evolution*, **21**, 394–399. 5

May, R.M. & Leonard, W.J. (1975). Nonlinear aspects of competition between three species. *SIAM Journal on Applied Mathematics*, **29**, 243–253. 66, 67, 71, 74, 85

McCann, K.S. (2000). The diversity–stability debate. *Nature*, **405**, 228–233. 13

Melbinger, A. & Vergassola, M. (2015). The impact of environmental fluctuations on evolutionary fitness functions. *Scientific Reports*, **5**, 15211. 2

Melbinger, A., Cremer, J. & Frey, E. (2010). Evolutionary game theory in growing populations. *Physical Review Letters*, **105**, 178101. 21

Melbinger, A., Cremer, J. & Frey, E. (2015). The emergence of cooperation from a single mutant during microbial life cycles. *Journal of The Royal Society Interface*, **12**, 20150171. 5, 21, 57, 135

Méndez, V., Assaf, M., Campos, D. & Horsthemke, W. (2015). Stochastic dynamics and logistic population growth. *Physical Review E*, **91**, 062133. 15, 25

Mitarai, N., Gunnarson, I., Pedersen, B.N., Rosiek, C.A. & Sneppen, K. (2016). Three is much more than two in coarsening dynamics of cyclic competitions. *Physical Review E*, **93**, 042408. 61

Mobilia, M. (2010). Oscillatory dynamics in rock–paper–scissors games with mutations. *Journal of Theoretical Biology*, **264**, 1–10. 67, 68, 70, 71, 150, 151, 152

Mobilia, M., Rucklidge, A.M. & Szczesny, B. (2016). The influence of mobility rate on spiral waves in spatial rock-paper-scissors games. *Games*, **7**, 24. 8, 67, 69, 71

Moran, P.A.P. *et al.* (1962). The statistical processes of evolutionary theory. *American Journal of Human Genetics*, **14**, 438–439. 15, 150

Morgenstern, O. & Von Neumann, J. (1944). *Theory of Games and Economic Behavior*. Princeton University Press. 13

Nahum, J.R., Harding, B.N. & Kerr, B. (2011). Evolution of restraint in a structured rock–paper–scissors community. *Proceedings of the National Academy of Sciences*, **108**, 10831–10838. 6, 59

Nash, J. (1951). Non-cooperative games. *Annals of Mathematics*, 286–295. 13

Nash, J. (1953). Two-person cooperative games. *Econometrica: Journal of the Econometric Society*, 128–140. 13

Nash, J.F. (1950). The bargaining problem. *Econometrica: Journal of the Econometric Society*, 155–162. 13

Nash, J.F. *et al.* (1950). Equilibrium points in n-person games. *Proceedings of the National Academy of Sciences*, **36**, 48–49. 13

Nee, S., May, R.M. & Harvey, P.H. (1994). The reconstructed evolutionary process. *Philosophical Transactions of the Royal Society of London. Series B: Biological Sciences*, **344**, 305–311. 15

Ni, X., Wang, W.X., Lai, Y.C. & Grebogi, C. (2010). Cyclic competition of mobile species on continuous space: Pattern formation and coexistence. *Physical Review E*, **82**, 066211. 61, 70

Nowak, M.A. (2006a). *Evolutionary Dynamics: Exploring the Equations of Life*. Harvard University Press. 15, 61, 70, 72, 74, 150

Nowak, M.A. (2006b). Five rules for the evolution of cooperation. *Science*, **314**, 1560–1563. 5

Nowak, M.A. & May, R.M. (1992). Evolutionary games and spatial chaos. *Nature*, **359**, 826–829. 5

Nowak, M.A. & Sigmund, K. (2004). Evolutionary dynamics of biological games. *Science*, **303**, 793–799. 4

Nowak, M.A., Sasaki, A., Taylor, C. & Fudenberg, D. (2004). Emergence of cooperation and evolutionary stability in finite populations. *Nature*, **428**, 646–650. 15

O'Dwyer, J.P. & Chisholm, R. (2014). A mean field model for competition: From neutral ecology to the Red Queen. *Ecology Letters*, **17**, 961–969. 47

Okasha, S. (2006). *Evolution and the Levels of Selection*. Oxford University Press. 57, 135

Paulsson, J. (2004). Summing up the noise in gene networks. *Nature*, **427**, 415–418. 32

Peltomäki, M. & Alava, M. (2008). Three- and four-state rock-paper-scissors games with diffusion. *Physical Review E*, **78**, 031906. 69

Pennisi, E. (2005). What determines species diversity? *Science*, **309**, 90–90. 1

Perc, M. & Szolnoki, A. (2010). Coevolutionary games-a mini review. *BioSystems*, **99**, 109–125. 70, 74

Petraitis, P.S., Latham, R.E. & Niesenbaum, R.A. (1989). The maintenance of species diversity by disturbance. *The Quarterly Review of Biology*, **64**, 393–418. 49, 57, 135

Postlethwaite, C. & Rucklidge, A. (2017). Spirals and heteroclinic cycles in a spatially extended rock-paper-scissors model of cyclic dominance. *EPL (Europhysics Letters)*, **117**, 48006. 67, 69, 71

Postlethwaite, C.M. & Rucklidge, A.M. (2019). A trio of heteroclinic bifurcations arising from a model of spatially-extended rock–paper–scissors. *Nonlinearity*, **32**, 1375. 67, 69

Provata, A., Nicolis, G. & Baras, F. (1999). Oscillatory dynamics in low-dimensional supports: A lattice Lotka-Volterra model. *The Journal of Chemical Physics*, **110**, 8361–8368. 68

Reichenbach, T. & Frey, E. (2008). Instability of spatial patterns and its ambiguous impact on species diversity. *Physical Review Letters*, **101**, 058102. 69

Reichenbach, T., Mobilia, M. & Frey, E. (2006). Coexistence versus extinction in the stochastic cyclic Lotka-Volterra model. *Physical Review E*, **74**, 051907. 60, 61, 63, 64, 74, 151, 152, 154

Reichenbach, T., Mobilia, M. & Frey, E. (2007a). Mobility promotes and jeopardizes biodiversity in rock–paper–scissors games. *Nature*, **448**, 1046–1049. 8, 69, 71

Reichenbach, T., Mobilia, M. & Frey, E. (2007b). Noise and correlations in a spatial population model with cyclic competition. *Physical Review Letters*, **99**, 238105. 8, 69, 71

Reichenbach, T., Mobilia, M. & Frey, E. (2008). Self-organization of mobile populations in cyclic competition. *Journal of Theoretical Biology*, **254**, 368–383. 8, 61, 69, 71

Reimann, P. (1995). Thermally driven escape with fluctuating potentials: A new type of resonant activation. *Physical Review Letters*, **74**, 4576. 140

Ridolfi, L., D'Odorico, P. & Laio, F. (2011). *Noise-Induced Phenomena in the Environmental Sciences*. Cambridge University Press. 2, 27

Roberts, E., Be'er, S., Bohrer, C., Sharma, R. & Assaf, M. (2015). Dynamics of simple gene-network motifs subject to extrinsic fluctuations. *Physical Review E*, **92**, 062717. 3, 141, 167

Rodriguez, M. & Pesquera, L. (1986). First-passage times for non-Markovian processes driven by dichotomic Markov noise. *Physical Review A*, **34**, 4532. 27

Rulands, S., Zielinski, A. & Frey, E. (2013). Global attractors and extinction dynamics of cyclically competing species. *Physical Review E*, **87**, 052710. 68

Samoilov, M.S., Price, G. & Arkin, A.P. (2006). From fluctuations to phenotypes: The physiology of noise. *Science's STKE*, **2006**, re17–re17. 32

Sancho, J. (1984). Stochastic processes driven by dichotomous Markov noise: Some exact dynamical results. *Journal of Mathematical Physics*, **25**, 354–359. 27

Sancho, J. & Miguel, M.S. (1983). Some results in the description of systems under the influence of dichotomous noise. *Progress of Theoretical Physics*, **69**, 1085–1090. 27

Sancho, J. & San Miguel, M. (1984). Theory of external two-state Markov noise in the presence of internal fluctuations. *Journal of Statistical Physics*, **37**, 151–172. 27

Sancho, J.M. (1985). External dichotomous noise: The problem of the mean-first-passage time. *Physical Review A*, **31**, 3523. 27

Sato, K., Konno, N. & Yamaguchi, T. (1997). Paper-scissors-stone game on trees. *Muroran Institute of Technology Report*, **47**, 109–114. 8, 61, 70

Schmid, G., Reimann, P. & Hänggi, P. (1999). Control of reaction rate by asymmetric two-state noise. *The Journal of Chemical Physics*, **111**, 3349–3356. 27

Schuster, P. & Sigmund, K. (1983). Replicator dynamics. *Journal of Theoretical Biology*, **100**, 533–538. 15

Semenov, N.N. *et al.* (1935). Chemical kinetics and chain reactions. 12

Sidhom, L. & Galla, T. (2020). Ecological communities from random generalized Lotka-Volterra dynamics with nonlinear feedback. *Physical Review E*, **101**, 032101. 13

Sinervo, B. & Lively, C.M. (1996). The rock–paper–scissors game and the evolution of alternative male strategies. *Nature*, **380**, 240–243. 6, 59

Sinervo, B., Miles, D.B., Frankino, W.A., Klukowski, M. & DeNardo, D.F. (2000). Testosterone, endurance, and Darwinian fitness: Natural and sexual selection on the physiological bases of alternative male behaviors in side-blotched lizards. *Hormones and Behavior*, **38**, 222–233. 59, 67

Smith, J.M. (1982). *Evolution and the Theory of Games*. Cambridge University Press. 3, 4, 14, 61, 70, 74, 85

Smith, J.M. (1996). The games lizards play. *Nature*, **380**, 198–199. 6

Smith, J.M. & Price, G.R. (1973). The logic of animal conflict. *Nature*, **246**, 15–18. 14

Smith, J.M. & Szathmary, E. (1997). *The Major Transitions in Evolution*. Oxford University Press. 5

Szabó, G. & Fath, G. (2007). Evolutionary games on graphs. *Physics Reports*, **446**, 97–216. 70, 72, 74, 85

Szabó, G. & Hauert, C. (2002). Phase transitions and volunteering in spatial public goods games. *Physical Review Letters*, **89**, 118101. 71

Szabó, G. & Szolnoki, A. (2002). Three-state cyclic voter model extended with Potts energy. *Physical Review E*, **65**, 036115. 61, 74

Szabó, G. & Tőke, C. (1998). Evolutionary prisoners dilemma game on a square lattice. *Physical Review E*, **58**, 69. 71

Szabó, G., Szolnoki, A. & Izsák, R. (2004). Rock-scissors-paper game on regular small-world networks. *Journal of Physics A: Mathematical and General*, **37**, 2599. 8, 61, 70

Szczesny, B., Mobilia, M. & Rucklidge, A.M. (2013). When does cyclic dominance lead to stable spiral waves? *EPL (Europhysics Letters)*, **102**, 28012. 8, 67, 68, 69, 71

Szczesny, B., Mobilia, M. & Rucklidge, A.M. (2014). Characterization of spiraling patterns in spatial rock-paper-scissors games. *Physical Review E*, **90**, 032704. 8, 67, 69, 71, 85

Szolnoki, A. & Szabó, G. (2004). Phase transitions for rock-scissors-paper game on different networks. *Physical Review E*, **70**, 037102. 8, 61, 70

Szolnoki, A., Mobilia, M., Jiang, L.L., Szczesny, B., Rucklidge, A.M. & Perc, M. (2014). Cyclic dominance in evolutionary games: A review. *Journal of the Royal Society Interface*, **11**, 20140735. 8, 66, 67, 68, 70, 71

Tainaka, K.i. (1989). Stationary pattern of vortices or strings in biological systems: Lattice version of the Lotka-Volterra model. *Physical Review Letters*, **63**, 2688. 61, 74

Tainaka, K.i. (1993). Paradoxical effect in a three-candidate voter model. *Physics Letters A*, **176**, 303–306. 61, 64, 74

Tainaka, K.i. (1994). Vortices and strings in a model ecosystem. *Physical Review E*, **50**, 3401. 8, 61, 70, 74

Taitelbaum, A., West, R., Assaf, M. & Mobilia, M. (2020). Population dynamics in a changing environment: Random versus periodic switching. *Physical Review Letters*, In Press, pre–print available at https://arxiv.org/abs/2002.10372. 46, 142, 144, 146

Taylor, D.R. & Aarssen, L.W. (1990). Complex competitive relationships among genotypes of three perennial grasses: Implications for species coexistence. *The American Naturalist*, **136**, 305–327. 59

Thattai, M. & Van Oudenaarden, A. (2001). Intrinsic noise in gene regulatory networks. *Proceedings of the National Academy of Sciences*, **98**, 8614–8619. 2

Thattai, M. & Van Oudenaarden, A. (2004). Stochastic gene expression in fluctuating environments. *Genetics*, **167**, 523–530. 32, 33, 45

Toupo, D.F. & Strogatz, S.H. (2015). Nonlinear dynamics of the rock-paper-scissors game with mutations. *Physical Review E*, **91**, 052907. 68, 71

Traulsen, A., Nowak, M.A. & Pacheco, J.M. (2006). Stochastic dynamics of invasion and fixation. *Physical Review E*, **74**, 011909. 71

Van Den Broeck, C. (1983). On the relation between white shot noise, gaussian white noise, and the dichotomic Markov process. *Journal of Statistical Physics*, **31**, 467–483. 27

Van den Broeck, C. & Hänggi, P. (1984). Activation rates for nonlinear stochastic flows driven by non-gaussian noise. *Physical Review A*, **30**, 2730. 27

Van Kampen, N.G. (1992). *Stochastic Processes in Physics and Chemistry*, vol. 1. Elsevier. 1, 73, 151

Venkat, S. & Pleimling, M. (2010). Mobility and asymmetry effects in one-dimensional rock-paper-scissors games. *Physical Review E*, **81**, 021917. 68, 74

Visco, P., Allen, R.J., Majumdar, S.N. & Evans, M.R. (2010). Switching and growth for microbial populations in catastrophic responsive environments. *Biophysical Journal*, **98**, 1099–1108. 2, 33

Volterra, V. (1926a). Fluctuations in the abundance of a species considered mathematically. *Nature*, **119**, 12–12. 12

Volterra, V. (1926b). Variations and fluctuations of the number of individuals in animal species living together. *Animal Ecology*, 409–448. 12

Wahl, L.M., Gerrish, P.J. & Saika-Voivod, I. (2002). Evaluating the impact of population bottlenecks in experimental evolution. *Genetics*, **162**, 961–971. 33

West, R. & Mobilia, M. (2020). Fixation properties of rock-paper-scissors games in fluctuating populations. *Journal of Theoretical Biology*, **491**, 110135. 2, 21

West, R., Mobilia, M. & Rucklidge, A.M. (2018). Survival behavior in the cyclic Lotka-Volterra model with a randomly switching reaction rate. *Physical Review E*, **97**, 022406. 2, 60, 74, 152, 155

Wienand, K., Lechner, M., Becker, F., Jung, H. & Frey, E. (2015). Non-selective evolution of growing populations. *PLoS One*, **10**. 2

Wienand, K., Frey, E. & Mobilia, M. (2017). Evolution of a fluctuating population in a randomly switching environment. *Physical Review Letters*, **119**, 158301. 2, 6, 21, 34, 42, 55, 96, 99, 118, 138, 161, 162, 163

Wienand, K., Frey, E. & Mobilia, M. (2018). Eco-evolutionary dynamics of a population with randomly switching carrying capacity. *Journal of The Royal Society Interface*, **15**, 20180343. 2, 6, 21, 34, 42, 55, 96, 99, 100, 136, 138, 139, 161, 162, 163

Wolf, D.M., Vazirani, V.V. & Arkin, A.P. (2005). Diversity in times of adversity: Probabilistic strategies in microbial survival games. *Journal of Theoretical Biology*, **234**, 227–253. 32

Xue, B. & Leibler, S. (2017). Bet hedging against demographic fluctuations. *Physical Review Letters*, **119**, 108103. 2

Yang, Q., Rogers, T. & Dawes, J.H. (2017). Demographic noise slows down cycles of dominance. *Journal of Theoretical Biology*, **432**, 157–168. 71

Yasui, Y. (2001). Female multiple mating as a genetic bet-hedging strategy when mate choice criteria are unreliable. *Ecological Research*, **16**, 605–616. 32

Zamudio, K.R. & Sinervo, B. (2000). Polygyny, mate-guarding, and posthumous fertilization as alternative male mating strategies. *Proceedings of the National Academy of Sciences*, **97**, 14427–14432. 6, 59